KINETICS OF GASEOUS REACTIONS OF THE OH RADICAL WITH SELECTED CYCLOALKENES AND AROMATIC COMPOUNDS

By

© TAKAKO KIMURA, B.A.

A Thesis

Submitted to the School of Graduate Studies

in Partial Fulfilment of the Requirements

for the Degree

Doctor of Philosophy

McMaster University

October, 1986

KINETICS OF GASEOUS REACTIONS OF THE OH RADICAL

DOCTOR OF PHILOSOPHY (1986)

McMASTER UNIVERSITY
Hamilton, Ontario

TITLE: Kinetics of Gaseous Reactions of the OH Radical with Selected Cycloalkenes and Aromatic Compounds

AUTHOR: Takako Kimura, B.A. (International Christian University)

SUPERVISOR: Dr. A. J. Yarwood

NUMBER OF PAGES: xvii, 237

ABSTRACT

The kinetics of the OH radical reactions with selected cycloalkenes and aromatic compounds were studied in the gas phase with the flash photolysis-resonance fluorescence technique.

Five OH-cycloalkene reactions were studied at temperatures between 295 and 428 K. The significance of the allylic hydrogen abstraction process relative to the addition process in these reactions is discussed. On the basis of the room-temperature rate constants, the significance of the OH radical reactions with cycloalkenes in the troposphere is considered. Arrhenius parameters were calculated for each reaction. The reactions all have negative apparent activation energies of ~4 - 5 kJ mol^{-1}; values similar to those of OH-alkene reactions. The factors which might determine the relative reactivity of various OH-alkene and OH-cycloalkene reactions are examined.

The kinetics of the OH-benzene reaction were studied at temperatures between 295 and 425 K. The validity of the previously proposed mechanism and the reasons for the discrepancies among the studies reported in the literature are examined by comparing the observed kinetics with the predictions of computer simulation of the mechanism. The temperature dependence of the OH-chlorobenzene reaction was studied in the same temperature range, and the kinetics were compared with those of the OH-benzene reaction.

The OH radical reactions were also studied at room temperature with six selected halogenated benzenes and biphenyl. The factors which might

determine the relative reactivity of these reactions and other previously reported OH-aromatic reactions are discussed.

The rate constants of various OH-chlorinated benzene reactions at room temperature were used as a model to estimate the relative reactivity of the OH-polychlorinated biphenyl reactions, and to discuss the significance of the reactions in determining the atmospheric lifetimes of polychlorinated biphenyls.

"And whatever you do in word or deed, do all in the name of the Lord Jesus, giving thanks through Him to God the Father." (From Apostle Paul's letter to the Colossians)

ACKNOWLEDGEMENTS

I wish to thank my research supervisor, Dr. A. J. Yarwood for making available to me all his resources, and for his guidance during the course of my graduate study.

I am grateful to the Department of Chemistry for their financial support and the opportunity of invaluable academic study in past years.

My appreciation to Mr. Claus Schonfeld for offering me so freely much practical advice and many ideas during the time of building the apparatus.

Thanks to Tom McLean, Faten Emara, and Rajini Senaratne in the next-door research laboratory for loaning me the extra things needed for the research and keeping company with me in the basement floor.

Thanks also to Mike Mallott for his skillful help in plotting graphs, and to Lydia Zengo for proof-reading this manuscript.

I appreciated all the roommates and housemates I have had during my stay at McMaster for making me feel at home in a foreign country.

My gratitude to my friends from Campus Crusade for Christ of Canada and Philpott Memorial Church for their continuous encouragement which kept me going even when I felt like giving up my study, and above all for feeding me with spiritual food in past years.

Finally, I cannot express how much I am grateful to my parents for their sacrificial support and patience with me. Without them I could never have come this far.

TABLE OF CONTENT

		Page
CHAPTER I	INTRODUCTION	1
	I.A. Role of the OH Radical in the Chemistry of the Polluted Atmosphere	2
	I.A.1. Concentration of the OH Radical in the Troposphere	2
	I.A.2. Reactivities of the OH Radical with Atmospheric Species	4
	I.A.3. Contribution of the OH Radical Reactions in the Overall Chemistry of the Troposphere	6
	I.B. Experimental Techniques for the Study of the Reaction Kinetics of the OH Radical	10
	I.B.1. Absolute Techniques	11
	I.B.1.a. Detection Methods Used in Absolute Techniques	11
	I.B.1.b. The Flash Photolysis Technique	11
	I.B.1.c. The Discharge Flow Technique	14
	I.B.2. Relative Rate Techniques	15
	I.C. Scope of the Present Study	17
CHAPTER II	EXPERIMENTAL	20
	II.A. The Reaction Cell	20
	II.B. Formation of the OH Radicals by Vacuum U.V. Flash Photolysis	24
	II.C. Detection of the OH Radicals by Resonance Fluorescence	27
	II.D. Preparation of the Reaction Gas Mixture	34

CHAPTER III KINETIC INFORMATION OBTAINED FROM THE FLASH PHOTOLYSIS-RESONANCE FLUORESCENCE TECHNIQUE 39

III.A. Intensity of the Fluorescence and the Concentration of the OH Radical 39

III.B. Decay Rates of the Concentration of the OH Radical and Rate Constants of Reactions 41

III.C. Possibility of Secondary Reactions 43

III.D. Effect of Diffusion on the Decay Curves of the Concentration of the OH Radical 48

III.E. Test Experiments 52

CHAPTER IV REACTIONS OF THE OH RADICAL WITH SELECTED CYCLOALKENES 56

IV.A. Experimental Results 56

IV.A.1. At Room Temperature 56

IV.A.2. Temperature Dependence of Rate Constants 68

IV.B. Discussion 76

IV.B.1. Comparison of the Results of the Present Study with Those Previously Reported 76

IV.B.2. Significance of the Allylic Hydrogen Abstraction 78

IV.B.2.a. Pressure Dependence of Rate Constants 78

IV.B.2.b. The Correlations with O Atom Reactions 79

IV.B.2.c. The Bond Dissociation Energy of Allylic C-H Bond 79

IV.B.2.d. Stable Product Study 81

IV.B.2.e. Stretching Force Constants 85

IV.B.3. Interpretations of the Temperature Dependence of the Rate Constants 89

IV.B.3.a. Collision Theory 91

IV.B.3.b. Transition-State Theory 93

IV.B.3.c. A Weakly-Bound Complex 95

IV.B.3.d. Consideration of Thermodynamic Parameters 97

IV.B.3.D.1. Potential Energy Surfaces of the OH-Alkene Reactions 97

IV.B.3.d.1.(a) Harpoon Model 99

IV.B.3.d.1.(b) Frontier Orbital Theory 102

IV.B.3.d.2. Entropy of Activation 105

IV.B.3.d.3. Free Energy Barrier of the Reaction 108

IV.B.4. Atmospheric Implication of the OH-Cycloalkene Reactions 111

IV.C. Summary of This Chapter 115

CHAPTER V REACTIONS OF THE OH RADICAL WITH SELECTED AROMATIC COMPOUNDS 117

V.A. Reactions of the OH Radical with Benzene and Chlorobenzene at Various Temperatures 117

V.A.1. The OH + Benzene Reaction 117

V.A.1.a. Experimental Results 117

V.A.1.b. Discussion 126

V.A.1.b.1. Comparison of the Present Results at Room Temperature with Those Previously Reported 126

V.A.1.b.2. Mechanism of the OH-Benzene Reaction and the Effect of Temperature 130

V.A.1.b.2.(a) Comparison of the Present Results with Those Previously Reported on the Temperature Dependence of

the Kinetics . . 131

V.A.1.b.2.(b) Curve Fitting and Computer Simulation of Decay Curves 138

V.A.1.b.3. A π Complex as an Intermediate in the OH-Benzene Reaction 148

V.A.2. The OH + Chlorobenzene Reaction. 150

V.A.2.a. Experimental Results 150

V.A.2.b. Discussion 154

V.B. Reactions of the OH Radical with Selected Halogenated Benzenes and Biphenyl at Room Temperature 162

V.B.1. Experimental Results 162

V.B.2. Discussion 169

V.B.2.a. Comparison of the Results of the Present Study with Those Previously Reported 169

V.B.2.b. The Factors Which Determine Relative Reactivities of the OH-Halogenated Benzene Reactions 173

V.B.2.c. Correlations of the Kinetics of the OH-Aromatic Reactions with Other Parameters 178

V.B.2.c.1. Correlation of the OH Radical and the O Atom Reactions with Aromatic Molecules 179

V.B.2.c.2. The Hammett Equation and OH-Aromatic Reactions 181

V.B.2.c.3. Correlation of Rate Constants of OH-Aromatic Reactions with Ionization Potentials 187

V.B.2.d. Implications of OH-Chlorinated Benzene Reactions on Polychlorinated Biphenyls in the Atmosphere 191

V.C. Summary of This Chapter 196

APPENDIX A PURITY LEVELS OF THE CHEMICALS 200

APPENDIX B COMPUTER SIMULATIONS OF THE REACTION SYSTEMS 203

B.1. Loss of the OH Radical in the Absence of a Reactant 204

B.2. Effect of Secondary Reactions 204

APPENDIX C ERROR ANALYSIS AND CONCENTRATION CALCULATIONS OF THE REACTANTS 207

C.1. Weights Used in Decay Curve Analysis 207

C.2. Detection of Non-Random Errors in Decay Curve Analysis 207

C.3. Calculation of the Concentration of a Reactant and Its Uncertainty 208

C.4. The Least-Square Cubic Method and Calculation of the Overall Accuracy 211

C.5. Calculation of Arrhenius Parameters 214

APPENDIX D MODEL STUDIES OF THE DECAY CURVES OF THE CONCENTRATION OF THE OH RADICAL BY DIFFUSION AND DIFFUSION PLUS A FIRST-ORDER REACTION 215

APPENDIX E TABULATION OF VARIOUS PARAMETERS USED IN FIGURES IV.13, IV.15, IV.16, V.20, V.21, AND V.22 220

E.1. Ionization Potential, Rate Constants of the OH Radical and the O Atom Reactions, and Reaction Cross Sections($\bar{\sigma}_{EXP}$) of Various Alkenes 220

E.2. Rate Constants of the OH Radical and the O Atom Reactions, Ionization Potentials, and $\Sigma\,\sigma^+$ of Various Aromatic Compounds 222

REFERENCES 224

LIST OF TABLES

		Page
Table I.1	Estimated Rates of Loss of Various Pollutant Molecules by Reactions with Reactive Species in the Troposphere	7
Table I.2	Principal Detection Methods of the OH Radical Used in Absolute Techniques and Their Working Concentration Ranges (from Reference 38)	12
Table III.1	Second-Order Rate Constants of the OH Radical Reactions with H_2, C_2H_4, and C_3H_6 at Room Temperature	55
Table IV.1	Observed First-Order Rate Constants of the OH-Cyclopentene Reaction at 295 K	57
Table IV.2	Second-Order Rate Constants of the OH Radical Reactions with Selected Cycloalkenes at Room Temperature	69
Table IV.3	Second-Order Rate Constants of the OH Radical Reactions with Selected Cycloalkenes at Various Temperatures	71
Table IV.4	Conventional Arrhenius Parameters of the OH Radical Reactions with Selected Cycloalkenes	75
Table IV.5	Comparison of Rate Constants of Hydrogen Abstraction by the OH Radical per Allylic C-H Bond Estimated by Various Groups	83
Table IV.6	Estimation of the Extent of Hydrogen Abstraction from Selected Alkenes and Cycloalkenes	90
Table IV.7	Arrhenius Parameters and Entropies of Activation at 350 K of Various OH-Alkene and OH-Cycloalkene Reactions	107
Table IV.8	Some Cycloalkenes Detected in the Troposphere	112
Table IV.9	Rate Constants of the OH and the O_3 Reactions with Some Cycloalkenes and Halflives of the Cycloalkenes due to Those Reactions in the Troposphere	114

Table V.1	Observed First-Order Rate Constants of the OH-Benzene Reaction at 295 K	119
Table V.2	High Pressure-Limit Second-Order Rate Constants of the OH-Benzene Reaction at Room Temperature	122
Table V.3	Second-Order Rate Constants of the OH-Chlorobenzene Reaction at Room Temperature and 310 K	153
Table V.4	Second-Order Rate Constants of the OH Radical Reactions with Selected Halogenated Benzenes and Biphenyl at Room Temeperature	170
Table V.5	Reported Rate Constans of the OH Radcial Reactions with Biphenyl and Chlorobiphenyls at Room Temperature	194
Table A	Purity Levels of Chemicals Used in the Present Study	201
Table E.1	Ionization Potentials, Rate Constants of the OH Radical and the O Atom Reactions, and Reaction Cross Sections (σ_{EXP}) of Various Alkenes	220
Table E.2	Rate Constants of the OH Radical and the O atom Reactions, Ionization Potentails, and $\Sigma \sigma^+$ of Various Aromatic Compounds	222

LIST OF FIGURES

		Page
Figure I.1	A Portion of a Proposed Generalized Mechanism of Gas-Phase Reactions in the Polluted Troposphere	9
Figure II.1	A Cross Section of the Flash-Photolysis Resonance Fluorescence Apparatus	21
Figure II.2	Another Cross Section of the Flash-Photolysis Resonance Fluorescence Apparatus	22
Figure II.3	Timing/Trigger/Flash Circuit	25
Figure II.4	Schematic Diagram of the Gas Flow System for the Resonance Lamp	28
Figure II.5	DC Power Supply Circuit of the Microwave Power Supply and an Added Capacitor	28
Figure II.6	Trigger/Detection System	30
Figure II.7	A Timing Diagram of a Typical Experimental Run with 1 msec Delay on the Minicomputer	32
Figure II.8	A Schematic Diagram of the Gas Flow System	35
Figure II.9	Two Ways to Introduce a Reactant/Argon Mixture	36
Figure III.1	Results of a Typical Experiment and Processing of the Data (OH + Cyclohexene Reaction at 295 K, P_{tot} = 50 torr, [Cycloalkene] = 7.65 x 10^{12} molecule cm^{-3})	
	(a) An Example of an Observed Decay Curve	44
	(b) A Decay Curve (a) Plotted in a Semi-Log Scale After Background Subtraction and a Fitted Curve	44
	(c) Weighted Residuals of a Fitted Curve	45
	(d) An Autocorrelation Function	45
Figure III.2	A Typical Decay Curve Observed in the Absence of a Reactant at Room Temperature	49

Figure III.3	k_{obs} versus Concentration Plot of the OH + H_2 Reaction at 295 K and P_{tot} = 100 torr	53
Figure III.4	k_{obs} versus Concentration Plot of the OH + C_2H_4 (T = 295 K, P_{tot} = 104 torr) and the OH + C_3H_6 (T = 294 K, P_{tot} = 99 torr) Reactions	54
Figure IV.1	k_{obs} versus Concentration Plot of the OH + Cyclopentene Reaction at 295 and 296 K	58
Figure IV.2	k_{obs} versus Concentration Plot of the OH + Cyclopentene Reaction at 331, 373, and 424 K (P_{tot} = 100torr)	59
Figure IV.3	k_{obs} versus Concentration Plot of the OH + Cyclohexene Reaction at 295 K	60
Figure IV.4	k_{obs} versus Concentration Plot of the OH + Cyclohexene Reaction at 332, 372, and 422 K	61
Figure IV.5	k_{obs} versus Concentration Plot of the OH + Cycloheptene Reaction at 296 K	62
Figure IV.6	k_{obs} versus Concentration Plot of the OH + Cycloheptene Reaction at 332, 375, and 425 K (P_{tot} = 101torr)	63
Figure IV.7	k_{obs} versus Concentration Plots of the OH + 1,3-Cyclohexadiene Reaction at 295 K	64
Figure IV.8	k_{obs} versus Concentration Plot of the OH + 1,3-Cyclohexadiene Reaction at 330, 369, and 428 K (P_{tot} = 100torr)	65
Figure IV.9	k_{obs} versus Concentration Plot of the OH + 1,4-Cyclohexadiene Reaction at 296 K	66
Figure IV.10	k_{obs} versus Concentration Plot of the OH + 1,4-Cyclohexadiene Reaction at 330, 368, and 426 K	67
Figure IV.11	Arrhenius Plot of the OH Radical Reactions with Cyclopentene, Cyclohexene, and Cycloheptene	73
Figure IV.12	Arrhenius Plot of the OH Radical Reactions with 1,3-Cyclohexadiene, and 1,4-Cyclohexadiene	74

Figure IV.13	Correlation Between the OH- and the O-Alkene Reactions at Room Temperature	80
Figure IV.14	Simplified Potential Energy Curves for the C-H and H-OH Bonds	87
Figure IV.15	Correlation Between Rate Constants of OH-Alkene Reactions and Lowest Vertical Ionization Potential (IP) of Alkenes	98
Figure IV.16	Reaction Cross Sections of a Harpoon Model (σ) and Experimental Cross Sections (σ_{EXP}) for OH-Alkene Reactions at Room Temperature as a Function of IP - EA	101
Figure IV.17	Profiles of H, T, S, and G for Halocarbene Reactions with Isobutene and Tetramethylethene Calculated by Houk et al (Reference 204)	110
Figure V.1	Some Examples of Observed Decay Curves for the OH + Benzene Reaction at Room Temperature	118
Figure V.2	k_{obs} versus Concentration Plot of the OH + Benzene Reaction at 295 K	120
Figure V.3	Apparent k_{obs} versus Concentration Plot of the OH + Benzene Reaction at 308 and 323 K (P_{tot} = 100 torr)	123
Figure V.4	Observed Decay Curves of the OH + Benzene Reaction at Three Different Temperatures with Similar Benzene Concentrations	124
Figure V.5	k_{obs} versus Concentration Plot of OH + Benzene Reaction at 392, 406, 416, and 424 K (P_{tot} = 100 torr)	125
Figure V.6	Temperature Dependence of the Second-Order Rate Constant of the OH + Benzene Reaction Studied by Various Groups	137
Figure V.7	$k_{app}(i)$ versus i-th Halflife of the OH + Benzene Reaction at 295 and 323 K :Results of a Simulation Study	141
Figure V.8	$k_{app}(1)$ versus Concentration Plot of OH + Benzene Reaction at 323 and 352 K : Results of a Simulation Study	143

Figure V.9	k_{app} and $(k_1[\text{benzene}] + k_4)^*$ versus Concentration Plots of the OH + Benzene Reaction at Temperature between 390 and 500 K.: Results of a Simulation Study	145
Figure V.10	k_{obs} versus Concentration Plot of the OH + Chlorobenzene Reaction at 295, 296, and 297 K	151
Figure V.11	k_{obs} versus Concentration Plot of the OH + Chlorobenzene Reaction at 310 and 328 K	152
Figure V.12	k_{obs} versus Concentration Plot of the OH + Chlorobenzene Reaction at 396 and 421 K (P_{tot} = 101 torr)	155
Figure V.13	$k_{app}(1)$ versus Concentration Plot of the OH + Chlorobenzene Reaction at 295, 310, 396, and 421 K : Results of a Computer Simulation	159
Figure V.14	k_{obs} versus Concentration Plot of the OH + Fluorobenzene Reaction at 295 and 296 K	163
Figure V.15	k_{obs} versus Concentration Plot of the OH + p-Difluorobenzene Reaction at 295, 296, and 298 K	164
Figure V.16	k_{obs} versus Concentration Plot of the OH Radical Reactions with o-Dichlorobenzene and 1,3,5-Trichlorobenzene at 295 K	165
Figure V.17	k_{obs} versus Concentration Plot of the OH + m-Dichlorobenzene Reaction at 296 K	166
Figure V.18	k_{obs} versus Concentration Plot of the OH + Bromobenzene Reaction at 296 and 297 K	167
Figure V.19	k_{obs} versus Concentration Plot of the OH + Biphenyl Reaction at 295 K	168
Figure V.20	Correlation of the Kinetics of the OH Radical and the O Atom Reactions with Aromatic Molecules at Room Temperature	180
Figure V.21	Correlation Between the Reactivity of the OH Radical towards Aromatic Molecules and $\Sigma\ \sigma^+$	184
Figure V.22	Correlation Between the Reactivity of the OH Radical towards Aromatic Molecules and the Vertical Ionization Potentials (IP) of Aromatic Molecules	188

Figure D (a) A Model Used to Study the Diffusion Pattern of OH Radicals in the Reaction Cell 216

Figure D (b) The Concentration of the OH Radical as a Function of Time and Radius in the Diffusion Model of (a) 216

Figure D (c) The Average Concentration of the OH Radical in the Central Area ($r \leq 0.8$ cm) as a Function of Time in the Absence of a Reaction 217

Figure D (d) The Average Concentration of the OH Radical in the Central Area ($r \leq 0.8$ cm) as a Function of Time in the Presence of a First-Order Reaction 219

CHAPTER I

INTRODUCTION

The hydroxyl (OH) radical was first recognized as an individual species in 1924 by Watson.[1] He proposed that the characteristic ultraviolet (u.v.) emission bands observed in flames and discharges through water vapour were due to the OH radical. The first absorption spectrum of the OH radical in partially dissociated water vapour at ~1900 K was observed soon after by Bonhoeffer and Reichardt.[2] The characterization of the OH radical spectrum enabled a study of the kinetics of this transient species. Oldenberg[3] was the first to monitor with an absorption technique the time profile of the OH radical in the discharge products of water vapour.

Although the importance of the OH radical had been known in the chemistry of flames and combustions[4-7] since the 1920's, it was less than two decades ago that its potential importance in the chemistry of the polluted atmosphere was first demonstrated.[8] Its interesting implications in atmospheric chemistry have led to extensive studies on the kinetics and mechanisms of the OH radical reactions with various inorganic and organic compounds in gas phase over the past fifteen years. These studies have been greatly aided by recent improvements in the experimental techniques used to obtain kinetic information on the OH radical.

This chapter briefly summarizes:

A. role of the OH radical in the chemistry of the polluted atmosphere,

B. experimental methods of studying the kinetics of the OH radical

reactions, and

C. scope of the present study.

I.A. Role of the OH Radical in the Chemistry of the Polluted Atmosphere

Leighton[9] first suggested in 1961 that the OH radical could be one of the intermediates in photochemical air pollution. In order to evaluate the significance of this radical in the polluted atmosphere, efforts have been made in three areas:

1. the estimation and measurement of the OH radical concentration in the troposphere,
2. the study of the reactivity of the OH radical with various atmospheric species and pollutant molecules, and
3. the study of the contribution of the OH radical reactions to the overall chemistry of the polluted atmosphere.

In the following sections, each of these areas will be described briefly.

I.A.1. Concentration of the OH Radical in the Troposphere

In the troposphere (an altitude of less than ~17 km), the active solar wavelengths are above 290 nm since the higher lying ozone (O_3) layer absorbs the radiation below 290 nm.[10] The major source of the OH radicals in the troposphere is probably the reaction of the excited oxygen atom ($O(^1D)$) with water (H_2O):

$$O(^1D) + H_2O \longrightarrow 2OH$$

where $O(^1D)$ might be created by the photolysis of O_3 at $\lambda < 319$ nm.[11] The incomplete combustion of the fossil fuels produces oxygenated organic

compounds, and their photochemical reactions in the polluted troposphere can create the hydroperoxy (HO_2) radical.[11] The disproportionation of the HO_2 radical forms hydrogen peroxide (H_2O_2), and photodissociation of H_2O_2 is an important source of the OH radical in the polluted troposphere:[11]

$$H_2O_2 + h\nu \longrightarrow 2OH \qquad \lambda < 320 \text{ nm}$$

The OH radical is also formed in the reaction of the HO_2 radical with nitric oxide (NO):[11]

$$NO + HO_2 \longrightarrow NO_2 + OH$$

The research on the determination of the concentration of the OH radical in the atmosphere did not make much progress until the 1970's. The global average concentration of the radical in the troposphere has been estimated to be $0.2 - 2.8 \times 10^6$ molecule cm^{-3} using the global balance of the concentrations of halocarbons[12-15] such as trichloromethane ($CHCl_3$) and trichloroethane (CCl_3CH_3), and the isotope carbon monoxide (^{14}CO).[16,17] The actual concentration of the radical in the troposphere varies depending on the local conditions, such as pressure, temperature, altitude, latitude, time, season, and chemical environment. The local average concentrations of the OH radical have been estimated from the rates of removal of some hydrocarbons from the local atmosphere,[18,19] or by the isotope tracing technique with ^{14}CO.[20] Several groups[21-26] have constructed contour maps of the OH radical concentration in the troposphere by computer modeling of the troposphere. They took into consideration basic photochemical reactions in the atmosphere, the atmospheric structure, and/or simple models of

transport processes.

Direct measurements have been also attempted. In the troposhpere, techniques have been used such as resonance absorption of sun light,[27,28] long-pass laser absorption,[29,30] spin trapping,[31] and laser excitation (or laser induced) resonance fluorescence.[32-35] With the last technique, the equipment was built in such a way that it could be carried by an aircraft to perform measurement in the higher troposphere.[32,33] These techniques, although very sensitive, still have difficulty detecting low concentrations of the OH radical in the troposphere. Recently measured day-time concentrations of the OH radical at various locations have been in the range of $< 5 \times 10^6$ molecule cm^{-3}.[29-31,34,35]

I.A.2. Reactivities of the OH Radical with Atmospheric Species

The recent progress in the kinetic study of the OH radical reactions was triggered by the research of Greiner in 1967.[8] He performed a series of studies on the OH-alkane reactions with the flash photolysis-kinetic spectroscopic technique. From the kinetic data obtained, he suggested that the OH radical could be important in the consumption of saturated hydrocarbons in the polluted atmosphere. Since then, the kinetics of elementary reactions of the OH radical have been studied with several hundred inorganic and organic compounds.[36-38] Technical improvements in the equipment have been made and more reliable kinetic data have become available. The three major techniques which have contributed most of the data will be described in section I.B. of this chapter. It has been found that in most cases the OH radical is more reactive by several orders of magnitude than other reactive species in the atmosphere such as ozone (O_3), the

ground-state oxygen atom ($O(^3P)$), and the hydroperoxy (HO_2) radical.

Studies of the products of the OH radical reactions have been carried out in two main ways. One way is by studying the immediate products of the elementary reactions of the OH radical. Since the immediate product is always another transient radical, the study requires highly sophisticated and very sensitive techniques, such as the low-pressure molecular beam or the discharge flow methods combined with (photoionization) mass spectroscopy.[39-45] Another way is by analyzing the stable products in a static system. In this method, the OH radicals are created in the static system by 1) photodissociation of nitrous oxide (N_2O) or NO_2 in the presence of molecular hydrogen (H_2), H_2O, or ethane (C_2H_6),[46,47] 2) photolysis of H_2O_2[47] or HONO,[48,49] 3) photodissociation of alkylnitrites (RONO) in the presence of nitric oxide (NO) and molecular oxygen (O_2),[50-55] or 4) photochemical reactions in NO_x/air mixture,[56,57] while a reactant is present. The initial reaction of the OH radical with a reactant is followed by a series of chain reactions until some stable products are formed or the species are lost on the walls. The stable products are analyzed with gas chromatography (GC),[46,47,49,57] gas chromatography-mass spectroscopy (GCMS),[49,53,56] differential optical absorption spectroscopy (DOAS),[53] or by long-path Fourier transform infrared spectroscopy (LPFTIR).[48,50-52,55] In addition, Kenley et al,[58,59] collected the stable products from a discharge flow system containing a mixture of $OH/O_2/NO$/reactant, and analyzed them with GC. One may deduce the mechanism of the reaction system from the results of qualitative and quantitative analysis of the stable products.

These product studies have shown that the OH radical initially reacts with a molecule either by abstracting a hydrogen atom from the molecule, or by adding itself to the molecule.

I.A.3. Contribution of the OH Radical Reactions in the Overall Chemistry of the Troposphere

The product of the average ambient concentration of the OH radical and the rate constant of its reaction with a reactant gives a rough estimate of the rate of loss of the reactant from the troposphere by the reaction with the OH radical. In Table I.1, this product is compared with those of other reactive species in the troposphere for the reactions with olefins, paraffins, and NO.[61] It is clear from the table that the OH radical is the species which dominantly consumes hydrocarbons by reaction, with the exception of olefins when the O_3 concentration is high.

As mentioned in the previous section, the immediate product of the OH radical reaction with a molecule is always a radical. One expects chain reactions to follow in the troposphere as well, until a termination reaction occurs. In order to estimate the significance of OH radical reactions in the overall chemistry of the polluted troposphere, it is important to assess not only how fast the OH radical would initially react with atmospheric species and pollutant molecules, but also to what products the following chain reactions would lead and how quickly. Many of the stable product studies mentioned in the previous section[48-57] were performed in simulated air, and provided information on the potential mechanisms of the degradation of reactants in the troposphere which are initiated by the OH radical.

Table I.1

Estimated Rates of Loss of Various Pollutant Molecules by Reactions with Reactive Species in the Troposphere

Reactive Species	Concentration of Species in Ambient Air (molecule cm^{-3})	Rate Constant of the OH Radical Reaction (cm^3 $molecule^{-1}$ sec^{-1})			Rate of Loss of Reactant in Ambient Air (sec^{-1})		
		Olefin	Paraffin	NO	Olefin	Paraffin	NO
OH	10^6 - 10^7	10^{-10} - 10^{-12}	10^{-12} - 10^{-13}	$3x10^{-30}$	10^{-3} - 10^{-6}	10^{-5} - 10^{-7}	$3x10^{-23}$ - 10^{-24}
$O(^3P)$	$[10^4]$	10^{-11} - 10^{-12}	10^{-14} - 10^{-15}	$1x10^{-31}$	10^{-7} - 10^{-8}	10^{-10} - 10^{-11}	10^{-27}
O_3	10^{11} - 10^{13}	10^{-17} - 10^{-18}	$< 10^{-20}$	$1.5x10^{-14}$	10^{-4} - 10^{-7}	$< 10^{-7}$	$1.5x10^{-1}$ - 10^{-3}
HO_2	$[10^8$ - $10^9]$	10^{-15} - 10^{-16}	10^{-20} - 10^{-22}	$1.7x10^{-13}$	10^{-6} - 10^{-8}	10^{-11} - 10^{-14}	$1.7x10^{-4}$ - 10^{-5}
CH_3O	$[\sim 10^7]$	$[10^{-16}]$		$[6x10^{-13}]$	$[10^{-9}]$		$[6x10^{-6}]$

Concentrations and rate constants were taken from reference 61.

A rate was calculated by multiplying a concentration with a rate constant.

The bracket signifies an estimated value.

The model air study helps to assess this even more realistically. It is done in two stages. First, in the laboratory, polluted air is simulated in a large environmental (or smog) chamber.[62-69] It is exposed to either simulated or real atmospheric conditions, such as light, temperature, and pressure. GC and in-situ LPFTIR are utilized as tools to identify some stable products and to monitor their concentrations as a function of time. When experimental conditions are reasonably well controlled, one can postulate a reaction mechanism for the system. In the second stage, if the rate constants of all the elementary reactions involved in the mechanism are known or can be estimated, rate equations for the species in the system can be numerically solved by computer.[66,67,69-75] The computer generates profiles of the concentrations versus time, which can be compared with corresponding experimental profiles. It is a very complex study. For example, a simulated atmosphere with only one organic pollutant, ethene, involves at least 70 reactions and 35 species.[70] Although many technical difficulties are encountered in these experiments as well as in the computations, certain features are predicted to be observed in the real atmosphere. The study seems to support a generalized mechanism for the gas-phase chemistry of the polluted troposphere, a part of which is shown in Figure I.1. Organic pollutants are expected to become peroxy radicals before further oxidization to carbonyl compounds. Although they are not shown in Figure I.1, fragmentations and isomerizations might also occur in the course of chain reactions. If the concentrations of organic pollutants are high, their oxidation processes might produce the concentrations of peroxy radicals and organic nitrates sufficient enough to promote NO-to-NO_2 conversion. The resulting higher NO_2/NO ratio might cause an increase in

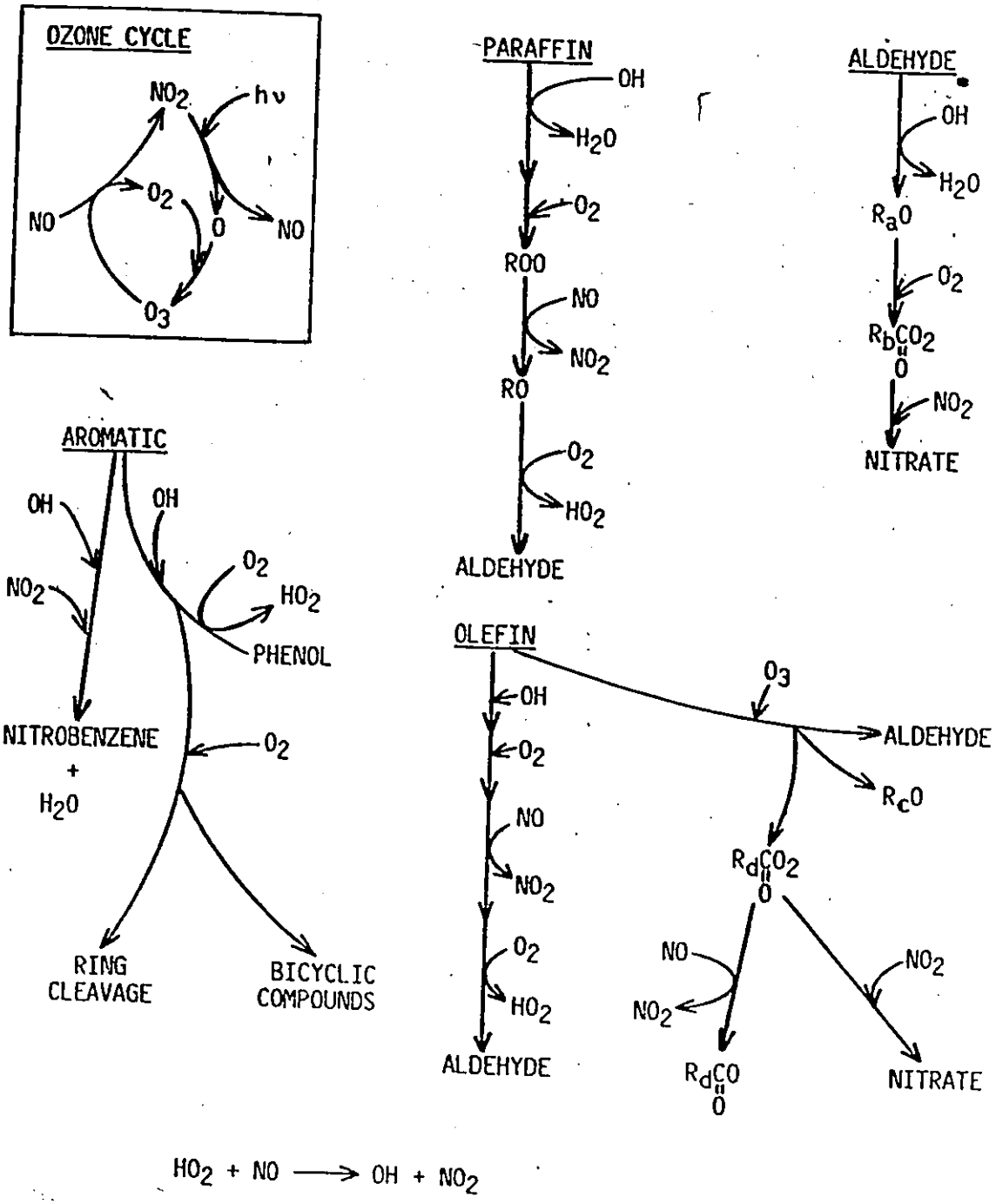

$$HO_2 + NO \longrightarrow OH + NO_2$$

Figure I.1

A Portion of a Proposed Generalized Mechanism of Gas-Phase Reactions in the Polluted Troposphere

ozone concentration in the troposphere through the ozone cycle.

It is now well established that the OH radical has a primary role in the gas-phase oxidation of many olefins, aromatics, and non-methane hydrocarbons as well as various inorganic compounds in the polluted troposphere. It was suggested therefore that the relative reactivities of the OH radical with various potential pollutant molecules be used, at least to a first approximation, as a measure of their "reactivity scales" under atmospheric conditions.[76]

I.B. Experimental Techniques for the Study of the Reaction Kinetics of the OH Radical

There has been much interest in the study of the basic reaction kinetics of transient species such as atoms and radicals, especially in the mechanistic studies and measurements of the rates of their reactions. Such studies require controlled production as well as sensitive and selective detection techniques. Measurement of rate constants at various temperatures would provide vital information on the energetics of these reactions. Recent improvements in these techniques have made available more reliable kinetic information on the OH radical reactions. In the past fifteen years, most of the OH radical kinetic data at temperatures below 500 K have been provided by three techniques: the flash photolysis technique, the discharge flow technique, and the relative rate technique. The first two are called absolute techniques since they directly determine the rates of the elementary reactions of the OH radical. The last method, on the other hand, deduces the rates based on the prior knowledge of the rate of a standard reaction occuring simultaneously in the system. These three

methods are briefly described in sections I.B.1. and I.B.2..

I.B.1. Absolute Techniques

I.B.1.a. Detection Methods Used in Absolute Techniques

Table I.2 shows the principal methods of the direct detection of the OH radical and their typical working concentration ranges.[38] Resonance fluorescence (RF), laser magnetic resonance (LMR), laser absorption (LA), and laser induced fluorescence (LIF) techniques have the advantage of lower detection limits. At the low concentration levels of those techniques, the secondary reactions, such as the OH-OH combination reaction and the reaction of the OH radical with the product are avoided, resulting in a longer inherent chemical lifetime of the radical and a simpler reaction mechanism. RF and LIF methods can be used at total pressures up to approximately atmospheric pressure[77] and a few atmospheres[78] respectively, if the pressure quenching of the fluorescence is not significant. In addition, the RF equipment is simpler than the other methods, relatively inexpensive, and can be applied to the detection of other atomic species with minor modifications.[79-85]

I.B.1.b. The Flash Photolysis Technique

In flash photolysis, a precursor molecule is photolyzed with a flash of light of appropriate wavelength to cause breaking of a bond to produce the OH radical. The vacuum ultra-violet (v.u.v.) flash photolysis of water is one method of forming OH radicals:[86]

$$H_2O + h\nu \longrightarrow H + OH \qquad \lambda < 180 \text{ nm}$$

Table I.2

Principal Detection Methods of the OH Radical Used in Absolute Techniques and Their Working Concentration Ranges (from Reference 38)

	(molecule cm^{-3})
Mass Spectrometry	$\sim 10^{12} - 10^{13}$
Electron Paramagnetic Resonance	$\sim 10^{11} - 10^{13}$
Resonance Absorption	$\sim 10^{12} - 10^{14}$
Laser Absorption	$\sim 10^{7}$
Resonance Fluorescence	$\sim 10^{9} - 10^{12}$
Laser-Induced Fluorescence	
Laser Magnetic Resonance	$\sim 10^{9} - 10^{11}$

HNO_3[87] and H_2O_2[88,89] are also used as OH precursors. They require longer photolysis wavelengths which are more readily available, and u.v. lasers have been used as a flash source.[90] In earlier studies, the OH radical was also produced from the reaction of $O(^1D)$ with a hydrogen containing substrate (H-R):

$$O(^1D) + H\text{-}R \longrightarrow OH + R$$

$O(^1D)$ was created by flash photolysis of N_2O,[91] NO_2,[92] or O_3.[92] A typical substrate was H_2.[91-93] Water is, however, an almost ideal precursor because it is relatively inactive to the OH radical and thermally stable compared with other precursors.[37] The number of OH radicals produced can be controlled by the flash energy and the concentration of the precursor.

The advantage of the flash photolysis technique is that the pressure in the reaction system can be varied over a wide range, as long as the photolysis of the precursor is not disturbed. This enables one to study pressure effects on the reaction. The disadvantage is that the kinds of reactants which can be studied are limited to those which do not undergo significant photolysis by the flash.

Since first applied by Stuhl and Niki[86] in the kinetic study of the OH radical, the resonance fluorescence technique has been the most commonly used detection method with flash photolysis. The time resolved profile of the fluorescence intensity is monitored after the flash as the OH radical concentration in the reaction zone decays with time by reaction and diffusion. The experimental details of the flash photolysis-resonance fluorescence (FPRF) technique are described in CHAPTER II.

I.B.1.c. The Discharge Flow Technique

In a discharge flow system, the OH radical is created by an electric discharge in a stream of the precursor/diluent gas. The most common source of the OH radical is the one introduced by Del Greco and Kaufman.[94] A H_2/diluent gas stream is passed through a microwave cavity where hydrogen atoms ($H(^2S)$) are created by discharge. NO_2 is added to the stream immediately after, and the fast reaction

$$H + NO_2 \longrightarrow OH + NO$$

produces OH radicals in the stream. Although this reaction is exothermic by 117 kJ mol^{-1}, and it can produce vibrationally excited OH radicals (v=1, 2, 3),[95] they are effectively deactivated to v=0 before a reactant is added under typical experimental conditions.[96]

A reactant is then added downstream. The detector is situated further downstream with a known variable distance, x, from the reactant addition port, where it detects OH radicals which have not yet reacted. The reactant concentration is usually greatly in excess of that of the OH radical, and the observed OH radical concentration varies exponentially with x.[97,98]

The advantage of the flow method is that the reaction region is separated from the zone where OH radicals are produced. This enables one to study reactants which cannot be studied with the flash photolysis technique because they undergo substantial photolysis by the flash. Some of the disadvantages are: the wall reactions can be serious in some cases and it is necessary to coat the wall carefully with an appropriate reagent;[99] the

maximum total pressure of the reaction system is limited to < 10 torr[98], and as a result, the extrapolation of the pressure effect on some reactions to atmospheric pressure may not be accurate.

When the discharge flow technique is combined with either the RF, LIF, or LMR techniques, it makes the determination of the stoichiometric coefficient of the reaction unnecessary. This is because the secondary reaction of the OH radical with the reaction product becomes negligible at the lower working concentration range of those detection methods.[38]

I.B.2. Relative Rate Techniques

In the absolute methods, efforts are made to minimize, if not to avoid completely, any influence from reactions other than the reaction of interest. The relative rate methods, on the other hand, involve a sequence of reactions in which the rate of the reaction of interest is measured relative to that of a standard reaction. Two conditions are therefore required. First, the mechanism of the employed reaction system must be known. Second, the absolute rate of the reaction with a standard compound must be known with a reasonable accuracy.

In the relative rate method, a chemical system is selected in which a reactant R and a standard compound S are predominantly consumed by the reactions with the OH radical with rate constants of k_R and k_S respectively. (If not, one must know at least the correction factors to be made due to other reactions.)

$$OH + R \longrightarrow P_R \qquad k_R$$

$$OH + S \longrightarrow P_S \qquad k_S$$

where P_R and P_S are products of the respective reactions. The rate constant of interest, k_R, is related with that of the standard reaction, k_S, by the following equation:

$$k_R = k_S \ln \frac{[R]_t}{[R]_0} / \ln \frac{[S]_t}{[S]_0}$$

where $[R]_t/[R]_0$ and $[S]_t/[S]_0$ are the concentrations at time t relative to those at time t_0 for a reactant and a standard respectively. There is no need to know absolute concentrations of the reactant or the standard compound in the system. Only the relative values are necessary. From the slope of the $\ln [R]_t/[R]_0$ versus $\ln [S]_t/[S]_0$ plot and the knowledge of k_S, the absolute rate constant k_R can be calculated.

The reaction system is contained in either a quartz cell whose walls are treated with sulfuric acid to avoid the wall effect,[100,101] or a larger (60 - 6400 L) pyrex,[102-105] all teflon,[106-110] or teflon coated[111-113] chamber. Operating temperatures are limited to those near room temperature. Concentrations of the reactants and the standard compounds are continuously monitored by either GC,[100-104,106-110] FTIR,[105,113] or DOAS.[111,112] A chemical system must be carefully selected to minimize complication of the kinetic analysis. Some examples of the systems used are: u.v. irradiation of mixtures such as HONO/air,[105] NO_x/air,[102-104,109] HONO/NO/air,[106] and CH_3ONO/NO/air.[107,108,110-113] Some non-photolytic systems also have been used.[114-116] Organic reactants and a standard compound are added to these systems. In all of the above systems, the OH

radical predominantly consumes the organic compounds.

The relative rate techniques provide an alternative way to investigate those reactions which would be difficult to study with the absolute techniques because of problems in handling or wall absorption.[36] Another advantage of this technique is that several reactants can be studied simultaneously. Results from this technique generally agree well with those from the flash photolysis and the discharge flow techniques.

I.C. Scope of the Present Study

The goal of the present study was to investigate the kinetics of the OH radical reactions in the gas phase with two groups of organic compounds, namely cycloalkenes and aromatic compounds because of the intrinsic interest in their reactivities and mechanisms, and the relevance of the results of the basic kinetic studies to the chemistry of a polluted atmosphere. Results of previous kinetic and mechanistic studies of these reactions will not be introduced in this chapter, but will be described in the discussion sections of CHAPTERS IV and V, since they need to be examined closely in order to interpret the results of the present study.

An experimental apparatus was constructed to study the kinetics of elementary reactions of the OH radical in the gas phase with the flash photolysis-resonance fluorescence (FPRF) technique. This technique was chosen because of its versatility concerning operating temperature and pressure conditions. Since this was the first investigation in this laboratory using the FPRF technique, the equipment will be described in detail. The equipment constructed initially was modified extensively to maximize the signal to noise (S/N) ratio, and the final version will be

described in CHAPTER II.

The determination of the kinetic information from the observed fluorescence will be discussed in CHAPTER III, together with the results of confirmatory data on the reactions of the OH radical with molecular hydrogen (H_2), ethene (C_2H_4), and propene (C_3H_6) at room temperature.

The first group of reactants investigated were cycloalkenes. Rate constants of the OH radical reactions with cycloalkenes have been obtained only with the relative rate techniques at room temperature in the past.[100,101,104,108,119] No temperature dependence of the rate constants has been reported previously. The results of the study of five OH-cycloalkene reactions with the FPRF technique at various temperatures and pressures will be presented in CHAPTER IV. The significance of abstraction of allylic hydrogens by the OH radical relative to the addition of the OH radical will be discussed. Several interpretations of the temperature dependence of rate constants of the OH-alkene reactions will be also examined in order to estimate the factors which might determine the reactivity of the OH radical toward various alkenes. Some cycloalkenes have been detected in the ambient atmosphere,[117,118] and they are thought to be one of the sources of the bifunctional carbonyl compounds found in the aerosol of photochemical smogs.[117] The OH radical might be one of the first species to initiate the oxidation of cycloalkenes in the troposphere. The significance of the OH-cycloalkene reactions in the troposphere will be discussed based on the rate constants obtained at room temperature.

The second group of reactants investigated were aromatic molecules, and the results are reported in CHAPTER V. The OH radical reactions with aromatic compounds have been found to show unique temperature dependence

when studied with the FPRF technique.[120-123] When the present study was first begun, only qualitative explanations had been given for the observed temperature dependence of the rate constants.[120,121] There were discrepancies in some of the results of the studies of the OH-benzene reaction reported by various groups.[120-123] The present study attempted to gain further insight into the mechanism of the OH-benzene reaction at higher temperatures by analyzing the observed kinetics more quantitatively. A similar analysis was attempted for the OH-chlorobenzene reaction as well. Six more halogenated benzenes were studied at room temperature to examine the halogen substituent effects on the rate constants. Factors which might determine the relative reactivities of various OH-halogenated benzene reactions will be discussed. The implications of a number of different correlations will also be considered: the correlation between the rate constants of various OH-aromatic reactions and those of O-aromatic reactions, the Hammett equation of the OH-aromatic reactions, and the correlation between the rate constants of OH-aromatic reactions and the ionization potentials of the aromatic molecules.

Direct study of the OH-polychlorinated biphenyl (PCB) reactions with the FPRF technique was not possible. The OH-biphenyl reaction was investigated at room temperature, and the reactivity of polychlorinated benzenes relative to benzene was used to model the reactivity of polychlorinated biphenyls relative to biphenyl. Since the fate of PCB's in the troposphere has been of much interest in recent years, the significance of the OH radical reactions with PCB's in the troposphere will be considered.

CHAPTER II

EXPERIMENTAL

In this study, the flash photolysis-resonance fluorescence technique was employed to study the kinetics of the OH radical reactions. Several groups[86,87,124-133] have previously reported their apparatus and the experimental conditions. Although the apparatus used in this study is similar in many respects to those described in the literature, a great amount of work was required to modify the equipment and to adjust the conditions of the experiments to achieve as good a signal-to-noise (S/N) ratio as possible. In this chapter, the final version of the apparatus is described, together with some of the attempts made to improve its efficiency and the S/N ratio. The main features of the apparatus are a reaction cell, the flash lamp unit, the resonance lamp-detector unit, and the gas mixing system. The relative positions of the first three are illustrated in Figures II.1 and II.2. Each unit will be described in detail in the following sections.

II.A. The Reaction Cell

The reaction cell was replaced twice before the final version was decided. The first two cells were a large Pyrex cylindrical cell (~2000 cm^3) and a quartz cell (~300 cm^3) of a similar design to the final version. The final version was a Pyrex cell (~300 cm^3). This was chosen for three main reasons: it was a reasonable size and the gas consumption during the

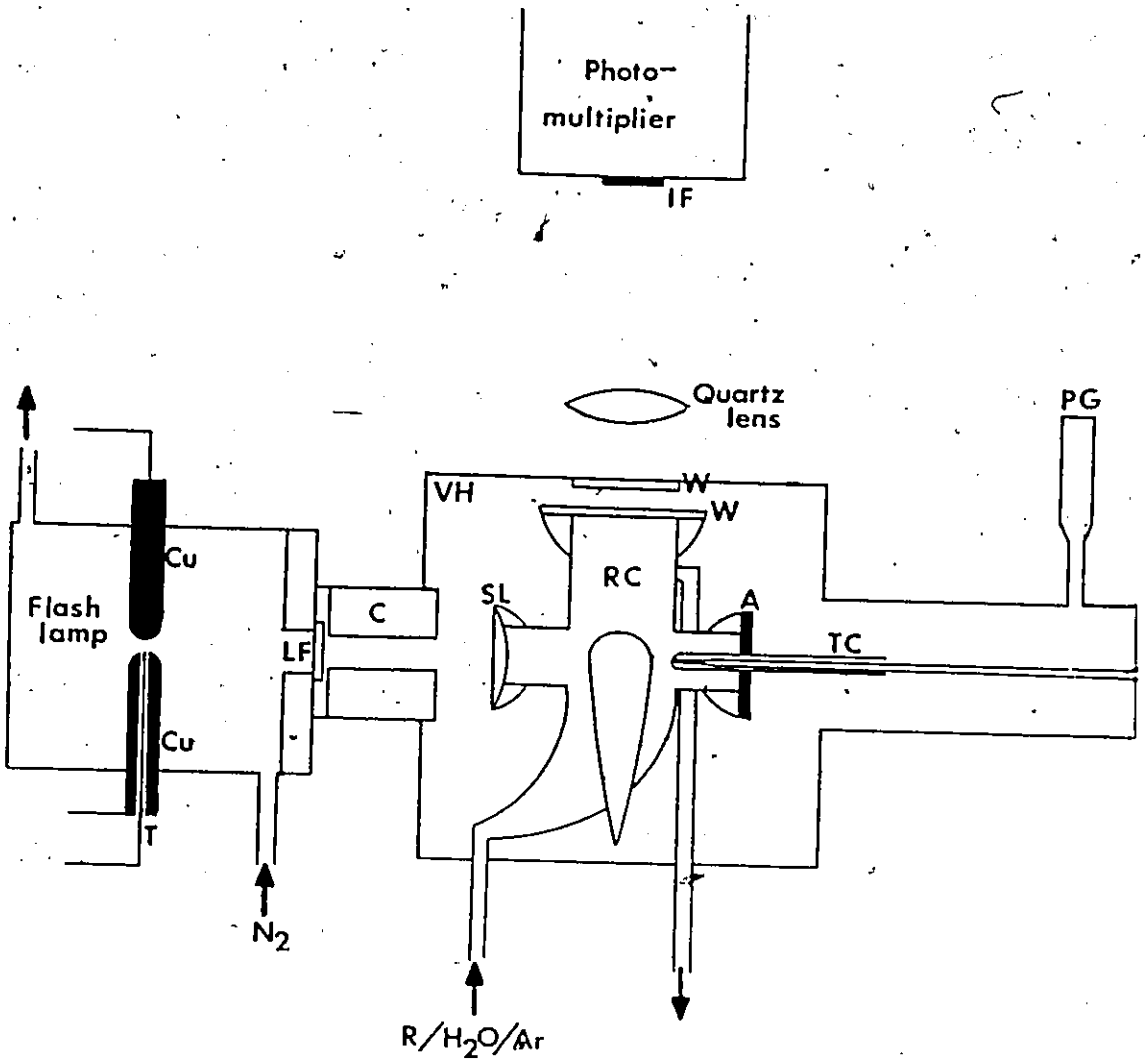

Figure II.1

A Cross Section of the Flash Photolysis-
Resonance Fluorescence Apparatus

VH : vacuum housing
W : quartz window
SL : Suprasil lens
TC : thermocouple
T : trigger pin
C : collimator
RC : reaction cell
IF : interference filter
PG : Pirani gauge
Cu : copper electrode
LF : LiF window
A : Aluminum plate

(Approximately 1/3 of the actual scale)

Figure II.2

Another Cross Section of the Flash Photolysis-Resonance Fluorescence Apparatus

CA : microwave discharge cavity
(For other symbols, see Figure II.1)

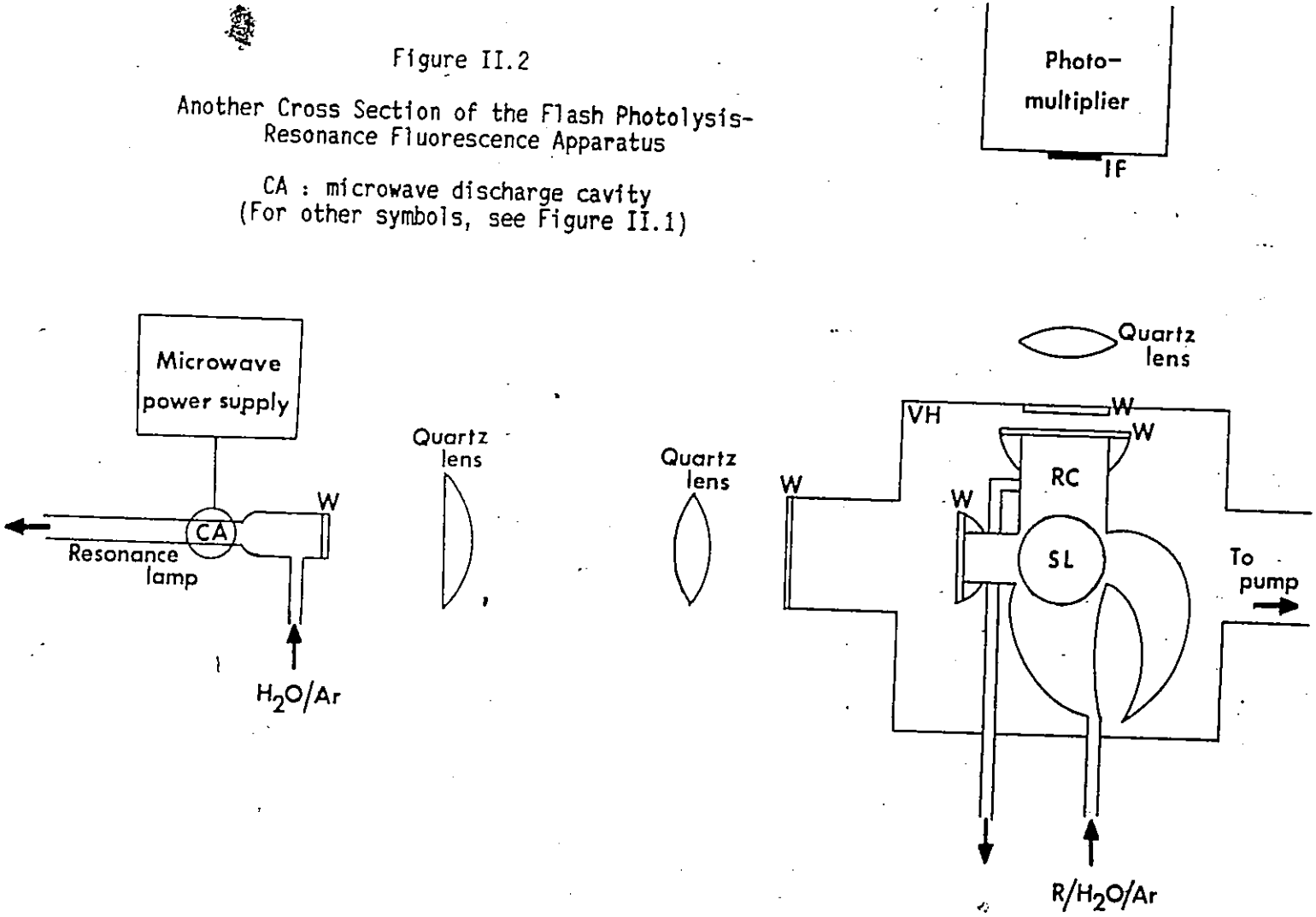

experiments was more economical than that for a larger cell; it was relatively easy to handle compared with a larger cell when fine optical adjustment had to be made; the scattered background light was significantly lower than the quartz cell. The cell was painted outside with black flat enamel paint, and wrapped with several layers of aluminum tape and then with a flexible electric heating tape (THERMOLYNE BriskHeat). It was covered with insulating glass wool, and placed in a stainless steel vacuum housing which served not only to provide a vacuum between the cell and the flash lamp but also to reduce the heat loss when the cell was heated to higher temperatures.

The cell had three ports at right angles to each other on which a Suprasil lens and two quartz windows were attached with Viton O-rings. A Suprasil lens (1.5" diameter and 5" focal length) faced a flash lamp which was mounted on one of the side ports of the vacuum housing. (Figure II.1) A quartz window (1.5" diameter) transmitted light from a resonance lamp and the light was focused onto a built-in Wood's horn opposite the window. (Figure II.2) Another quartz window (6 cm diameter) faced a detection unit mounted on the vacuum housing. The cell had an additional Wood's horn opposite this third port.

A glass-capsuled retractable copper-constantan thermocouple was inserted in the cell opposite the Suprasil lens. (Figure II.1) During experiments the cell temperature was monitored just outside the zone viewed by the detector, so that the detector was not affected by light scattered by the thermocouple. The cell could be heated by passing an electric current through the heating tape. The aluminum tape wrapped around the cell provided good heat conduction through the wall of the

irregular-shaped cell. An additional thermocouple was attached on the outside wall of the cell to monitor the wall temperature as the cell was heated up and cooled down. The variation of the temperature across the cell around and through the reaction zone was monitored at various temperatures between room temperature and 423 K. It was found that the maximum temperature variation within the reaction zone was 1 degree at 423 K. The maximum temperature attained in this cell was ~430 K.

The pre-mixed gas of water, reactant, and argon was passed through the cell continuously at a controlled pressure and flow rate. Section II.D of this chapter will describe the gas flow system of the present study.

II.B. Formation of the OH Radicals by Vacuum U.V. Flash Photolysis

The OH radical was produced by the vacuum u.v. flash photolysis of water vapour. The schematic diagram of the flash lamp and electrical circuit is illustrated in Figure II.3. The flash lamp was made of cylindrical acrylic plastic (4" i.d. and 4 1/2" long). One end of the cylinder was mounted on a side port of the vacuum housing (Figure II.1), and a lithium fluoride (LiF) plate (1" diameter) was used for the window.

Two 1/2"-diameter copper electrodes were inserted opposite to one another through the side wall with O-ring seals. Their tips were ground to spherical shape. It was found that these thick spherically shaped electrodes provided faster discharge time (the full-width at half maximum (fwhm) was ~ 2 μsec) than the pointed 1/8"-diameter tungsten electrodes used earlier. A tungsten trigger pin (1/16"-diameter) was coaxially inserted in one of the copper electrodes and insulated with teflon. This copper electrode was grounded. (Figure II.3)

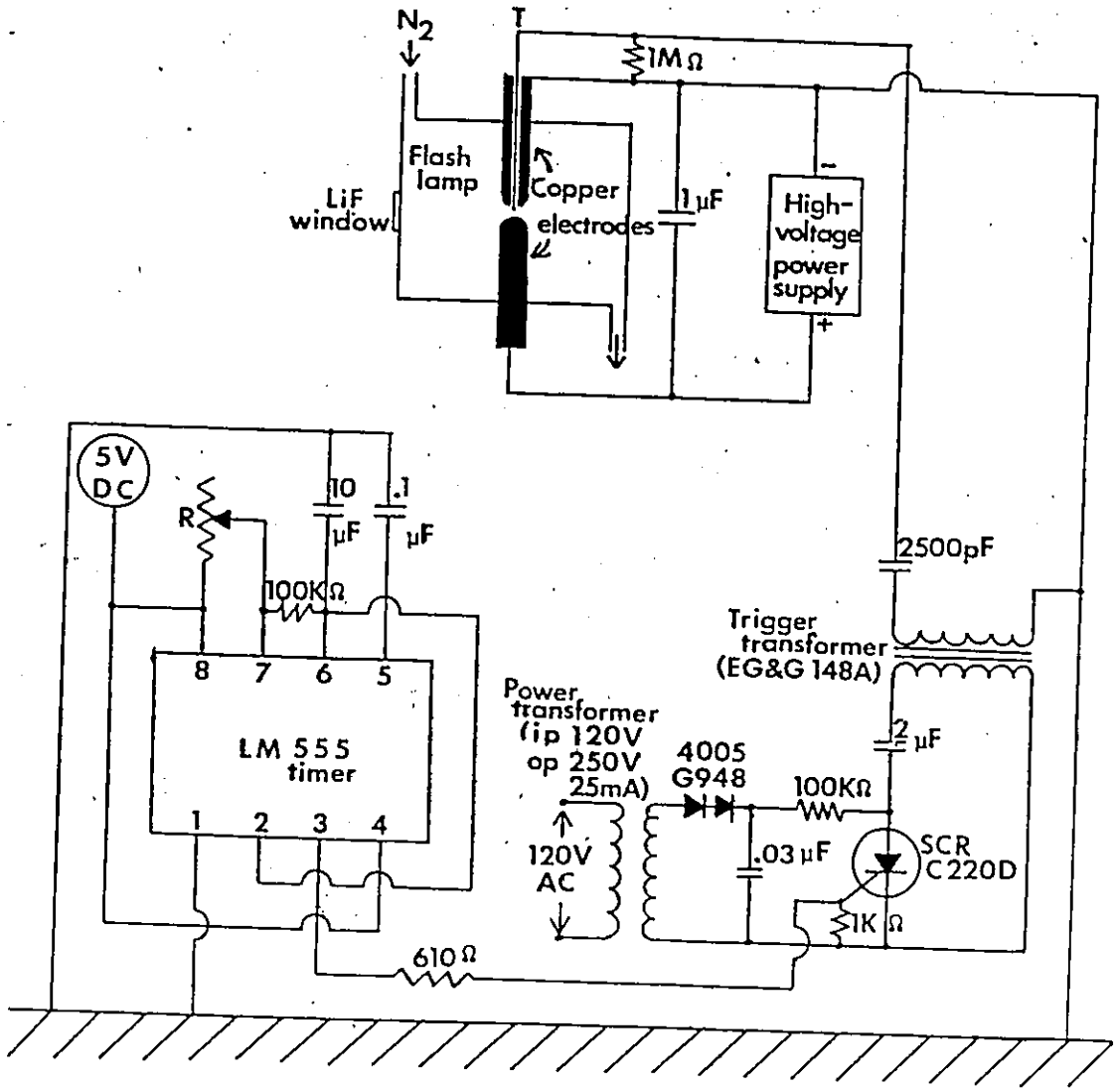

Figure II.3

Timing/Trigger/Flash Circuit

T : trigger pin
R : variable resistor to determine the time interval of flashes
5VDC : home-made 5 V DC power supply

The lamp was continuously purged with prepurified nitrogen at atmospheric pressure with a relatively high flow rate (> 3000 cm^3 min^{-1}). This high pressure and flow rate served to reduce sputtering of the electrodes on the window.

A 1 μF capacitor (Sprague Clorinol Capacitor 1-0-30000 VDC, S-3-427H) was connected to the copper electrodes. It was charged up to a high voltage (normally of 5 - 10 kV). A timing circuit (Figure II.3) generated repetitive pulses with the desired interval (normally of 2 - 3 sec.) which were fed into a flash-trigger circuit. The latter sent high voltage pulses (-12 kV) to the trigger pin inducing breakdowns of the potential between the copper electrodes. Each breakdown was followed by a recharge.

The trigger transformer and the flash unit were contained in a box shielded with copper and brass sheets to reduce the propagation of electromagnetic noise to other equipment. All signal and trigger circuit cables of the apparatus were also carefully shielded to minimize the disturbance from electrical noise.

The light pulse generated by the electrical breakdown of the flash lamp passed through the LiF window, and onto a Suprasil lens which made the light beam parallel. The Suprasil material transmits wavelengths longer than ~165 nm, and the dissociation of water molecules begins at wavelengths shorter than ~180 nm. The photolysis of a water molecule between 165 and 180 nm creates a hydrogen atom (H) and a OH radical both in their ground electronic states:[37,134]

$$H_2O + h\nu \longrightarrow H(^2S) + OH(X^2\Pi) \qquad 165 < \lambda < 180 \text{ nm}$$

The actinometric experiments with ethene[135,136] were conducted under the

same geometrical conditions as those of the actual experiments, and the computer aided simulation of the reaction system (see CHAPTER III.B) was also performed. The initial concentration of the OH radical after each flash was estimated to be less than 10^{11} molecule cm^{-3} in the center of the reaction cell under typical experimental conditions of the present study.

II.C. Detection of the OH Radicals by Resonance Fluorescence

The resonance lamp was made of quartz, and a quartz window was attached to it with an O-ring. Argon was bubbled through distilled water at room temperature and at atmospheric pressure. The water/argon (H_2O/Ar) mixture flowed through the lamp at a pressure of about 10 torr. (Figure II.4) A continuous light emission was caused by an electrodeless discharge through the mixture in a microwave type 5 cavity[137] (OPTHOS INSTRUMENT CO.) excited by a power supply (RAYTHEON, MICROTHERM Model CMD4, 2450 Mc). An additional 100 μF capacitor reduced ripples on the DC power which was applied to a magnetron of the microwave power supply. (Figure II.5) Various optical arrangements were tested on the resonance lamp output to obtain better S/N ratios. The final version was a compromise between a higher intensity light beam of the resonance lamp and a higher background scattered light. The first quartz lens (2-1/2" diameter and 6" focal length) collected the light from the lamp and made it almost parallel, then the second quartz lens (2" diameter and 12" focal length) focused the light beam onto the Wood's horn opposite a quartz window. (Figure II.2)

The major emission band of this lamp was due to the $OH(A^2\Sigma^+ \longrightarrow X^2\Pi)$ transition at ~308 nm.[86] The light beam intersected the flash light

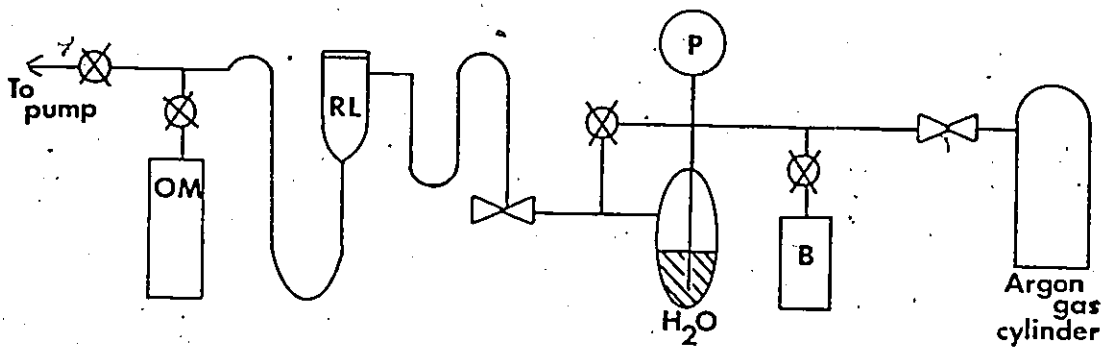

Figure II.4

Schematic Diagram of the Gas Flow System
for the Resonance Lamp

OM : oil manometer
RL : resonance lamp
⋈ : metering valve
P : Bourdon pressure gauge
B : bubbler
⊠ : Teflon stopcock

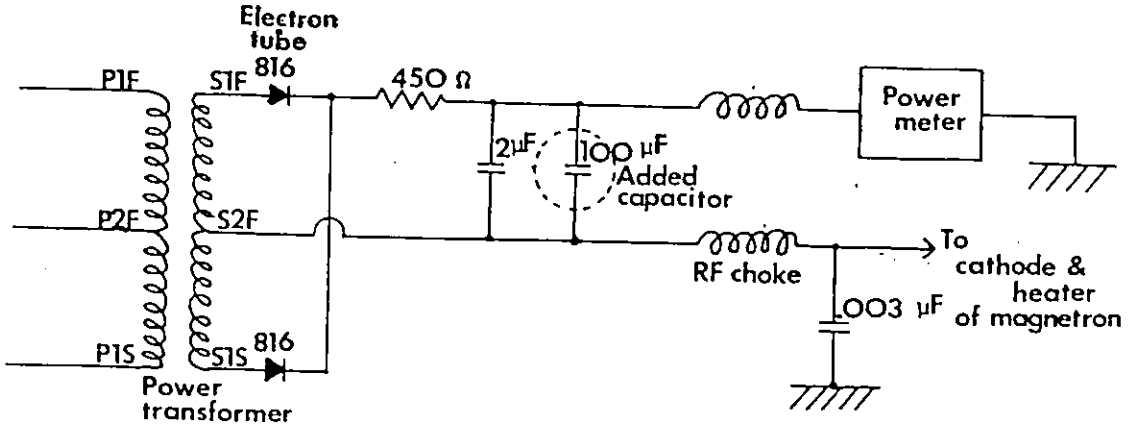

Figure II.5

DC Power Supply Circuit of the Microwave Power Supply
(REYTHEON MICROTHERM MODEL CMD4 2450 Mc)
and an Added Capacitor

beam in the center of the reaction cell creating an effective reaction zone of 2-3 cm^3. This reaction zone was away from the cell wall, and the effect of wall reactions was minimized. Some of the ground-state OH radicals ($X^2\Pi$) in the reaction zone absorbed the resonance light, and subsequently emitted fluorescence isotropically.

A portion of the fluorescence was observed by a photomultiplier (AMPEREX 56DUVP) through an interference filter (CORION, center wavelength 308.3 nm, fwhm 2.6 nm, maximum transmittance 14%). The light scattered by the cell walls and by Rayleigh scattering by the gas molecules in the cell was also observed by the detector as a background. The background signal consists mainly of the scattered light of the resonance lamp light since it has the same wavelength as the fluorescence light, and minor contributions from the background noise of the photomultiplier and the scattered light from the flash. Since the observed fluorescence is weak, improvement of the S/N ratio was crucial. Various optical arrangements were tested to collect the fluorescence light with different lenses and filters. In the final version, a quartz lens (2" diameter and 2" focal length) was placed in such a way that the center of the reaction cell (~2 cm diameter) formed a diminished image on the interference filter (1/2" x 1/2").

To improve the S/N ratio further, the single photon counting technique was employed. The pulse output was taken from the photomultiplier and processed as illustrated in Figure II.6. The signal was first fed into an amplifier/discriminator circuit (ORTEC 9301, 454, and 436), and the resultant output was collected in a minicomputer (NICOLET INSTRUMENT CORP. NIC-1180 Data Processor) which was run in the multi-channel scaling mode.

The minicomputer was triggered by a pulse from a photodiode which

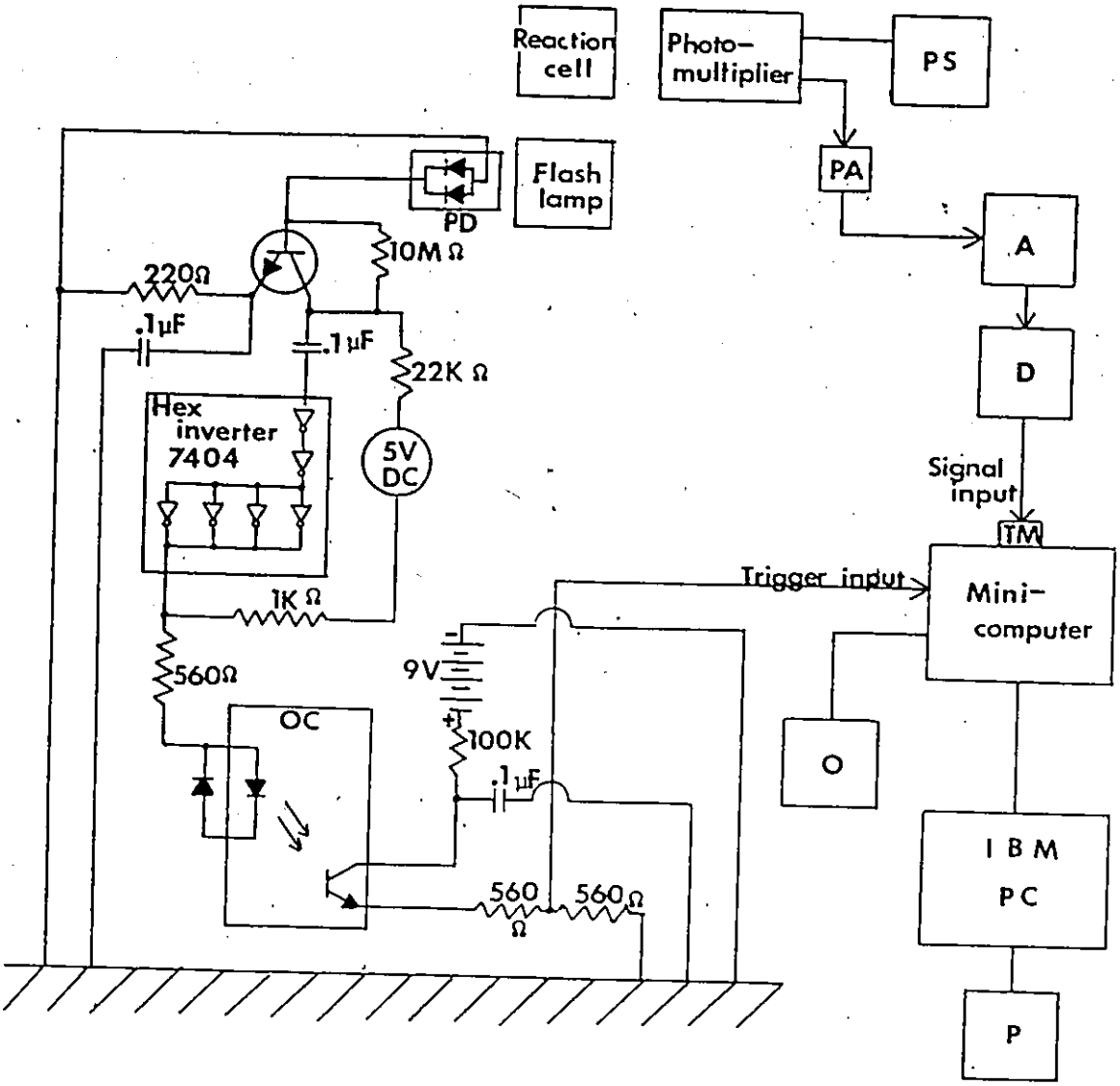

Figure II.6

Trigger/Detection System

PA : ORTEC Fast Preamplifier 9301
A : ORTEC Timing Filter Amplifier 454
D : ORTEC 100 MHz Discriminator 436
O : Oscilloscope (NICOLET INSTRUMENT CORP. 5110)
OC : Optocoupler

PS : high votage power supply
PD : photodiode (EG&G SGD-100A)
TM : 75 terminator
P : MANNESMAN TALLY Printer (MT 160)

viewed the flash. An optocoupler was placed between a photodiode circuit and the minicomputer to eliminate any large electrical spike at the computer trigger input. (Figure II.6) Since the optocoupler has a slow response time, there was a 25 μsec. dead time between the flash and the pulse sent to the trigger input of the minicomputer. Any additional delay time could be controlled on the minicomputer. Figure II.7 illustrates a timing diagram of a typical experimental run when 1 msec of delay time was added on the minicomputer.

The data were obtained as the number of photons observed during a fixed dwell time (normally 0.05 - 6 msec) in a channel as a function of time after the flash. In order to improve the S/N ratio, fluorescence profiles were accumulated in the minicomputer by repetitive flashes. In the photon counting technique, the S/N ratio is defined as

$$S/N = \frac{\text{signal counts above the background}}{\text{the square root of the background counts}}$$

An initial S/N ratio of at least 40 was attained. This provided at least four halflives of the fluorescence decay data which were above the average background count by more than twice its square root. Accumulated data could be seen on the oscilloscope connected to the computer. The collected data were then transfered to an IBM PC in which all numerical analyses were performed.

Photons observed above the background after the flash were assigned to the OH radical for the following four reasons:

a. Those photons were detected after passing through a very narrow-band interference filter whose maximum transmittance was at the wave-

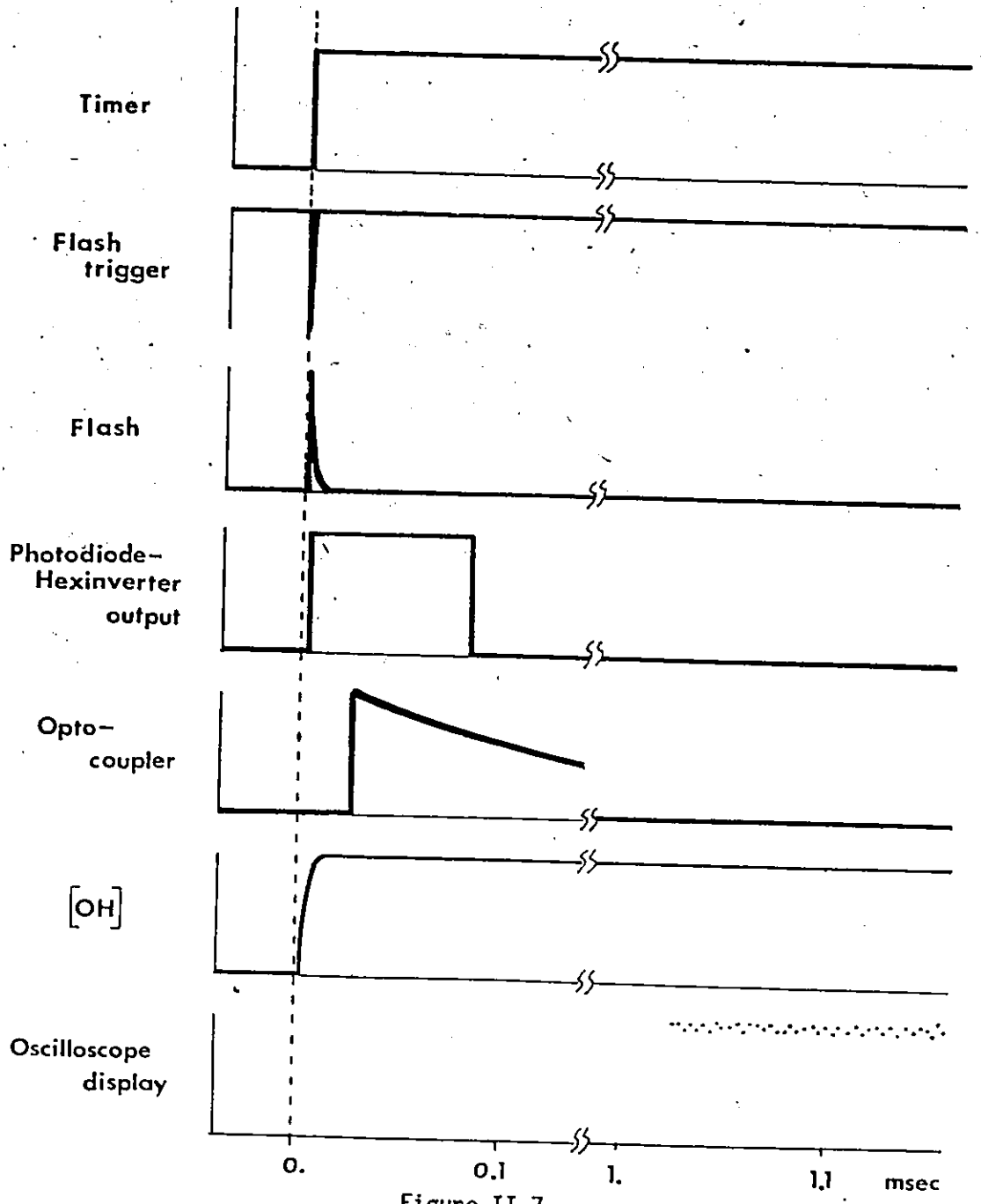

Figure II.7

A Timing Diagram of a Typical Experimental Run with 1 msec Delay on the Minicomputer

(Vertical axes are arbitrary unit of voltage or intensity)

length region of fluorescence of the OH radical.

b. When air was introduced into the vacuum housing, no photons were observed above the background. This is because the air blocked vacuum u.v. light from entering into the reaction cell, and the OH radical was not created.

c. When the resonance lamp was blocked off, no photons above the background were observed after the flash. This supports the conclusion that the observed photons were those of fluorescence.

d. The initial intensity of decay curves of the observed photons was proportional to the flash energy, and also depended on the concentration of water in the reaction cell.

One can be confident that the observed photons above the background were due to the fluorescence of the OH radical in the reaction cell.

An attempt was made to use the timing circuit described in section II.B. to trigger both the minicomputer and flash so that the background noise might be collected before the flash was fired. Although many efforts were made, the electromagnetic noise from the flash circuit made it impossible to operate such a timing-trigger circuit consistently. The background was therefore collected a long time after the flash (usually ~1 sec.) where the the fluorescence would be negligible.

A gating circuit for another photomultiplier (EMI 6256S) was also devised so that the photocathode would be inactive during the flash. This could have protected the photocathode from the intense scattered light of the flash. This attempt was unsuccessful for two reasons. The first was that electromagnetic disturbance from the flash initiated the trigger pulse to the gating circuit earlier than desired. The second was a limitation of

the design of the dynodes of the photomultiplier. A circuit was devised to raise the potential of the first dynode to that of the photocathode to inactivate the latter during the flash. The overall potential was not changed. This, however, caused a higher inter-dynode potential between the first and second dynodes resulting in higher dark noise. The limited time available did not allow the pursuit of further modifications. Instead, efforts were geared towards adjustment of the optics to reduce the unwanted scattered light as much as possible without losing too much of the fluorescence intensity.

II.D. Preparation of the Reaction Gas Mixture

Figure II.8 shows the schematic diagram of the gas flow system. Small amounts of the H_2O/Ar mixture and the reactant/argon (R/Ar) mixture were added to a stream of diluent argon gas. The amounts of each mixture added to the stream were calculated from the flow rates. All flow rates were measured with calibrated capillary flowmeters.

The H_2O/Ar mixture was made by bubbling argon through distilled water at room temperature and at atmospheric pressure.

Two methods were used to make R/Ar mixtures. When the reactant was gaseous (test reactants) or a relatively volatile liquid (cycloalkenes, benzene, fluorobenzenes) at room temperature, a R/Ar mixture of a known ratio was made in a 12-l bulb using an electronic manometer (DATAMETRICS Type 1023).(Figure II.9(a)) It was left to mix for two to three hours before use. When the reactant was a cycloalkene, a circulating pump was connected to the bulb for more efficient mixing. A portion of the mixture was taken into the main argon stream while the pressure in the bulb and the

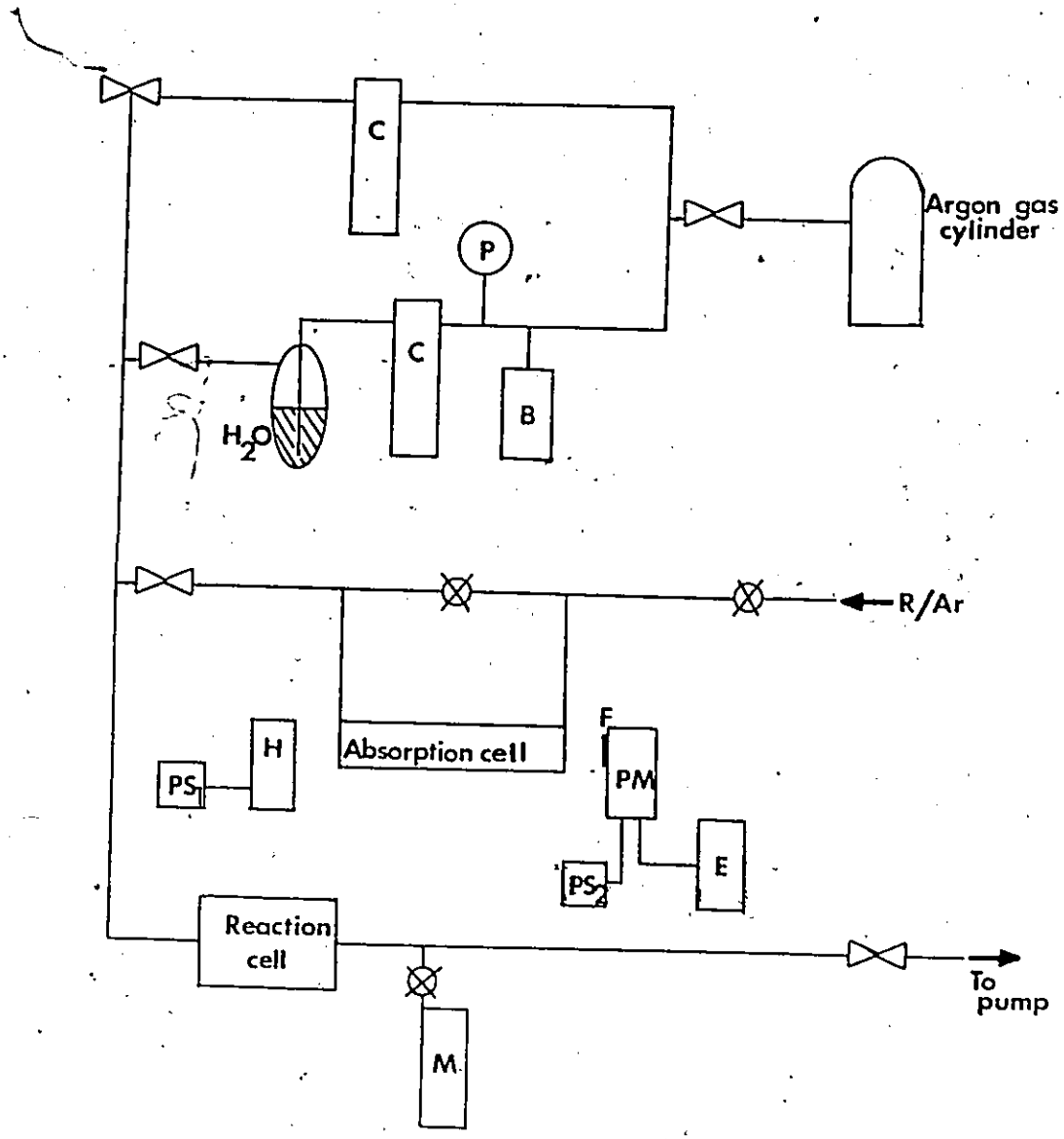

Figure II.8

A Schematic Diagram of the Gas Flow System

C : capillary flowmeter
B : bubbler
PM : photomultiplier (RCA 1P28)
E : electrometer (Keithley Instrument 610B)
PS : power supply
F : Mercury fine filter
P : Bourdon pressure gauge
H : low-pressure mercury lamp
M : mercury manometer
R/Ar : reactant/argon mixture from Figure II.7
⋈ : metering valve
⊗ : Teflon stopcock

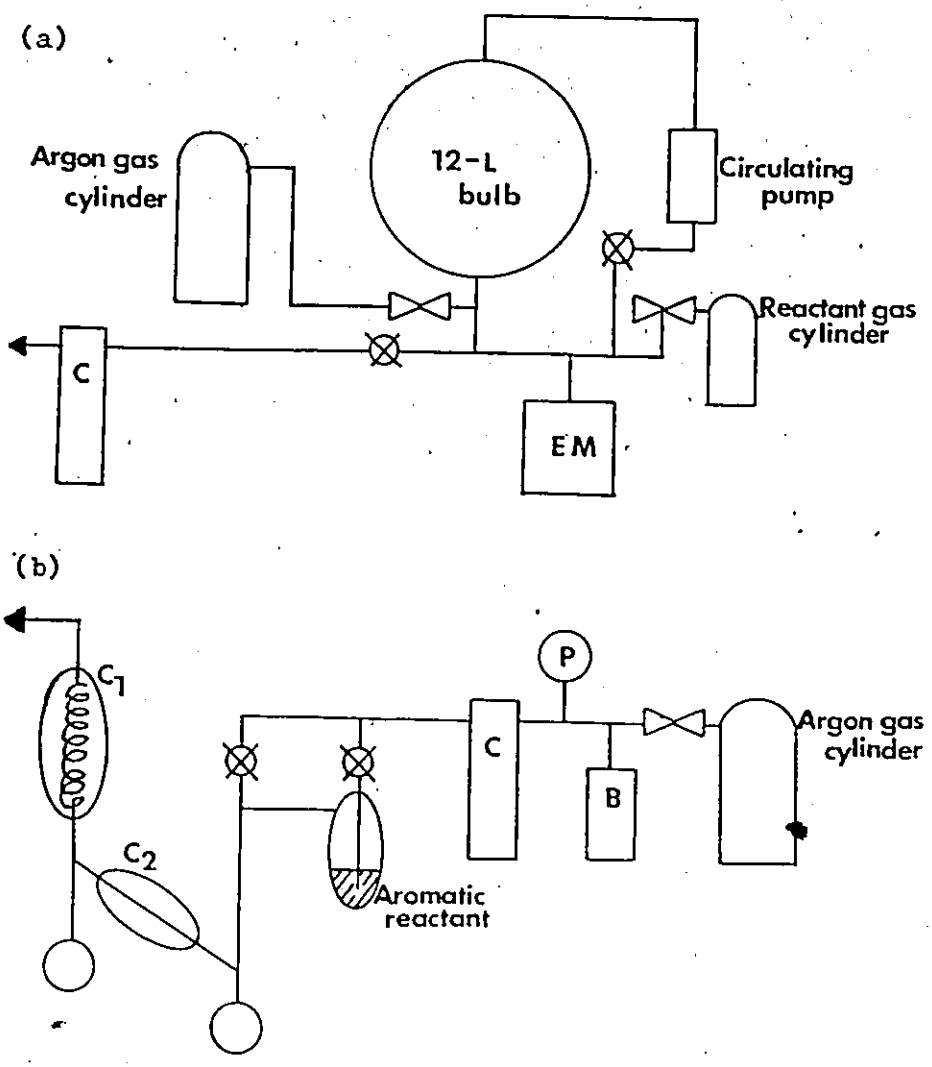

Figure II.9

Two Ways to Introduce a Reactant/Argon Mixture

EM : electronic manometer
C_1, C_2 : condensers
(For other symbols, see Figure II.8.)

flow rate of the mixture through a metering valve were continuously monitored with the electronic manometer and a capillary flowmeter respectively. When the reactant was an aromatic liquid of low volatility, argon was bubbled through a mixing cell which contained the reactant at atmospheric pressure and at room temperature. (Figure II.9(b)) The mixture was then passed through two condensers at a constant temperature lower than that of the cell to make a consistent mixture with the desired mixing ratio. The vapour pressures of the reactant at the condenser temperature were calculated from the equations given in the literature.[138]

In the case of aromatic reactants, the R/Ar mixture was passed through an absorption cell, either 6.5 or 50 cm long, to check the mixing ratio before it was added to the main stream. (Figure II.8) Two quartz windows were sealed on the ends of the cell. Absorption at 253.7 nm from a low-pressure mercury lamp (RAYMASTER Spectral Omnirange Lamp) was monitored. The wavelength was selected by a mercury line filter (CORION SM-2537-2). The transmitted light was detected by a photomultiplier (RCA 1P28) and measured on an electrometer (KEITHLEY INSTRUMENT 610B). Absorption was calibrated with known pressures of aromatics in the cell.

When a reactant was a solid (1,3,5-trichlorobenzene or biphenyl), the first mixing method could not be used because of an extremely low vapour pressure of the solid. With the second method, solid deposited on walls of the condensers causing inconsistent mixing ratio. After testing various combinations of temperatures of the mixing cell and of the condensers, it was found best to immerse the mixing cell in a constant temperature bath of the same temperature as the condensers, which was slightly below the room temperature (~290 K). From observed u.v. absorption of the mix-

ture, this method provided a constant mixing ratio over various flow rates of argon through the mixing cell and over a long period of time. The vapour pressure equations for 1,3,5-trichlorobenzene[139] and biphenyl[140] were used to calculate their vapour pressure at the temperature of the condensers. They were also roughly checked by taking a sample from the absorption cell with a gas-tight syringe and analyzing it with GC using naphthalene as a standard. The vapour pressure obtained from the gas analysis agreed with that calculated from the equation within 15%.

The reaction mixture containing water and the reactant in argon gas was passed through the reaction cell. The total pressure of the mixture was measured with a mercury manometer. The flow rate of the mixture (typically 50 - 70 cm^3 sec^{-1}) was always sufficiently fast that each flash photolyzed a fresh mixture. As the flow rate of the R/Ar mixture was varied in order to provide various reactant concentrations in the reaction cell, the flow rate of the main argon stream was adjusted in such a way that the total pressure as well as the total flow rate of the gas through the reaction cell was maintained constant. When the flow rate of the R/Ar mixture was changed, enough time was allowed for the reactant concentration in the cell to stabilize.

The purities of gases and reactants used in this study are listed in APPENDIX A. For argon gas of different purities, no difference was observed in the OH radical kinetics with either prepurified or ultra-high-purity gas.

CHAPTER III

KINETIC INFORMATION OBTAINED FROM THE FLASH PHOTOLYSIS RESONANCE FLUORESCENCE TECHNIQUE

III.A. Intensity of the Fluorescence and the Concentration of the OH Radical

In resonance fluorescence experiments, the intensity of the fluorescence is proportional to the concentration of the electronic ground-state OH radicals in the reaction zone if two conditions are met.[141] First the OH radical concentration must be low enough that the absorption of the excitation light in the zone is linearly proportional to the concentration. From Beer's law,

$$\ln \frac{I_0}{I_0 - I_a} = \sigma \, l \, N$$

where I_0 is the intensity of the incident excitation light, I_a is the intensity of the absorbed light, σ is the absorption cross section, l is the path length, and N is the number concentration of molecules in the lower electronic state (the ground state in this case). If $I_a \ll I_0$, this equation can be approximated to

$$\frac{I_a}{I_0} = \sigma \, l \, N$$

The intensity of the fluorescence I_F is proportional to I_a,

$$I_F = \Phi_F I_a$$

where Φ_F is the quantum efficiency of fluorescence. Under the above condition of absorption,

$$I_F = \Phi_F \sigma l N I_0$$

This implies that the intensity of fluorescence would be directly proportional to the concentration of the ground-state OH radical if the intensity of the incident light is kept constant. Under the experimental conditions, $N \approx 10^{11}$ molecule cm^{-3} and $l = 1.5$ cm (the depth of the reaction zone). With $\sigma = 5.3 \times 10^{-17}$ cm^2 molecule,[142] I_a/I_0 was estimated to be $\approx 8 \times 10^{-6}$. Therefore; the first condition was met in the present study.

The second condition is that the line shape of the resonance source should be "as close to nonreversed as is practical."[141] If the excitation source is reversed and weak in its intensity at the desired wavelength of excitation, non-linear absorption might be seen even at low concentrations. High-resolution emission spectra of resonance lamps of this type have been reported by some groups,[86,92,143] and no reversal has been observed. The intensity of the observed fluorescence in the present study was directly proportional to the flash energy and water concentration within the range of the experimental conditions. The decay curves followed simple exponential behavior over four to five halflives as long as the reaction mechanism involved was a simple first-order reaction. This again supports the assumption that the fluorescence was within the linear range in all the experiments.

The observed intensity of fluorescence, therefore, was proportional

to the concentration of the OH radical in the reaction zone under the experimental conditions of the present study.

III.B. Decay Rates of the Concentration of the OH Radical and the Rate Constants of Reactions

Once the OH radicals are formed in the reaction zone by flash photolysis, they might undergo the following sequence of reactions in the absence of a reactant:

$H_2O + h\nu \longrightarrow H + OH$	1
$OH \longrightarrow$ lost by diffusion	2
$OH + OH \longrightarrow H_2O + O$	3
$OH + OH + M \longrightarrow H_2O_2 + M$	4
$OH + O \longrightarrow O_2 + H$	5
$OH + H + M \longrightarrow H_2O + M$	6
$H_2O_2 + OH \longrightarrow HO_2 + H_2O$	7
$H_2O_2 + H \longrightarrow H_2O + OH$	8
$H_2O_2 + H \longrightarrow H_2 + HO_2$	9
$OH + HO_2 \longrightarrow H_2O + O_2$	10
$H + HO_2 \longrightarrow 2OH$	11
$H + HO_2 \longrightarrow H_2 + O_2$	12
$O + HO_2 \longrightarrow OH + O_2$	13
$2HO_2 \longrightarrow H_2O_2 + O_2$	14
$HO_2 + H_2O \longrightarrow OH + H_2O_2$	15

where M is a diluent gas molecule. Assuming first-order rates for the loss

of all species by diffusion, and using available rate constants of all other reactions 3 - 15,[144] simulations of the reaction system were performed for various initial conditions at room temperature by numerically solving the rate equations with computer.(APPENDIX B.1) Results indicated that the reactions 3 - 15 had a negligible influence on the OH radical decay when the initial concentration is less than 5×10^{11} molecule cm^{-3}, and that the loss by diffusion (the reaction 2) was the predominant path in the absence of a reactant. Under such conditions, the rate equation of the OH radical is effectively

$$-\frac{d[OH]}{dt} = k_2[OH]$$

When a reactant R is added, the reaction

$$OH + R \longrightarrow P \qquad 16$$

is added where P is its product. The rate equation of the OH radical concentration becomes

$$-\frac{d[OH]}{dt} = k_{16}[R][OH] + k_2[OH] \qquad (i)$$

Since all experiments were performed under the condition of $[OH] \ll [R]$, the decays of the OH radical concentration were expected to appear first-order (exponential) with a rate constant k_{obs},

$$-\frac{d[OH]}{dt} = k_{obs}[OH] \qquad (ii)$$

where

$$k_{obs} = k_{16}[R] + k_2 \qquad (iii).$$

Figure III.1(a) shows an example of such a first-order decay of fluorescence intensity observed in one of the experiments. The average background had to be subtracted from the observed decay curve, and the resultant curve was plotted on a semi-log scale. (Figure III.1(b)) The slope of this plot is $-k_{obs}$ which was computed with the linear least square method with a proper weight on each logarithmic value. (APPENDIX C.1) Randomness of weighted residuals (Figure III.1(c)) was checked by plotting an autocorrelation function (Figure III.1(d)). (See also APPENDIX C.2) Decay curves were observed at various reactant concentrations [R]. (APPENDIX C.3) When the linear relationship between k_{obs} and [R] was observed as expected from the equation (iii), its slope was computed with the least squares cubic method which takes into account random errors in both k_{obs} and [R]. The slope was the second-order rate constant k_{16}. (APPENDIX C.4)

III.C. The Possibility of Secondary Reactions

In the presence of a reactant, one might expect the following reactions in addition to the reaction (16):

$$R + h\nu \longrightarrow A \qquad 17$$

$$OH + A \longrightarrow \qquad 18$$

$$OH + P \longrightarrow \qquad 19$$

where the reaction 17 is the photolysis of a reactant by the flash, and A is its product. The reactions 18 and 19 are potential secondary reactions in the presence of a reactant. If they contribute significantly to the decay of the OH radical concentration, the rate equation (i) becomes

$$-\frac{d[OH]}{dt} = k_{16}[OH][R] + k_2[OH] + k_{18}[OH][A] + k_{19}[OH][P] \qquad (iv)$$

Figure III.1

Results of a Typical Experiment and Processing of the Data

(OH + Cyclohexene Reaction at 295 K, P_{tot} = 50 torr,
[Cyclohexene] = 7.65×10^{12} molecule cm^{-3})

(a) An Example of an Observed Decay Curve
(Dwell time = 100 μsec, 400 flashes)

(b) A Decay Curve (a) Plotted in a Log-Linear Scale After Background Subtraction and a Fitted Curve

(c) Weighted Residuals of a Fitted Curve

(d) An Autocorrelation Function

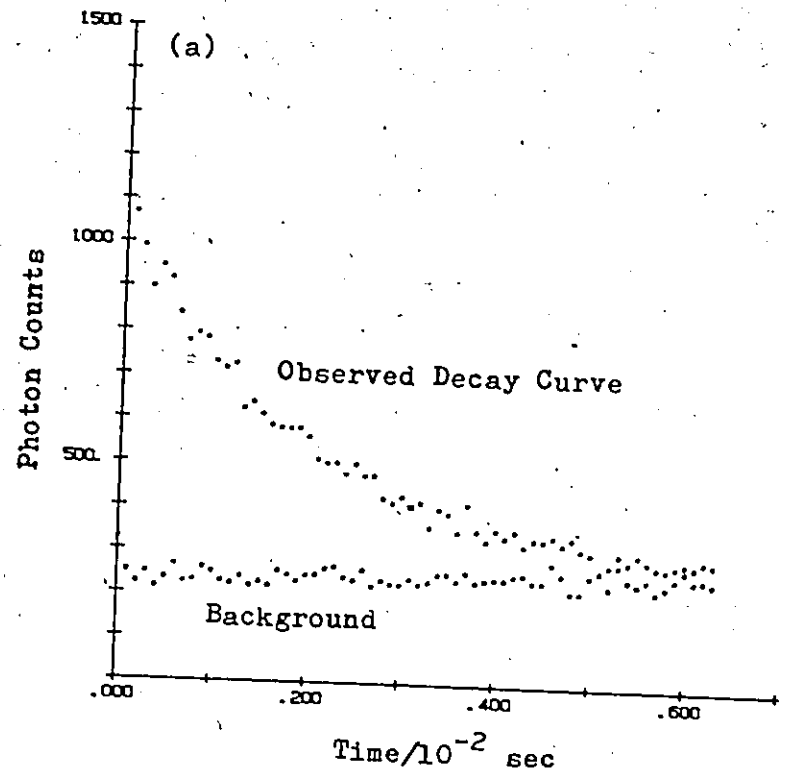
(a)
1500
1000
500
Photon Counts
Observed Decay Curve
Background
.000
.200
.400
.600
Time/10^{-2} sec

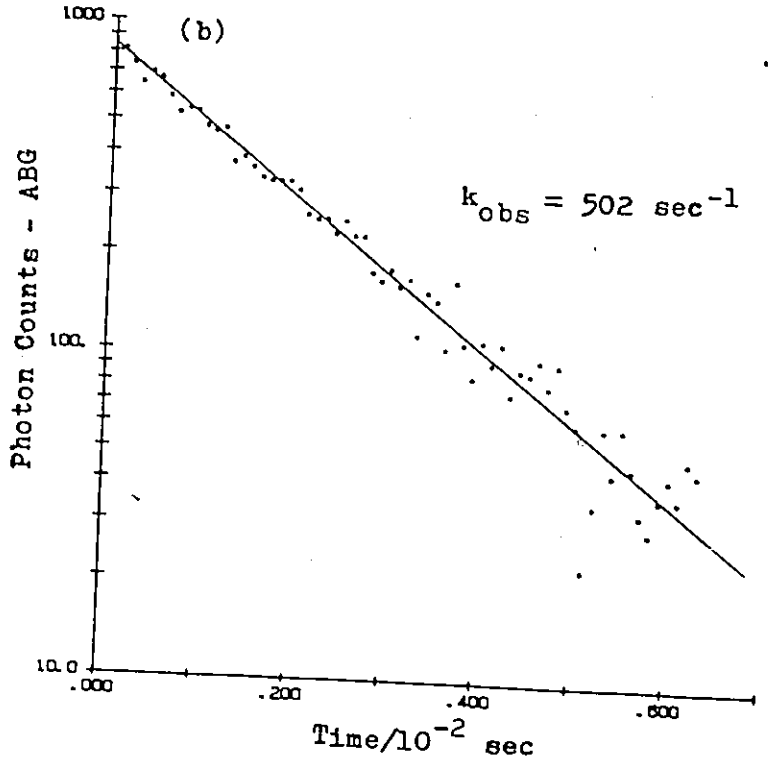
(b)
1000
100
10.0
Photon Counts - ABG
k_{obs} = 502 sec^{-1}
.000
.200
.400
.600
Time/10^{-2} sec

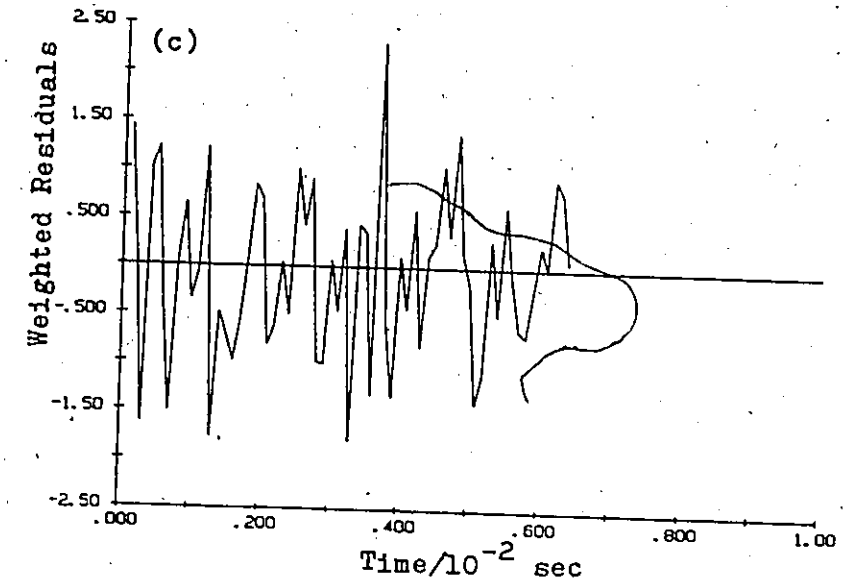
(c)
Weighted Residuals
2.50
1.50
.500
-.500
-1.50
-2.50
.000
.200
.400
.600
.800
1.00
Time/10^-2 sec

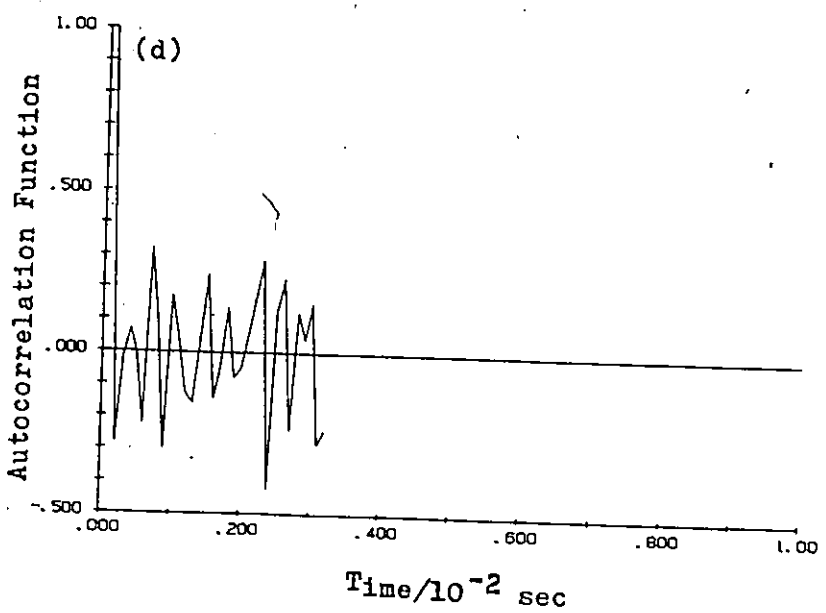
(d)
Autocorrelation Function
1.00
.500
.000
-.500
.000
.200
.400
.600
.800
1.00
Time/10^-2 sec

The initial concentration of A (i.e. $[A]_0$) will be proportional to the intensity of the incident flash light at a constant concentration since

$$[A]_0 = \xi_{R\rightarrow A}\, \sigma_R\, I_0\, [R]$$

where $\xi_{R\rightarrow A}$ is the quantum efficiency of photolysis of R to produce A, and σ_R is the absorption cross section of R. If reaction 18 is significant, a change in the flash energy should directly cause a change in the observed decay rate of the OH radical concentration. Using H_2, an alkene, or a cycloalkene as a reactant, no effect of the flash energy was observed in the decay rates when the flash energy was varied by a factor of two. The decay rates measured in most OH-aromatic reactions in the present study showed a slight dependence on flash energy but only within two least-square standard deviations of k_{obs}. The only exception was the OH-benzene reaction, which will be discussed in CHAPTER V.A.1. Computer simulations of a reaction system involving reactions 16 and 18 were performed in a similar manner to that described in the previous section. (APPENDIX B.2) They showed that the determination of the rate constant k_{16} would not be affected by the reaction with the photolysis product beyond the overall accuracy of the technique employed if $[A]_0 \leq [OH]_0$.

If the reaction 16 is much faster than the diffusion loss 2 and the diffusion loss of a photolytic product P, then

$$[P] \approx [OH]_0 - [OH]$$

If reaction 19 is significant, one might expect to observe the increasing deviation from exponentiality with time as the product P is accumulated.

The deviation would be enhanced by higher flash energy. No such deviation was observed in the experiments. Computer simulations of a reaction system involving reactions 16 and 19 showed that under extreme conditions (see Appendix B.2), the deviation with increased rate becomes noticeable at longer time (the second and the third halflives) where the concentration of the OH radical is lower. This deviation, however, may not be detectable under the present experimental conditions, and would not contribute significantly in the determination of k_{obs}.

Reactions with impurities in the diluent argon gas were another possible effect on the observed kinetics of the OH radical. In the absence of a reactant, the rate of the OH radical decay was approximately inversely proportional to the total pressure of argon diluent gas over the range of 50 and 200 torr. This indicates that the reactions with impurities in argon were negligible compared with the loss by diffusion. Prepurified and ultra-high-purity argon gases did not show any difference in the kinetics of the OH radical reactions.

Impurities in cycloalkenes and aromatics were analyzed and listed in Table A of the APPENDIX A. Levels of poly-enes in monoalkenes were very low, and it was estimated that the rate constant of monoalkenes would be affected by poly-enes by < 0.7 % when rate constants of poly-enes are taken into considerations. Impurities in aromatics are aromatics with similar rate constants. With the observed impurity levels, the rate constants of the aromatics of the present study should not be affected by more than 1%, except for m-dichlorobenzene (2.5%).

III.D. The Effect of Diffusion on the Decay Curves of the Concentration of the OH Radical

In the past, first-order kinetics have always been assumed for the loss of the OH radical by diffusion from the reaction zone in flash photolysis-resonance fluorescence experiments. The first-order approximation is applicable when dealing with loss of active species by diffusion in a bulk reaction system, such as H_2-O_2 reaction in a vessel.[145] In the flash photolysis-resonance fluorescence technique, one observes the concentration of the OH radicals in a small volume in the center of a reaction cell which is defined by the intersection of the light beams of the flash and the resonance lamps. The observed pattern of decay by diffusion is quite different from that of a bulk system, and there is no reason to presume that the loss of the OH radicals is first-order under the present experimental conditions.

Non-exponential (i.e. non-first-order) decays of the OH radical concentration were observed in the absence of a reactant (Figure III.2). The decay rate was initially faster and slowed down later as compared with an exponential decay. To ensure that this non-exponentiality was not due to effects other than diffusion, decays in the absence of a reactant were studied under various experimental conditions. Similar non-exponentiality was observed as the concentration of the radical was varied over the factor of 30 or more. This was done by varying the flash energy, the concentration of water in the reaction cell, and the density of a screen in front of the flash lamp. There was no significant change in decay rates and the features of decay curves as long as the total pressure and the total flow rate were kept constant. The intensity of the resonance lamp also had no

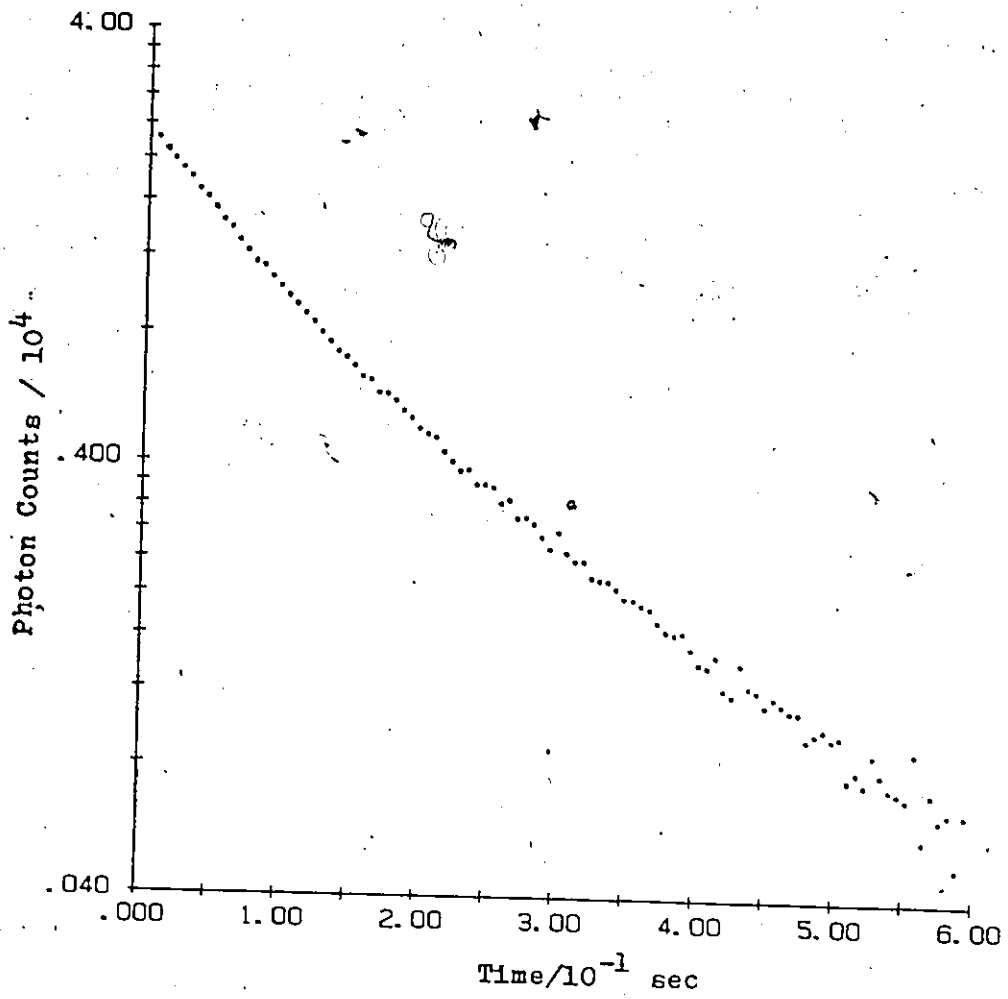

Figure III.2

A Typical Decay Curve Observed in the Absence of a Reactant at Room Temperature

effect on them. The decay rate increased as the total pressure was reduced, and decreased as the total pressure was increased. When the flow rate of the gas through the cell was increased at a constant total pressure, the initial steeper part of the decay curve became slightly extended. When the flow was stopped, non-exponentiality was still observed. When the temperature of the reaction cell was raised to ~393 K, the decay rate became faster by a few sec^{-1} but the general features of the curve were similar to those at room temperature. All of the above observations support the conclusion that the non-exponentiality was due to the pattern of diffusion in the reaction zone.

A simple model of diffusion was studied using computer simulation. (APPENDIX D) In the model, it was assumed that the OH radicals were initially created uniformly in a cylinder with a diameter of 1.6 cm in the center of a cylindrical reaction cell with a diameter of 4 cm. The diffusion equation was therefore modelled in two dimension, and it was numerically solved by computer under given initial conditions and boundary conditions. The average concentration within the central diameter of 1.6 cm was calculated as a function of time. The time profile calculated for the average concentration showed a similar pattern to that obtained from the experimental decay curves. The actual experimental conditions were more complicated than those in the model. The reaction zone was not exactly cylindrical because it was intersected by the resonance light beam. There was also a slow flow of gas through the cell. The reaction cell was not a simple cylinder. The zone viewed by the photomultiplier was not defined precisely and the flash excitation beam might not have been exactly uniform. Although these complications do not allow quantitative analysis

of the contribution of diffusion to the experimental decay curves, the calculations strongly suggest that the non-exponentiality observed in the present experimental system in the absence of a reactant is due to diffusion.

There was a concern whether this non-exponentiality of loss of the OH radical by diffusion would affect the analysis of decay curves in the presence of a reactant. A first-order reaction was added to the above model and the diffusion-reaction equations were solved numerically in a similar way to that described above (APPENDIX D). The results indicate that if the overall first-order rate constant is high enough (100 sec^{-1} or higher), the variation of the diffusion rate during three to four halflives of decay curves was negligible compared with the typical error levels encountered in experiments. One must look carefully at decay curves when the first-order rate constant of the reaction is smaller than 100 sec^{-1}. In this study, the concentrations of reactants were chosen, when possible, in such a way that the observed first-order rate constants had values between 100 sec^{-1} and 600 sec^{-1}. The latter value was the practical limit set by the sensitivity of the apparatus. In some cases, the decay curves had to be observed with the first-order rate constants less than 100 sec^{-1} for practical reasons (CHAPTER V.A.). In such cases, decay curves were carefully analyzed using an autocorrelation function plot to detect any deviation from the exponentiality.

Recently Tully and Goldsmith[146] observed similar non-exponentiality in the OH radical fluorescence decay with their laser photolysis-laser-induced fluorescence technique at lower total pressures and/or higher temperatures in the absence of a reactant. Since the non-exponentiality in

their data was observed within 20 msec after the laser flash they had to correct the decay curves in the presence of a reactant by assuming a functional form, constaht x $(1 + 4\ rt)^{-\alpha}$ for diffusion. Values of r and α were obtained by fitting the function to a decay curve obtained in the absence of a reactant. This correction assumes that the diffusion rate is independent of the reaction. In the simulation of the present study, this assumption was supported when the reaction of interest was the dominant path for the loss of the OH radical. One must carefully treat the effect of diffusion loss according to the specific experimental conditions.

III.E. Test Experiments

Prior to the study of the reactions of interest, experiments were performed to test the experimental system. The OH radical reactions with hydrogen (H_2), ethene (C_2H_4), and propene (C_3H_6) were observed at room temperature (295 K) and with the total pressure of 100 torr argon. Figures III.3 and 4 show k_{obs} versus the reactant concentration plots for these three reactions. Indicated error bars on the figures are one standard deviation of the least square calculations of the slopes of decay curves. Table III.1 tabulates the second-order rate constants, together with previously reported rate constants obtained with the same technique. The rate constants of the two alkenes studied are known to depend on the total pressure, and literature values were selected which had been obtained under similar experimental conditions. In all three cases, the rate constants measured in the present study agree very well with those reported earlier. Experimental results obtained with this system, therefore, can be considered reliable.

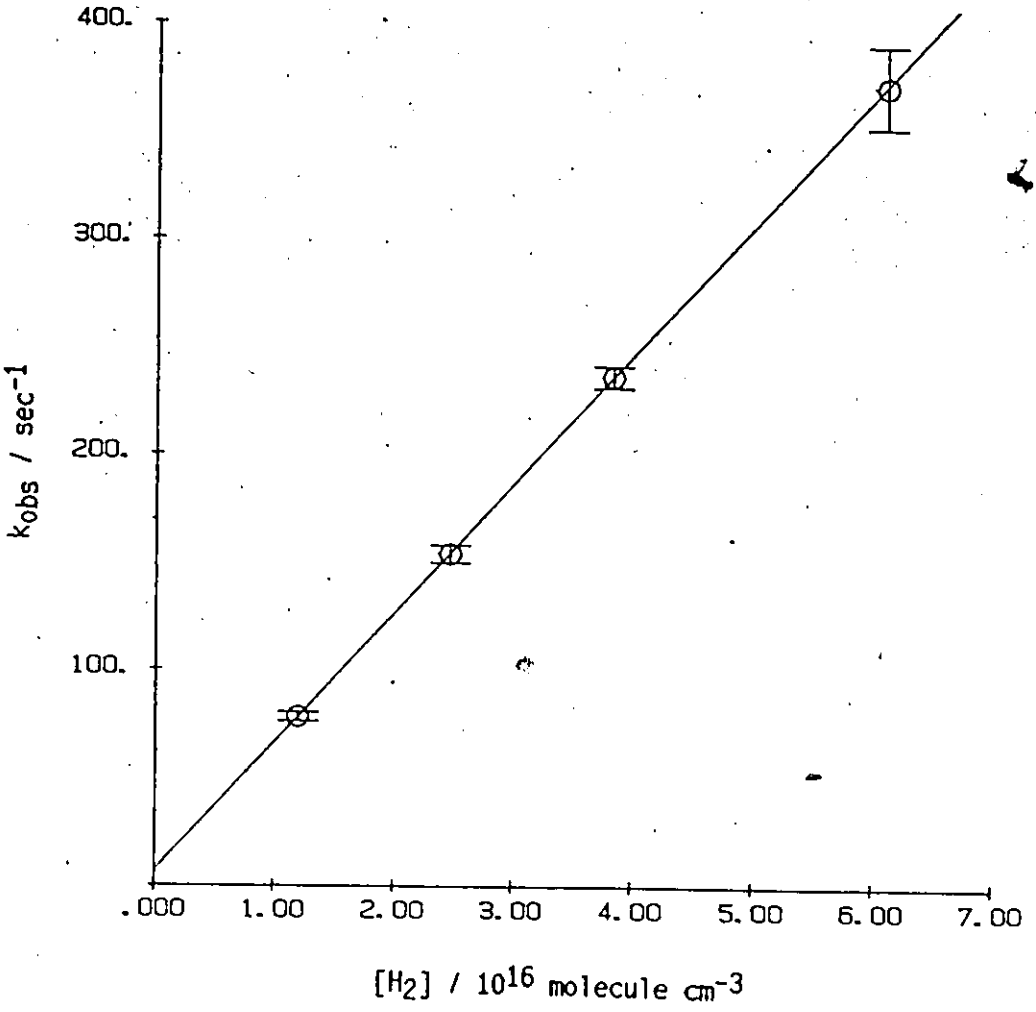

Figure III.3

k_{obs} Versus Concentration Plot of the OH + H_2 Reaction
at 295 K and P_{tot} = 100 torr

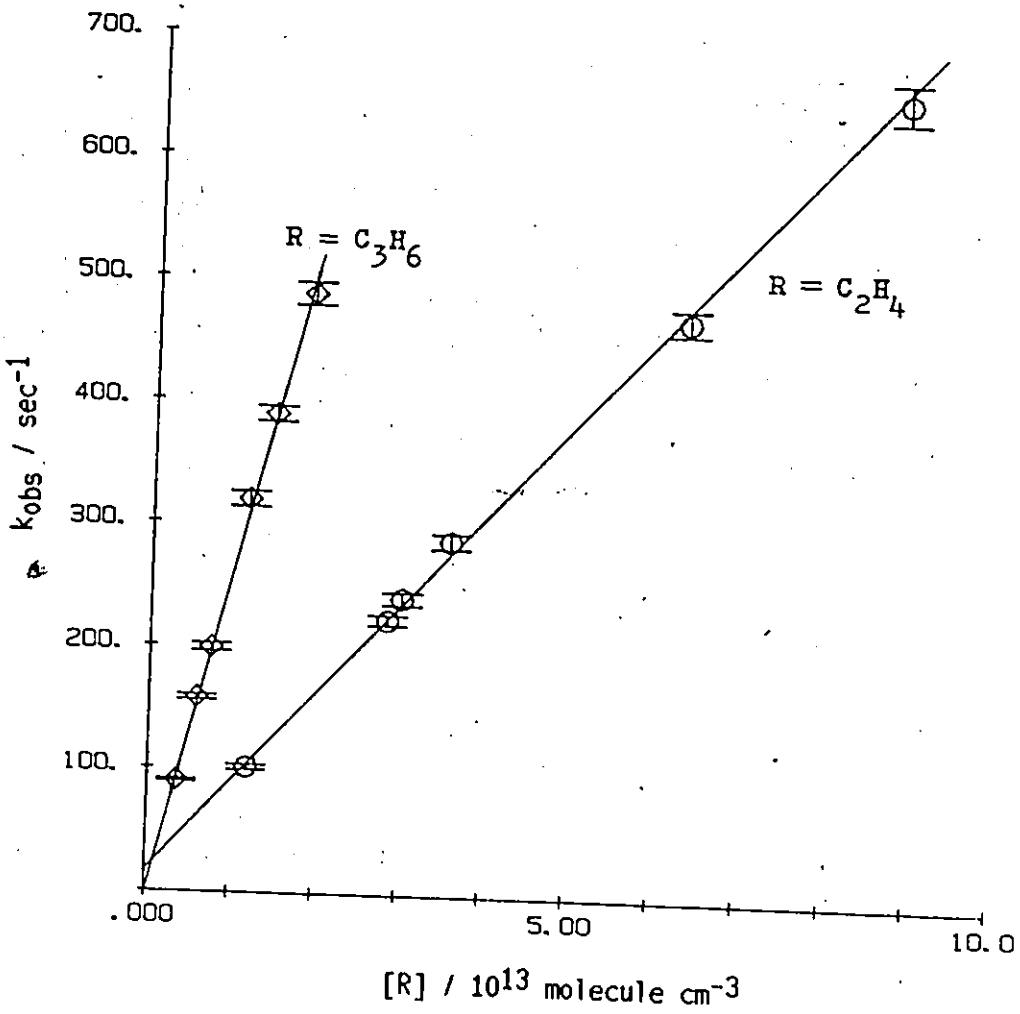

Figure III.4

k_{obs} Versus Concentration Plot of
the OH + C_2H_4 (T = 295 K, P_{tot} = 104 torr) and
the OH + C_3H_6 (T = 294 K, P_{tot} = 99 torr) Reactions

Table III.1

Second-Order Rate Constants of the OH Radical Reactions with H_2, C_2H_4, and C_3H_6 at Room Temperature

Reactant	k (cm^3 $molecule^{-1}$ sec^{-1} / 10^{-12})	Temp. (K)	Ptot(torr)		Reference
H_2	(5.98 + 0.03a) x 10^{-3}	295	100	Ar	This work
	(7.1 + 1.7b) x 10^{-3}	298	20	He	86
	(6.97 + 0.70b) x 10^{-3}	298	15	Ar	126, 147
	(6.08 + 0.37a) x 10^{-3}	298	50	Ar	126
	(5.64 + 0.60a) x 10^{-3}	295	100	Ar	148
	(5.8 + 1.0) x 10^{-3}	295	760	Air	149
C_2H_4	7.40 + 0.35a	295	104	Ar	This work
	4.72 + 0.60a	300	100	He	150
	6.82 + 0.68b	299	74.7	Ar	151
	7.85 + 0.79b	299	224.9	Ar	151
	7.3 + 1.5	296	96.8	Ar	133
	6.21 + 0.16a	291	100	He	152
	7.3 + 1.0	295	760	Air	149
C_3H_6	27.2 + 1.3a	295	99	Ar	This work
	25.1 + 2.5b	297	50	Ar	153
	26.3 + 1.2c	298	200	He	154
	29.9 + 6.6	297	96	Ar	133
	26.9 + 0.4a	293	200	He	146
	22 + 4	295	760	Air	149

a : two standard deviations

b : the overall accuracy estimated

c : the maximum possible error estimated

CHAPTER IV

REACTIONS OF THE OH RADICAL WITH SELECTED CYCLOALKENES

IV.A: Experimental Results

IV.A.1. At Room Temperature

The kinetics of OH radical reactions at room temperature were studied with five cycloalkenes; cyclopentene, cyclohexene, cycloheptene, 1,3-cyclohexadiene, and 1,4-cyclohexadiene. In all measurements simple exponential decays were observed. An example of decay curves observed in the OH-cyclohexene reaction has been shown in Figure III.1 of the previous chapter. For all of the five reactions, first-order rate constants were measured at various reactant concentrations. The total pressure of the reaction mixture was varied beween 50 and 200 torr. Table IV.1 lists the observed first-order rate constants of the OH-cyclopentene reaction at 295 K as an example. Flash energies were also varied over the range 18 to 40 J while the reactant concentration was maintained constant. The observed kinetics of the reactions were not affected by the variation in the flash energy in any of the five reactions. Regardless of the total pressure used, observed rate constants of decays were directly proportional to the concentration of the reactant in all of the reactions. Figures IV.1, 3, 5, 7, and 9 show observed first-order rate constants versus concentration plots at room temperature for the five reactions at three total pressures (50, 100, and 200 torr). Indicated error bars are one standard deviation obtained by the least square calculations of the slopes of the decay

Table IV.1

Observed First-Order Rate Constants of the OH-Cyclopentene Reaction at 295 and 296 K

P_{tot} /torr	Flash Energy /J	[Cyclopentene] /molecule cm^{-3}	k_{obs} /sec^{-1}
50	25	2.06 ± 0.03	130 ± 3
	25	3.75 ± 0.05	224 ± 8
	25	4.83 ± 0.06	285 ± 6
	25	6.19 ± 0.07	378 ± 7
	25	8.13 ± 0.09	474 ± 10
100	25	0.90 ± 0.03	63.9 ± 1.0
	18	1.94 ± 0.03	119.4 ± 2.6
	25	1.95 ± 0.03	121.4 ± 2.3
	40	1.97 ± 0.04	121.6 ± 2.3
	25	3.89 ± 0.05	225 ± 4
	25	5.68 ± 0.07	318 ± 9
	25	7.92 ± 0.10	428 ± 9
200	25	1.08 ± 0.03	75.9 ± 1.9
	25	3.00 ± 0.05	180 ± 4
	25	4.72 ± 0.08	272 ± 5
	25	6.97 ± 0.11	398 ± 10
	25	9.10 ± 0.14	523 ± 12

Indicated errors are one standard deviation.
T = 295 K for experiments with P_{tot} = 50 and 100 torr.
T = 296 K for experiments with P_{tot} = 200 torr.

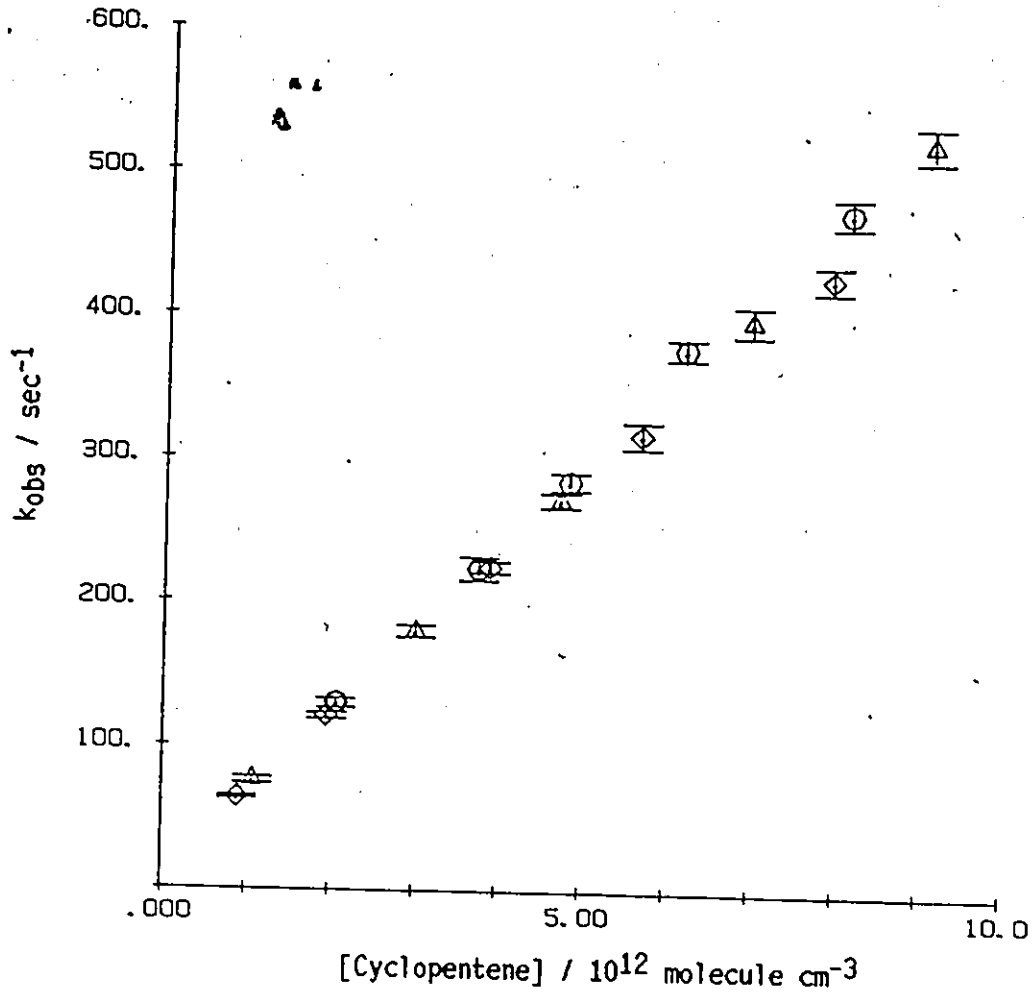

Figure IV.1

k_{obs} versus Concentration Plot of the OH + Cyclopentene Reaction at 295 and 296 K

○ T = 295 K, P_{tot} = 50 torr
◇ T = 295 K, P_{tot} = 100 torr
△ T = 296 K, P_{tot} = 200 torr

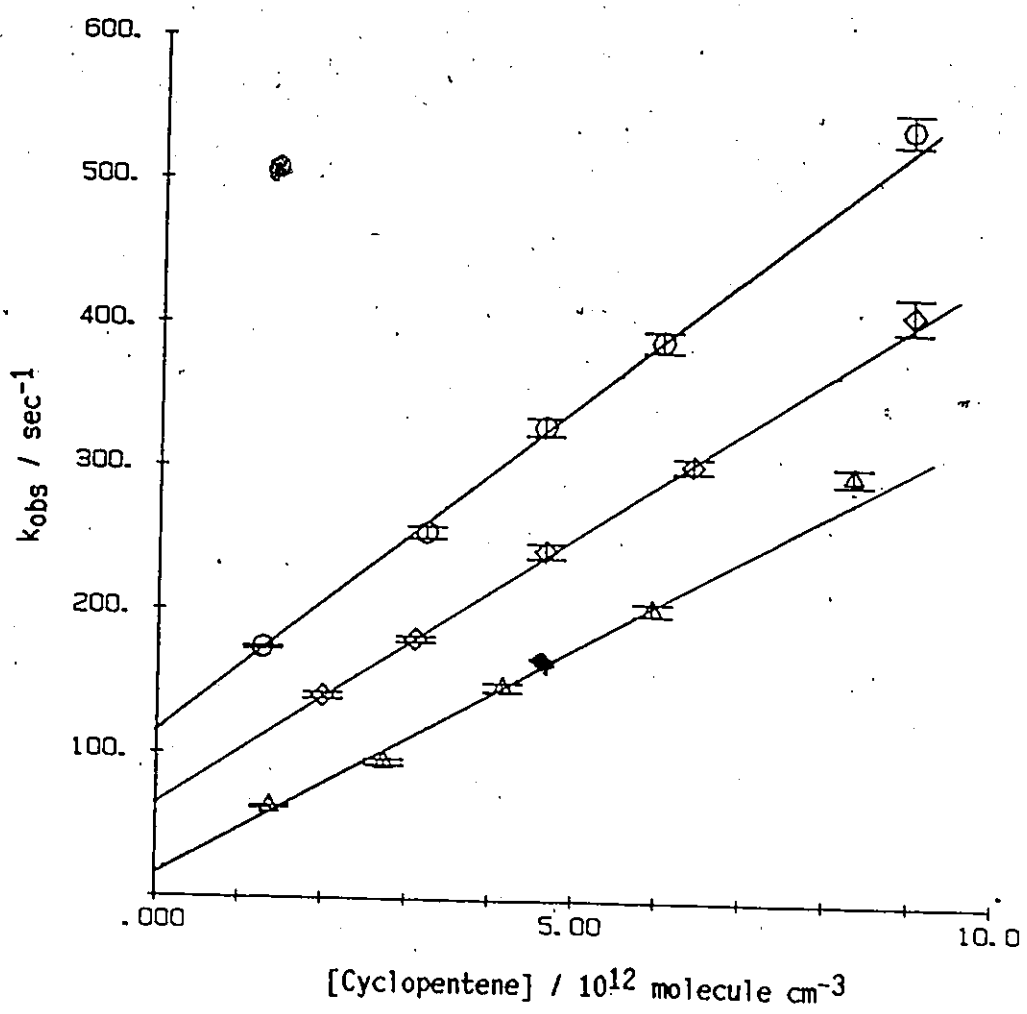

Figure IV.2

k_{obs} versus Concentration Plot of the OH + Cyclopentene Reaction at 331, 373, and 424 K (P_{tot} = 100torr)

○ T = 331 K (Shifted upward by 100 sec^{-1})
◇ T = 373 K (Shifted upward by 50 sec^{-1})
△ T = 424 K

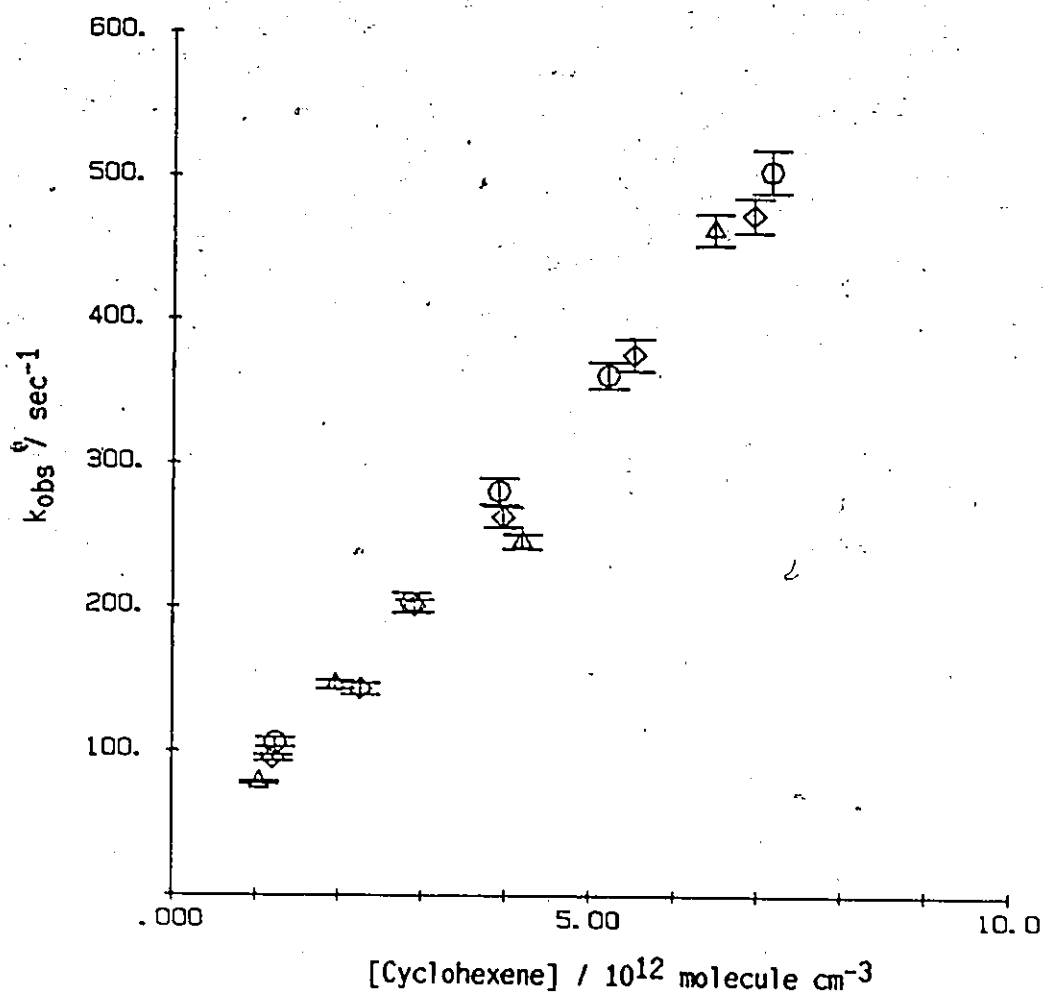

Figure IV.3

k_{obs} versus Concentration Plot of the OH + Cyclohexene Reaction at 295 K

○ P_{tot} = 50 torr
◇ P_{tot} = 100 torr
△ P_{tot} = 200 torr

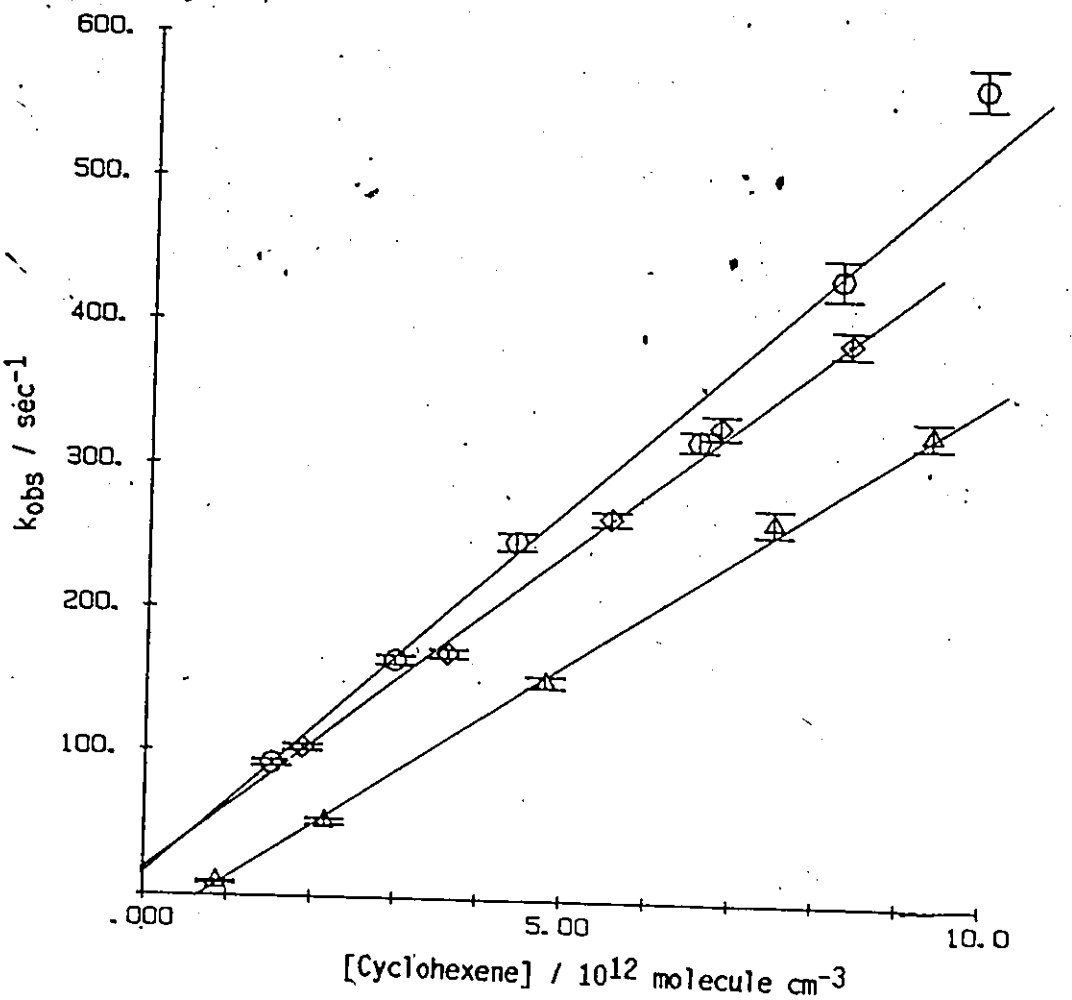

Figure IV.4

k_{obs} versus Concentration Plot of the OH + Cyclohexene Reaction at 332, 372, and 422 K

○ T = 331 K, P_{tot} = 101 torr
◇ T = 373 K, P_{tot} = 100 torr
△ T = 424 K, P_{tot} = 100 torr (Shifted downward by 40 sec^{-1})

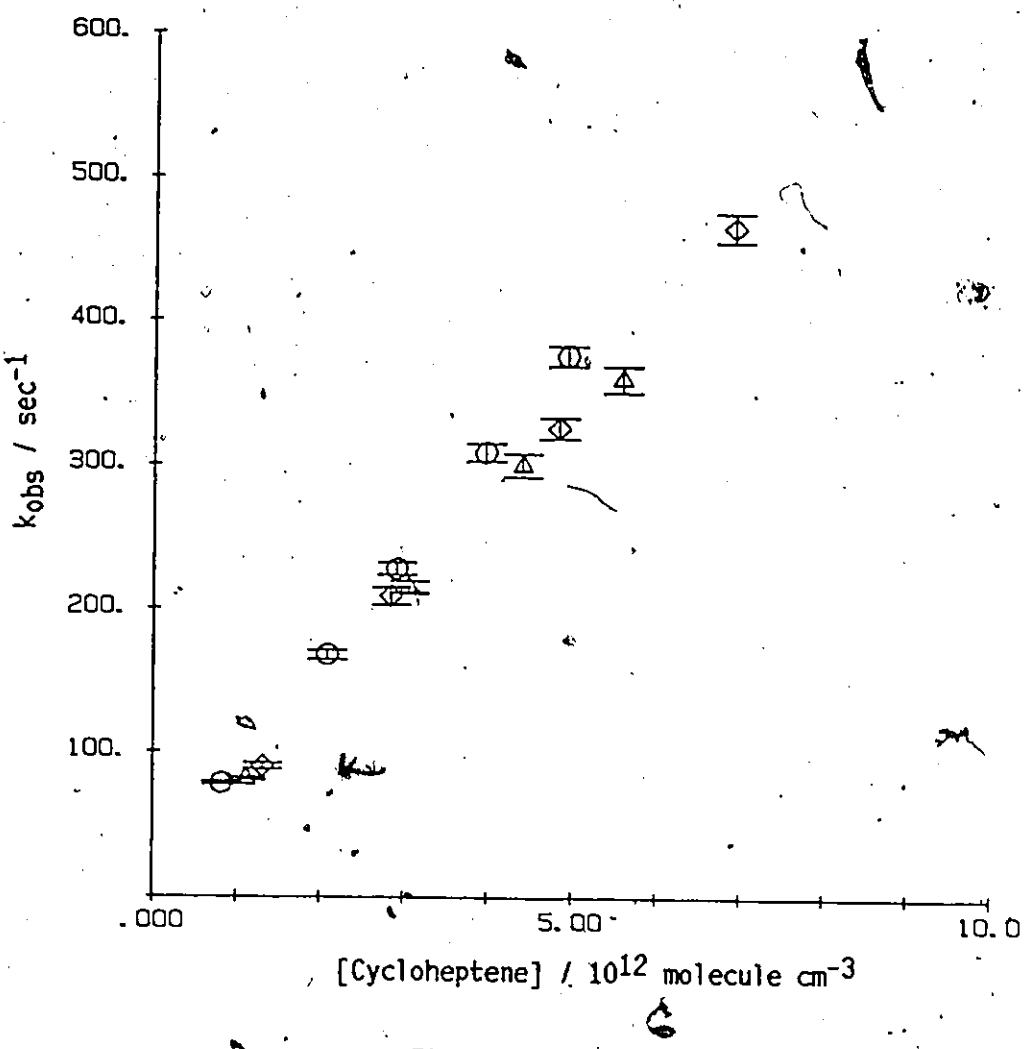

Figure IV.5

k_{obs} versus Concentration Plot of the OH + Cycloheptene Reaction at 296 K

○ P_{tot} = 50 torr
◇ P_{tot} = 100 torr
△ P_{tot} = 200 torr

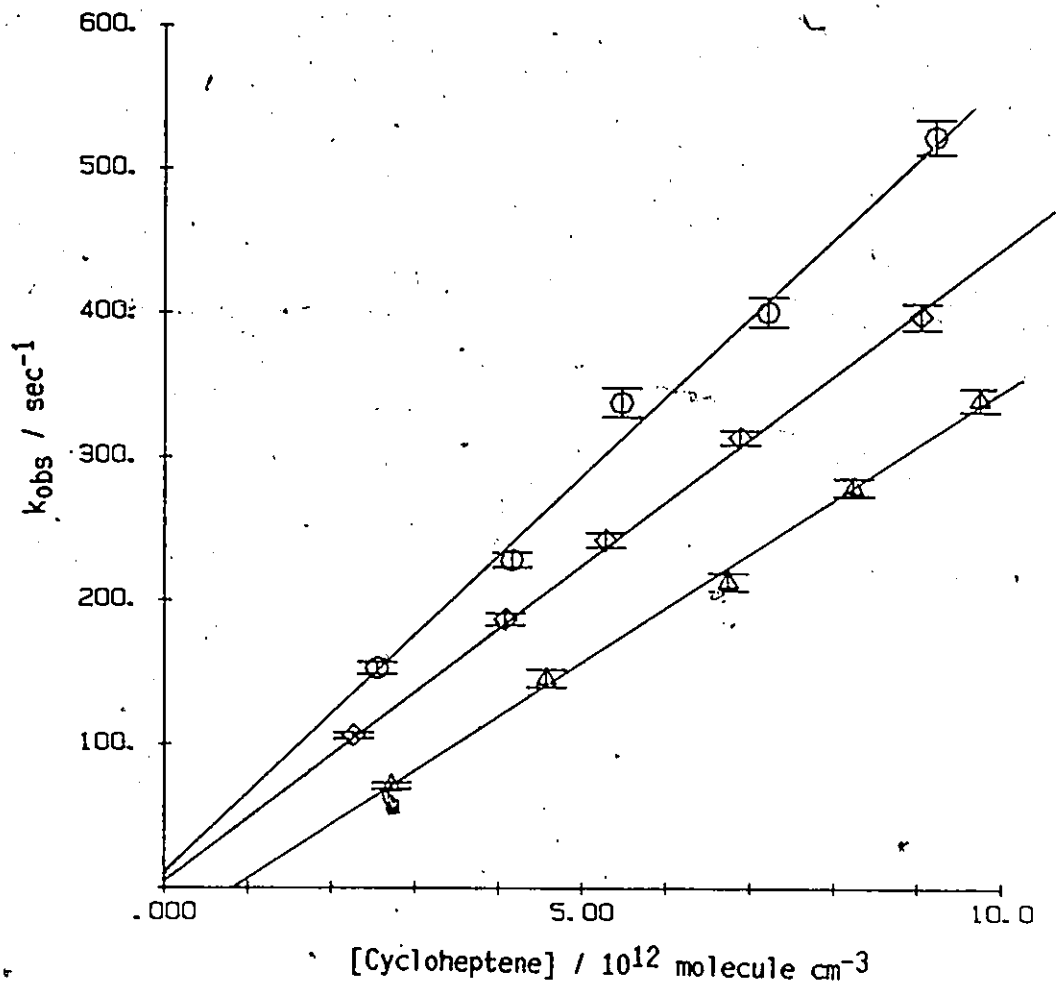

Figure IV.6

k_{obs} versus Concentration Plot of the OH + Cycloheptene Reaction at 332, 375, and 425 K (P_{tot} = 101torr)

○ T = 332 K
◇ T = 375 K
△ T = 425 K (Shifted downward by 50 sec^{-1})

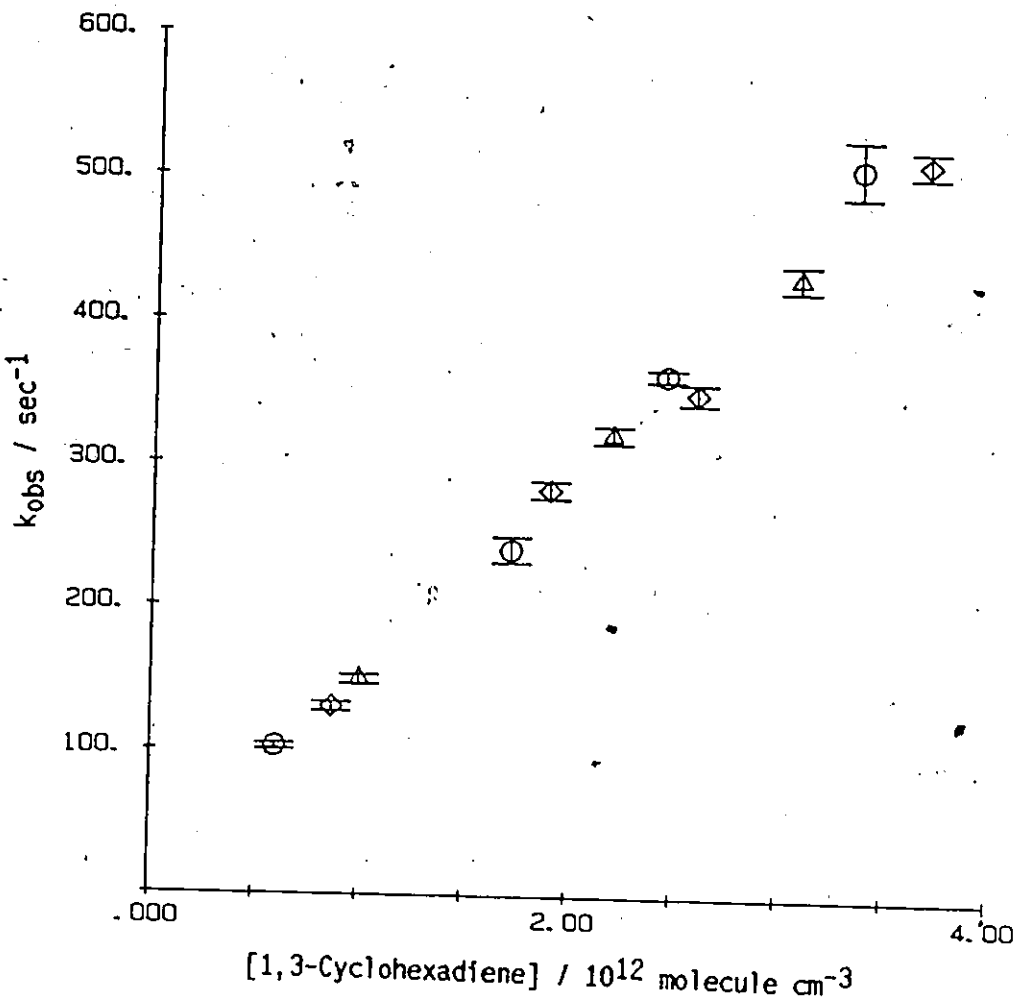

Figure IV.7

k_{obs} versus Concentration Plot of the OH + 1,3-Cyclohexadiene Reaction at 295 K

○ P_{tot} = 51 torr
◇ P_{tot} = 100 torr
△ P_{tot} = 200 torr

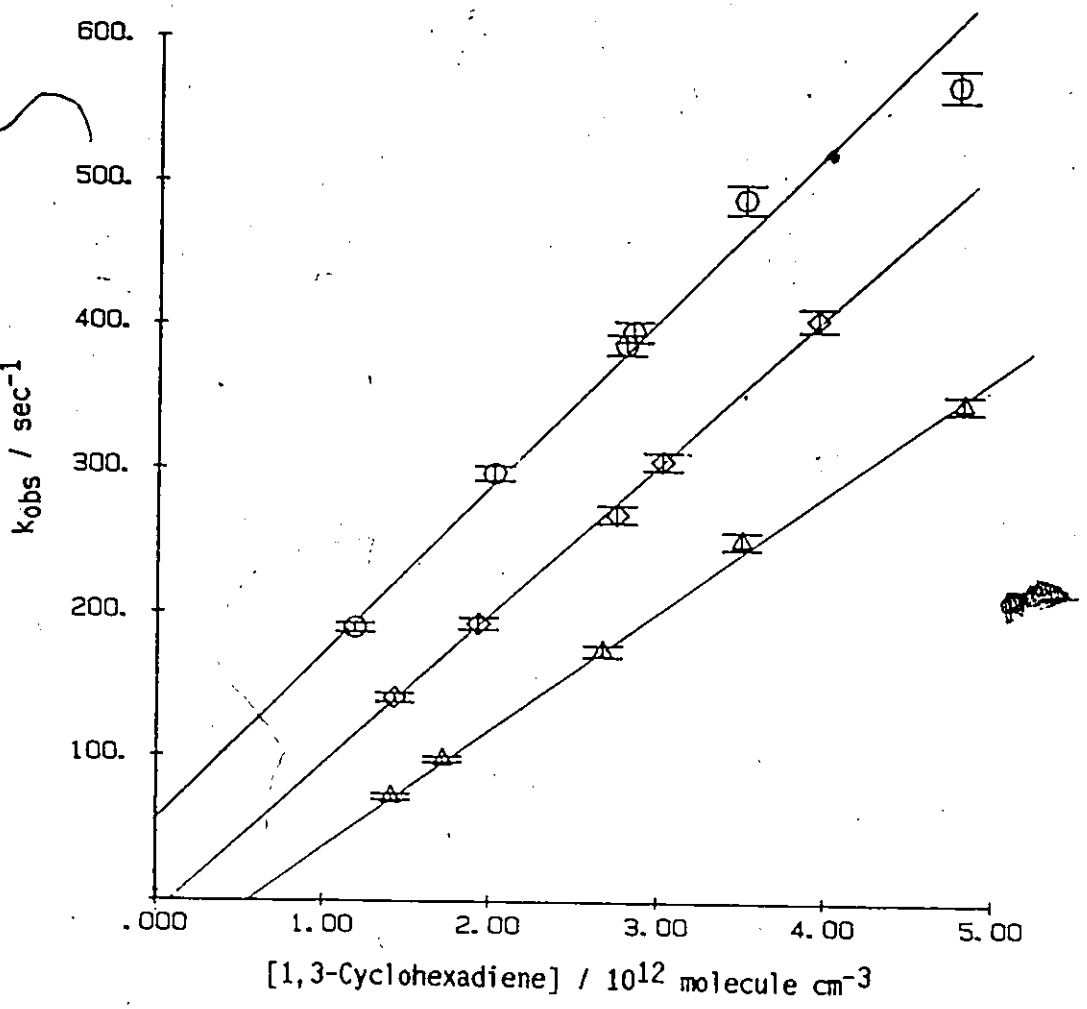

Figure IV.8

k_{obs} versus Concentration Plot of the OH + 1,3-Cyclohexadiene Reaction at 330, 369, and 428 K (P_{tot} = 100torr)

○ T = 330 K (Shifted upward by 50 sec^{-1})
◇ T = 369 K
△ T = 428 K (Shifted downward by 50 sec^{-1})

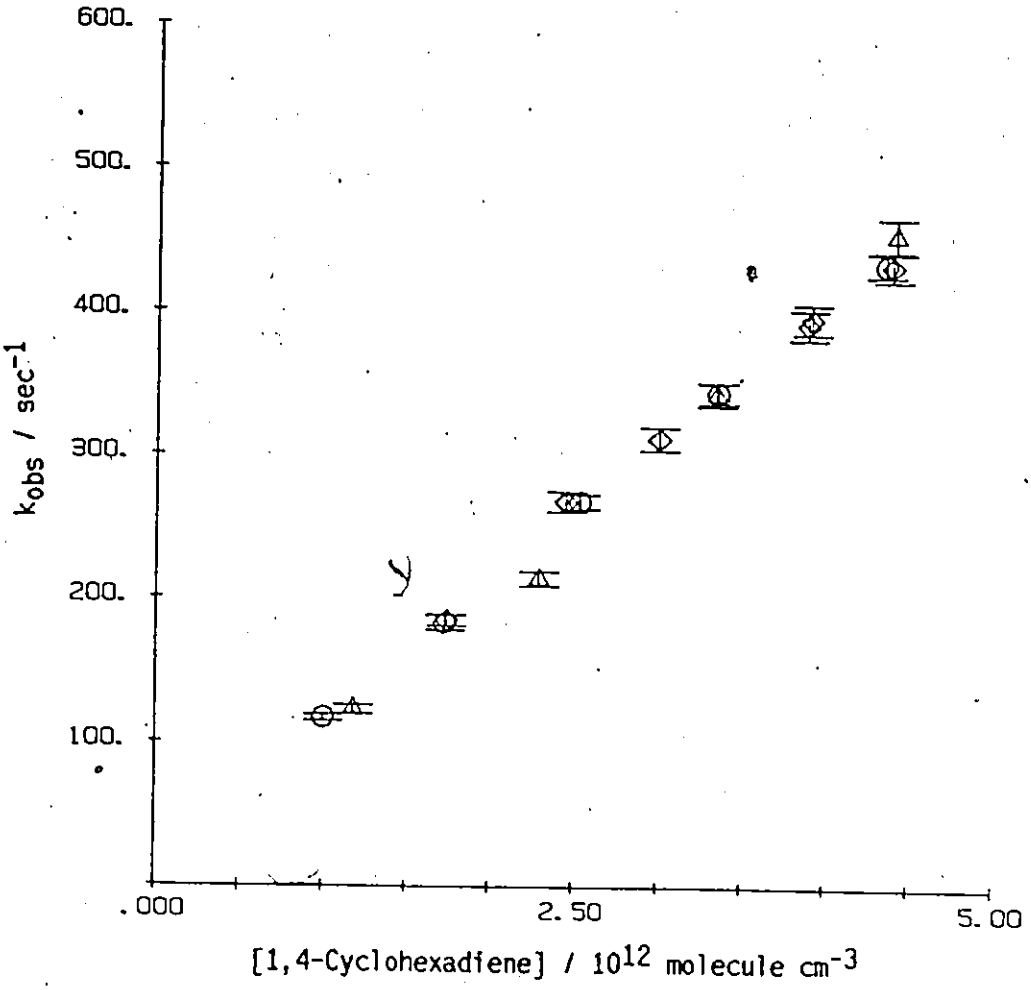

Figure IV.9

k_{obs} versus Concentration Plot of the OH + 1,4-Cyclohexadiene Reaction at 296 K

○ P_{tot} = 50 torr
◇ P_{tot} = 100 torr
△ P_{tot} = 200 torr

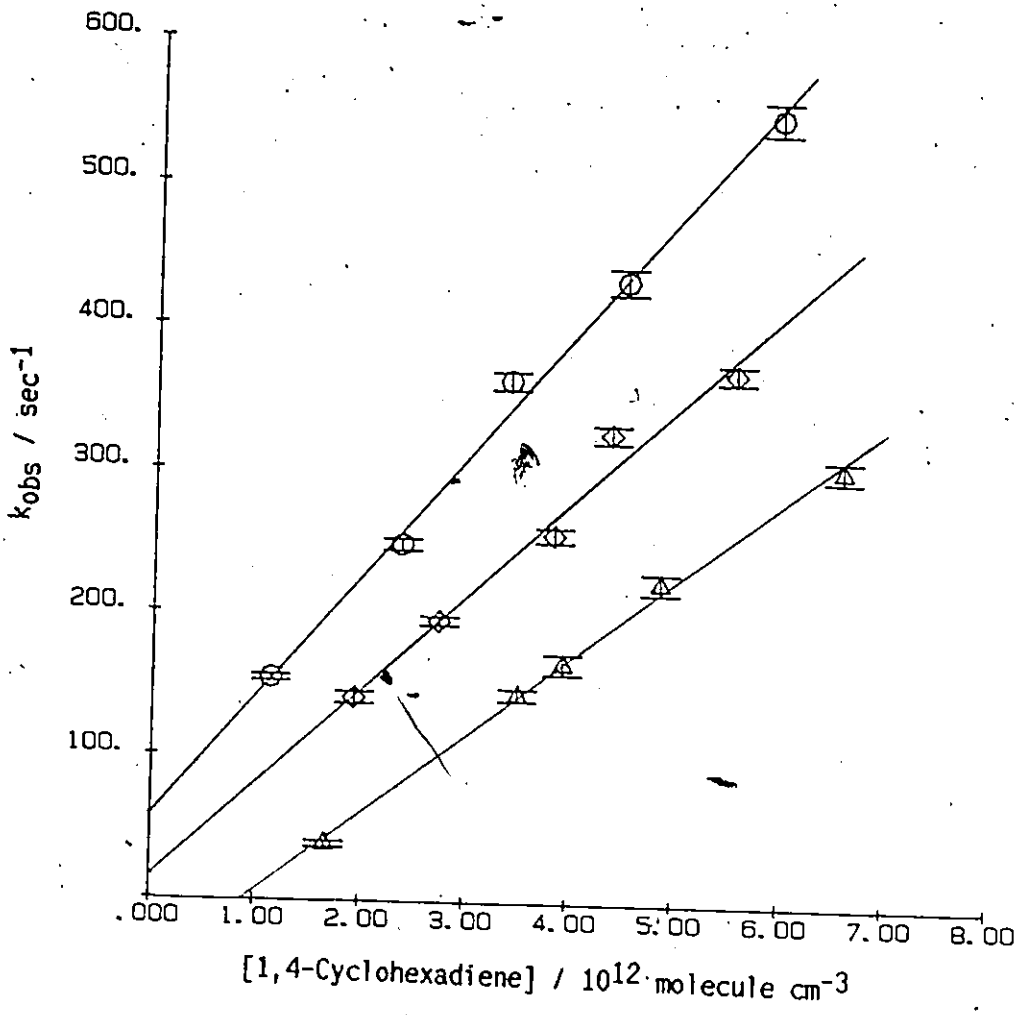

Figure IV.10

k_{obs} versus Concentration Plot of the OH + 1,4-Cyclohexadiene Reaction at 330, 368, and 426 K

○ T = 331 K, P_{tot} = 101 torr (Shifted upward by 50 sec^{-1})
◇ T = 373 K, P_{tot} = 100 torr
△ T = 424 K, P_{tot} = 100 torr (Shifted downward by 50 sec^{-1})

curves. Since most of standard deviations associated with the concentrations were smaller than the symbols used in the figures, they are not indicated in the figures in order to avoid confusion. The slopes of the plots in the five figures (i.e. second-order rate constants) were calculated and listed in Table IV.2 together with available literature values. The best-fitted lines were not drawn on some of the figures to allow a clear representation of the data. The second-order rate constants obtained at various total pressures were essentially constant within the experimental errors. Literature values of the rate constants of the five reactions had been obtained by the relative rate techniques. Their values have been recently revised by Atkinson[38] with new recommended rate constants of the standard reactions. Both the originally reported values and the revised values are shown in Table IV.2.

IV.A.2. Temperature Dependence of Rate Constants

The same five reactions were studied at three temperatures above room temperature. The upper limit of the temperature accessible with the present apparatus was ~430 K. The total pressure of the reaction mixture was maintained at 100 torr in all the higher temperature studies. In all experiments, simple exponential decays were observed at each temperature, and observed rate constants were directly proportional to the concentration of the reactant. Figures IV.2, 4, 6, 8, and 10 are plots of the decay rate versus the concentration at three different temperatures for the five reactions. Indicated error bars are one standard deviation as described in the previous section. Resultant second-order rate constants at higher temperatures are listed in Table IV.3 together with the rate constants

Table IV.2

Second-Order Rate Constants of the OH Radical Reactions with Selected Cycloalkenes at Room Temperature

Reactant	Rate Constant / 10^{-12} cm^3 $molecule^{-1}$ sec^{-1}	T / K	Reference
Cyclopentene	50 torr 57.8 ± 2.6a	295	
	100 torr 52.9 ± 1.2a	295	This work, b
	200 torr 54.8 ± 0.5a	296	
	67.0 ± 2.4a (63.9)	298	108, c
Cyclohexene	50 torr 65.4 ± 3.0a		
	100 torr 64 ± 6a	295	This work, b
	200 torr 63 ± 8a		
	67.4 ± 1.7a (64.3)	298	108, c
	65.5 (62.4)	303	104, d
	75.7 ± 15.1 (73.4)	305	119, e
	64.6 ± 2.5 (64.1)	297	100, f
	65.5 (62)	300	160, g
	67.6	300	161, g
Cycloheptene	50 torr 65 ± 4a		
	100 torr 68 ± 5a	296	This work, b
	200 torr 72.5 ± 1.0a		
	74.1 ± 2.3 (70.8)	298	108, c
1,3-Cyclohexadiene	51 torr 140 ± 12a		
	100 torr 135 ± 12a	295	This work, b
	200 torr 138 ± 5a		
	163 ± 5a (156)	298	108, c
1,4-Cyclohexadiene	50 torr 96.0 ± 3.0a		
	100 torr 96 ± 6a	296	This work, b
	200 torr 100 ± 14a		
	99.4 ± 4.1a (94.8)	298	108, c
	99.4 ± 3.1 (98.6)	297	100, f

(Continued)

(Continued)

a : Indicated error limits are two least-square standard deviations of the slopes of plots

b : Flash photolysis-resonance fluorescence technique

c - g : Relative rate techniques

c : Relative to k(OH + 2-methy-1,3-butadiene) = 101 (96) x 10^{-12}

d : Relative to k(OH + cis-2-butene) = 54.6 (52.0) x 10^{-12}

e : Relative to k(OH + 2-methylpropene = 49.5 (48.0) x 10^{-12}

f : Relative to k(OH + 1,5-hexadiene = 62.1 (61.6) x 10^{-12}

g : Relative to k(OH + ethene) = 8.45 (8) x 10^{-12}

(Rate constants of the standard compounds were those recently revised by Atkinson. See reference 38. The values in the brackets are from those reported earlier. All rate constants are in cm^3 $molecule^{-1}$ sec^{-1}.)

Table IV.3

Second-Order Rate Constants of the OH Radical Reactions with Selected Cycloalkenes at Various Temperatures

Reactant	T / K	Rate constant / 10^{-12} cm^3 $molecule^{-1}$ sec^{-1}
Cyclopentene	295	54.3 ± 1.9
	331	46.0 ± 2.4
	373	37.8 ± 1.2
	424	32 ± 4
Cyclohexene	295	65.1 ± 2.7
	332	52 ± 5
	372	44.6 ± 3.0
	422	37.1 ± 2.0
Cycloheptene	296	71.9 ± 2.7
	332	55 ± 5
	375	44.2 ± 1.2
	425	37.5 ± 1.8
1,3-Cyclohexadiene	295	137 ± 5
	330	116 ± 14
	369	103 ± 5
	428	81.8 ± 2.8
1,4-Cyclohexadiene	296	96.1 ± 2.6
	330	85 ± 7
	368	66 ± 10
	426	55.6 ± 2.2

The mean values of rate constants at room temperature were used. Indicated errors of the room temperature values are the two standard deviations of the larger values of internal and external consistencies. All other indicated errors are two least-square standard deviations of slopes of k_{obs} versus concentration plots.

measured at room temperature. Indicated errors in the table are two standard deviations. Overall accuracies of rate constants (see APPENDIX C.4) were estimated to be fairly constant over the temperature range of the present study. When the least square fit was good the overall accuracy was estimated to be ~8%, and with worst fit it was estimated to be ~15%. In general it was ~10%. The values of the rate constants at room temperature are the means of second-order rate constants obtained at three different total pressures, and their indicated errors are two standard deviations of the larger values of internal and external consistencies.[156] In all reactions, the second-order rate constants decreased as the temperature was increased. Figures IV.11 and 12 are conventional Arrhenius plots (ln k versus 1/T) of the second-order rate constants of the five reactions. Table IV.4 lists for each reaction the apparent activation energy E_a and pre-exponential factor A of the conventional Arrhenius equation

$$k = A \exp(-E_a/RT) \qquad \text{(iv.1)}$$

where R is the gas constant. The Arrhenius parameters of the present study are the first values reported, and there are no literature values available to compare with them.

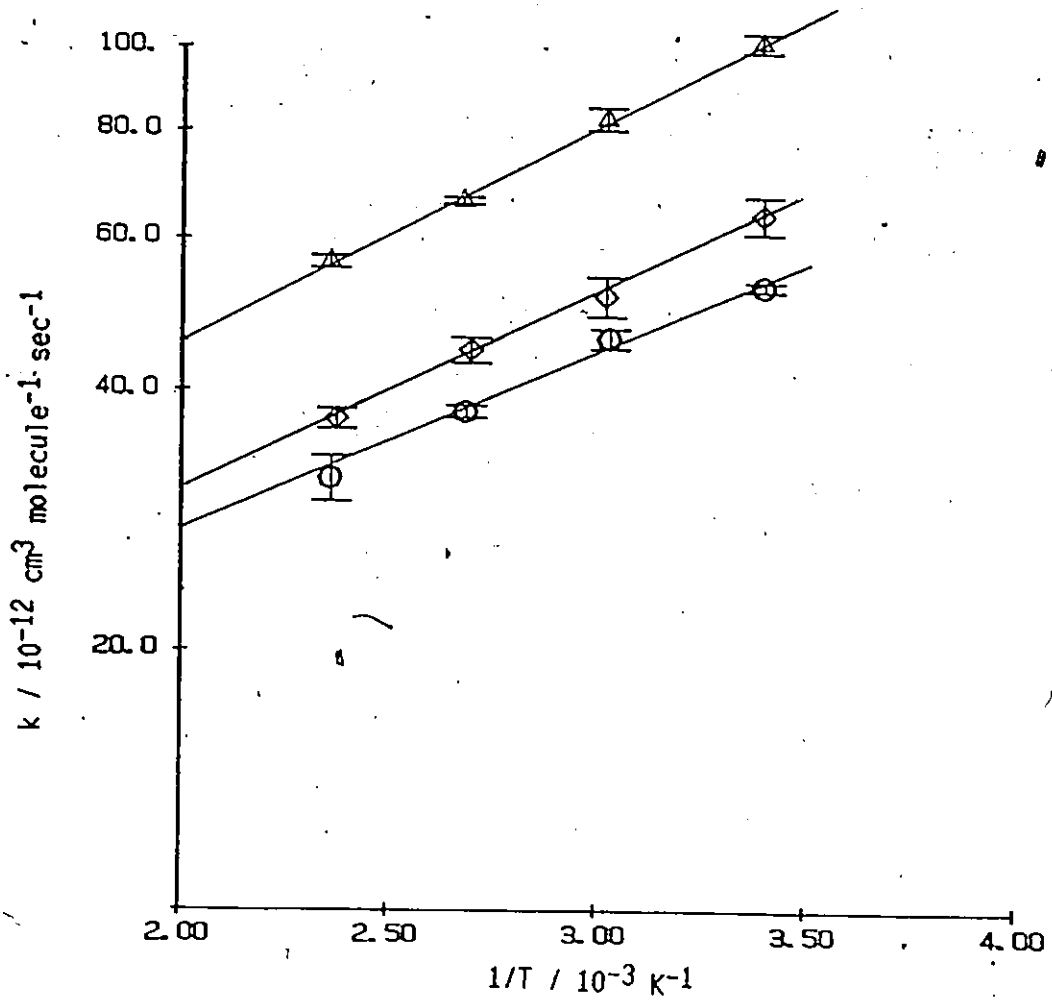

Figure IV.11

Arrhenius Plot of the OH Radical Reactions with Cyclopentene, Cyclohexene, and Cycloheptene

○ OH + Cyclopentene
◇ OH + Cyclohexene
△ OH + Cycloheptene (Rate constants are multiplied by 1.5 for clarity in the figure.)

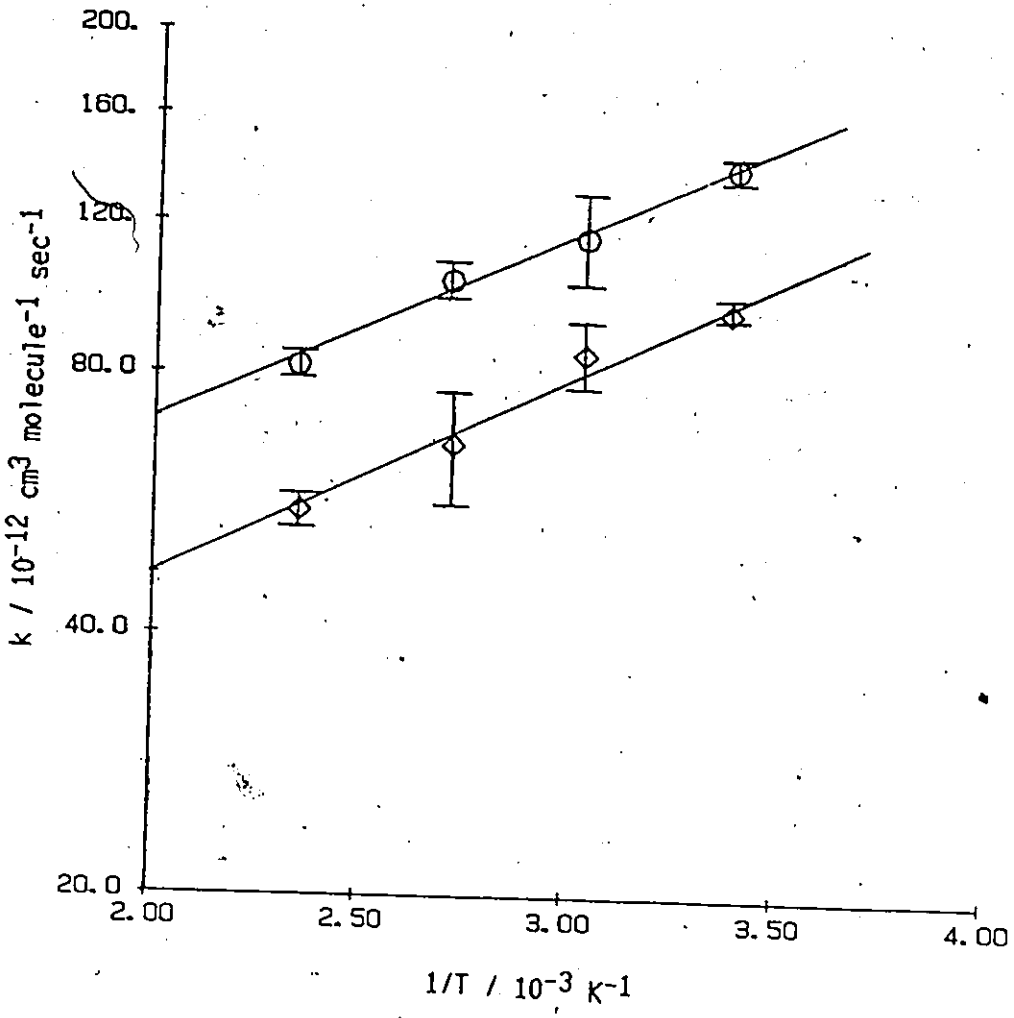

Figure IV.12

Arrhenius Plot of the OH Radical Reactions with 1,3-Cyclohexadiene and 1,4-Cyclohexadiene

○ OH + 1,3-Cyclohexadiene
◇ OH + 1,4-Cyclohexadiene

Table IV.4

Conventional Arrhenius Parameters of the OH Radical Reactions with Selected Cycloalkenes

Reactant	A / 10^{-12} cm^3 $molecule^{-1}$ sec^{-1}	Ea / kJ mol^{-1}
Cyclopentene	9.6 ± 1.8	-4.3 ± 0.5
Cyclohexene	10.1 ± 1.9	-4.6 ± 0.5
Cycloheptene	7.9 ± 1.2	-5.4 ± 0.4
1,3-Cyclohexadiene	26.4 ± 3.4	-4.1 ± 0.4
1,4-Cyclohexadiene	16.0 ± 2.3	-4.4 ± 0.4

Indicated errors are two least-square standard deviations.

IV.B. Discussion

In this section, first, the results of the present study at room temperature will be compared with those previously reported. Secondly, the significance of the process of allylic hydrogen abstraction at room temperature will be discussed and compared with that of the addition process. Thirdly, since the OH-cycloalkene reactions showed a temperature dependence of their rate constants similar to that of other OH-straight-chain alkene reactions, the theories used to interpret such temperature dependence will be discussed, based on not only the results of the present study but also previously reported results for other OH-alkene reactions. Finally, implications will be examined of the rate constants obtained at room temperature for the OH-cycloalkene reactions on the chemistry of the atmosphere.

IV.B.1 Comparison of the Results of the Present Study with Those Previously Reported

All the literature values listed in Table IV.2 had been obtained by relative rate techniques, and the results of the present study are the first values determined by an absolute technique. One of the disadvantages of the relative rate technique is that the accuracies of the rate constants depend largely on the accuracies of those of the standard reactions. The values derived for the absolute rate constants have to be revised when new recommended values of the rate constants of the standard reactions appear. The most recent revision of the rate constants determined by the relative rate technique appeared in 1986.[38] Rate constants obtained by absolute techniques are, therefore, very useful to evaluate those obtained by relative rate techniques. The results of the present study agree very well

with literature values especially for cyclohexene, cycloheptene, and 1,4-cyclohexadiene. The values of cyclopentene and 1,3-cyclohexadiene are smaller than those reported by Atkinson et al.[108] The rate constants obtained with the present study are generally smaller than those obtained by the relative rate technique, especially so after the recent revision. Atkinson[38] estimated the uncertainties of the standard reactions used to obtain the literature values in Table IV.1 to be 15 - 20 %. The 1,3-cyclohexadiene reaction is close to the upper limit of rate constants which can be determined with the flash photolysis-resonance fluorescence technique, and the overall accuracy of this reaction in the present study was estimated to be 15 %. When the overall accuracies of both techniques (10 - 20%) are taken into account, the apparent discrepancies are within those accuracies. The reasonable agreement between results from two totally different techniques supports the reliability of both techniques.

As Atkinson et al[108] pointed out, there seems to be no significant ring effect on the rate constants of the OH radical reaction with the cycloalkenes at room temperature. Rate constants of the OH radical reactions with cycloalkenes are close to those with the corresponding straight-chain alkenes. For example, the rate constants of the OH-cis-2-butene and the OH-2,4-hexadiene reactions are 57.1 and 135 x 10^{-12} cm^3 $molecule^{-1}$ sec^{-1} respectively.[38] They can be compared with the rate constants of the OH-cyclopentene and the OH-1,3-cyclohexadiene reactions (54.3 and 137 x 10^{-12} cm^3 $molecule^{-1}$ sec^{-1} respectively). Atkinson et al[108] found that this was true also for some bicycloalkenes. The OH-cycloalkene reactions, therefore, seem to be insensitive to the ring structures.

IV.B.2. The Significance of Allylic Hydrogen Abstraction

The OH radical reacts with alkenes either by addition to a double-bonded carbon, or by abstraction of a hydrogen atom from alkenes. Cyclopentene is taken as an example to show these paths:

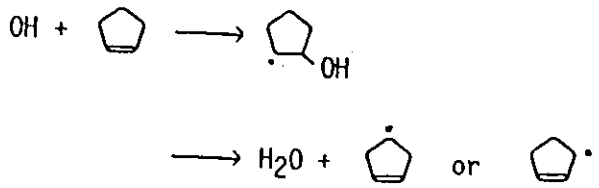

The relative importance of the two processes has been examined in the past for several OH-alkene reactions occurring in the gas phase[43-45,47,96,97,162-166] as well as in the solution phase,[167] and the addition path is considered to be at least a major path if not predominant. Qualitative estimations of the significance of the hydrogen abstraction path, especially the allylic hydrogen abstraction have been inconclusive. Sections IV.B.2.a. to d. will consider four different approaches which have been used in the past to estimate this relative importance in various OH-alkene reactions. An additional approach will be introduced in section IV.B.2.e..

IV.B.2.a. Pressure Dependence of Rate Constants

One way of investigating the relative importance of the addition and abstraction processes is to study the reaction at various total pressures. Addition reactions often show a dependence of the rate constants on pressure. The energy-rich adducts, which are usually formed, can easily dissociate to reform the reactants unless they are energetically stabilized by collisions with other molecules,

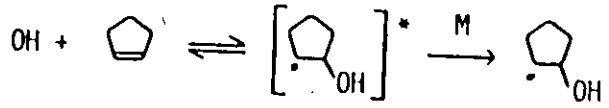

where * denotes an energy-rich adduct. For larger alkenes (>C_4),[43] however, the high pressure limit is reached at lower pressures than those of the typical experiment. As expected the reactions of the present study did not show any pressure dependence of the rate constants between 50 and 200 torr. The pressure effect cannot be used to evaluate the relative importance of the two process in OH-cycloalkene reactions of the present study.

IV.B.2.b. Correlation with O Atom Reactions

Several groups[108,163,168,169] have suggested a correlation between rate constants of the O atom and the OH radical reactions with various alkenes. In Figure IV.13, rate constants of literature values are plotted on a log-log scale. The rate constants of the present study are also plotted on the figure and are represented by filled symbols. They are consistent with the general trend. Both the O atom and the OH radical seem to exhibit electrophilic character in their reactivity trends,[36] as do $S(^3P)$ and ozone.[36] Since the O atom reacts with alkenes predominantly via addition,[173] the fairly linear correlation for a variety of alkenes strongly suggests that the OH-alkene reactions also occur predominantly by addition, although this correlation is not direct evidence. Further aspects of the correlation will be considered in section IV.B.3..

IV.B.2.c. Bond Dissociation Energies of Allylic C-H Bonds

For the reactions of the OH radical with alkanes, a linear relationship was found between ln k for the hydrogen abstraction by the OH

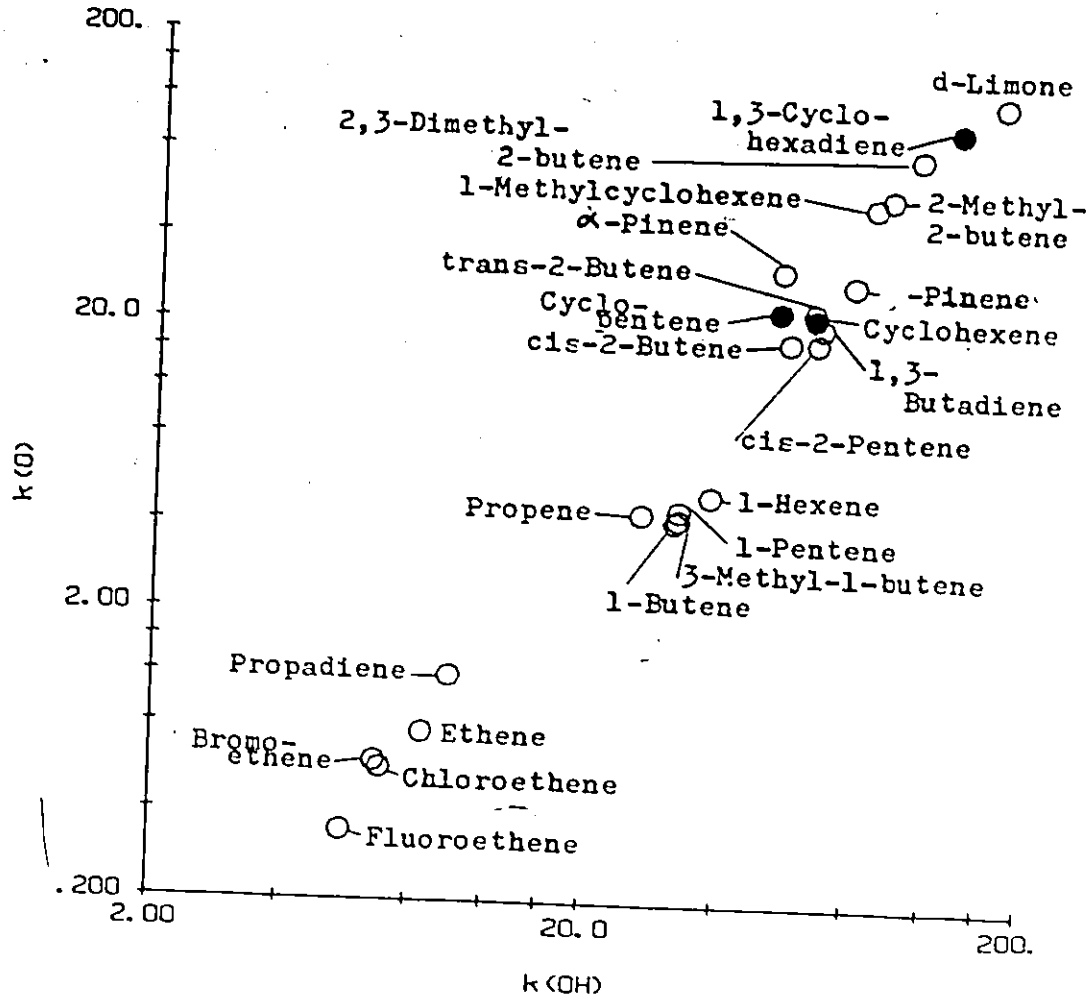

Figure IV.13

Correlation Between the OH- and the O-Alkene Reactions at Room Temperature

Both axes are in 10^{-12} cm^3 $molecule^{-1}$ sec^{-1}. k(OH)'s are rate constants of the OH-alkene reactions. They are taken from reference 38 except those from this work. When k(OH) is from this work, a symbol is filled in the figure. k(O)'s are rate constants of the O-alkene reactions. They are taken from references 168, 170, 171, and 172. When several rate constants are available for a reaction, their mean was taken. k(O)'s of cycloheptene and 1,4-cyclohexadiene are not available.

radical per C-H bond and the C-H bond dissociation energy (BDE).[168,174-176] Since the BDE's of allylic C-H bonds are smaller than those of alkyl C-H bonds, one might expect the abstraction of a hydrogen atom from allylic C-H bonds to be faster than that from alkyl C-H bonds. For example, the BDE's of primary, secondary, and tertiary alkyl C-H bonds are 410, 398, and 385 kJ mol^{-1} respectively, while that of an allylic C-H bond of 1,3-cyclohexadiene is 306 kJ mol^{-1}.[177] If the relationship found in alkyl C-H bonds is extended to allylic C-H bonds, one would expect extremely high rate constants for allylic hydrogen abstraction. For example, for 1,3-cyclohexadiene one would expect from Figure 3 of the reference 175 a value of ~1.4 x 10^{-8} cm^3 $molecule^{-1}$ sec^{-1} per allylic C-H bond. This value is not only larger than the observed overall rate constant (1.37 x 10^{-10} cm^3 $molecule^{-1}$ sec^{-1}) by a factor of ~100, but is also larger than the collision frequency. This clearly shows that the correlation holds only for alkyl C-H bonds and not for allylic C-H bonds. A possible reason for the lack of correlation will be discussed in section IV.B.2.e..

IV.B.2.d. Stable Product Study

Since Ohta's investigation of the stable products of the reaction[165] was the only direct study on the relative importance of the hydrogen abstraction from cycloalkenes, his results will be examined in detail in this section. In his experiment, the mixture of the OH radical precursor (either CH_3ONO or H_2O_2)/ cyclohexadiene (1,3- or 1,4-)/O_2/ N_2 was photolyzed at appropriate wavelengths to produce OH radicals from the precursor at room temperature. He analyzed by gas chromatography, not only the amount of alkene removed, but also the amount of benzene formed. He

assumed, under his experimental conditions, that all the benzene was formed as a result of allylic hydrogen abstraction by the OH radical. He estimated that 8.9% and 15.3% of reacted alkenes underwent the abstraction process with 1,3- and 1,4-cyclohexadienes respectively. From those results he estimated the rate constant of allylic hydrogen abstraction by the OH radical to be ~3.8×10^{-12} cm^3 $molecule^{-1}$ sec^{-1} per allylic C-H bond. This value is larger than the rate constant of the tertiary hydrogen abstraction (2.1×10^{-12} cm^3 $molecule^{-1}$ sec^{-1} per allylic C-H bond[109]), but not as large as was expected from ln k versus BDE plot described in the previous section. Since BDE's of most allylic C-H bonds lie between those of cyclohexadienes and a tertiary C-H bond, Ohta predicted that the rate constant of the allylic hydrogen abstraction per C-H bond would lie between 2.1 - 3.8×10^{-12} cm^3 $molecule^{-1}$ sec^{-1}.

His conclusion, however, can be questioned in two respects: the use of the BDE relation, and his experimental results. First, although Ohta continued to use the BDE relation, it may be no longer an appropriate parameter to correlate with the relative reactivities of allylic hydrogen abstraction by the OH radical for reasons described in section IV.B.2.c..

Secondly, the predictions by Ohta[165] of the range of values for the rate constants of hydrogen abstraction from allylic C-H bonds might be overestimates. His prediction disagrees with the estimates made by some other groups. Estimated rate constants of allylic hydrogen abstraction by various groups are compared in Table IV.5. As Ohta himself pointed out,[165] Biermann et al [44] had earlier estimated the rate constant of the allylic hydrogen abstraction from propene (BDE = 361 kJ mol^{-1} [177]) to be 0.27 x

Table IV.5

Comparison of Rate Constants of Hydrogen Abstraction by the OH Radical per Allylic C-H Bond Estimated by Various Groups

Rate constant per allylic C-H bond	Reference
2.1 - 3.8 (general)	Ohta (165)[a]
0.27 (propene)	Biermann et al (44)[b]
0.06 (propene)	Tully and Goldsmith (146)[c]
0.0017 (propene)	Smith et al (178)[c]
3 (1-butene)	Biermann et al (44)[b]
< 1.57 (1-butene)	Hoyermann and Siervert (45),[b] Atkinson et al (166)[d]
1.9 (1-pentene)	Biermann et al (44)[b]

a. The range was estimated as that between rate constant of tertially alkyl C-H bond and that of allylic C-H bond of cyclohexadiene. The latter was obtained from the stable product (benzene) analysis of the reaction.
b. From mass spectroscopic study
c. From extrapolation of the Arrhenius equation at higher temperature to room temperature.
d. From stable product analysis with GC

10^{-12} cm^3 $molecule^{-1}$ sec^{-1} per allylic C-H bond from their study of the reaction by discharge flow-photoionization mass spectrometry, which was smaller than that predicted by Ohta by an order of magnitude. Recently, Tully and Goldsmith[146] and Smith et al[178] studied the OH-propene reaction with the laser photolysis and the laser pyrolysis techniques respectively, combined with the laser induced fluorescence technique at high temperatures (700 ~ 896 K and 960 ~ 1090 K respectively) where the addition path is thougfit to be practically closed because of the fast backward reaction. The rate constants of the abstraction at room temperature, when the Arrhenius equations obtained by them were extrapolated, were even smaller (0.06 and 0.0017 x 10^{-12} cm^3 $molecule^{-1}$ sec^{-1} per allylic C-H bond respectively at 295 K[146,178]) than the value reported by Biermann et al.[44]

Ohta's predictions of the rate constants of the allylic hydrogen abstraction from 1-butene and 1-pentene do agree with the experimental results of Biermann et al (3 and 1.9 x 10^{-12} cm^3 $molecule^{-1}$ sec^{-1} respectively).[44] The values obtained by Biermann et al are, however, questionable as pointed out by the authors themselves,[44] since they indicated that the abstraction from 1-butene was faster than that from 1-pentene by a factor of ~1.5. There is no reason to expect such a relationship. Hoyermann and Siervert[45] and Atkinson et al[166] estimated the extent of abstraction by the OH radical from 1-butene to be less than 10% of the overall reaction from their studies of the reaction with mass spectroscopy and gas chromatography respectively. This implies a rate constant of less than 1.57 x 10^{-12} cm^3 $molecule^{-1}$ sec^{-1} per allylic C-H bond.

It is possible that the rate constants of allylic hydrogen abstrac-

tion from cyclohexadienes were overestimated in Ohta's experiment. He assumed that in his experiment the formation of benzene was always via allylic hydrogen abstraction by the OH radical, as long as the O_2 pressure was maintained high enough to suppress the abstraction by the CH_3O radical when CH_3ONO was used. There might have been hydrogen abstraction by species other than the OH radical, such as the adducts and other products in the reaction system causing overestimation of the extent of hydrogen abstraction from cyclohexadienes. Since Ohta did not analyze any products other than benzene, it is desirable to study the other products of the reaction in order to verify his assumption.

IV.B.2.e. Stretching Force Constants

The OH radical is very reactive, and activation energies of hydrogen abstraction reactions from various alkanes are less than 17 kJ mol^{-1}. The reactions are always exothermic because of the relative stability of the H-OH bond compared to the C-H bond. This suggests that the C-H bond would not be much affected by an approaching OH radical. The OH radical might be relatively distant from the C-H bond at the transition state where the C-H bond is not significantly broken yet. In this type of radical reaction, the nature of the bonds to be broken (i.e. their bond energies and polarities) and the stability of the resultant radicals exert little influence on the activation energies.[179,180] Therefore, a different correlation should be used to predict the relative importance of abstraction by the OH radical from allylic C-H bonds.

Szwarc[181] suggested that when a hydrogen atom was abstracted by a very reactive radical, the transition state could be classed as an 'early

transition state' and that the difference in C-H stretching force constants might determine the relative reactivities of hydrogen abstraction in such cases. This is illustrated in Figure IV.14. For example, the benzylic primary C-H bond has a smaller dissociation energy than that of the aliphatic tertiary C-H bond. If the potential energy curve of the H-OH bond cuts across the potential energy curve of a C-H bond at point A (i.e. an early transition state), the activation energy of hydrogen abstraction from benzylic C-H bond (III) will be higher than that from aliphatic tertiary C-H bond (II). If it cuts across at point B (i.e. a late transition state), the opposite occurs. A change in the C-H stretching frequency does not necessarily correspond to a change in BDE.[182] For example, the bond energies of ethane C-H, benzylic C-H of toluene, and allylic C-H of propene are 411, 368, and 361 kJ mol^{-1} respectively.[175] Since all of these C-H bonds are primary, their stretching frequencies are similar.[183] Rate constants of the OH radical reactions with these three compounds at 700 - 900 K are very similar.[122,146,184,185] If one assumes the hydrogen abstraction process is predominant at these high temperatures in OH-toluene and OH-propene reactions, this implies that the three kinds of C-H bonds exhibit similar reactivities towards the OH radical.

Although the exact extent of the abstraction process cannot be evaluated for OH-cycloalkenes until more accurate experimental results become available, it can be roughly predicted for the five reactions of the present study if one assumes the relationship between the stretching force constant and the relative reactivity of hydrogen abstraction as described above. Since allylic C-H bonds have stretching frequencies similar to

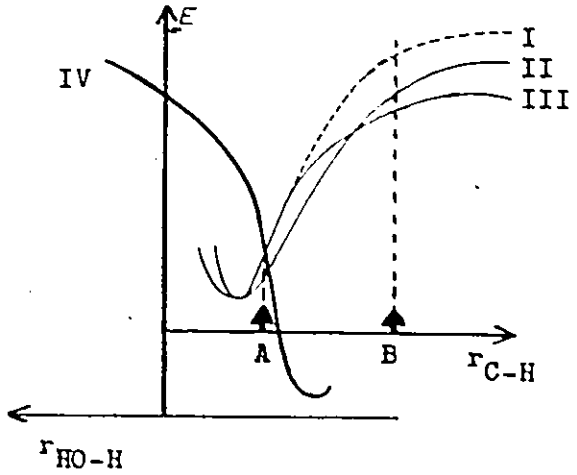

Figure IV.14

Simplified Potential Energy Curves for the C-H and H-OH Bonds

I : Aliphatic primary C-H
II : Aliphatic tertiary C-H
III : Aromatic primary C-H
} from reference 181

IV : Hypothetical H-OH

those of normal alkyl C-H bonds,[183] the reactivity of the OH radical toward an allylic C-H bond might be expected to be similar to that toward alkyl C-H bond of the same order. There are substantial kinetic data available in the OH-saturated organic reactions which undergo hydrogen abstraction. Atkinson[38] used the group additivity technique to estimate rate constants of hydrogen abstraction from various saturated organics. This additivity rule[38] to calculate the overall rate constant of hydrogen abstraction from a saturated organic,[38]

$$k_{abs} = \Sigma\,[k_{prim}\,F(x)] + \Sigma\,[k_{sec}\,F(x)\,F(y)] + \Sigma\,[k_{tert}\,F(x)\,F(y)\,F(z)]$$

might be also used for that from an alkene where $k_{prim} = 0.144$, $k_{sec} = 0.838$, $k_{tert} = 1.83 \times 10^{-12}$ cm^3 molecule^{-1} sec^{-1}. F(i)'s are substituent group factors given in reference 38. For example, cyclopentene has three methylene groups, two of which are allylic and the other is alkyl:

k_{abs}(cyclopentene)

$$= 2 \times [k_{sec}\,F(-CH_2-)\,F(-CH=)\,R(5)] + k_{sec}\,F(-CH_2)^2\,R(5)$$

$$= 2 \times [0.835 \times 1.29 \times 1.0 \times 0.8] + 0.835 \times 1.29^2 \times 0.8$$

$$= 1.72 + 1.11$$

$$= 2.83$$

(in 10^{-12} cm^3 molecule^{-1} sec^{-1})

where R(5) is the five-membered ring factor, and F(-CH=) was assumed to be 1.0. According to this calculation, rate constant of allylic hydrogen abstraction was estimated to be $1.72/4 = 0.43 \times 10^{-12}$ cm^3 molecule^{-1} sec^{-1} per allylic C-H bond. This value should be compared with those in Table IV.5. Similar calculations were performed for the other four cycloalkenes,

and the estimated overall abstraction rate constants are listed in Table IV.6. Three more alkenes were added in the table for comparison. From the estimation in the table, it is clear that abstraction is expected to be very minor at room temperature for any of the listed alkenes and cycloalkenes, and within the typical uncertainty levels of the experimental technique.

The arguments presented in sections IV.B.2.a. to e. can be summarized as follows: the extent of hydrogen abstraction by the OH radical from the cycloalkenes studied here is expected to be very small (< 10%) compared with the addition reaction, although further experimental verification would be very valuable. The following discussion will proceed on the assumption that the addition reaction is the predominant process.

IV.B.3. Interpretations of the Temperature Dependence of the Rate Constants

The temperature dependence of the rate constants was studied in order to gain some insight into the origin of the relative reactivities of the OH radical with various alkenes, and the dynamics of the reactions. The negative temperature dependence of the rate constants noticed in the present study (Table IV.3) has been observed in all other OH-alkyl-substituted alkene reactions previously reported. (See Table IV.7 in page 107.) What is unique about the OH-alkene reactions is that not only are the apparent activation energies negative but also their values are usually 4 - 5 kJ mol^{-1}. (Table IV.7) Since the values of apparent activation energies are almost constant for the variety of OH-alkene reactions, it is not possible to predict the source of their relative reactivities from the difference in their energetic properties. The negativity of the values

Table IV.6

Estimation of the Extent of Hydrogen Abstration from Selected Alkenes and Cycloalkenes

Reactant	Overall rate constant of the OH radical reaction (k_o)a	Estimated Hydrogen abstraction rate constant (k_{abs})a,e	k_{abs}/k_o
Propene	26.3b	0.144	0.005
1-Butene	31.4b	1.02	0.033
1-Pentene	31.9c	2.35	0.074
Cyclopentene	54.3d	2.83	0.052
Cyclohexene	65.1d	3.96	0.061
Cycloheptene	71.9d	5.08	0.071
1,3-Cyclohexadiene	137 d	1.73	0.013
1,4-Cyclohexadiene	96.1d	1.34	0.014

a : In 10^{-12} cm^3 $molecule^{-1}$ sec^{-1}
b : Recommended in Reference 38
c : Reference 186
d : This work's results
e : Calculated as explained in the text

cannot be explained in the context of the conventional Arrhenius equation if a simple elementary reaction is assumed. A non-Arrhenius equation of the form

$$k = B\ T^{b} \exp\ (-E_0/RT) \qquad \text{(iv.2)}$$

might be employed to describe the temperature dependence of rate constants, where B' and b are empirical parameters.[187] If the threshold energy E_0 is assumed to be zero, the apparent negative activation energy of ~4 - 5 kJ mol^{-1} in the conventional Arrhenius equation (iv.1) corresponds to $b \approx -1.5$ in equation (iv.2). There have been three interpretations proposed in the literature to explain the observed temperature dependence of the OH-alkene reactions. In the following sections IV.B.3.a. to c. each interpretation will be examined in terms of its strengths and weaknesses, and an additional proposal will be presented in section IV.B.3.d..

IV.B.3.a. Collision Theory

According to the simple collision theory,[188] the rate constant of a bimolecular reaction in a thermally equilibrated system is derived as

$$k(T) = \left(\frac{8}{k_B{}^3 \pi \mu}\right)^{1/2} T^{-3/2} \int_{E_0}^{\infty} E\ \sigma(E)\ \exp(-E/k_B T)\ dE \qquad \text{(iv.3)}$$

where k_B is the Boltzmann constant, μ is the reduced mass of reactants, E is the relative kinetic energy of reactants, and $\sigma(E)$ is the reaction cross section. σ is a function of energy and it is zero when E is smaller than the threshold energy E_0. This equation cannot be solved in general because the exact form of σ is not usually known. The apparent activation energy

of the conventional Arrhenius equation E_a can be defined from (iv.1) as

$$E_a = - R \frac{d \ln k(T)}{d (1/T)} \qquad \text{(iv.4)}$$

By substituting (iv.3) into (iv.4),[187,189]

$$E_a = \frac{N_a \int_{E_0}^{\infty} E^2 \sigma(E) \exp(-E/k_B T) \, dE}{\int_{E_0}^{\infty} E \sigma(E) \exp(-E/k_B T) \, dE} - 1.5RT \qquad \text{(iv.5)}$$

where N_a is the Avogadro's number. This can be written as[187]

$$E_a = \langle E_r \rangle - \langle E \rangle \qquad \text{(iv.6)}$$

where the first term $\langle E_r \rangle$ is the average relative kinetic energy of reactive collisions and the second term $\langle E \rangle$ is the average relative kinetic energy of all collisions in the system. According to equations (iv.5) and (iv.6), the apparent activation energy E_a must be larger than $-\langle E \rangle$ (i.e. $-1.5RT$). At 350 K, which is the middle of the typical temperature range of the study, $-1.5RT = -4.4$ kJ mol^{-1}. This is approximately equal to the apparent activation energies observed in OH-alkene reactions. For $\langle E_r \rangle$ to approach zero in order to make E_a approach $\langle E \rangle$ in equation (iv.6), E_0 in equation (iv.5) must approach zero, and the reactive cross section must have a form of a Dirac function,[189]

$$\sigma = \text{constant} \times \delta(E-E_0) \qquad \text{(iv.7)}$$

It implies that the reaction is accessible only at one extremely low energy channel, which is not realistic. Thus the simple collision theory is not sufficient to explain the observed negative temperature dependence unless an extreme condition is assumed.

IV.B.3.b. Transition-State Theory

According to the transition-state theory,[190] the rate constant of a bimolecular reaction is derived as

$$k(T) = \tau \left(\frac{k_B T}{h}\right) \left(\frac{Q(ROH^{\ddagger})}{Q(OH)Q(R)}\right) \exp(-\Delta E/k_B T) \qquad \text{(iv.8)}$$

where τ is the transmission coefficient, $(k_B T/h)$ is the frequency factor, h is the Planck's constant, Q's are partition functions per unit volume of the transition state ($ROH^{\ddagger}$) and reactants (OH and R), and ΔE is the difference between the zero-point energies of the transition state and reactants. The negative temperature dependence of k must be explained from the pre-exponential factor [151,153]

$$A(T) = \tau \left(\frac{k_B T}{h}\right) \left(\frac{Q(ROH^{\ddagger})}{Q(OH)Q(R)}\right) \qquad \text{(iv.9)}$$

Each partition function in equation (iv.9) is often assumed to be a product of translational, vibrational, and rotational partition functions,

$$Q(i) = Q_t(i)\, Q_v(i)\, Q_r(i)$$

and all partition functions vary with temperature:

$$Q_t = (2\pi m k_B T/h^2)^{1.5}$$

$$Q_r = 8\pi^2 I k_B T/h^2 \text{ for a linear molecule}$$

$$Q_r = \pi^{0.5} \{8\pi^2 (I_x I_y I_z)^{1/3} k_B T/h^2\}^{1.5} \text{ for a non-linear molecule}$$

$$Q_v = \prod \{1 - \exp(-hc\,\omega_j/k_B T)\}$$

where m is the total mass of a molecule, I's are moments of inertia, ω_j is the vibrational wavenumbers, and j runs through all vibrational degrees of freedom of a molecule. $\{1 - \exp(-hc\,\omega_j/k_B T)\}$ approaches 1 as ω_j/T becomes larger, and $k_B T/hc\,\omega_j$ as ω_j/T becomes smaller. At the temperature range of the present study (< 425 K), $Q_v(OH) \sim 1$. If both the reactant molecule and the transition state are non-linear,

$$A(T) = \text{constant} \times T^{-1.5} \times \{Q_v(ROH^{\ddagger})/Q_v(R)\} \qquad \text{(iv.10)}$$

If $\Delta E = 0$, and $Q_v(ROH^{\ddagger})/Q_v(R)$ is independent of temperature, the rate constant would show the temperature dependence $T^{-1.5}$ as observed in the OH-alkene reactions. This assumes that the vibrational modes due to the newly formed C-OH bond in the transition state do not have very low frequencies and that the remaining vibrational modes cancel out between the transition state and the reactant. While the latter is a reasonable assumption, there is presently no available information to evaluate the frequency of the newly formed bond. Thus although this theory can explain the observed negative temperature dependence, information is required on the vibrational modes of the transition state in order to evaluate the assumption.

IV.B.3.c. A Weakly Bound Complex

In the last two approaches, it was assumed that the observed rate constant was that of a genuine elementary reaction. Singleton and Cvetanovic[191] used a mechanism involving a weakly bound complex as an intermediate to explain the activation energies of the $O(^3P)$-alkene reactions. A similar mechanism might be applied to the OH-alkene reactions:

$$OH + R \longrightarrow C \qquad (A)$$

$$C \longrightarrow OH + R \qquad (B)$$

$$C \longrightarrow Add \qquad (C)$$

where C is a weakly bound complex and Add is an adduct (a product). The reactions (A), (B), and (C) do not depend on pressure, since the negative activation energies have been measured in experiments which were at the high pressure limit. When the steady-state approximation is applied to the complex, the observed rate constant of the loss of the OH radical would be

$$k_{obs} = \frac{k_A}{1 + k_B/k_C}$$

By substituting the Arrhenius equation for three rate constants,

$$k_{obs} = \frac{A_A \exp(-E_A/RT)}{1 + (A_B/A_C) \exp\{-(E_B-E_C)/RT\}}$$

For the complex formation (A), the activation energy is zero or near zero. If $k_B >> k_C$,

$$k_{obs} = (A_A A_C/A_B) \exp\{-(E_C-E_B)/RT\}$$

and the apparent activation energy E_a is (E_C-E_B). When $E_B > E_C$, E_a appears negative.

There are two main difficulties in this interpretation. The first is the uncertainty of the existence of the complex. It has never been experimentally identified in the OH-alkene reactions. Making a prediction of the characteristic properties of the complex is difficult since there is almost no variation in the apparent activation energies of the OH radical reactions with a variety of alkenes. This is in contrast to the O-alkene reactions where various values of the activation energies were observed, indicating the possibility of differing relative stabilities of the complexes formed from various alkenes. The second difficulty arises when the mechanism is modified to explain the pressure dependence of the rate constants observed in the OH-ethene and OH-propene reactions below their high pressure limits.[116,133] The rate constant of the OH-ethene reaction depends on the total pressure up to 225 torr, and the OH-propene reaction up to 10 torr in argon at room temperature.[38] The pressure dependence is usually considered to be due to the formation of an energy-rich adduct before it is stabilized by collisions with other molecules as mentioned in section IV.B.2.a.. If the mechanism with a weakly bound complex is applied to explain the pressure dependence of these reactions, at least either reaction (A) and (B), or (C) must be pressure dependent, and the mechanism would become more complicated. On the other hand, a mechanism without an intermediate complex has been successfully applied to explain the observed pressure dependence of the reactions above 1 torr.[116,133]

Although the existence of the complex allows the explanation of the

negative activation energy, it does not explain why the values of negative energies are almost constant for various OH-alkene reactions and complicates explanation of the pressure dependence of the OH-ethene and the OH-propene reactions.

IV.B.3.d. Consideration of Thermodynamic Parameters

There are two questions which have to be answered in order to verify any interpretation of the temperature dependence of the rate constants described in the previous sections (IV.B.3.a. - c.). One is whether or not there is a potential minimum (i.e. an intermediate complex) and/or a potential barrier along the reaction coordinate. Another is closely related to the first: whether the main factor in determining the reactivity is the energetics of the reaction or else the structures and internal motions of the reacting molecules. Unfortunately there are no reported molecular orbital calculations of the potential energy surfaces of the OH-alkene reactions to assist in an examination of these questions. Consequently, in this section three thermodynamic parameters of the reaction systems will be considered based on the experimental results in order to obtain some clues as to the dynamics of the reactions. These parameters are the potential energy, the entropy, and the free energy

IV.B.3.d.1. Potential Energy Surfaces of the OH-Alkene Reactions

Although the apparent activation energies do not show any correlation with any characteristic properties of alkenes, Gaffney and Levine[168] and Gusten et al[192] pointed out that the rate constants at room temperature seemed to show a correlation with the lowest vertical ionization potential (IP) of alkenes. Figure IV.15 shows a plot of ln k versus IP as suggested

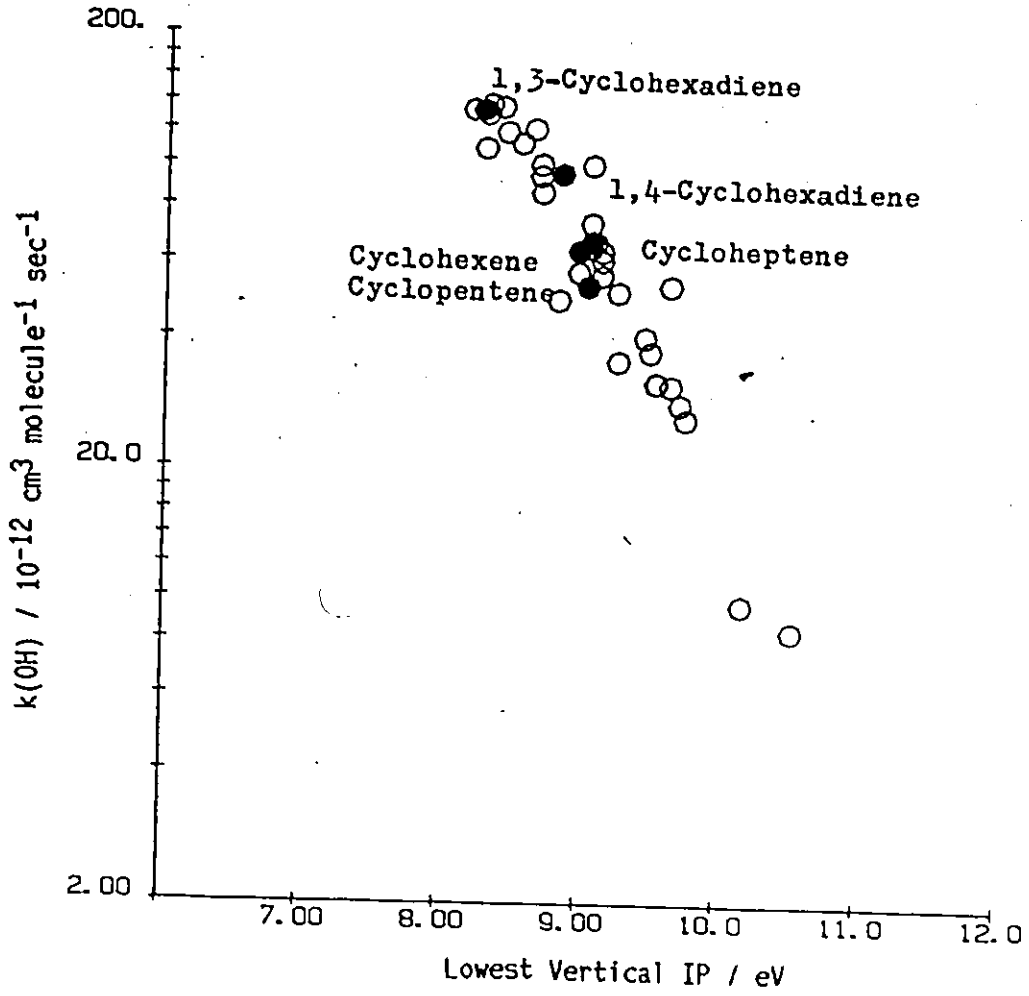

Figure IV.15

The Correlation Between Rate Constants of OH-Alkene Reactions and Lowest Vertical Ionization Potentials (IP) of Alkenes

Rate constants are from reference 38 and this work (filled).
Vertical ionization potentials are taken from references 168, 192, 193, and 194.
Values used to plot this figure are tabulated in APPENDIX E.1.

by them, however, the values of the rate constants are those recently revised by Atkinson[38] and from the present study. The values used in Figure IV.15 are tabulated in APPENDIX E.1.. A similar relationship has been observed in the OH-aromatic reactions[195] and this will be discussed in the next chapter.

The lowest IP of an alkene indicates the availability of π electrons to be removed. There are two models of the potential energy surfaces which predict a correlation between the rate constant and the IP of the alkene: the harpoon model and the frontier orbital theory model. These models will be examined in turn.

IV.B.3.d.1.(a) Harpoon Model

Rinke and Zetzsch[195] suggested applying a harpoon model[196] of the reaction to explain the ln k-IP relationship of OH-aromatic reactions. The harpoon model was originally suggested for the reactions between an alkali metal (A) and a halogen atom (B). The atom A is considered "to toss out its valence electron to hook atom B, which it hauls in with the coulombic force of attraction."[197] Electron transfer takes place at a distance less than r_h where the coulombic attraction between A^+ and B^- is equal to (IP(A) - EA(B)) where EA is the electron affinity:

$$e^2/r_h = IP(A) - EA(B)$$

If A and B approach within the distance r_h, the reaction takes place since the coulombic force between A^+ and B^- is strongly attractive there. The reaction cross section becomes

$$\sigma = \pi r_h^2 = \pi [e^2/\{IP(A) - EA(B)\}]^2$$

When this model is applied to the OH-alkene reactions (i.e. A = alkene, and B = OH), a linear relationship is expected between ln σ and ln (IP(A) - EA(B)) as shown with a solid line in Figure IV.16. The average experimental reactive cross section of the OH-alkene reactions can be approximated to

$$\bar{\sigma}_{EXP} = k\ (\pi\mu/8k_BT)^{1/2}$$

where $(\pi\mu/8k_BT)^{1/2}$ is the average relative velocity of reactants at the temperature T and μ is the reduced mass of the reactants. The values of $\bar{\sigma}_{EXP}$ are also plotted in Figure IV.16. Calculated values of $\bar{\sigma}_{EXP}$ are listed in APPENDIX E.1. together with the values of the ionization potentials used. The observed cross sections vary with (IP - EA) more sharply than those expected from the harpoon model and the majority of $\bar{\sigma}_{EXP}$ are smaller than σ from a harpoon model. The model was originally used to explain large reactive cross sections (50 - 100 A^2) of alkali metal-halogen atom reactions. At such large separation, it is reasonable to assume that the coulombic attraction is dominant. Since the observed reactive cross sections of OH-alkene reactions are much smaller, the characteristics of intermolecular interactions might be very different from the long-range ones.

Ruiz and Bayes[199] and Paltenghi et al[200] also observed smaller cross sections than those expected from the harpoon model when they studied alkyl radical reactions with O_2 and O_3. In those reactions as well, ln k

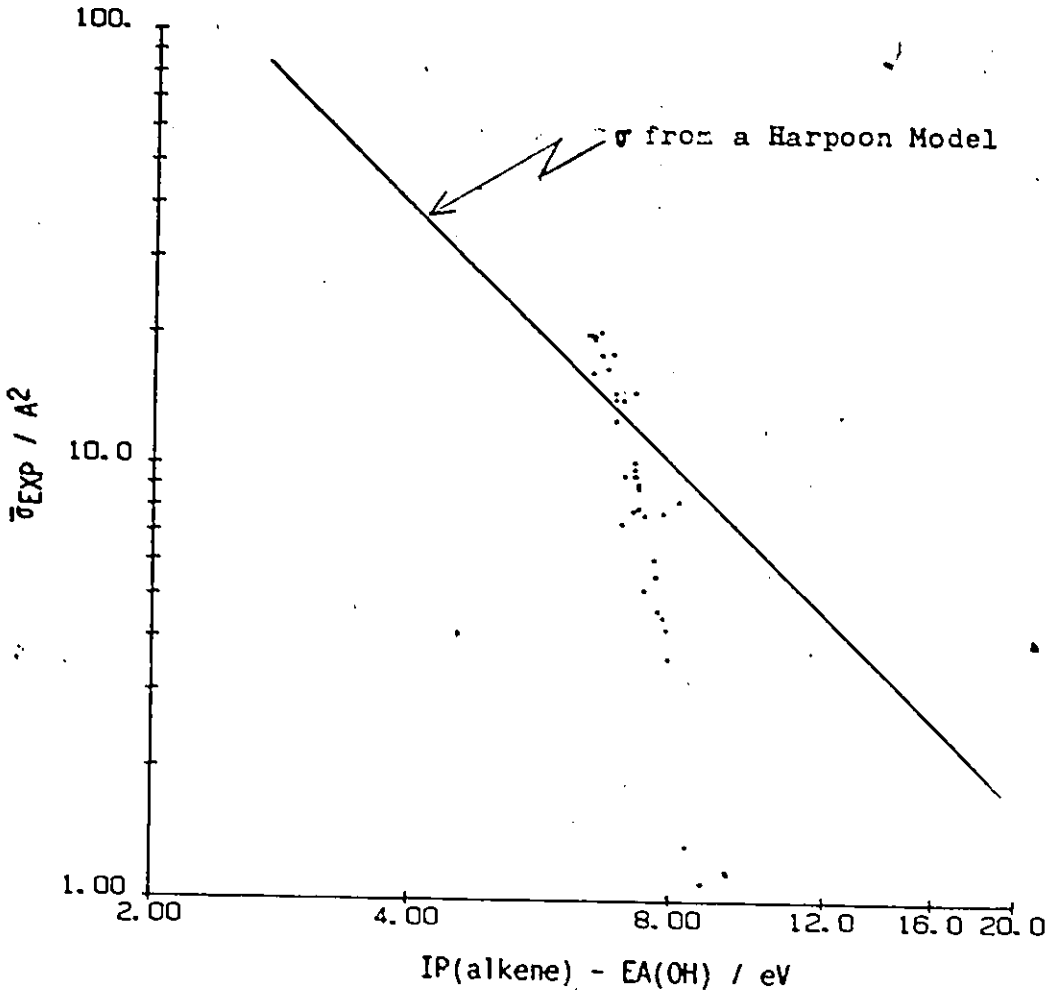

Figure IV.16

Reaction Cross Sections of a Harpoon Model (σ) and Experimental Cross Sections (σ_{EXP}) for OH-Alkene Reactions at Room Temperature as a Function of (IP - EA)

IP's are taken from references 168, 192, 193, and 194.
EA(OH) = 1.83 eV (Reference 198)
Dots are σ_{EXP}, and their values are tabulated in APPENDIX E.1.
(See page 100.)
The solid line indicates σ from a Harpoon Model.

was observed to correlate with (IP - EA), and there seems to be no potential barrier in those reactions.[199,200] They attempted to reproduce the experimentally observed trend of rate constants with (IP - EA) in their theoretical calculation of rate constants. They assumed that the ground-state radical-reactant surface (neutral) was made attractive at a large radical-reactant distance r due to the perturbation by the ion-pair surface. They assumed a long-range potential energy curve:

$$V = \frac{-H^2}{\{(IP - EA) - e^2/r\}} + \frac{H^2}{(IP - EA)}$$

where H is an empirical parameter. Although the assumption was crude and the equation was empirical, they succeeded in reproducing the trend of relative reactivities of the reactions. They suggested that the perturbation between the neutral ground surface and the ion-pair surface should be significant even for reactants with small reaction cross sections. According to this model, the smaller the IP is, the earlier the potential surface becomes attractive. Whether there is a similar ion-pair surface effect in OH-alkene reactions is not known yet.

IV.B.3.d.1.(b) Frontier Orbital Theory

Another explanation for the correlation between ln k and IP might be supplied by frontier orbital theory. According to perturbation theory, when two molecules interact weakly, an energy change is brought about:[201]

$$\Delta E = e_Q + e_K - D + e_P$$

where ΔE is the change of the energy of reactants as they are brought together from their infinite separation, e_Q is the coulombic interaction

energy, e_K is the exchange interaction, D is the stabilization energy due to the electron delocalization interaction, and e_P is the polarization interaction energy. In most non-ionic reactions, D is found to be the most significant.[201] The frontier orbital theory[202] predicts that the interaction between the singly occupied molecular orbital (SOMO) of the OH radical and the highest occupied molecular orbital (HOMO) of an alkene molecule determines the magnitude of D:

$$D = \frac{C_r^2 \gamma_r^2}{e(SOMO) - e(HOMO)}$$

where e(SOMO) and e(HOMO) are the energy of the SOMO of the OH radical and that of the HOMO of an alkene respectively, C_r is the coefficient of the HOMO at the interacting atom r of the alkene, and γ is the exchange integral. e(SOMO) and e(HOMO) can be approximated to -EA(OH) and -IP(alkene) respectively.[201] The idea is that the destabilization caused by bond-breaking in the alkene as the OH radical approaches is compensated by the stabilization obtained by the delocalization of electronic charge over the whole OH-alkene adduct. Alkenes have only a limited range of IP values (~3 eV). Although D is expected to show a curvature when it is plotted against IP over a large range of IP, it might appear linearly related to IP over a small range of IP. Often the relative reactivities are interpreted as being due to the differences in D which affect the activation energies. The result is that a smaller value for the IP of an alkene leads to a larger value of D, a smaller E_a, and finally a larger k value. It is known that the apparent activation energies of O-alkene and S-alkene reactions corre-

late with the IP of the alkenes.[81] On the other hand, the apparent activation energies of the OH-alkene reactions are negative, and without much variation from one alkene to another. One might assume that there is no barrier in the potential energy surface of the OH-alkene reactions. In such a case, the larger the D value is, the earlier the attractive surface might set in along the reaction coordinate, resulting in the larger reactive cross section. This might be part of the reason that the ln k's of the OH-alkene reactions at room temperature could still correlate with those of the O-alkene reactions (or with those of S-alkene reactions) although the OH-alkene reactions do not seem to have any variation in the activation energies and the O-alkene and the S-alkene reactions do. EA's of O and S atoms and the OH radical are, however, in the order O (1.46 eV) < OH (1.83 eV) < S (2.08 eV).[198] One might wonder why the OH radical does not show various activation energies like the O and the S atoms. In addition, the OH radical is more reactive than the O and the S atoms at room temperature. One might also wonder why the OH radical is more reactive than the S atom which has a higher EA. The main difference between the OH radical and the O and the S atoms are, while the product of the reaction of the OH radical with an alkene is always a radical, the O atoms (and most likely the S atom also) produce triplet biradicals.[173] The results of the study of the distribution of the stable and unstable products of the O-ethene reactions have been successfully interpreted with a triplet biradical as an intermediate. The fraction of the intermediates which leads to a ground-state singlet surface by intersystem crossing depends on the total pressure.[173] OH-alkene reactions, on the other hand, do not show such product distribution.

One of the advantages of this theory is its ability to predict regio-selectivities. The theory predicts that the OH radical will preferentially attack the carbon of the double bond which has the higher C_r value. A product study of the OH-propene reactions found a preference for attack at the terminal carbon[162] which has a higher C_r value. There are, however, some uncertainties associated with this interpretation of the correlation shown in Figure IV.15 since an observed rate constant k is a sum of the partial rate constants of the OH radical reactions at the two carbons of the double bond with different C_r values. Experimental studies of partial reactivities at the two carbons of various OH-alkene reactions would be helpful to examine the validity of this interpretation.

IV.B.3.d.2 Entropy of Activation

In the previous section, relative reactivities were interpreted in terms of how early the attractive surface would set in, assuming the entropy behaviour does not vary much from one alkene to another. In this section, the contribution of the entropy to the relative reactivities will be examined. For a bimolecular reaction, the change of the entropy from the reactant state to the transition state (the entropy of activation) $\Delta S^{\ddagger}$ (in J deg^{-1} mol^{-1}) is,[203]

$$\Delta S^{\ddagger} = R \ln(A\, h/k_B T^2 e^2 R')$$

where R is the gas constant in J deg^{-1} mol^{-1}, A is the pre-exponential factor of the conventional Arrhenius equation in cm^3 $molecule^{-1}$ sec^{-1}, h is the Planck's constant, k_B is the Boltzmann constant, T is the temperature

(350 K was used since it was approximately the middle of the temperature range studied for most of the reactions), and R' is 1.3624×10^{-22} atm cm^3 $molecule^{-1}$ deg^{-1}. $\Delta S^{\neq}$ here is the standard-state entropy of activation $\Delta S^{o\neq}$ where the standard states chosen are one atmosphere pressure of an ideal gas. In the following discussions, all ΔS's are the standard entropy changes. Table IV.7 lists the values of $\Delta S^{\neq}$ calculated from pre-exponential factors obtained at high pressure limits of various OH-alkene reactions in the literature as well as from the present study. The values of $\Delta S^{\neq}$ are close to those of the overall entropy change of the reaction, ΔS_R, calculated using the additivity rules of Benson[203], assuming the product is an OH substituted alkyl radical. For example, $\Delta S^{\neq}$ and ΔS_R are -117 and -113 J deg^{-1} mol^{-1} for the OH-ethene reaction. This indicates the transition state for this reaction resembles the product (1-hydroxy-2-ethyl radical) in its structure. $\Delta S^{\neq}$ and ΔS_R are -104 and -121 for the OH-cyclopentene reaction, and -95 and -129 for the OH-1,3-cyclohexadiene reaction respectively in J deg^{-1} mol^{-1}. The structures of their transition states would less closely resemble those of the product states since the differences between $\Delta S^{\neq}$ and ΔS_R are larger than that for ethene reaction. Although the variation of $\Delta S^{\neq}$ among various OH-alkene reactions is fairly small (-95 to -117 J deg^{-1} mol^{-1}), the values of $\Delta S^{\neq}$ (or A) roughly correlates with IP. The smaller the IP is, the smaller the magnitude of $\Delta S^{\neq}$. If the IP determines the intermolecular distance between the OH radical and an alkene molecule at the transition state as described in the previous section (IV.B.3.d.1.), it implies that $\Delta S^{\neq}$ is a function of the intermolec-

Table IV.7

Arrhenius Parameters[a] and Entropies of Activation[b] at 350 K of Various OH-Alkene and OH Cycloalkene Reactions

Alkene	A[c]	$-E_a$ /kJ mol^{-1}	$-\Delta S^{\ddagger}$ / J deg^{-1} mol^{-1}
Ethene	2.03	3.4	117
Propene	4.85	4.2	110
1-Butene	6.53	3.9	107
Isobutene	9.51	4.2	104
cis-2-Butene	10.9	4.1	103
trans-2-Butene	10.1	4.6	103
3-Methyl-1-butene	5.32	4.4	109
2-Methyl-2.butene	19.2	3.7	98
Cyclopentene	9.6	4.3	104
Cyclohexene	10.1	4.6	103
Cycloheptene	7.9	5.4	106
1,3-Butadiene	13.9	3.9	101
2-Methyl-1,3-butadiene	25.5	3.4	96
1,3-Cyclohexadiene	26.4	4.1	95
1,4-Cyclohexadiene	16.0	4.4	100
α-Pinene	12.0	3.7	102
β-Pinene	23.6	3.0	96

a : Arrhenius parameters used here are those recommended in reference 38 except for the five cycloalkenes of the present study

b : See text for the equation to calculate $\Delta S^{\ddagger}$

c : In 10^{-12} cm^3 molecule^{-1} sec^{-1}

ular distance at the transition state, i.e. the earlier the transition state is, the larger $\Delta S^{\ddagger}$ is, implying a relatively looser transition state.

IV.B.3.d.3. Free Energy Barrier of the Reaction

The observations made in sections IV.B.3.d.1. and 2. indicate that there are many similarities between the OH-alkene reactions and the cycloaddition of singlet halocarbenes (a^1A_1) to alkenes. The recent study by Houk et al[204] is very noteworthy. They performed ab initio calculations of the cycloaddition of difluoro-, dichloro-, and dibromocarbenes (CF_2, CCl_2, and CBr_2) to alkenes. The CCl_2 addition reactions are particularly interesting. Relative reactivities with the various alkenes indicate the electrophilic character of the singlet dichlorocarbene.[205] It has been found experimentally that the relative reactivities of various alkenes are fairly independent of temperature for CCl_2 cycloaddition,[206,207] which is also true for OH-alkene reactions since the apparent activation energies are fairly constant. In the preliminary calculations, Houk et al[204] found neither an intermediate complex nor a potential energy barrier along the reaction coordinate in the CCl_2 reactions with ethene, propene, and isobutene. For CCl_2-alkene reactions, the potential energy at the transition state was found to be smaller than the reactant state. They also found that the entropy decreased linearly with the intermolecular distance r when r was smaller than 4 A in cycloadditions of CF_2, CCl_2, and CBr_2 to ethene. The entropy curve was found to be fairly independent of the nature of the carbenes. They approximated the entropy surface for $r \leq 4$ A to[204]

$$S\ (\text{cal deg}^{-1}\ \text{mol}^{-1}) = 10.35\ r(A) - 56.67$$

Combining the semi-empirical curves (inverted Morse functions) of potential energy with the above entropy equation, they obtained the free energy curves shown in Figure IV.17 for cycloadditions of CF_2, CCl_2, and CBr_2 to isobutene and 2,3-dimethyl-2-butene. Although no potential barrier was assumed in CCl_2 and CBr_2 reactions, substantial free energy barriers were observed in those reactions. The position of the transition state was determined mainly by how early the floor of the potential curve dropped. The magnitude of the free energy barrier was determined mainly by the entropy at the transition state. The earlier the potential curve became attractive, the earlier the transition state was attained and the smaller the magnitude of $\Delta S^{\ddagger}$. The values of $\Delta H^{\ddagger}$ were negative in the CCl_2 and CBr_2 reactions. In the case of the CCl_2 reactions, $\Delta H^{\ddagger}$ turned out to be fairly constant as the reactant was varied. The prediction of the model was that the relative reactivities would be independent of temperature and this was observed experimentally. Thus, the results of their calculations for the CCl_2-alkene reactions show many similarities to the OH-alkene reactions. Houk et al[204] interpreted the results of their calculations as implying that even when there is no potential energy barrier, there is "a dynamic barrier arising from the fact that the low-frequency translation and rotations of reactants are converted into relatively high-frequency vibration of the product"[204] which narrows the reaction path. If this is true also for the OH-alkene reactions, the temperature independence of the ratio of the vibrational partition functions in equation (iv.10) of transition-state theory (page 94) might be appropriate in the interpretation using a transition-state theory model. It is not known yet what this

Figure IV.17

Profiles of ΔH, $T\Delta S$, and ΔG for Halocarbene Reactions with Isobutene and Tetramethylethene Calculated by Houk et al (Reference 204)

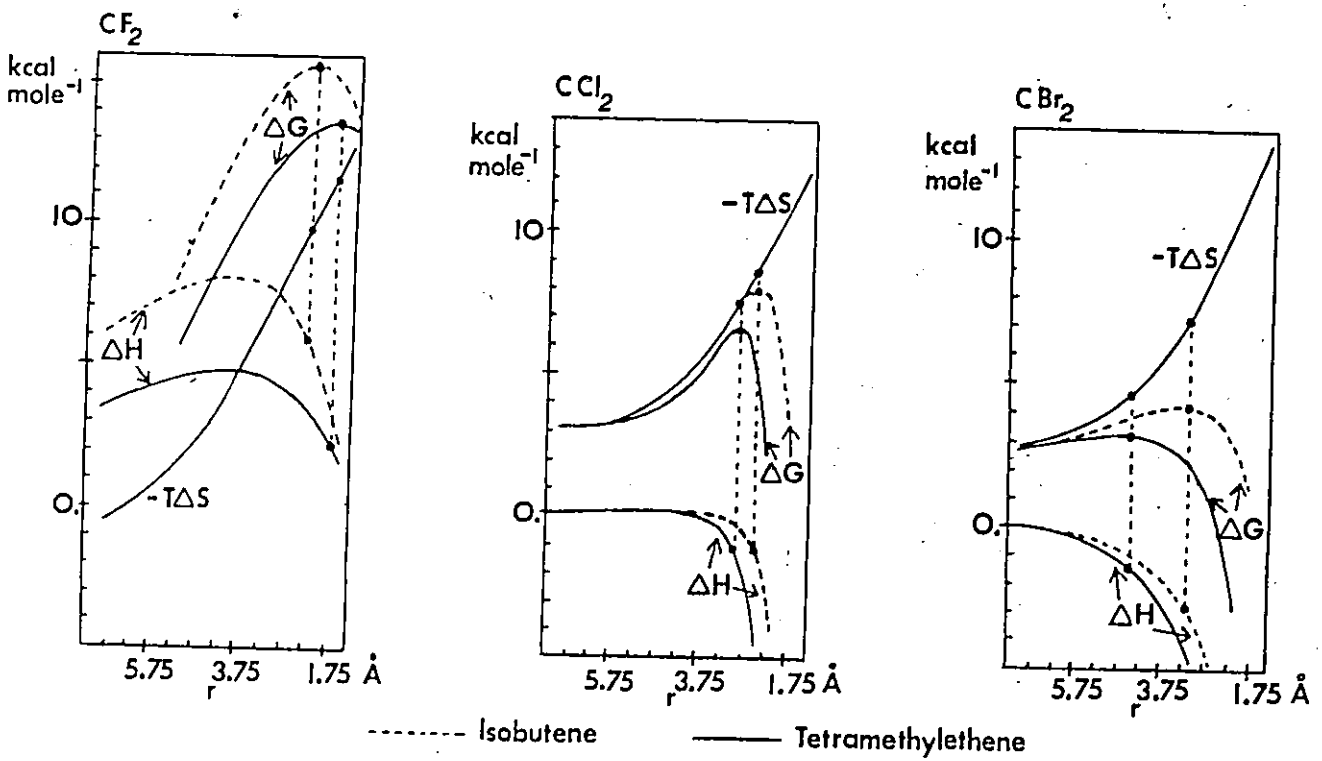

implies in the collision theory.[204]

It is also interesting to note that in the calculations reported by Houk et al,[204] the less reactive CF_2 showed a variety of potential energy barriers depending on the alkene partner. As a result, the potential barrier determined the free energy barrier in this case, and the transition state would occur at a similar intermolecular distance r resulting in a similar $\Delta S^{\ddagger}$, i.e. similar pre-exponential factors for various alkenes. This CF_2 case seems to be very similar to the behaviour of the O-alkene reactions. It is known experimentally that the relative reactivities of CCl_2 and CF_2 with various alkenes correlate at room temperature,[205] as do the OH- and the O-alkene reaction reactivities. Since substantial experimental data for OH-alkene reaction have now become available, theoretical studies, i.e. ab initio calculation of the potential surfaces of the OH-alkene reactions, should be pursued soon to explain the unusual features of the reactions.

IV.B.4. The Atmospheric Implication of the OH-Cycloalkene Reactions

Some cycloalkenes have been detected in the ambient air, gasoline, and automobile exhaust. (Table IV.8)[117,118] From smog chamber experiments, it has been known that even when they are present as traces in the NO_x/air mixture, cycloalkenes and dialkenes can form aerosols more easily than straight-chain monoalkenes.[117] Organic aerosols of photochemical smogs have been found to contain a significant amount of difunctional compounds (dicarboxylic acids, dialdehydes, oxocarboxylic acids, oxo-alcohols),[208,209] and cycloalkenes are considered to be their major source.[117]

Table IV.8

Some Cycloalkenes Detected in the Troposphere[a]

Cycloalkene		
Cyclopentene	A, G, FF	2 - 9 ppb[b]
1-Methylcyclopentene	A, G	Detected[c]
3-Methylcyclopentene	A, G	
Cyclohexene	A, G, RA	10.7 ppb[b]
1-Methylcyclohexene	A, RA	4.7 ppb[b]
3-Methylcyclohexene	A, G	
4-Methylcyclohexene	A, G	
1,4-Cyclohexadiene	RC	Detected[c]

A : Automobile exhaust
G : Gasoline
FF : Forest fire
RA : Rubber abrasion
RC : Refuse combustion
a : From reference 117 (pp466,467) and 118 (pp96 - 102)
b : Detected in Los Angeles
c : Detected but no quantitative measurement is available

In the gas phase, cycloalkenes are thought to react first with either the OH radical or O_3 to become involved in the atmospheric reactions. Table IV.9 compares the rate constants of the OH radical and the O_3 reactions with the five cycloalkenes of the present study. Although the OH radical reacts with alkenes much faster than O_3, their relative importance depends on the concentrations of the OH radical and O_3 in the ambient air. Table IV.9 also lists halflives of the cycloalkenes due to the OH reaction only and those due to both the OH radical and the O_3 reactions. The concentrations of the OH radical and O_3 assumed to be constant at 3×10^5 and 10^{12} molecule cm^{-3} respectively.[210] These concentrations are the average annual concentration and the background concentration respectively. The concentration of O_3 can reach several tenths of ppm (1ppm = 2.5×10^{13} molecule cm^{-3}) during the daytime in the summer and the early fall when the atmosphere is polluted.[210] The concentration of the OH radical also will increase approximately proportionally during the same period of the year.[210] The overall relative importance of the two reactions would be maintained almost the same[210] except at local points where the OH radical concentration builds up more quickly than the O_3 concentration. From the comparisons of halflives in Table IV.9, it is clear that the O_3 reactions would be largely responsible for the initial reaction of cycloalkenes except for 1,4-cyclohexadiene with which O_3 reacts relatively slowly. As pointed out in section IV.B.1 of this chapter, the OH radical reacts with cycloalkenes insensitively to their ring structures. Although the reasons are not known yet, O_3 has been observed to have some steric preferences in

Table IV.9

Rate Constants of the OH and the O_3 Reactions with Some Cycloalkenes and Halflives of the Cycloalkenes due to Those Reactions in the Troposphere

Cycloalkene	$k_{OH} \times 10^{12}$ a	$t_{1/2(OH)}$ b	$k_{O3} \times 10^{16}$ c	$t_{1/2(OH\&O_3)}$ d
Cyclopentene	54.3	12	2.75	0.66
Cyclohexene	65.1	10	1.04	1.6
Cyclheptene	71.9	8.9	3.19	0.57
1,3-Cyclohexadiene	137.4	4.7	19.7	0.096
1,4-Cyclohexadiene	96.1	6.7	0.639	2.08

a : From this work's results, in cm^3 $molecule^{-1}$ sec^{-1}

b : $t_{1/2(OH)} = \ln 2/(60.^2 k_{OH}[OH])$ assuming $[OH] = 3 \times 10^5$ molecule cm^{-3}

c : From reference 211 in cm^3 $molecule^{-1}$ sec^{-1}

d : $t_{1/2(OH\&O_3)} = \ln 2/\{60.^2(k_{OH}[OH] + k_{O3}[03])\}$ assuming $[OH] = 3 \times 10^5$ and $[O_3] = 10^{12}$ molecule cm^{-3}

Both $t_{1/2}$'s are in hours.

its reactions with cycloalkenes.[211] The OH radical, therefore, can become an important source of initial reactions of cycloalkenes in the atmosphere only under the following conditions:

1. under the local conditions which build up the OH radical concentration more quickly than that of O_3,
2. with a cycloalkene whose reaction with O_3 is stericly hindered.

IV.C. Summary of This Chapter

The OH-cycloalkene reactions proceed either by addition or by hydrogen abstraction. Various previously reported estimations of the relative importance of hydrogen abstraction, especially allylic hydrogen abstraction, were examined. Although more direct experimental studies are necessary to determine the exact extent of allylic hydrogen abstraction, it was concluded that allylic hydrogen abstraction should be of a similar order to that of alkyl hydrogen abstraction. Thus, the addition process is expected to be predominant in the reactions of the OH radical with cycloalkenes.

The rate constants of the OH-cycloalkene reactions depend on temperature in a manner similar to that displayed by the rate constants of the OH-alkene reactions. In terms of the conventional Arrhenius equation theory, all exhibit activation energies which are negative and have values approximately 4 - 5 kJ. This corresponds to the temperature-dependent factor of $T^{-1.5}$ in the non-Arrhenius equation. This feature of the kinetics has been considered from three view points. Simple collision theory cannot explain the behaviour unless an unrealistic assumption was made. Transition state theory can explain the observed value of negative

apparent activation energies if the newly formed C-OH bond does not have low vibrational frequencies. A theory involving a weakly bound complex can explain the negative activation energies, but cannot explain why their magnitudes were almost constant for the variety of alkenes and cycloalkenes. Comparison of the relative reactivities and thermodynamic parameters of various OH-alkene and the OH-cycloalkene reactions with those of the cycloaddition of singlet dichlorocarbene to alkenes suggests many similarities between these reactions. It was proposed that the model used to explain the kinetics of dichlorocarbene cycloaddition reactions might be extended to cover the interpretation of the OH-alkene reactions. The model involves no potential energy barrier or minimum, but does involve a free energy barrier, which determines the relative reactivity of various alkenes. It was suggested that ab initio molecular orbital calculations should be performed to determine the potential energy surfaces for the OH-alkene reactions.

The OH-cycloalkene reactions would not be as significant as the O_3-cycloalkene reactions in the troposphere because of the relatively high concentration of O_3, although the rate constants of the OH reactions are much higher than those of the O_3 reactions. The OH reactions would become significant only when the O_3 concentration is relatively low and/or the O_3 reactions are stericly hindered.

CHAPTER V

REACTIONS OF THE OH RADICAL WITH SELECTED AROMATIC COMPOUNDS

V.A. Reactions of the OH Radical with Benzene and Chlorobenzene at Various Temperatures

V.A.1. The OH + Benzene Reaction

V.A.1.a. Experimental Results

The OH-benzene reaction was studied at temperatures between room temperature (295 K) and 424 K. At room temperature it was studied at three different total pressures: 50, 100, and 200 torr. Decay curves at room temperature deviated from the single exponential form at longer times. Figure V.1 shows some examples of such decay curves at room temperature. Apparent first-order rate constants were determined from approximately the first three halflives where the deviation from exponentiality was negligible. Table V.1 lists observed first-order rate constants with various benzene concentrations at room temperature for three different total pressures. As seen in the table, when the flash energy was varied from 18 to 36 J with a constant benzene concentration, decay curves remained exponential at least for the first four halflives, but observed first-order rate constant slightly increased with the flash energy. For the rest of the benzene concentrations, the flash energy was maintained at 25 J. Figure V.2 shows the rate constants versus concentration plots at room temperature for three different total pressures. Indicated error bars are one standard deviation of the least square calculations. The observed

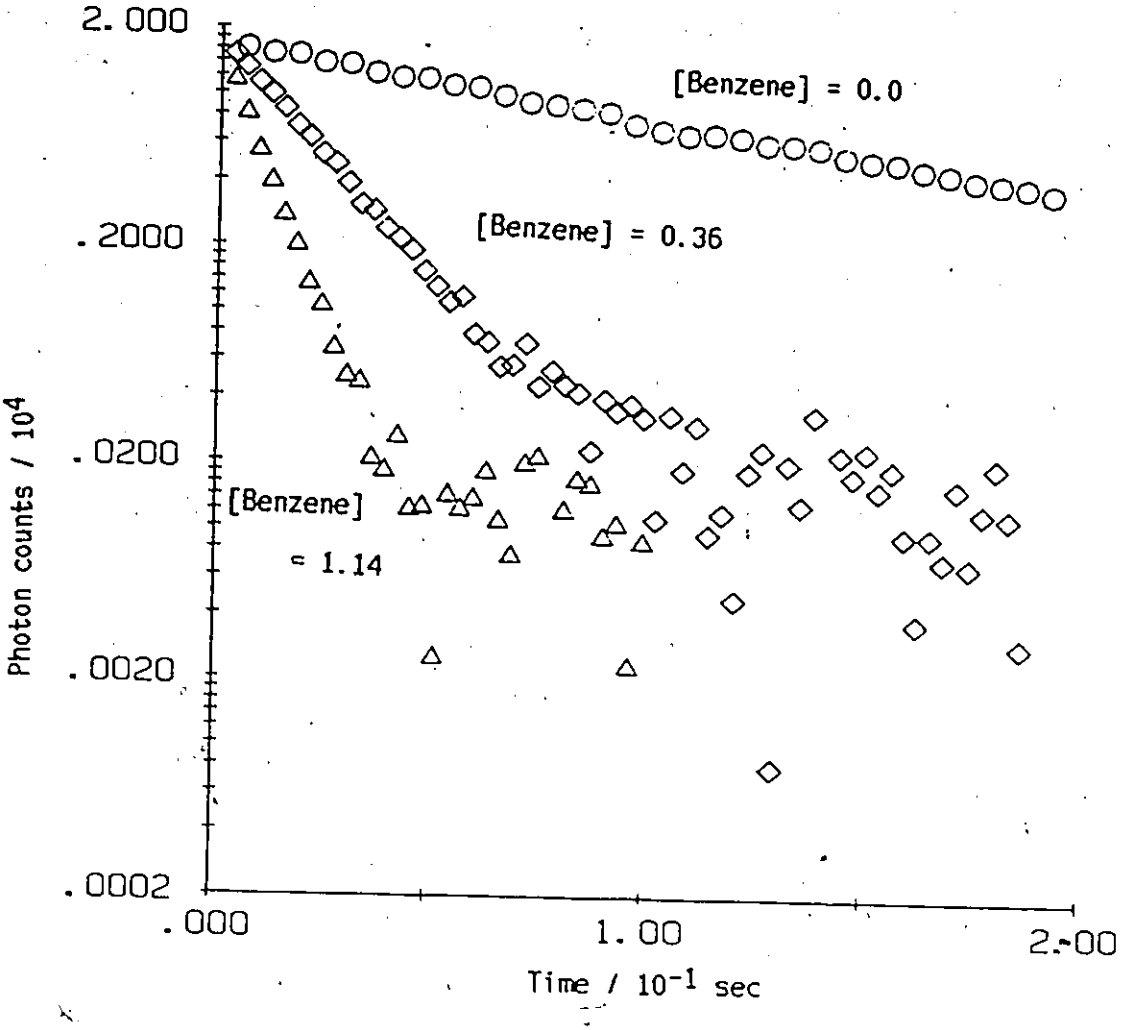

Figure V.1

Some Examples of Observed Decay Curves for the OH + Benzene Reaction at Room Temperature

The average background has been subtracted.
Benzene concentrations are in 10^{14} molecule cm^{-3}.

Table V.1

Observed First-Order Rate Constants of the OH-Benzene Reaction at 295 K

P_{tot}/torr	[Benzene]/10^{14} molecule cm^{-3}	k_{obs}/sec^{-1} (a)
49	0.47 ± 0.03	74.0 ± 1.0
	0.92 ± 0.06	(b)103.1 ± 2.0
	0.92 ± 0.06	109.1 ± 1.6
	0.92 ± 0.06	(c)117.4 ± 1.6
	1.34 ± 0.09	165 ± 3
	2.15 ± 0.14	243 ± 7
	3.01 ± 0.19	341 ± 7
100	0.53 ± 0.04	86.0 ± 1.5
	1.10 ± 0.08	152 ± 4
	2.03 ± 0.14	260 ± 5
	2.83 ± 0.20	356 ± 9
	3.44 ± 0.24	429 ± 12
200	0.66 ± 0.05	108.7 ± 2.1
	1.48 ± 0.10	190 ± 4
	2.31 ± 0.14	288 ± 13
	3.43 ± 0.21	406 ± 12
	5.57 ± 0.34	641 ± 44

The flash energies used are
a : 25 J (unless otherwise indicated)
b : 18 J
c : 36 J

Indicated errors are one standard deviation of the least square calculations.

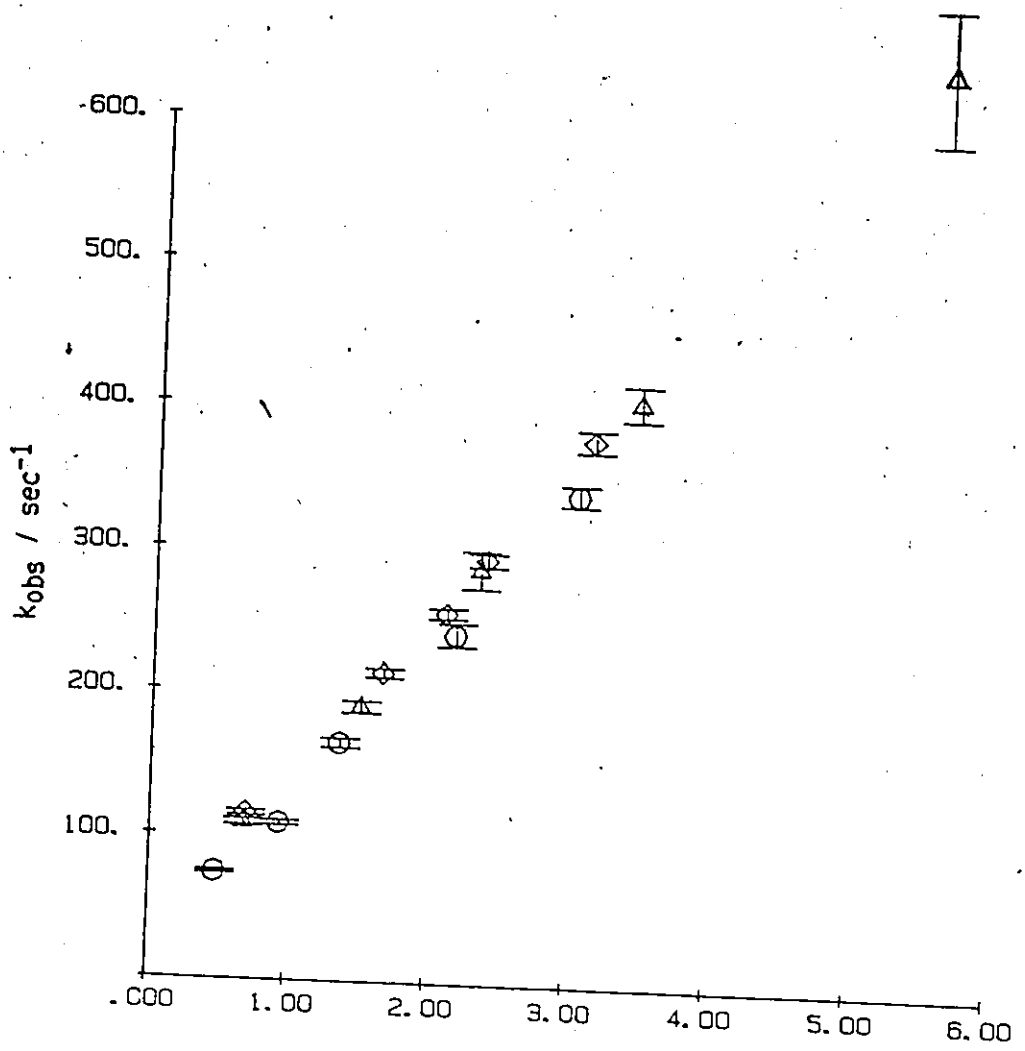

Figure V.2

k_{obs} versus Concentration Plot of the OH + Benzene Reaction at 295 K

○ P_{tot} = 49 torr
◇ P_{tot} = 100 torr
△ P_{tot} = 200 torr

first-order rate constants were proportional to the concentration of benzene. The second-order rate constants at room temperature are compared with literature values in Table V.2.

In the studies of the reaction at higher temperatures, the total pressure was maintained at 100 torr, and the flash energy at 25 J. At 308 K, the deviation from the exponentiality set in at a slightly earlier time. About two halflives were used to determine decay rates at this temperature. Apparent first-order rate constants are plotted against the concentration of benzene in Figure V.3. Error bars are not indicated. The slope gave a second-order rate constant of 1.2×10^{-12} cm^3 $molecule^{-1}$ sec^{-1}, which is higher than that at room temperature. At 323 and 340 K, the non-exponentiality set in even earlier. In Figure V.4, an example of decay curves at 340 K is compared with those at 295 K and 418 K with similar benzene concentrations. The slopes of decay curves at 323 and 340 K were initially large and then became smaller until eventually they corresponded to the decay rates in the absence of a reactant. For example, at 340 K, the rate approached ~20 sec^{-1} at longer time. From the initial slopes, k_{obs}'s were roughly calculated at 323 K and plotted in Figure V.3. They were roughly linearly correlated with the concentration of reactant with the slope of 1×10^{-12} cm^3 $molecule^{-1}$ sec^{-1}. No attempt was made to calculate the slopes at 340 K since the non-exponentiality became very obvious within the first halflife at this temperature. Above 392 K, the observed decay curves were all simple exponential, an example of which at 418 K is shown in Figure V.4. The plots of the first-order rate constants versus the concentration of benzene were, however, not linear as shown in Figure V.5. Therefore,

Table V.2

High-Pressure-Limit Second-Order Rate Constants of the OH-Benzene Reaction at Room Temperature

T (K)		$k / 10^{-12}$ cm^3 molecule^{-1} sec^{-1}	P (torr)	Reference
295		1.02 ± 0.10[a]	50 Ar	
		1.05 ± 0.04[a]	100 Ar	This
		1.07 ± 0.04[a]	200 Ar	work[f]
	Average	1.06 ± 0.03[a']		
298		1.59 ± 0.12[b]	100 He	212[f]
298		1.24 ± 0.12[c]	50, 100, &200 Ar	213[f]
298		1.20 ± 0.15[c]	~100 Ar	120[f]
298		1.24 ± 0.09[a]	50 ~ 200 Ar	122[f]
295		0.88 ± 0.04[d]	100 Ar	131[g]
298		1.16 ± 0.25	42, 112 He	123[g]
296		1.0 ± 0.2[c]	100 He	195[g]
304		< 2.62		102[h]
300		0.85[e]		160[h]
~300		0.93		161[h]

a : Two standard deviations
a': Two standard deviations(Internal consistency)
b : One standard deviation
c : The estimated overall accuracy
d : Three standard deviations
e : The uncertainty is a factor of 2
f : The flash photolysis-resonance fluorescence technique
g : The laser photolysis-resonance fluorescence technique
h : The relative rate technique

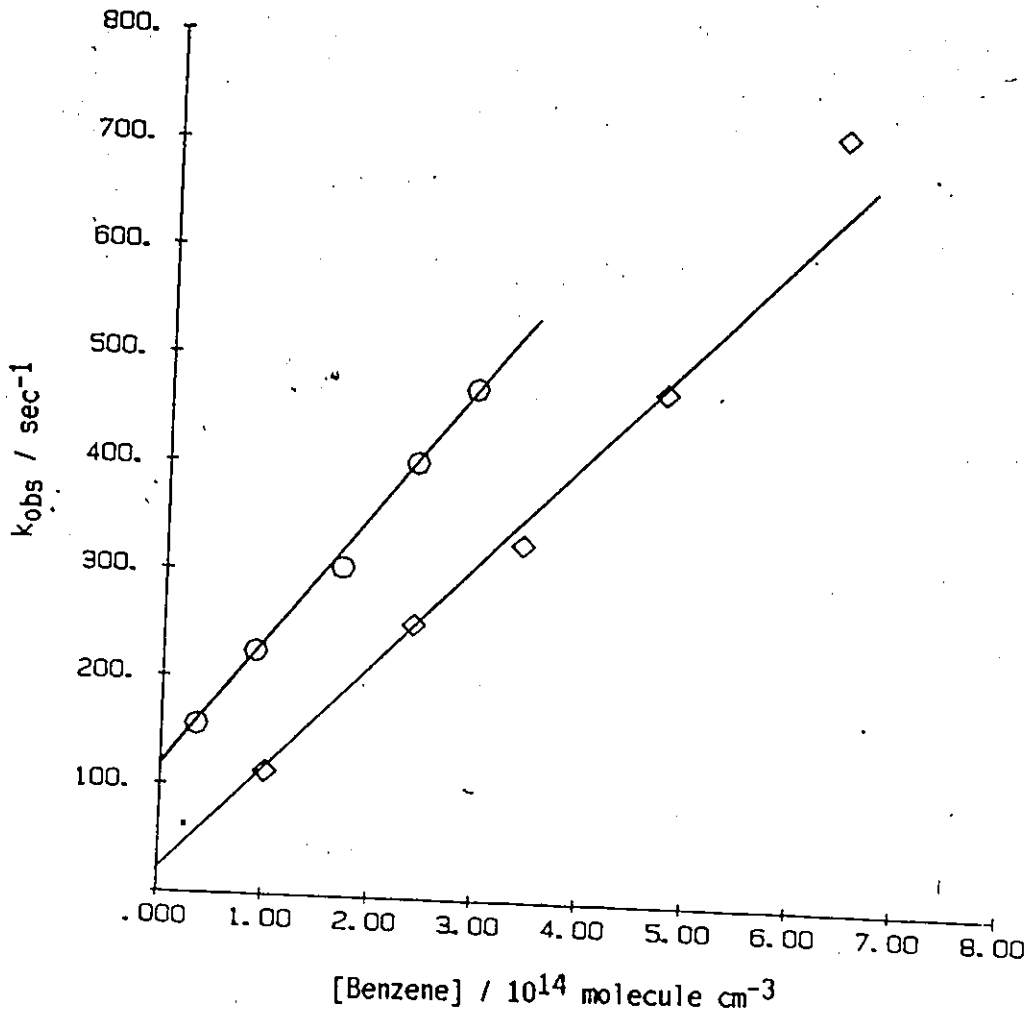

Figure V.3

Apparent k_{obs} versus Concentration Plot of the OH + Benzene Reaction at 308 K and 323 K (P_{tot} = 100 torr)

○ T = 308 K (Shifted upward by 100 sec^{-1})
◇ T = 323 K

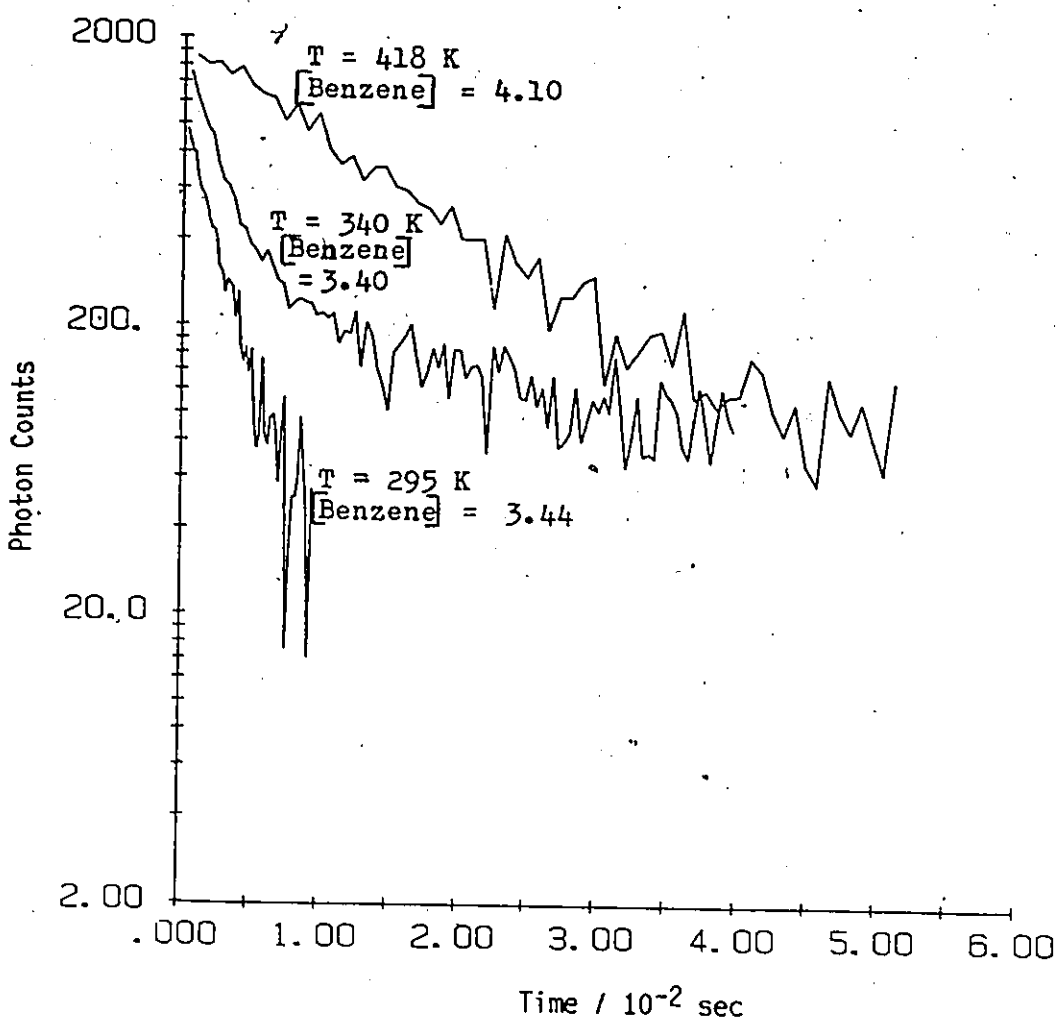

Figure V.4

Observed Decay Curves of the OH + Benzene Reaction at Three Different Temperatures with Similar Benzene Concentrations

Benzene concentrations are in 10^{14} molecule cm^{-3}.

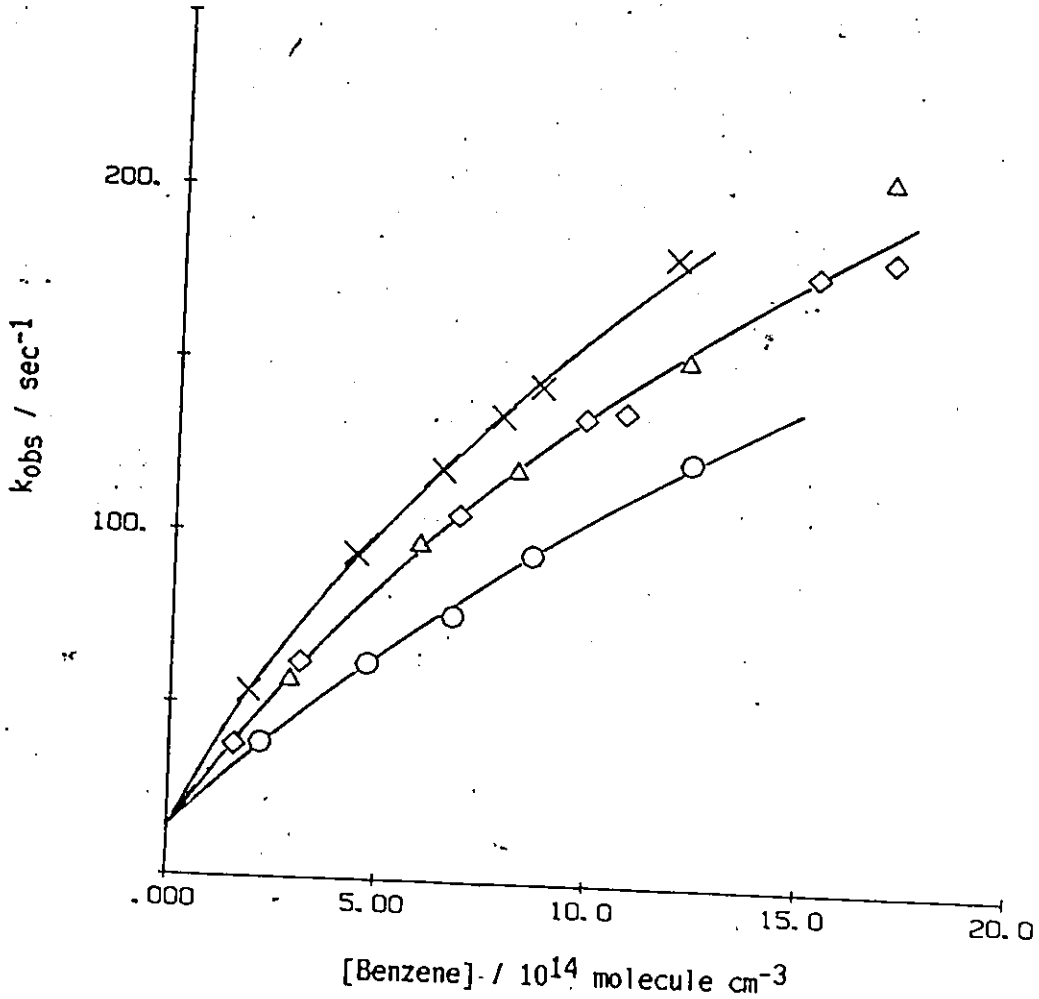

Figure V.5

k_{obs} versus Concentration Plot of the OH + Benzene Reaction at 392, 406, 416, and 424 K (P_{tot} = 100 torr)

○ T = 392 K
◇ T = 406 K
△ T = 416 K
× T = 424 K

the second-order rate constants were not calculated above 392 K. (Approximate tangential slopes of the k_{obs} versus concentration plot are 0.13, 0.16, 0.16, and 0.21 x 10^{-12} cm^3 $molecule^{-1}$ sec^{-1} at 392, 406, 416, and 424 K respectively.) Observed decay rates at temperatures above 392 K were very slow compared with those at room temperature. (Compare decay curves observed at 295 and 418 K in Figure V.4.) The maximum temperature of this study was 424 K. At higher temperatures, observed rate constants showed a dependence on the flash energy similar to that at room temperature.

V.A.1.b. Discussion

In this section, first the room temperature results of the OH-benzene reaction will be compared with those previously reported. Second, the mechanism of the reaction will be discussed with emphasis on the kinetic behaviour at higher temperatures. Finally the possibility of a π complex as an intermediate in the reaction will be considered.

V.A.1.b.1. Comparison of the Present Results at Room Temperature with Those Previously Reported

The rate constant of the OH-benzene reaction is known to depend on the total pressure at low pressures.[123,212] Above 50 torr, it has been observed to be independent of the pressure when argon is the diluent gas.[122,123,195,213] No significant pressure dependence was observed between 50 and 200 torr in the present study. (Table V.2) The variation of the rate constant within this pressure range was within two least-square standard deviations. Therefore, 50 torr can be considered above the high-pressure limit. The overall accuracy of the room temperature rate constant was estimated to be ~20%. This relatively high uncertainty is due to the

cablibration of the concentration using u.v. absorption at 253 nm. Previously reported values of the rate constants at room temperature vary from 0.88 to 1.59 x 10^{-12} cm^3 $molecule^{-1}$ sec^{-1} from flash (or laser) photolysis-resonance fluorescence experiments as shown in Table V.2. The value of the rate constant at room temperature of the present study agrees within experimental error with most of the listed values. The value 1.59 x 10^{-12} cm^3 $molecule^{-1}$ sec^{-1} reported by Davis et al[212] is the highest value obtained with the FRRP technique. The reason for the discrepancy between their value and all the other values is not known. The value 0.88 x 10^{-12} cm^3 $molecule^{-1}$ sec^{-1} reported by Wahner and Zetzsch[131] is the lowest. Since the same group (Rinke and Zetzsch[195]) recently reported a somewhat higher value (1.0 x 10^{-12} cm^3 $molecule^{-1}$ sec^{-1}), there seems to be a systematic error in the value obtained earlier by Wahner and Zetzsch[131]. Presently available results from the relative rate techniques[102,160,161] are not as precise as those from the absolute techniques. The values obtained by the absolute techniques are within the range of values estimated with the relative rate techniques. Recently, Atkinson[38] recommended a value of 1.28 x 10^{-12} cm^3 $molecule^{-1}$ sec^{-1} with an uncertainty of 30% as the room-temperature (298 K) rate constant of the OH-benzene reaction. This was calculated from the Arrhenius equation which was derived from ten rate constants obtained by Hansen et al[213], Perry et al[120], Tully et al[122], and Lorenz and Zellner[123] in the temperature range between 244 and 325 K using absolute techniques. (Four of the ten rate constants were measured at room temperature.) This recommended value is higher than the values of the rate constant actually obtained at room temperature by the same groups

although they are within the estimated uncertainty. Therefore, the recommended value seems to be slightly overestimated. This is largely because the rate constants obtained at temperatures lower and higher than room temperature are scattered. It would be more reasonable to take the recommended value at room temperature from the average of the values obtained at room temperature: 1.15×10^{-12} cm^3 $molecule^{-1}$ sec^{-1} is obtained from the values measured with absolute techniques shown in Table V.2 except the values reported by Davis et al[212] and Wahner and Zetzsch.[131]

The variation of the observed first-order rate constant with the flash energy is somewhat larger than can be accounted for by random error. As described in CHAPTER III, the presence of secondary reactions can lead to an effect of the flash energy on the observed kinetics of the reaction. Since the flash energy effect was observed only in the OH-benzene reaction, and not in the experiments with H_2, alkenes, or cycloalkenes, its potential source is the reaction of the OH radical with either a photolysis product (R·) of benzene or a product of the OH-benzene reaction. The variation of the flash energy did not alter the exponentiality of the decay curves, and the simulation study (See APPENDIX B.2.) suggests that the reaction with a photolysis product of benzene might be the source. In the present study the range of the experimental conditions was limited and it was not possible to investigate systematically the significance of this secondary process. It would be ideal to vary the flash energy (especially to the lower energies) at various benzene concentration. This would require significant further improvement in the S/N ratio. Four groups[122,195,212,213] have studied the OH-benzene reaction using the same vacuum u.v flash photolysis of H_2O as the source of OH radicals. Results

of Davis et al[212] indicated a similar small trend when the flash energy was varied between 45 and 180 J with a CaF_2 window ($\lambda > 125$ nm) in front of the flash lamp, but they did not make any comments on it. Hansen et al[213] (and Perry et al[120]) claimed that the variation of the flash energy between 25 and 50 J with a LiF window ($\lambda > 105$ nm) did not show any change in rate constants beyond the experimental errors, but the size of their experimental errors is not clear. Tully et al[122] used a Suprasil lens ($\lambda > 165$ nm), and claimed that the variations in the photolysis flux or in the initial concentration of the OH radical did not show any indication of significant secondary reactions, but the details of their investigation were not reported. Rinke and Zetzsch[195] reported that the second-order rate constant did not change as a LiF window was replaced with a Suprasil window ($\lambda > 165$ nm) with the flash energy of 15 J although individual k_{obs}'s became somewhat smaller according to Figure 5 of their paper. Lorenz and Zellner[123] used laser photolysis of HNO_3 at either 248 or 193 nm as a OH radical source, but did not observe any influence of the laser energy on the rate constant. Since neither quantum yields are known of various photolysis products of benzene under vacuum u.v. radiation in the gas phase, nor the rate constants of the OH radical reactions with them, it is not possible at present to estimate quantitatively the extent of the effect of the reactions of the OH radical with the photolysis products of benzene. If the results of the present study were more susceptible to the secondary reactions with the photolysis products than those reported by other groups, one would expect the rate constant of the OH-benzene reaction obtained in the present study to be higher than those obtained by other groups. (See

APPENDIX B.2.) The rate constant obtained in the present study, however, agrees well with the majority of the rate constants previously obtained by other groups using different flash energies and windows. Therefore, the rate constants reported in the present study are reliable second-order rate constants free from significant secondary reactions, at least within the estimated overall accuracy (20%).

V.A.1.b.2. Mechanism of the OH-Benzene Reaction and the Effect of Temperature

The OH radical can react with benzene either by addition to the benzene ring, by hydrogen abstraction, or by direct hydrogen elimination:

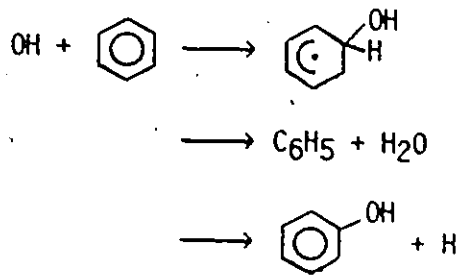

At room temperature, however, the latter two processes can be considered to be very minor because there was no isotope effect on the kinetics of the reaction at room temperature,[122,123] and also from the extrapolation of results at higher temperatures[120,122,123,214] where the first process becomes practically negligible because of its fast backward reaction. Kinetics of the reaction at higher temperature will be discussed later in this section.

The pressure dependence of the rate constants observed at lower total pressures (< 40 - 50 torr in argon) at room temperature[123,212] indicates the formation of an energy-rich adduct in the addition process

which is stabilized by collisions with other molecules:

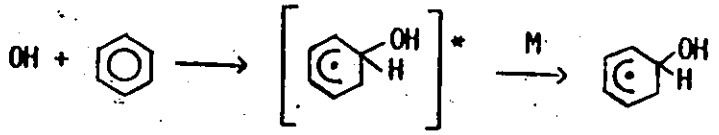

The study of the reaction at various temperatures might reveal the energetics of this addition process.

V.A.1.b.2.(a) Comparison of the Present Results with Those Previously Reported on the Temperature Dependence of the Kinetics

The temperature dependence of the OH-benzene reaction was first studied by Perry et al[120] at temperatures between room temperature and 422 K with a flash photolysis-resonance fluorescence technique. Tully et al[122] extended the study to the temperature range 250 - 1017 K and used the same technique. Tully et al[122] observed four ranges of temperatures which showed different apparent kinetics. They can be summarized as follows;

(i) At room temperature and below

---Exponential decays were observed.

---A linear relationship was observed between k_{obs} and the concentration of benzene.

---No isotope effect was observed with d_6-benzene.

(ii) 320 - 390 K

---Non-exponential decays were observed.

---The initial slopes versus the concentration plot was "concave upward" at lower rates and linear at higher rates at 352 K.

---The overall rate decreased with temperature.

(iii) 400 - 500 K

---Exponential decays were observed.

---A non-linear ("concave downward") relationship was observed between k_{obs} and the concentration.

---The overall rate increased with temperature.

(iv) Above 500 K

---Exponential decays were observed.

---A linear relationship was observed between k_{obs} and the concentration.

---The second-order rate constant increased with temperature more rapidly than in the range (i).

---A significant isotope effect was observed with d_6-benzene.

Perry et al[120] had made similar observations earlier in ranges (i) and (ii). They, however, had reported a linear relationship between k_{obs} and the concentration in temperature range (iii). Tully et al[122] commented that this was probably because the range of first-order rate constants studied by Perry et al[120] was too small to observe the concave shape. The observed temperature dependence of the reaction at the high pressure limit was qualitatively explained with the following mechanism by both groups:[120,122]

$$OH + C_6H_6 \longrightarrow H_2O + C_6H_5 \qquad (1)$$

$$OH + C_6H_6 + M \longrightarrow C_6H_6OH + M \qquad (2)$$

$$C_6H_6OH + M \longrightarrow OH + C_6H_6 + M \qquad (-2)$$

$$C_6H_6OH \longrightarrow \text{LOSS BY DIFFUSION} \qquad (3)$$

$$OH \longrightarrow \text{LOSS BY DIFFUSION} \qquad (4)$$

Although Lin and Lin[215] a few years later claimed from their calculations that the direct hydrogen elimination was more important than hydrogen abstraction (1) at higher temperatures, recent experiments by Madronich and Felder[214] indicated the opposite. For the present discussion, both are considered to be included in the rate constant k_1. The observed kinetic behaviour in the various temperature ranges was qualitatively explained by this mechanism as follows. At lower temperatures (range (i)), reactions (1) and (-2) are slow compared with reaction (2). At higher temperatures (ranges (iii) and (iv)), reaction (-2) becomes very significant, reaction (2) is practically closed, and reaction (1) becomes dominant. Range (ii) is where the transition takes place between these two phenomena. Whether non-exponentiality would be observed or not depends on two things: the lifetime of the adduct which is determined primarily by k_{-2}, and the time scale of the experiments which is determined by the kind of experimental technique used. Perry et al[120] roughly estimated the rate constant k_{-2} = 100 sec^{-1} at 350 K which is the middle of the temperature range where the non-exponentiality was observed in decay curves with the flash photolysis-resonance fluorescence technique. They also calculated its activation energy by assuming the pre-exponential factor $A_{-2} = 3 \times 10^{13}$ sec^{-1} which was taken from that of the decomposition of cyclohexadienyl radical. The estimated activation energy was $E_{-2} = 78.2 \pm 8.4$ kJ mol^{-1}.[120]

More quantitative analyses of the mechanism were desired in order to examine whether all of the observed features of the reaction, especially in ranges (ii) and (iii), could be explained. The present study initially intended to quantitatively analyze decay curves at various temperatures

using the proposed mechanism to obtain not only k_2 but also k_1 and k_{-2} more precisely for benzene, and to extend the study to halogenated aromatics. Later, Wahner and Zetzsch[131] showed in their paper that the previously proposed mechanism predicted a biexponential form for the decay curves of the OH radical concentration.

$$I/I_0 = [OH]/[OH]_0 = I_{0f} \exp(-k_f t) + I_{0s} \exp(-k_s t) \qquad (v.1)$$

where I/I_0 is the observed intensity of fluoresence relative to the initial intensity, $[OH]/[OH]_0$ is the concentration of the OH radical relative to the initial value, and

$$I_{0f} = \frac{(k_f - d)^2}{bc + (k_f - d)^2} \qquad (v.2)$$

$$I_{0s} = \frac{bc}{bc + (k_f - d)^2} \qquad (v.3)$$

$$k_f = \frac{a + d}{2} + \left(\frac{(a - d)^2}{4} + bc \right)^{1/2} \qquad (v.4)$$

$$k_s = \frac{a + d}{2} - \left(\frac{(a - d)^2}{4} + bc \right)^{1/2} \qquad (v.5)$$

$$a = k_1[C_6H_6] + k_2[C_6H_6] + k_4 \qquad (v.6)$$

$$b = k_{-2} \qquad (v.7)$$

$$c = k_2[C_6H_6] \qquad (v.8)$$

$$d = k_{-2} + k_3 \qquad (v.9)$$

They also found that at lower temperatures, the ratio of I_{0f}/I_{0s} could be approximated to

$$\frac{I_{0f}}{I_{0s}} \approx \frac{(k_1 + k_2)^2}{k_{-2}k_2}[C_6H_6] + \text{constant} \qquad (v.10)$$

From their experimentally obtained decay curves at longer times at 295 and 312 K, similar to the curves shown in Figure V.1, they estimated I_{0f}/I_{0s} for a limited range of benzene concentrations. The range was limited because I_{0s} became too small to estimate at higher benzene concentrations. The initial slopes of the decay curves were assumed to be proportional to $(k_1 + k_2)[C_6H_6]$, and $k_1/(k_1 + k_2)$ was assumed to be 0.05 from the estimation by Perry et al.[120] The values of k_{-2} were estimated to be 1.95 and 11.5 sec^{-1} at 295 and 312 K respectively. The activation energies of k_{-2} (i.e. E_{-2}) were estimated to be 74.5 ± 5.7 kJ mol^{-1} at 295 K by assuming the same pre-exponential factor $A_{-2} = 3 \times 10^{13}$ sec^{-1} as that used by Perry et al,[120] and 80 ± 15 kJ mol^{-1} at 312 K when A_{-2} was assumed to be 3×10^{14} sec^{-1}. They showed that the decay curves at long times at room temperature could be fitted to the biexponential function (v.1) with rate constants of k_1, k_2, and k_{-2} obtained as described above. The agreement between the calculated and the experimental decay curves seemed to be fairly good except that the longer tail of experimentally observed curves appeared to decay slightly faster than the calculated curves (in Figure 3 of their paper[131]). Their method can be used only in lower temperature range where

k_{-2} is very small in order to satisfy the conditions of their approximation. About the same time, Lorentz and Zellner[123] studied the reaction at temperatures between 244 and 523 K with the laser photolysis-resonance fluorescence technique using HNO_3 as a OH precursor. In their paper, however, there was no report of non-exponentiality of decay curves in temperature range (ii), although the overall rate decreased with temperature, consistent with the results by Perry et al,[120] Tully et al[122], and the present study. No curvature was observed in k_{obs}-concentration plot in range (iii) by Lorentz and Zellner.[123]

The present study reported the results of experiments in temperature ranges (i), (ii), and (iii) of Tully et al.,[122] and attempted to clarify some of the inconsistencies noted in the literature. Although an attempt was made to use a quartz reaction cell to extend the study to higher temperatures, it was unsuccessful because of high scattered background light levels. Observations made in the present study in ranges (i) to (iii) are in agreeement with those by Tully et al[122], except that the overall rates of the reaction in the present study were generally smaller than theirs. Figure V.6 summarizes graphically the temperature dependence of the reaction studied by Perry et al[120], Tully et al[122], Lorentz and Zellner,[123] Madronich and Felder,[214] and the present study. Although the general trends of overall rates from the various studies are very similar, there are quantitative discrepancies, especially in temperature ranges (ii) and (iii). As Lorentz and Zellner pointed out,[123] a part of the reason for the discrepancy is due to the way the overall rate constant was determined when the decay curve was not exponential within the experimental time

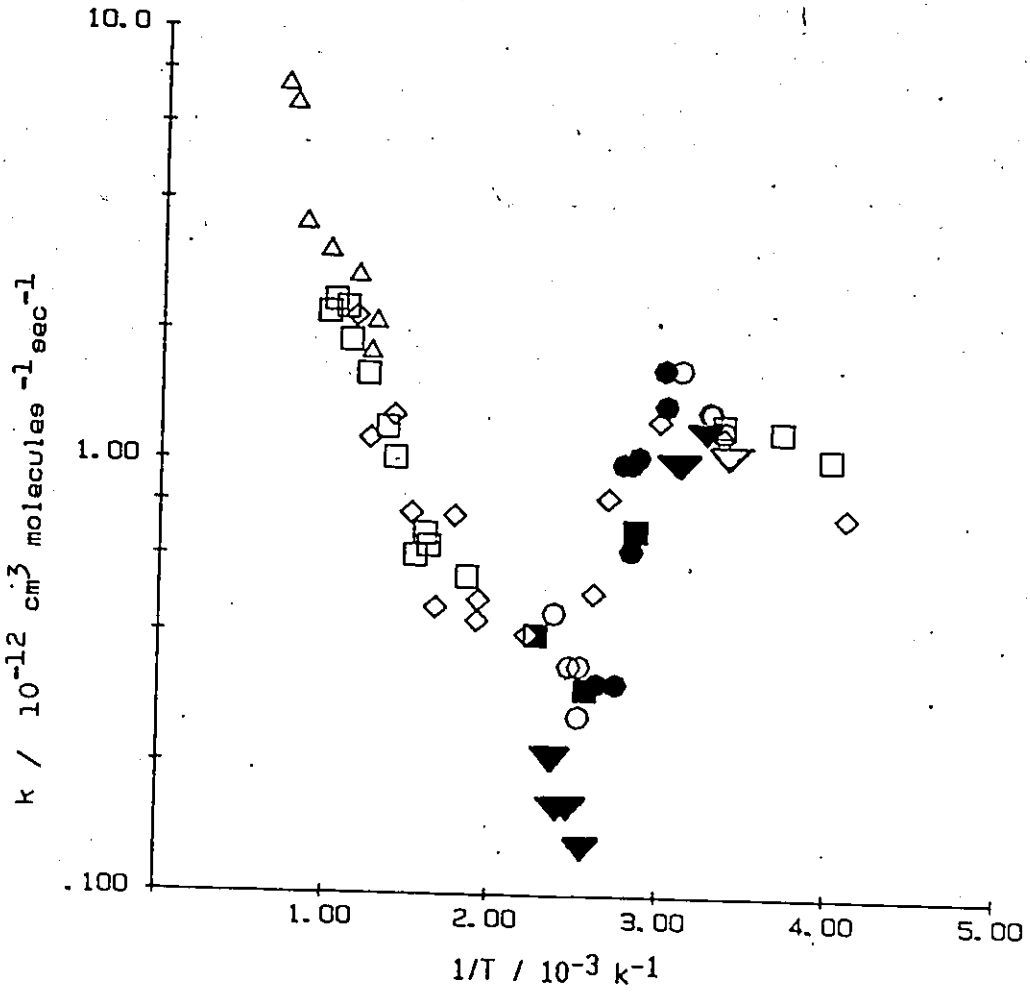

Figure V.6

Temperature Dependence of the Second-Order Rate Constant of the OH + Benzene Reaction Studied by Various Groups

Perry et al (Reference 120)
Lorenz and Zellner (References 38 & 123)
Madronich and Felder (Reference 214)
Tully et al (Reference 122)
This work

Filled symbols are either where non-exponential decay curves were observed and their initial slopes were used to calculate k_{obs}, or where non-linearity was observed in k_{obs} versus concentration plots, and their tangential slopes were taken as apparent k.

scale. This, however, applies only in temperature range (ii), since exponential decays were observed in range (iii). Potential reasons for these discrepancies were investigated, and they will be described in the following section.

V.A.1.b.2.(b) Curve Fitting and Computer Simulation of Decay Curves

Since the proposed mechanism predicts a very explicit form (v.1) for the decay curves of the OH radical concentration, it was decided to attempt to fit a biexponential function (v.1) directly to observed decay curves. I_{0f}, k_f, I_{0s}, and k_s could then be determined in the intermediate temperature range (ii) without making assumptions or approximations such as those made by Wahner and Zetzsch.[131] A non-linear least square method, Marquardt's algorithm,[216] was employed for the curve fittings. Since at room temperature I_{0s} is very small under the typical experimental conditions, it was thought that decay curves at slightly higher temperatures (311 K and 340 K) might be easier to fit. Decay curves with fairly good S/N ratios were collected in the experiments for which curve fittings were attempted. Although various methods were used to estimate the initial values of the parameters, experimental data could not be fitted to a biexponential function with any reasonable precision. There seem to be two major reasons for the failure, even if one could assume that the mechanism was correct. First, the values of k_f and k_s were always very different ($k_f/k_s > 10$), and consequently dwell times of multichannel analyzer appropriate for k_f were not appropriate for k_s and vice versa. Therefore, it was difficult to set the criteria to determine the appropriate dwell time and the goodness of the fit. Secondly, since k_s was of the order of a few

sec^{-1} in the temperature ranges (i) and (ii) with typical concentrations of benzene, this slower exponential curve would have been susceptible to the variation in the rate of diffusion as mentioned in CHAPTER III.D..

An alternative approach to the interpretation of the experimental data obtained in the different temperature ranges was chosen. The decay curves were simulated by computer calculation of the equation (v.1) at the various temperatures and using benzene concentrations in the typical experimental range. Because of the limited temperature range of the present study, the Arrhenius equations of k_1, k_2, and k_{-2} from the literature were used. The computer simulations were used to check whether the mechanism, and specifically equation (v.1), could explain the observations made by Tully et al[122] and the present study, especially in ranges (ii) and (iii). They may also be able to explain why there are discrepancies in the experimental results reported by the different groups. The following rate constants were used in computations:

$k_1 = 3.5 \times 10^{-11} \exp(-2300/T)$ cm^3 $molecule^{-1}$ sec^{-1} (Reference 214)

$k_2 = 3.1 \times 10^{-12} \exp(-270/T)$ cm^3 $molecule^{-1}$ sec^{-1} (Reference 122)

$k_{-2} = 3. \times 10^{13} \exp(-9020/T)$ cm^3 $molecule^{-1}$ sec^{-1} (Reference 131)

$k_3 = 2. \times (T/295.)$

$k_4 = 8. \times (T/295.)$

The function of k_4 was chosen to fit observed decay curves without reactant at various temperatures. A similar temperature dependence factor was used for k_3.

The apparent rate constants k_{app} were calculated from simulated

decay curves:

$$k_{app}(i) = \frac{\ln 2.}{t(i) - t(i-1)}$$

where i stands for i-th halflife, and t(i) is the time when the concentration of the OH radical becomes $1/2^i$ of the initial concentration. $k_{app}(i)$ is, therefore, the (approximated) first-order rate constant during the i-th halflife. The value of k_{app} was usually calculated for the first four to six halflives (i.e. i=1,2,$\cdots$,6). If all $k_{app}(i)$ values from a simulated decay curve coincide, it indicates that the curve cannot be distinguished from the single exponential curve since its halflife is constant. The following observations (1) --- (4) were made from the computed results of $k_{app}(i)$'s and their comparison with experimental results.

(1) 295K (range (i))---Figure V.7 shows some examples of k_{app} versus i-th halflife plots of simulated decay curves. The magnitude of k_{app} clearly decreases with time indicating the second exponential component in equation (V.1) becomes significant with time. The variations within the first three halflives are, however, within 10%, and the average value of $k_{app}(1)$ to $k_{app}(3)$ is approximately k_2[benzene] + k_4. Thus, using the first three halflives to determine the k_2 value at room temperature in the experiments can be justified according to the proposed mechanism. It was also found that the decay rate approaches 2 sec^{-1} at long time (> 50 msec) in any of the simulated decay curves, while in the experiments it was slightly faster, i.e. 5 ~ 15 sec^{-1}. This might be because the assumption of the first-order decay for the diffusion process of the OH radical might be

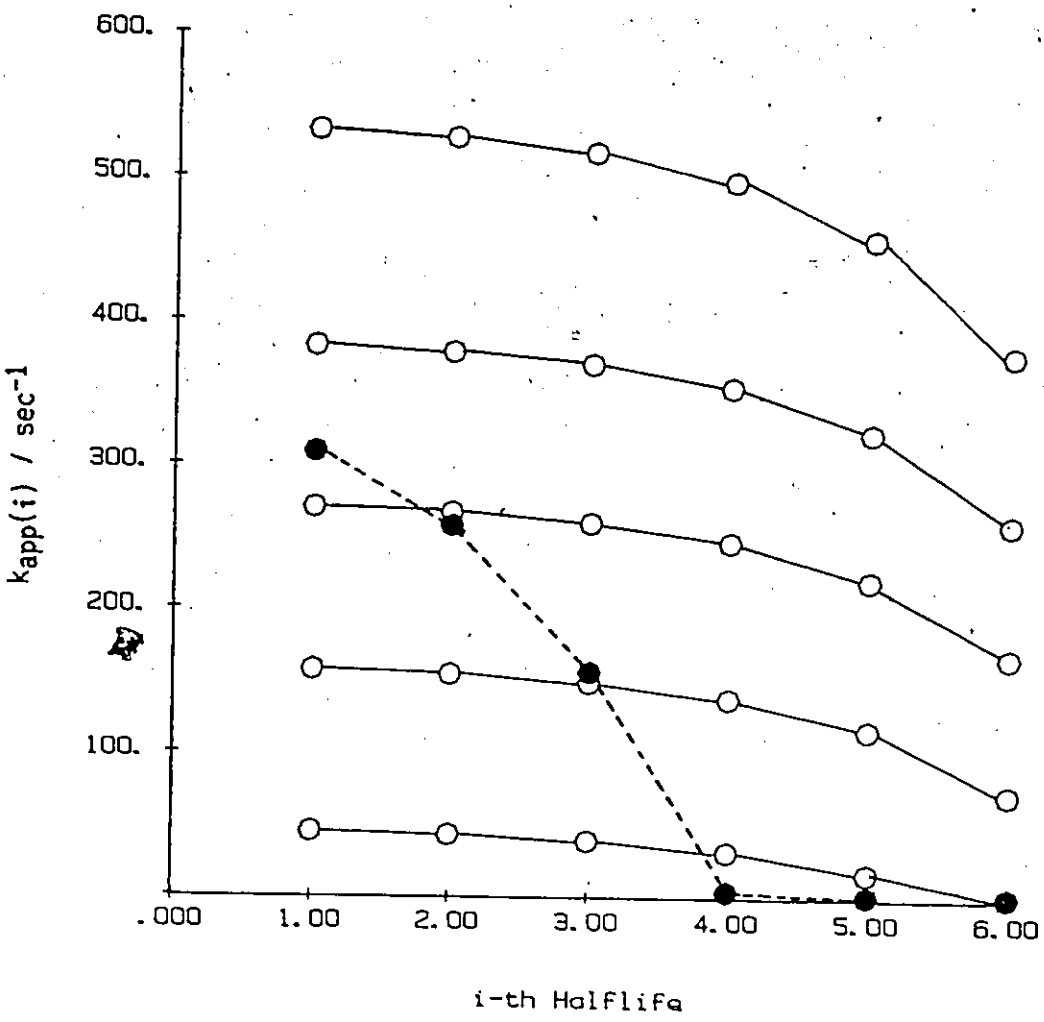

Figure V.7

$k_{app(i)}$ versus i-the Halflife of the OH + Benzene Reaction at 295 and 323 K : Results of a Simulation Study

Blank symbols : 295 K
Filled symbols : 323 K

inappropriate at longer times in the experiments.

(2) 323 ~ 352 K (range (ii))---The k_{app} values at these temperatures decrease very markedly with time in simulated decay curves, and non-exponentiality becomes apparent within 1 ~ 2 halflives; an example, shown by a dashed line is given in Figure V.7. The solid line in Figure V.8 shows a plot of $k_{app}(1)$ versus the concentration of benzene at 323 K which appears linear. The slope of the plot is smaller than the value of k_2 at room temperature. This is in accordance with the result of the present study except for the difference in the absolute values of the slopes. This is because the value of k_2 obtained from the Arrhenius equation by Tully et al[122] was higher than that of the present study. The plot of $k_{app}(1)$ versus concentration at 352 K gives a concave upward curve at lower concentrations and becomes linear at higher concentration with a slope approaching k_2.(The dashed line in Figure V.8) This is in accordance with the observation by Tully et al[122] at the same temperature. The simulation predicts that the observations of such concave upward curves followed by linear regions depend on the delay time used in the experiments. With longer delay times one might observe concave downward curves instead of concave upward curves, since the most of the fast component of the biexponential form would be missed, and the observed decay curves would become similar to those in range (iii). The decay rates at longer time (> 50 msec) due to the second component of the biexponential curve in simulated decay curves are less than 10 sec^{-1} while in experiments they were faster (~ 20 sec^{-1}). This could be caused by diffusion problem mentioned previously.

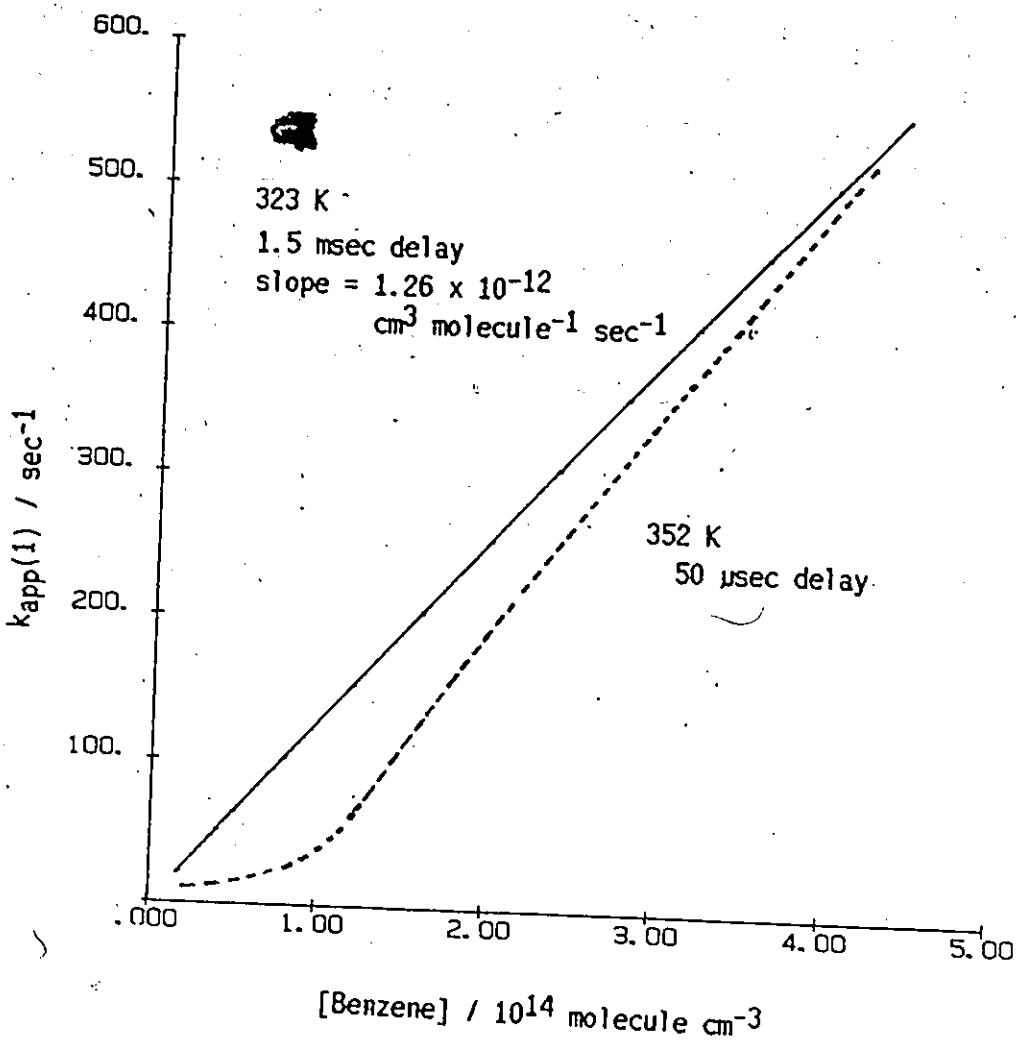

Figure V.8

$k_{app(1)}$ versus Concentration Plot of the OH + Benzene Reaction at 323 and 352 K : Results of a Simulation Study

(3) 390 ~ 500 K (ranges (iii) and (iv))---Above 390 K, when a delay time the same as the experiments was used, simulated decay curves were single exponential again (i.e. all $k_{app}(i)$'s are constant) and $k_{app} = k_s$ (in equation v.1). This agrees with the results of the present study as well as those by Perry et al [120] and Tully et al.[122] The first exponential component is so fast at these temperatures that only the second component would be observed by the time the multichannel analyzer is triggered in the flash photolysis-resonance fluorescence technique. Figure V.9 shows in the solid lines the simulation results as a plot of k_{app} versus the concentration at various temperatures between 390 and 500 K. At lower temperatures, curves are "downward concave" as observed by Tully et al[122] as well as in the present study. The dashed linear lines in the same figure indicate k_1[benzene] + k_4, i.e. sum of the abstraction (and/or elimination) rate constant and the diffusion rate constant at corresponding temperatures. As the temperature increases the two lines become closer, so that at 500 K they cannot be distinguished, and k_{app} becomes linear with concentration. This supports the observation by Tully et al[122] of normal second-order kinetics above 500 K, and according to the proposed mechanism, the determination of the Arrhenius parameters of abstraction process (1) from the kinetic data obtained above 500 K is justified.

(4) Sensitivity of Decay Curves toward E_{-2} and an Additional Reaction of the Adduct---It was found that the temperature range (ii) in the simulation results was very sensitive to the activation energy of reaction (-2), and the value of 75 kJ mol^{-1} proposed by Wahner and Zetzsch[131] seemed to be a reasonable value to fit the results of the present study if the pre-

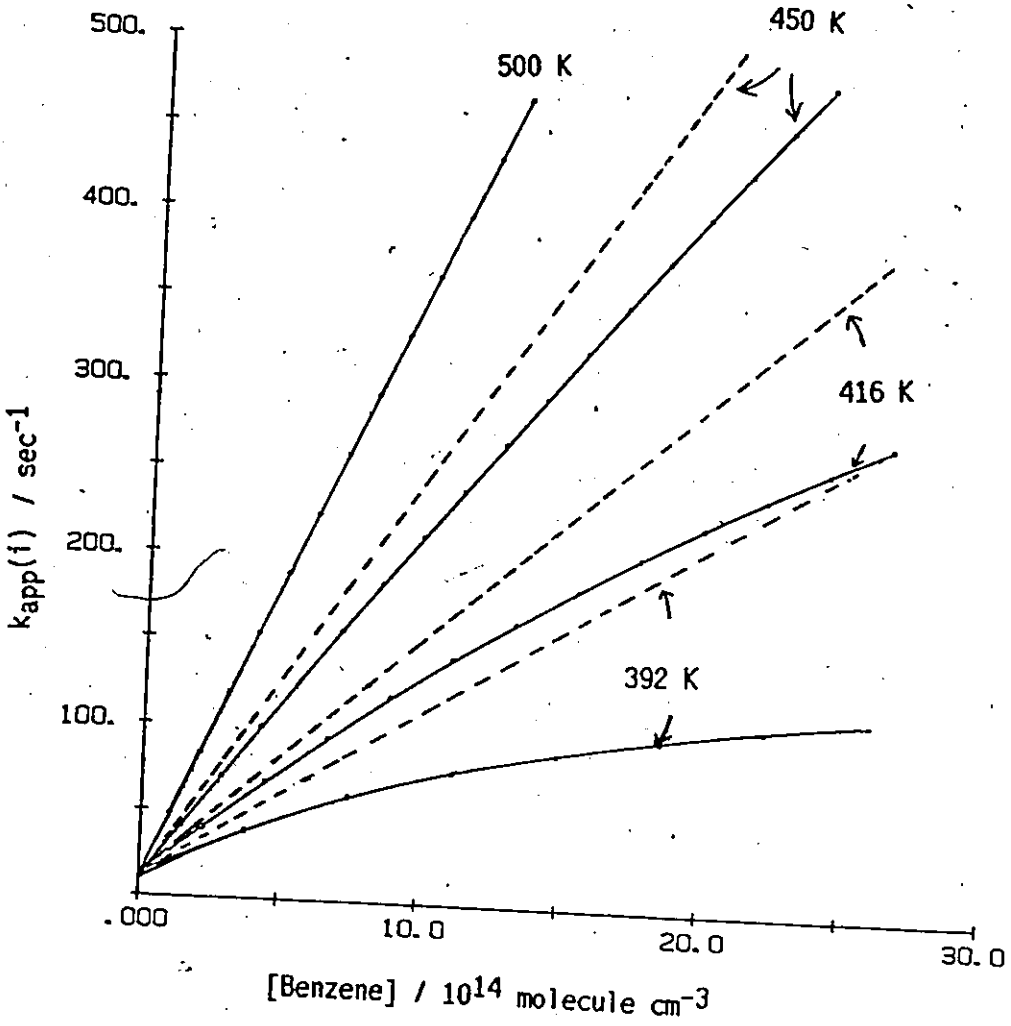

Figure V.9

k_{app} and k_1[benzene] + k_4 versus Concentration Plot of the OH + Benzene Reaction at Temperatures between 390 and 500 K : Results of a Simulation Study

——— k_{app}
----- k_1[benzene] + k_4

exponential factor 3×10^{13} sec^{-1} was assumed. (The variation of A_{-2} by a factor of 10 affects E_{-2} by only ~6 kJ mol^{-1} within the temperature range of the present study.) As E_{-2} becomes larger, the non-exponentiality range (ii) shifts to a higher temperature, and vice versa. If E_{-2} is changed by 10 kJ mol^{-1}, range (ii) shifts by 40 - 50 degrees. If the proposed mechanism is correct, E_{-2} is essentially the dissociation energy of C-OH bond of the adduct.[120] Therefore, where range (ii) is located is an indication of the energetic stability of the adduct state relative to that of the reactant state. Tully[152] and Tully and Goldsmith[146] studied the temperature dependence of the OH-ethene and OH-propene reactions at temperatures between 291 and 591 K and 293 and 896 K respectively, with the laser photolysis-laser induced fluorescence technique. They observed the temperature dependence of these reactions to be very similar to those of OH-benzene reactions, but range (ii) was shifted to higher temperatures than that of the OH-benzene reaction. For example, range (ii) was located at temperatures > 438 K for ethene[152] and 500 ~ 700 K for propene[146] reactions. Since the mechanism of these reactions seems to be similar to the proposed mechanism of the OH-benzene reaction, and the pre-exponential factors A_{-2} of these reactions (2.4×10^{13} sec^{-1}) calculated from those of their forward reactions are similar to A_{-2} of the OH-benzene reaction (3.0×10^{13} sec^{-1}), the shift of range (ii) to lower temperatures for the benzene reaction indicates that the adducts of OH-benzene are less stable than the adducts of OH-ethene and OH-propene. This difference might be because some resonance stabilization is lost in the adduct formation of the

OH-benzene reaction.

When there is a path for the thermalized adduct to undergo reactions other than dissociation back to the reactants, with a first-order rate constant k_5, equations v.7 and v.9 become

$$b = k_{-2} + k_5 \qquad (v.7')$$

$$d = k_{-2} + k_3 + k_5 \qquad (v.9')$$

The severity of the non-exponentiality of decay curves in range (ii) and non-linearity of k_{obs} versus concentration plots in range (iii) diminishes as the rate of the additional path (k_5) is increased. It also gives higher overall rates in both ranges (ii) and (iii). This might partly explain why the rates obtained by Lorentz and Zellner[123] are generally higher than those in other studies done in these ranges. There might have been a reaction of the adduct with HNO_3 and/or NO_2(as a photolysis product or an impurity in HNO_3). In ranges (ii) and (iii), relatively higher concentrations of benzene had to be used in the experiments because of the slower overall rate of the reaction. The adduct reaction with benzene or photolysis products of benzene might become very significant in those ranges. This might have caused some discrepancies among the various studies if their experimental conditions (e.g. the concentration ranges and the flash energies) differed from each other. The reason for the smaller overall rates of the reaction observed in the present study in ranges (ii) and (iii) than those reported in other studies might be that the experimental conditions of the present study were relatively free from secondary reactions in those ranges.

In summary, the proposed mechanism can explain the observed effect of temperature on the kinetics of the OH-benzene reaction, particularly the results by Tully et al[122] and the present study. The main reasons for the deviations seem to be the uncertainties associated with the diffusion loss of the OH radical at longer time when the reactant is present, and additional adduct reactions which might become significant, particularly in temperature ranges (ii) and (iii).

V.A.1.b.3. A π Complex as an Intermediate in the OH-Benzene Reaction

Perry et al[120] pointed out the possible existence of a π complex as an intermediate in the reaction of the OH radical with benzene. Radicals would not readily form a Dewar-type π complex with a molecule which involves a covalent bond since an extra electron has to reside in an antibonding orbital.[217] The π complex of the OH radical-benzene, if it exists, might be a complex which is not covalently linked, such as donor-acceptor, charge-transfer, molecular complex. The definition of a π complex itself has been ambiguous in the past.[217] One might define a π complex as one in which the OH radical is not localized on a particular carbon atom of the benzene molecule but has freedom to move around the ring because it interacts with the π electrons of the benzene ring as a whole. A σ complex might be defined as one in which the OH radical is localized on a particular carbon. Perry et al,[120] proposed a mechanism for the OH-benzene reaction involving a π complex as an intermediate:

$$\text{OH} + \text{benzene} \underset{b}{\overset{a}{\rightleftharpoons}} \pi \text{ complex} \underset{d}{\overset{c}{\rightleftharpoons}} \sigma \text{ complex}$$

Recently, Fritz et al[218] observed the hydroxylcyclohexadienyl radical (σ

complex) at room temperature using long-path continuous wave-u.v.-laser absorption at 308 nm after the laser photolysis of HNO_3 in the presence of benzene. They found that the initial rate of formation of the hydroxyl-cyclohexadienyl radical was equal to the decay rate of the OH radical within the experimental error. This might indicate that the σ complex is readily formed at room temperature and that the dissociation to produce extra OH radicals observed at higher temperatures is that of the σ complex. The observed kinetics can be interpreted simply without assuming a π complex as an intermediate. However, since the quantum yield of the σ complex is not yet known, the possibility still remains that the π complex might exist in equilibrium with the σ complex. In this case, the π complex would be relatively stable and its dissociation would be responsible for the production of extra OH radicals at higher temperatures. Molecular orbital calculations would be helpful to find out whether the OH-benzene system has any potential minimum as the reactants approach one another. If it does, it would be interesting to see whether or not the OH radical is localized at a particular carbon on the benzene ring at the potential minimum.

V.A.2. The OH + Chlorobenzene Reaction

V.A.2.a. Experimental Results

The OH radical reaction with chlorobenzene was studied at temperatures between room temperature and 421 K at a total pressure of 100 torr. In addition, it was studied at 50 and 200 torr at room temperature. Decay curves deviated from the single exponential form at longer time at room temperature (295, 296, and 297 K) and at 310 K, i.e. similar to the OH-benzene reaction at room temperature. Approximately the first three halflives were used to calculate first-order rate constants at those temperatures. When the flash energy was varied between 18 and 36 J, the observed first-order rate constant increased with the flash energy, but the variation was within two standard deviations of the least square calculations of the rate constant. For the rest of the experiments, the flash energy was maintained at 25 J. Observed rate constants are plotted against the concentration in Figures V.10 and 11. Indicated error bars are one standard deviation of the least square calculations. Table V.3 lists the second-order rate constants at those temperatures together with available literature values. The variation of the total pressure did not affect the rate constant at room temperature as seen in the table. The rate constant at 310 K was the same as that at room temperature. The estimated overall accuracies of the rate constants at those temperatures are ~9%. At 328 K, the decay curves deviated markedly from exponentiality after the second halflife. The first-order decay rates obtained from the first two halflives were very close to those at room temperature. (Figure V.11) At 361 K, non-exponentiality set in within the first halflife and the decay rates of the slower part of the curves were ~20 sec^{-1}. At 396 K, decay

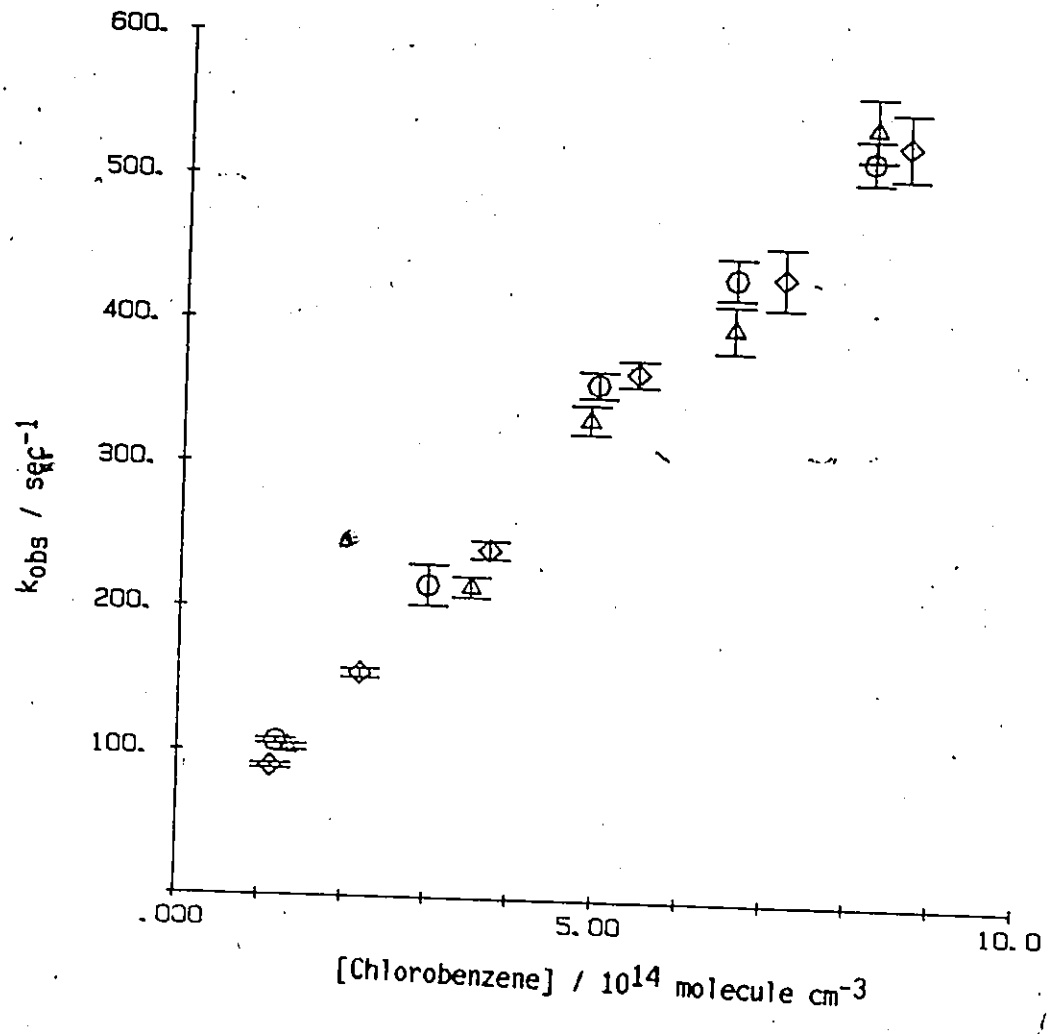

Figure V.10

k_{obs} versus Concentration Plot of OH + Chlorobenzene Reaction at 295, 296, and 297 K

T = 295 K, P_{tot} = 51 torr
T = 296 K, P_{tot} = 100 torr
T = 297 K, P_{tot} = 198 torr

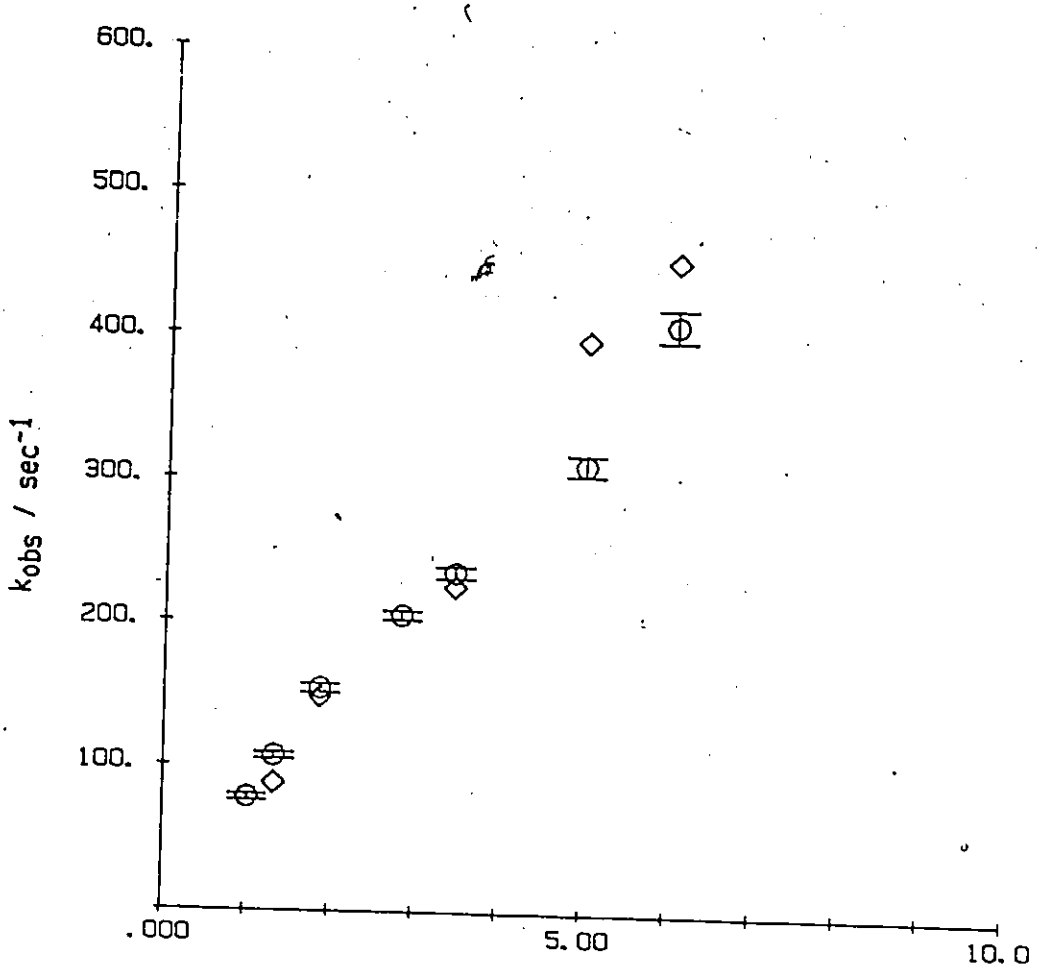

Figure V.11

k_{obs} versus Concentration Plot of the OH + Chlorobenzene Reaction at 310 and 328 K

○ T = 310 K, P_{tot} = 100 torr
◇ T = 328 K, P_{tot} = 101 torr

Table V.3

Second-Order Rate Constants of the OH-Chlorobenzene Reaction at Room Temperature and 310 K

T(K)	Ptot (torr)	k / 10^{-12} cm^3 $molecule^{-1}$ sec^{-1}	Reference
295	51	0.62 ± 0.04[a]	
296	100	0.61 ± 0.03[a]	This work[b]
297	198	0.60 ± 0.06[a]	
	Average	0.61 ± 0.02[a']	
296		0.67	220[b]
299		0.94 ± 0.12[a]	219[c]
310	100	0.62 ± 0.06[a]	This work[b]

a : Two standard deviations
a': Two standard deviations (Internal consistency)
b : The flash photolysis-resonance fluorescence technique
c : The relative rate technique, relative to k(benzene) = 1.29 x 10^{-12} cm^3 $molecule^{-1}$ sec^{-1}.
The originally reported value was 0.88 x 10^{-12} cm^3 $molecule^{-1}$ sec^{-1} using k(benzene) = 1.2 x 10^{-12} cm^3 $molecule^{-1}$ sec^{-1}.

curves were exponential again except for about the first 15 msec, which contained the faster component. At 421 K, decay curves were exponential. At 396 and 421 K, decay rates increased slightly with the concentration. (Figure V.12) The decay rates were very slow, and the range of values of k_{obs} studied was limited to less than 100 sec^{-1} at these temperatures. Experiments with higher concentrations of chlorobenzene were not attempted, as direct photolysis of the chlorobenzene would have interfered with the kinetics. At 421 K, the rate constant increased with an increase in the flash energy by more than two least-square standard deviations, although the decay curve remained exponential. No determination was made of the second-order rate constants at these temperatures. Error bars are not shown in Figure V.12 since standard deviations of k_{obs} were smaller than the size of the symbols used.

V.A.2.b. Discussion

While the manuscript of the present study was being written, Atkinson, Aschmann, Winer, and Pitts[219] reported the rate constant of the reaction determined using a relative rate technique. Their value was more recently revised by Atkinson[38] using the new recommended rate constant of the standard reaction. Their paper also referred to a rate constant of the same reaction reported earlier at a conference by Zetzsch.[220] Zetzsch[220] utilized the same experimental technique as the present study. The rate constants obtained in the present study (0.61×10^{-12} cm^3 $molecule^{-1}$ sec^{-1}) and by Zetzsch[220] (0.67×10^{-12} cm^3 $molecule^{-1}$ sec^{-1}) are in very close agreement. The value 0.94×10^{-12} cm^3 $molecule^{-1}$ sec^{-1} obtained by

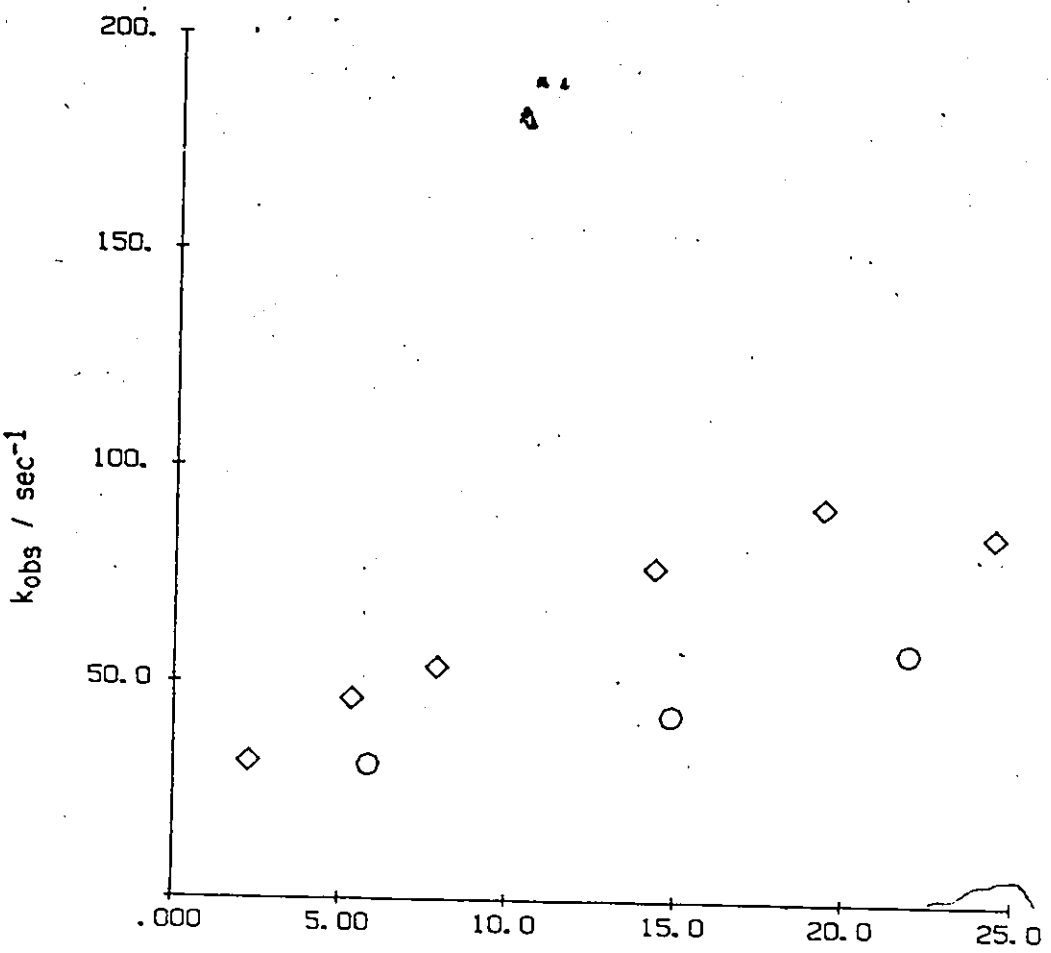

Figure V.12

k_{obs} versus Concentration Plot of the OH + Chlorobenzene Reaction at 396 and 421 K (P_{tot} = 101 torr)

○ T = 396 K
◇ T = 421 K

Atkinson et al[219] is higher than that obtained by Zetzsch[220] as well as that obtained in the present study. This discrepancy is partly because of the higher rate constant of the OH-benzene reaction (1.29×10^{-12} cm^3 $molecule^{-1}$ sec^{-1}) used by Atkinston[38] as a standard than that obtained directly in the present study (1.06×10^{-12} cm^3 $molecule^{-1}$ sec^{-1}). The relative reactivity of the chlorobenzene compared with benzene at room temperature will be discussed in the next section (V.B.) together with a comparison with the reactions of some other halogenated benzenes. In the present section, the temperature dependence of the OH-chlorobenzene reaction will be discussed. There is no previously reported temperature study of the OH-chlorobenzene reaction to compare with the results of the present study. The temperature dependence of the kinetics of the OH-chlorobenzene reaction will be compared with that of the OH-benzene reaction.

The bond energies of the C-Cl bond of chlorobenzene and the Cl-OH bond are 398 and 251 kJ mol^{-1} respectively.[198] The chlorine atom abstraction by the OH radical, therefore, would be strongly endothermic and can be excluded from the mechanism of the OH-chlorobenzene reaction in the temperature range of the present study. By the analogy with the OH-benzene reaction, the first step of the reaction would be either the OH radical addition to the benzene ring, hydrogen abstraction, or direct elimination of a hydrogen atom. In addition, there might be direct chlorine elimination from the ring. The temperature dependence of the OH-chlorobenzene reaction is very similar to that of the OH-benzene reaction. The only difference is that the intermediate temperature range (ii) described in section V.A.1.b.2 of this chapter is shifted to higher temperatures for the OH-chlorobenzene reaction than for the OH-benzene reaction. If one

interprets the temperature dependence of this reaction in a manner similar to that for the OH-benzene reaction, the shift of range (ii) indicates that the dissociation energy of the adduct (E_{-2}) might be larger for the chlorobenzene adduct, assuming that the pre-exponential factors (A_{-2}) of the two reactions are not significantly different. Rinke and Zetzsch[195] studied the OH-1,2,4-trichlorobenzene at temperatures between 273 and 368 K, and even at 368 K, range (ii) had not set in. The shift of range (ii) to the higher temperatures might be a common feature of chlorinated benzenes; in contrast, it shifts very slightly to the lower temperatures with alkyl benzenes.[120] The higher value of E_{-2} for chlorobenzene could be due to the higher stability of the adduct formed from chlorobenzene because of the resonance participation of p-orbital electrons of a chlorine atom with the benzene π system. The OH radical reactions with methoxybenzene and cresols also show slightly higher values of E_{-2} than that of the benzene reaction, and they have been attributed to the relative stabilization of the adducts due to the resonance participation of p-orbital electrons of an oxygen atom.[121]

In the present study, the rate constants at 295 and 310 K appeared to be the same. If the addition process is predominant at those temperatures, as in the OH-benzene reaction, the activation energy of the OH radical addition to chlorobenzene must be very small or even zero. That is not surprising since both the OH-benzene and the OH-1,2,4-trichlorobenzene reactions have been observed to have only small activation energies (2.2[122], 3.7[120], 4.2[123] kJ mol^{-1} for the former and 3.6[195] kJ mol^{-1} for the latter have been reported).

Curve fittings similar to those described in section V.A.1.b.2.(b) were performed for the OH-chlorobenzene at room temperature using Marquardt's algorithm[216] and an eigenfunction expansion method.[222] This attempt was unsuccessful for reasons probably similar to those described in the section on OH-benzene reaction. In addition, the observed decay curves might deviate from a biexponential function if the temperature dependence of the addition-dissociation process differs at the three positions on the benzene ring which are ortho, meta, and para to the chlorine substituent.

A computer simulation similar to the one described for the OH-benzene reaction system (see section V.A.1.b.2.(b)) was performed for the OH-chlorobenzene system. The rate constant of hydrogen abstraction from chlorobenzene was assumed to be 5/6 of that from benzene. The rate constant of the OH radical addition was assumed to be independent of temperature with the room temperature value. Several trial calculations indicated that the activation energy of ~80 kJ mol^{-1} for the dissociation of the adduct (E_{-2}) best described the observed temperature ranges (ii) and (iii) when the pre-exponential factor A_{-2} was assumed to be 3×10^{13} sec^{-1}. The general trend and features of simulated decay curves at various temperatures agree fairly well with the experimental observations. Figure V.13 shows from the simulation results the plot of $k_{app}(1)$ versus the concentration at several temperatures. They should be compared with Figures V.10 - 12. As mentioned in the previous section on the OH-benzene reaction, non-exponentiality of the decay curves or non-linearity of k_{obs} versus concentration plots might not appear so severely if there were any significant reactions for the thermalized adduct other than its dissocia-

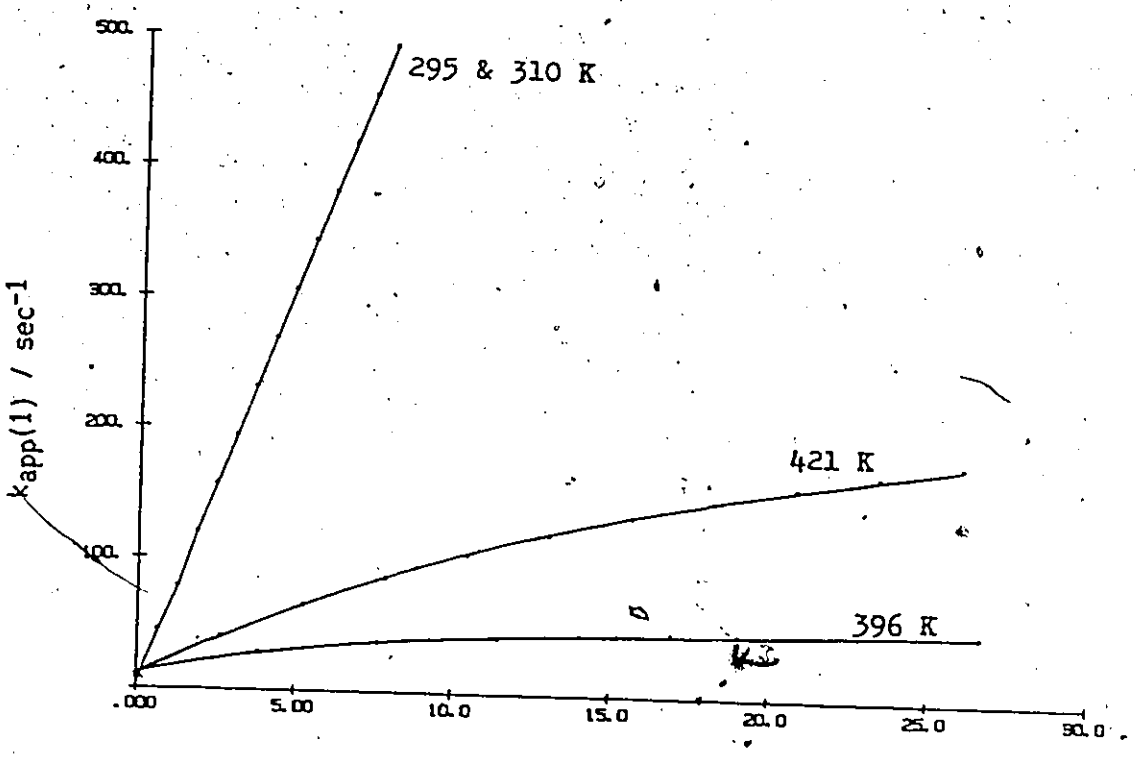

Figure V.13

$k_{app}(1)$ versus Concentration Plot of the OH + Chlorobenzene Reaction at 295, 310, 396, and 421 K : Results of a Computer Simulation

1.5 msec of delay time was used except for 396 K (15 msec).

tion back to the reactants. Since under the assumptions made above, the simulated decay curves and their rates at ranges (ii) and (iii) agree fairly well with those experimentally observed, it is unlikely that the thermalized adduct would undergo, to a significant extent, reactions other than dissociation back to reactants. It is also unlikely that the direct elimination of a chlorine atom from chlorobenzene occurs at a significant rate. Even if it occurs, the rate would be similar to that of hydrogen abstraction/elimination from benzene, hence insignificant compared with the addition path. The only reported example of the direct elimination of a halogen substituent by the OH radical was observed by Koster and Adams[221] in the OH-fluorinated benzene reactions in solution phase. From their results, they proposed a fluorine elimination reaction in addition to the OH addition reaction to the benzene ring:[221]

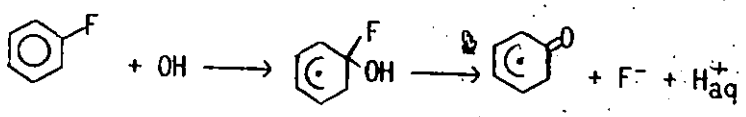

The rate constant of the elimination reaction per fluorine in the OH-polyfluorinated benzenes was, however, observed to be very small compared with the rate constant of the addition to fluorobenzene. Although the elimination mechanism in the OH-chlorobenzene reaction in the gas phase may not be exactly the same, the OH radical would have to first attack the ipso carbon (i.e. the carbon with a chlorine atom attached). This would be expected to have a substantial activation energy since the ipso carbon has lower electron density and also because there might be a steric hindrance from a bulky chlorine atom. The process might, however, become significant at higher temperatures.

It would be desirable to obtain kinetic information on the addition and other processes separately in order to analyze quantitatively the decay curves observed in the temperature range of the present study. Kinetic study of the reaction at temperatures lower than room temperature and higher than 425 K would provide this information. This would involve major redesign of the reaction cell and the vacuum housing to make them suitable for those temperatures ranges, and was not attempted.

V.B. Reactions of the OH Radical with Selected Halogenated Benzenes and Biphenyl at Room Temperature

V.B.1. Experimental Results

The OH radical reactions were studied at room temperature with six other halogenated benzenes: fluorobenzene, p-difluorobenzene, o-dichlorobenzene, m-dichlorobenzene, 1,3,5-trichlorobenzene, and bromobenzene. The study was also done with biphenyl as a reactant. Approximately the first three halflives of the decay curves were used to obtain first-order rate constants at various reactant concentrations. The total pressure was varied between 50 and 100 or 200 torr. For o-dichlorobenzene, the reaction was studied at one total pressure. During the calibration of the u.v. absorption of o-dichlorobenzene vapour, it was found that the o-dichlorobenzene was absorbed in the apparatus (probably on the O-rings), and the long-term exposure of the apparatus to o-dichlorobenzene was undesirable. In the experiments on the OH-o-dichlorobenzene reaction whose results are reported here, the reactant mixture was flushed through the reaction cell for a time long enough that the concentration of o-dichlorobenzene in the cell reached its steady state level. In the study of 1,3,5-trichlorobenzene, because of its low vapour pressure the total pressure was limited in order to maintain the same total flow rates as those used for studies of other reactions. It was, therefore, maintained at 100 torr. The same was true for biphenyl. The pressure was varied within a limited concentration range for the biphenyl reaction. All the compounds studied in this section did not show any variation in observed rate constants beyond two standard deviations of the least square calculations when the flash energy was varied between 18 and 40 J. Figures V.14 - 19 show k_{obs} versus concentra-

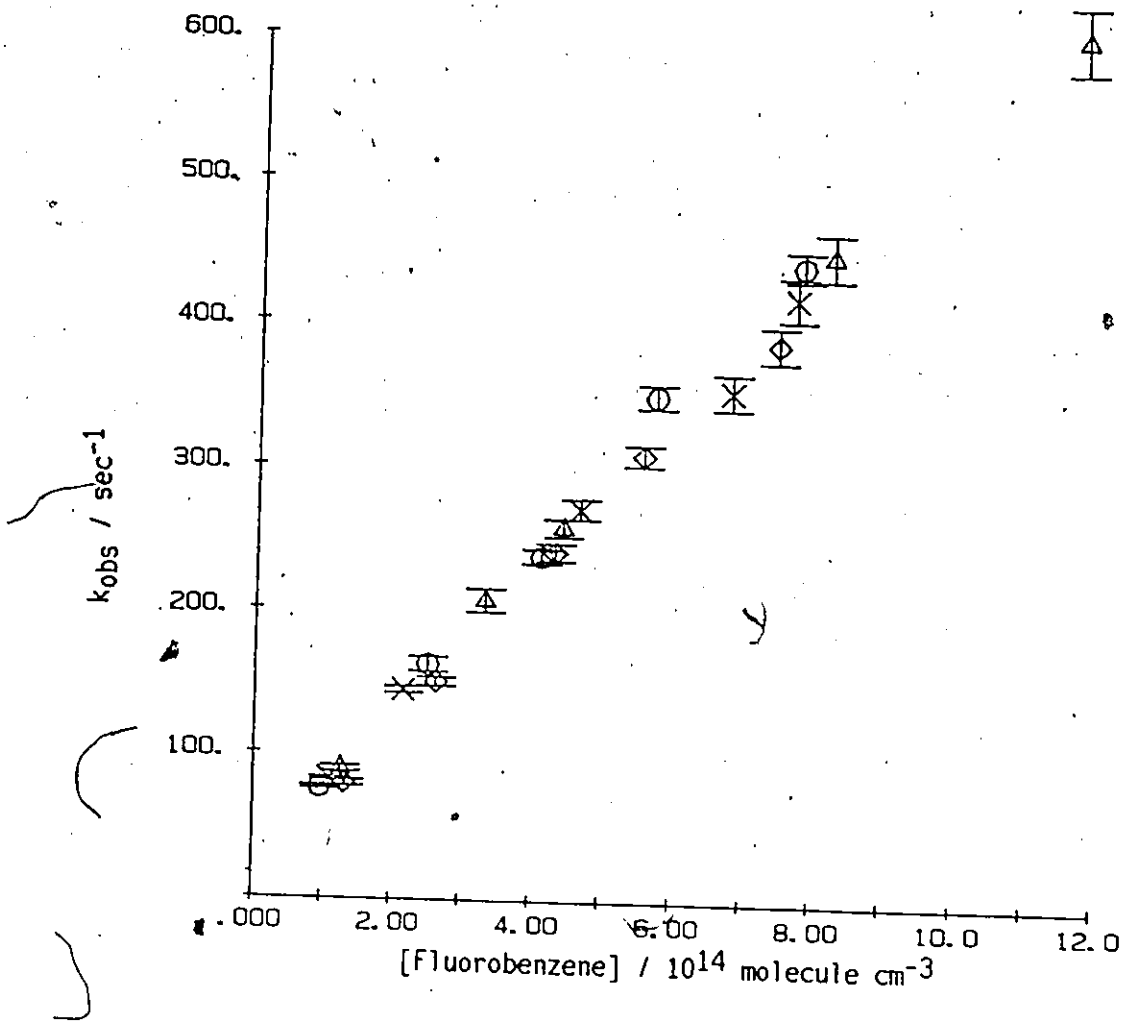

Figure V.14

k_{obs} versus Concentration Plot of the OH + Fluorobenzene Reaction at 295 and 296 K

T = 295 K, P_{tot} = 50 torr
T = 295 K, P_{tot} = 100 torr
T = 295 K, P_{tot} = 100 torr
T = 296 K, P_{tot} = 200 torr

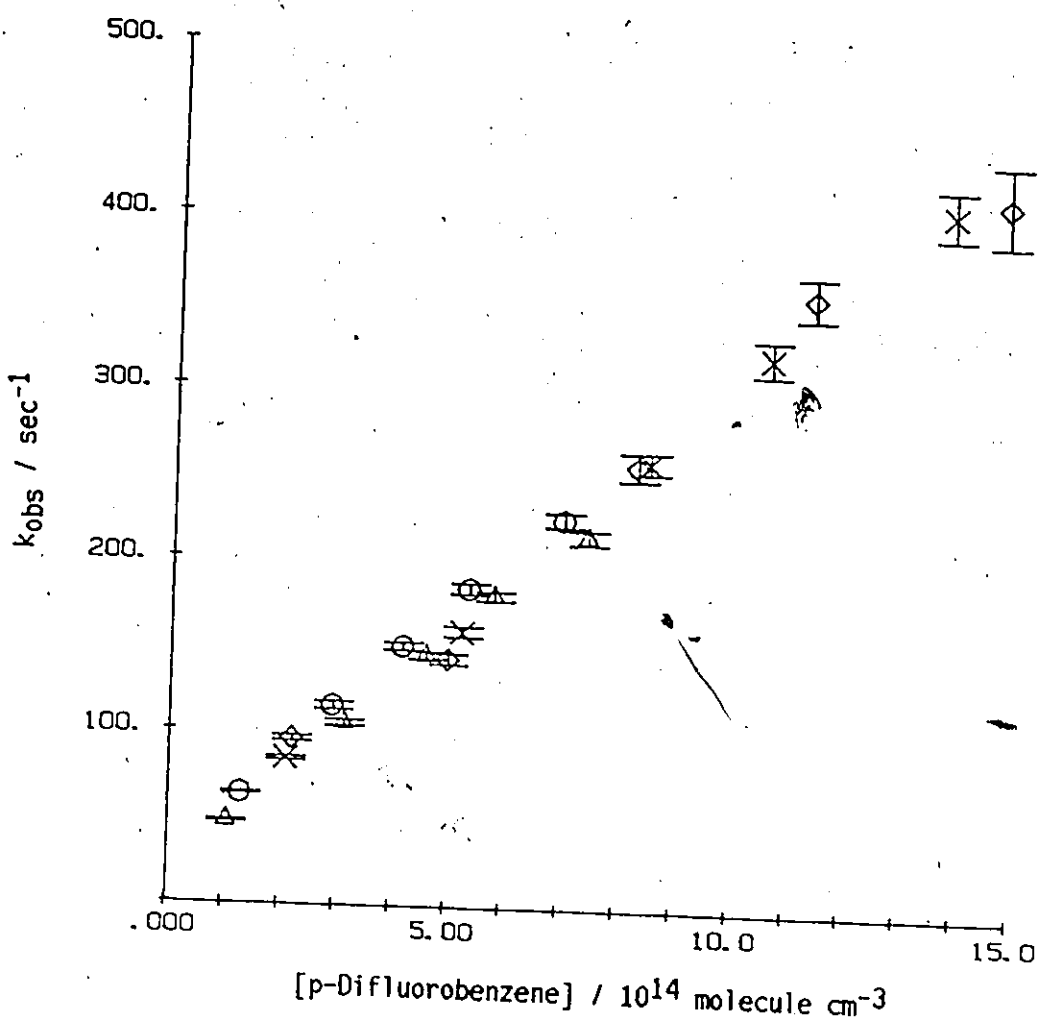

Figure V.15

k_{obs} versus Concentration Plot of the OH + p-Difluorobenzene Reaction at 295, 296, and 298 K

○ T = 298 K, P_{tot} = 50 torr
◇ T = 296 K, P_{tot} = 50 torr
△ T = 295 K, P_{tot} = 100 torr
× T = 296 K, P_{tot} = 100 torr

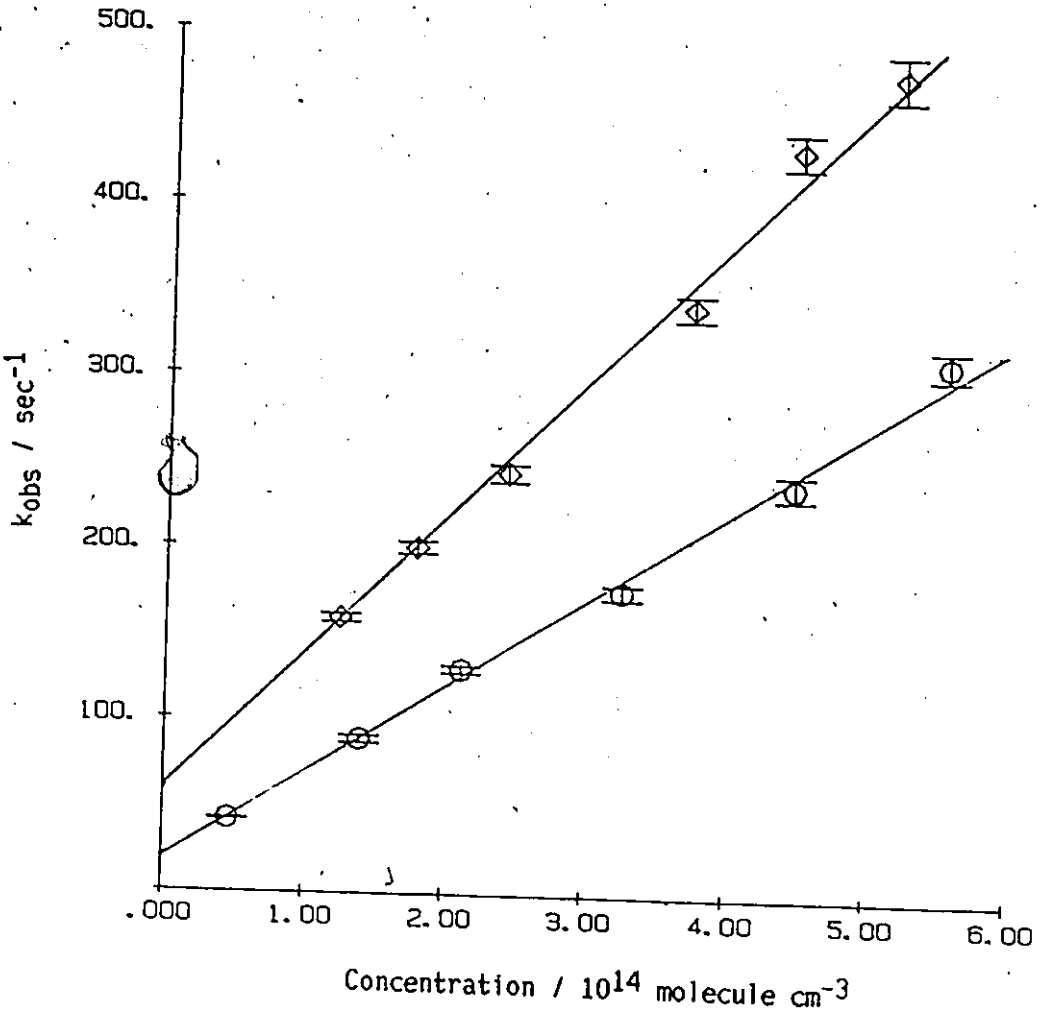

Figure V.16

k_{obs} versus Concentration Plot of the OH Radical Reactions with o-Dichlorobenzene and 1,3,5-Trichlorobenzene at 295 K

○ o-Dichlorobenzene (T = 295 K, P_{tot} = 50 torr)
◇ 1,3,5-Trichlorobenzene (T = 295 K, P_{tot} = 100 torr, Shifted upward by 40 sec^{-1})

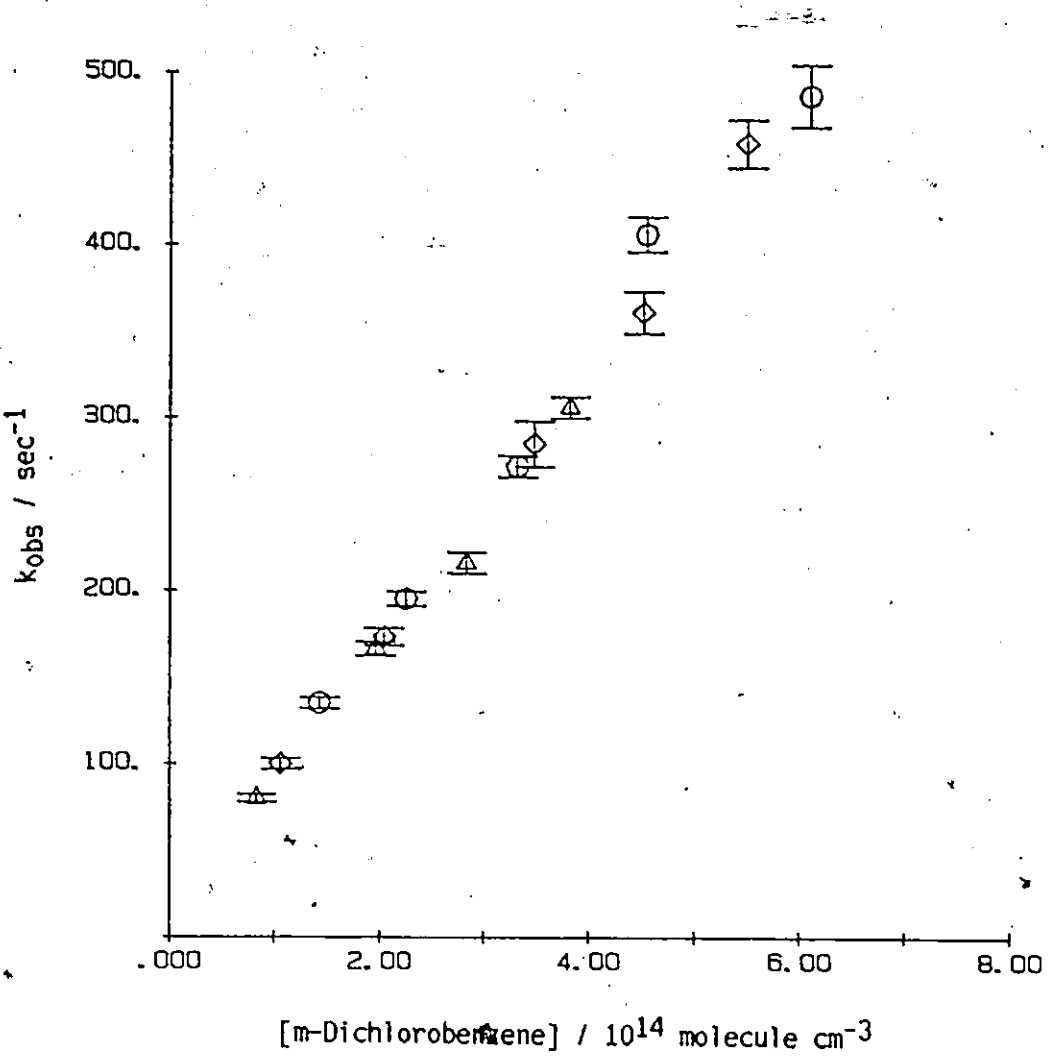

Figure V.17

k_{obs} versus Concentration Plot of the OH + m-Dichlorobenzene Reaction at 296 K

○ P_{tot} = 50 torr
◇ P_{tot} = 100 torr
△ P_{tot} = 200 torr

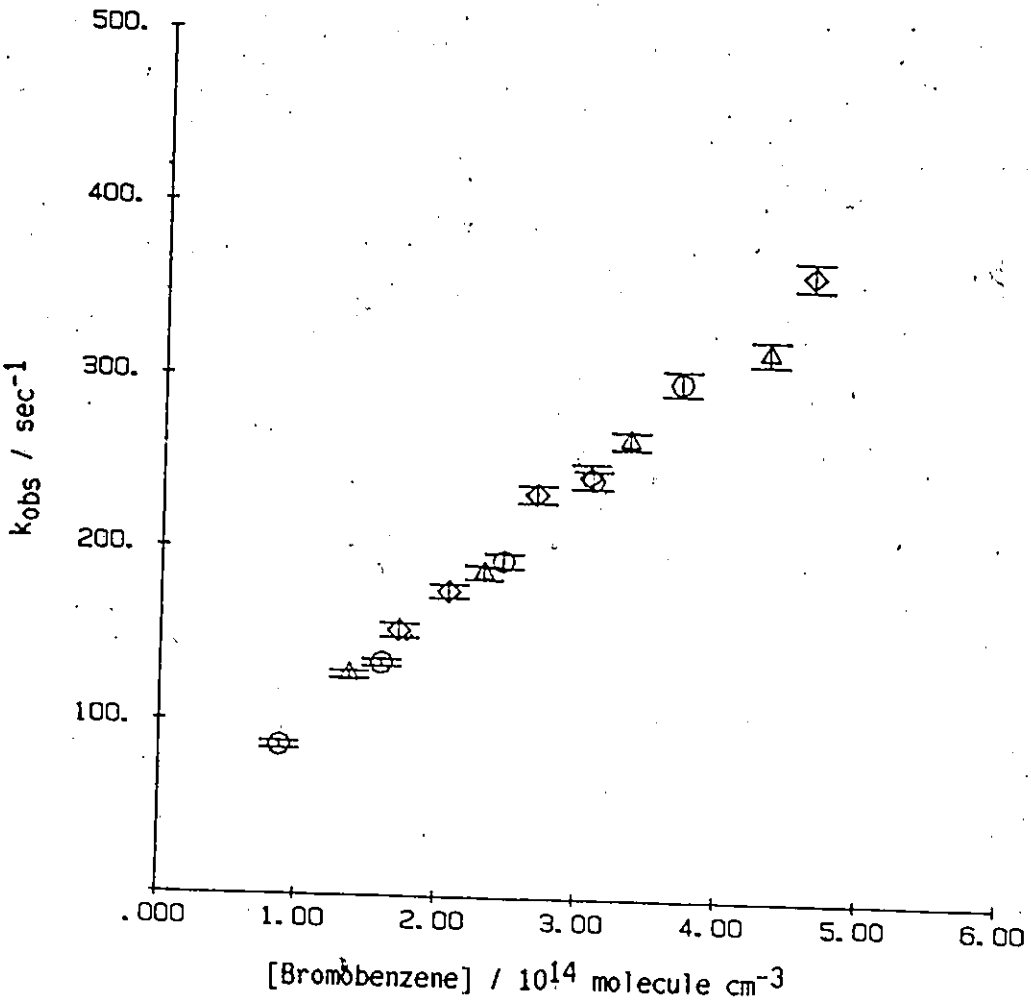

Figure V.18

k_{obs} versus Concentration Plot of the OH + Bromobenzene Reaction at 296 and 297 K

○ T = 297 K, P_{tot} = 51 torr
◇ T = 296 K, P_{tot} = 101 torr
△ T = 296 K, P_{tot} = 100 torr

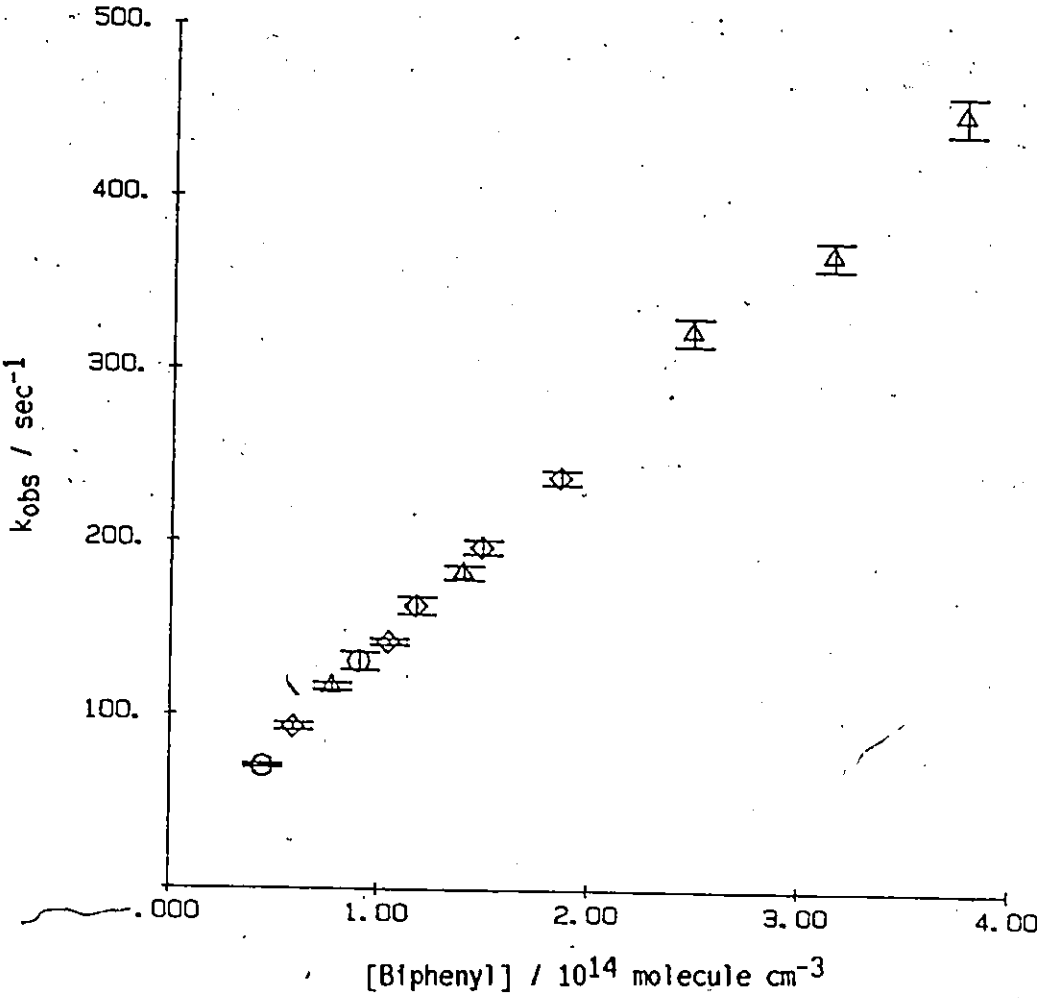

Figure V.19

k_{obs} versus Concentration Plot of the OH + Biphenyl Reaction at 295 K

○ P_{tot} = 50 torr
◇ P_{tot} = 100 torr
△ P_{tot} = 201 torr

tion plots for the seven reactions. Indicated error bars are one standard deviation of the least square calculations. No best fitted line was drawn in the figures (except for Figure V.16) to allow a clear representation of the experimental data. Variation of the total pressure did not alter the observed kinetics of the reactions. Table V.4 lists the second-order rate constants of the seven reactions together with available literature values. The rate constants of benzene, other chlorinated benzenes, and iodobenzene are also listed in the same table for comparison. The overall accuracies of the second-order rate constants in the table are: ~8% for fluorobenzene and di-chlorobenzenes, ~14% for bromobenzene, 1,3,5-trichlorobenzene, and biphenyl.

V.B.2. Discussion

In this section, first the results of the present study will be compared with the previously reported results by other groups. Secondly, the discussion will focus on the factors which might determine the relative reactivities of the OH-halogenated benzene reactions. Several correlations of the kinetics of the OH-aromatic reactions with other characteristic properties of aromatic molecules will be discussed in terms of their relevance to understanding the reaction mechanism. Lastly, the potential reactivities of polychlorinated biphenyls in the atmosphere will be considered based on the reactivities of the OH radical toward chlorinated benzenes and biphenyl.

V.B.2.a. Comparison of the Results of the Present Study with Those Previously Reprted

There are no literature values available for the rate constants of

Table V.4

Second-Order Rate Constants of the OH Radical Reactions with Selected Halogenated Benzenes and Biphenyl at Room Temperature

Reactant		This work	Literature
Fluorobenzene	50 torr	0.544 ± 0.030	0.54 ± 0.05, Ref.38
	100 torr	0.531 ± 0.024	
	100 torr	0.520 ± 0.030	
	200 torr	0.51 ± 0.04	
	Average	0.529 ± 0.015	
p-Difluorobenzene	50 torr	0.296 ± 0.014	
	50 torr	0.25 ± 0.06	
	100 torr	0.275 ± 0.008	
	100 torr	0.268 ± 0.020	
	Average	0.278 ± 0.011	
Chlorobenzene		0.61 ± 0.02	See Table V.2
o-Dichlorobenzene	100 torr	0.510 ± 0.024	0.42 ± 0.02, Ref.131
m-Dichlorobenzene	50 torr	0.79 ± 0.09	0.72 ± 0.02, Ref.131
	100 torr	0.78 ± 0.03	
	200 torr	0.74 ± 0.06	
	Average	0.77 ± 0.03	
p-Dichlorobenzene			0.32 ± 0.02, Ref.131
1,2,4-Trichloro benzene			0.532 ± 0.05, Ref.195
1,3,5-Trichloro-benzene	100 torr	0.79 ± 0.06	
Bromobenzene	51 torr	0.72 ± 0.04	0.70 ± 0.07, Ref.38
	100 torr	0.73 ± 0.05	
	100 torr	0.68 ± 0.03	
	Average	0.71 ± 0.06	
Iodobenzene			0.93 ± 0.05, Ref.38

(continued)

(continued)			
Benzene		1.06 ± 0.03	See Table V.1
Biphenyl	50 - 200 torr	11.7 ± 0.4	8.2 ± 0.8a, Ref.223 5.8 ± 0.8, Ref.220 7.76 ± 0.68b, Ref.110

All rate constants are in 10^{-12} cm^3 $molecule^{-1}$ sec^{-1}.
All indicated errors are two standard deviations. For the average value of the rate constants, the standard deviation was taken from the larger value of the internal consistency and external consistency.
All rate constants in the literature were obtained with the flash photolysis-resonance fluorescence technique unless otherwise indicated.

a : with a relative rate technique, relative to k(cyclohexane) = 7.28 x 10^{-12} cm^3 $molecule^{-1}$ sec^{-1}

b : with a relative rate technique, relative to k(n-nonane) = 10.3 x 10^{-12} cm^3 $molecule^{-1}$ sec^{-1}

the OH radical reactions with p-difluorobenzene or 1,3,5-trichlorobenzene. While the present study was in progress, the rate constants of the reactions with o- and m-dichlorobenzenes were reported by Wahner and Zetzsch[131] who used the same experimental technique as the present study. Their values, 0.42 and 0.72 x 10^{-12} cm^3 $molecule^{-1}$ sec^{-1} for o- and m-dichlorobenzene respectively, are smaller than those in the present study, 0.51 and 0.77 x 10^{-12} cm^3 $molecule^{-1}$ sec^{-1} respectively. As mentioned in section V.A.1.b., their value of the benzene reaction in the same study was also smaller (0.88 x 10^{-12} cm^3 $molecule^{-1}$ sec^{-1}) than that of the present study (1.06 x 10^{-12} cm^3 $molecule^{-1}$ sec^{-1}). The same group[195] recently reported a higher rate constant for the benzene reaction (1.0 x 10^{-12} cm^3 $molecule^{-1}$ sec^{-1}). There must have been some systematic error in the earlier study[131] which led to smaller values of the rate constants, most likely in the determination of the concentrations of reactants in the reaction cell. In the present study, the concentrations of aromatic compounds in the mixture of the reactant/argon stream were checked by the absorption of 253 nm light. The rate constants of the present study are, therefore, more reliable for the o- and m-dichlorobenzenes.

In 1986 Atkinson, in a review article[38], referred to unpublished values of rate constants for the OH-fluorobenzene and the OH-bromobenzene reactions obtained by Zetzsch. Those rate constants (0.54 and 0.70 x 10^{-12} cm^3 $molecule^{-1}$ sec^{-1} for fluorobenzene and bromobenzene respectively) are in excellent agreement with the results of the present study (0.53 and 0.71 x 10^{-12} cm^3 $molecule^{-1}$ sec^{-1} respectively).

The rate constant of the OH-biphenyl reaction has been studied at

room temperature with a relative technique[110,223] as well as with the flash photolysis-resonance fluorescence technique.[220] The value obtained in the present study (11.7 x 10^{-12} cm^3 $molecule^{-1}$ sec^{-1}) is higher than the other values reported in the literature (5.8 ~ 8.2 x 10^{-12} cm^3 $molecule^{-1}$ sec^{-1}). The discrepancy is probably due to the systematic errors associated with the determination of the biphenyl concentration in the reaction mixture. In the present study, great care was taken to ensure that the argon gas flowing from the condenser was saturated with biphenyl at the temperature of the condenser, and that the saturation was maintained at a constant level. (See CHAPTER II.D.) The accuracy of the rate constant of the present study of the OH-biphenyl reaction is primarily determined by the accuracy of the vapour pressure equation. Its uncertainty was estimated to be < 6.1%.[140] While the present experimental technique does not require the rate constant of the standard reaction, the relative rate method[110,223] is susceptible to systematic errors associated with the uncertainties of the rate constant of the standard reaction. For example, Atkinson[38] estimated an uncertainty of 20% for the standard OH-cyclohexane reaction, used in one of the studies of the OH-biphenyl reaction.[223] Considering the difficulties in both techniques of dealing with compounds with such low vapour pressures, the agreement of the rate constants from these different techniques is not unreasonable.

V.B.2.b. The Factors Which Determine Relative Reactivities of the OH-Halogenated Benzene Reactions

From the rate constants listed in Table V.4, one recognizes that the variations in the values of the rate constants are small. All rate

constants in Table V.4 are within the factor of 40 of each other. This low substance selectivity is a general feature of the OH-aromatic reactions. Among the reported rate constants at room temperature, the slowest is the OH-nitrobenzene reaction (0.21×10^{-12} cm^3 $molecule^{-1}$ sec^{-1})[220] and the fastest is the OH-N,N-dimethylaniline reaction (148×10^{-12} cm^3 $molecule^{-1}$ sec^{-1})[38]. Since the variation of the rate constants among various aromatic molecules is relatively small, and the rate constant of the OH-N,N-dimethylaniline reaction is close to the collisional frequency, OH-aromatic reactions are generally fast. According to the reactivity-selectivity principle,[224] one might expect the relatively low substance and positional selectivities of the OH-aromatic reactions as observed in the present study.

In Table V.4, the following relative reactivity relationships are observed for halogenated benzenes:

ⓐ $F < Cl < Br < I < H$

ⓑ $p\text{-}Cl_2 < o\text{-}Cl_2 < Cl < m\text{-}Cl_2 < H$

ⓒ $1,2,4\text{-}Cl_3 < Cl < m\text{-}Cl_2 \sim 1,3,5\text{-}Cl_3 < H$

For the reactions listed in Table V.4 the rate constants of the OH-halogenated benzene reactions are all smaller than that of the OH-benzene reaction. Since halogen atom abstraction by the OH radical from a benzene ring is endothermic, as was shown for the OH-chlorobenzene reaction in the previous section V.A.2.b., it would not be significant at room temperature. The addition of the OH radical to the ring, the hydrogen atom abstraction from the ring, and/or direct elimination of a hydrogen or chlorine atom by the OH radical might be the first step of the reaction, similar to the OH-

benzene reaction. In the study of the OH-chlorobenzene reaction (section V.A.2.b.), it was concluded that the experimental results supported the predominance of the addition process at room temperature, and that the other processes were significant only to an extent similar to those in the OH-benzene reaction. In the OH-benzene reaction, only 5 - 7% of the total reaction is attributed to non-addition processes at room temperature.[38] Similarly, the addition reaction is expected to predominate in other OH-halogenated benzene reactions.

A similar relative reactivity relationship ⓐ (F < Cl < Br < H) has been observed in CF_3 radical reactions with halogenated benzenes in gas phase.[225] Since both the OH radical and the CF_3 radical exhibit an electrophilic character in their reactivities, one might expect their reactivities toward halogenated benzenes to be affected by the change in the electron density on the benzene ring due to halogen substituents. Two features of halogen atoms are noteworthy: the electronegativities of halogen atoms, and the ability of halogen p-orbital electrons to conjugate with the benzene π-orbital electrons. Since the electronegativities of halogens and hydrogen atoms are in the order of F > Cl > Br > I > H, the electron density of the ring carbons (primarily the σ-electron densities) would decrease, in the order of H > I > Br > Cl > F especially at the positions close to a halogen atom. On the other hand, the p-orbital electrons of a halogen atom might conjugate with π electrons of the benzene ring resulting in higher π electron density on the ring especially at ortho and para positions to the halogen substituent. This ability of conjugation increases in the order of F < Cl < Br < I. Both effects of halogen atoms predict the relative reactivities of an electrophile with the mono-

halogenated benzene to be F < Cl < Br < I, as observed in the present study. Although the rate constants of all the OH-monohalogenated benzene reactions are smaller than that of the benzene reaction, it does not necessarily mean that the electronegativity effect overpowers the conjugation effect. The observed rate constant k is a composite of the rate constants for individual reactions at the six different positions of the ring. Since the two effects influence the six positions in various degrees, one cannot separate their relative importance based only on the overall rate constant. A study of the positional selectivities is needed, and this is not available at present. It would be helpful to study quantitatively the stable products of the OH-halogenated benzene reactions to gain further insight.

The relative reactivities ⓑ (p-Cl_2 < o-Cl_2 < Cl < m-Cl_2 < H) and ⓒ (1,2,4-Cl_3 < Cl < m-Cl_2 ~ 1,3,5-Cl_3 < H) indicate some interesting features of a chlorine substituent. If the electronegativity effect of chlorine were predominant, one would expect the decreasing reactivities in the order of benzene > mono- > di- > tri-chlorobenzenes regardless of the positions of chlorine atoms. The experimental results show that m-dichlorobenzene and 1,3,5-trichlorobenzene react with the OH radical faster than other mono-, di-, and tri-chlorobenzenes. The increase in reactivity by the presence of an additional chlorine atom in the meta position might be due to the conjugation effect. Thus the conjugation effect seems to be important and sensitive to the position of chlorine atoms.

So far, the effects of halogen substituents have been considered from the reactants' point of view, i.e. the electron density on the ring carbons of the reactant. One might argue that both the electronegativity

effect and the conjugation effect would affect the stability of the adduct (the product) resulting in the observed relative reactivities. Whether the transition state of the reaction resembles the reactant state or the product state cannot be distinguished from the observed substituent effects. The activation energy is close to zero or very small in OH-chlorobenzene (see section V.A.2.), OH-1,2,4-trichlorobenzene,[195] and OH-benzene[38] reactions, and the reactions are exothermic by ~80 kJ mol^{-1}. The transition states of these reactions seem to be closer in their energies to the reactant states than to the product states. On the other hand, the entropy of activation of the OH-benzene reaction calculated by Lorenz and Zellner[123] suggests that the transition state might be structurally closer to the product, i.e. a fairly tight transition state. If so, the Hammond postulate[226] would not apply to the OH aromatic reactions. The basic idea of the postulate is that "similar energies correspond to similar structure".[226] The OH-aromatic reactions seem to have transition states closer to the reactant states in energy but closer to the product states in structure. In such reactions the substituent effects on the reactant state or the product state would not apply to the transition state in the same manner.

Even if the transition state does not resemble either the reactant or the product state, the question to be answered is whether the halogen substituents affect the reaction energetically or stericly to exhibit the observed relative reactivities. Benzene and 1,2,4-trichlorobenzene have been observed to have very small positive activation energies: 2.2,[122] 3.7,[120] 4.2[123] kJ mol^{-1} for benzene, and 3.6 kJ mol^{-1} for 1,2,4-trichloro-

benzene.[195] Since no significant temperature dependence was observed in the rate constant of the OH-chlorobenzene reaction between 295 K and 310 K in the present study, its activation energy must be zero or very small. Thus, the relative reactivities of the OH-halogenated benzene reactions (and most likely the other substituted benzenes also) do not seem to be determined by the height of the activation energy barriers if one assumes an elementary reaction. More studies are needed of the temperature dependence of various OH-halogenated benzene reactions in the lower temperature range, i.e. lower than room temperature, in order to investigate whether there is any significant variation in their activation energies. This would necessitate a completely new reaction cell design to accomodate low temperatures.

V.B.2.c. Correlations of the Kinetics of the OH-Aromatic Reactions with Other Parameters

In this section, the relative reactivities of OH-halogenated benzene reactions will be examined in the context of general trends in reactivities of OH-aromatic reactions. Correlations of rate constants of a series of reactions with other parameters which characterize reactants are often helpful not only in predicting rate constants of reactions which have not been measured yet but also in finding the factors which might determine the relative reactivities of a series of reactions. In this section, the applicability and implications of three previously proposed correlations will be discussed.

V.B.2.c.1. Correlation of the OH Radical and the O Atom Reactions with Aromatic Molecules

As in the alkene reactions discussed in CHAPTER IV, there seems to be a correlation between the rate constants of the O atom-aromatic reactions and those of the OH radical-aromatic reactions at room temperature, as pointed out by Atkinson[169]. Figure V.20 shows the correlation using rate constants of several OH- and O-aromatic reactions previously reported as well as of the reactions reported in the present study (filled symbols). The overall rate constants of the OH reactions were corrected to give the rate constants of the addition components of the reactions using Table XV of reference 38. The values of rate constants are listed in APPENDIX E.2.. The O atom reacts with aromatic molecules primarily via addition.[234] Although the addition mechanism of the OH radical might have some similarity to that of the O atom, there are distinct differences between the two species. While the relative reactivities of the O atom reactions are determined primarily by the magnitude of the activation energies, at least among benzene, toluene, and xylenes,[227-229] those of the OH radical do not seem to show any consistent correlation with the activation energies.[36,122,123,195] This is somewhat similar to alkene reactions as pointed out in CHAPTER IV. Another difference is that while the pre-exponential factors of the O-aromatic reactions are of the order of 10^{-11} cm^3 $molecule^{-1}$ sec^{-1},[227-229] those of the OH-aromatic reactions (addition) are of the order of 10^{-12} cm^3 $molecule^{-1}$ sec^{-1}.[36,122,195] If both reactions are one-step reactions, this indicates that the transition states of the OH-aromatic reactions are generally tighter than those of the O-

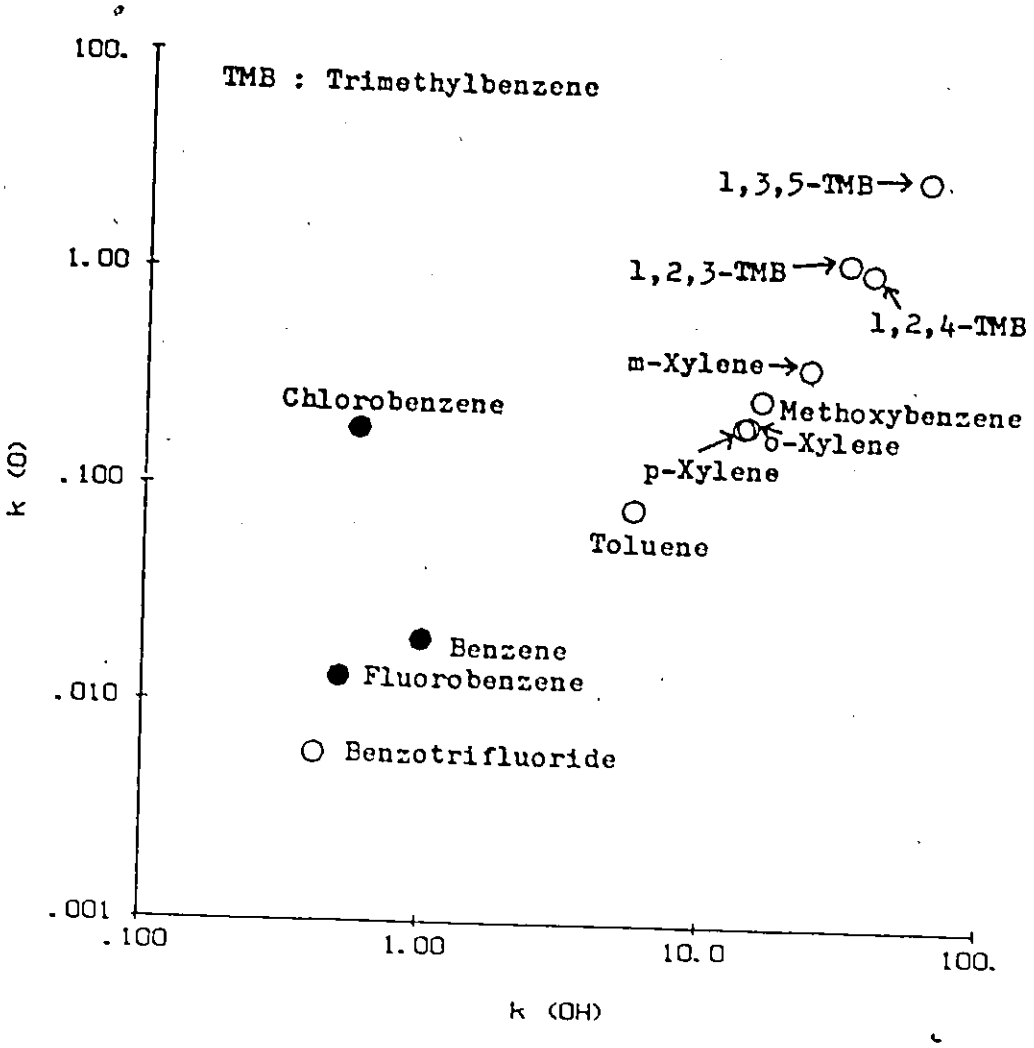

Figure V.20

Correlation of the Kinetics of the OH Radical and the O atom Reactions with Aromatic Molecules at Room Temperature

k(OH)'s are taken from reference 38 and the present study. When k(OH) is from the present study, its symbol is filled in the figure.
k(O)'s are taken from references 227 - 233. When several literature values are available, their mean is taken.

aromatic reactions, and that the orientation of the incoming OH radical can be very important.

There are only two rate constants available for the reactions of the O atom with halogenated benzenes: fluorobenzene and chlorobenzene. The O atom reacts with chlorobenzene faster than with fluorobenzene, which is a similar behaviour to that of the OH radical. The O-chlorobenzene reaction, however, was observed to be faster than the O-benzene reaction, which is different from the observation made for the OH radical. Although the rate constant of the O-chlorobenzene reaction should be confirmed experimentally, it does at least suggest the significance of the conjugation effect of a chlorine substituent in the OH radical and the O atom reactions.

V.B.2.c.2. The Hammett Equation and OH-Aromatic Reactions

Since the OH radical exhibits an electrophilic character in its reactivity, one might expect some similarities between its reactions with aromatic compounds and the electrophilic aromatic substitution reactions which have been extensively studied in organic chemistry. In many S_E2 reactions, the rate determining step of the substitution reaction is the first attack by an electrophile E^+ (often a cation) to form an intermediate:

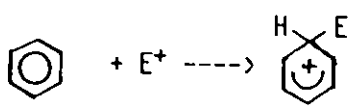

The reactivities of various aromatic compounds are usually interpreted in terms of the relative stability of the intermediate due to inductive, resonance, and steric effects of the substituents. The following Hammett

equation is often used to characterize the substituent effects on the relative reactivities of S_E2 reaction of various mono-substituted benzenes:[235]

$$\log (k_{Xi}/k_H) = \rho \sigma_i^+(X)$$

where k_{Xi} is the partial rate constant of a substituted benzene with a substituent X at i-th position to the reaction site, k_H is the rate constant of benzene reaction per carbon, ρ is the reaction constant, $\sigma_i^+(X)$ is the electrophilic substituent constant of a substituent X at i-th position to the reaction site obtained from the solvolysis of t-cumyl chloride for m- and p-substituents.[236] σ_i^+ is zero for benzene, and the values of σ_i^+ reflect the extent of change in electron density at the reaction site in the transition state due to substituents, and are independent of the nature of the reactions.[237] A negative value of σ_i^+ indicates an electron donating nature and a positive value indicates an electron withdrawing nature of a substituent on the reaction.[238] For poly-substituted benzenes, the additivity rules are often employed to estimate their effects at a reaction site. The slope indicates the nature of the reaction.[238]

Zetzsch[220] and Atkinson[38] correlated the rate constants of the OH-aromatic reactions with the sum of the electrophilic substituent constants $\Sigma \sigma^+$. Since no study on the positional selectivities had been done except for toluene, some assumptions had to be made to plot the correlation. Their basic assumptions were that the para effect and the ortho effect were equivalent and that $\Sigma \sigma^+$ of the position where the OH radical was predicted

to react the fastest among the six carbons of the benzene ring was taken to represent the substituent constant of the molecule. Figure V.21 shows the plot of k versus $\Sigma \sigma^+$ on a semi-log scale. Filled symbols indicate the reactions of the present study. The values of $\Sigma \sigma^+$ and the rate constants (corrected for addition) used in the figure are tabulated in APPENDIX E.2.. There seems to be a general correlation, and Atkinson[38] obtained the expression:

$$\log k(cm^3 \text{ molecule}^{-1} \text{ sec}^{-1}) = - 11.64 - 1.31 \Sigma \sigma^+$$

Most of the experimentally obtained rate constants are within a factor of two of the values calculated from the the above correlation equation. Exceptions are 1,2,4-trichlorobenzene, fluorobenzene, bromobenzene, N,N-dimethylaniline, p-chloroaniline, o-nitrophenol, and n-propylpentafluorobenzene.[38] The results for p-difluorobenzene and chlorobenzene obtained in the present study also do not fit within a factor of two to the above expression. A better correlation is seen if only alkyl benzenes (shaded symbols) and benzene are taken into consideration. The negative slope of the plot indicates that the reactions are electrophilic.[237] Its small magnitude indicates that the change in charge (or electron density) at the reaction site is small during the reaction, which is very common in radical reactions.[237] The limitation of this correlation, however, should be kept in mind. The assumption that the ortho effect and the para effect are equivalent is not valid at least for the OH-toluene reaction and most likely for the reactions with other alkyl benzenes. The addition of the OH radical at the ortho position has been found to be dominant in the OH-

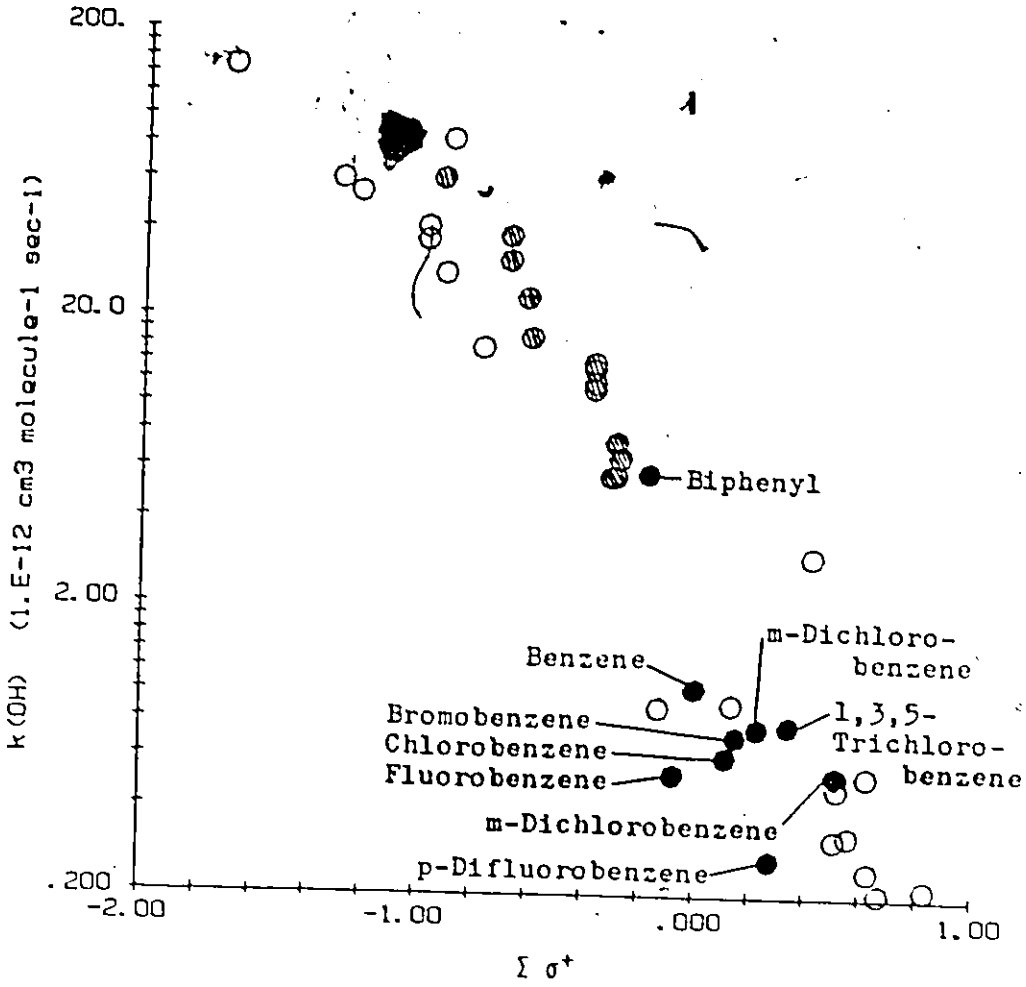

Figure V.21

Correlation between the Reactivity of the OH Radical towards Aromatic Molecules and $\Sigma \sigma^+$

Rate constants are taken from reference 38 and the present study (filled symbols).
The values of $\Sigma \sigma^+$ are taken from reference 38.
Both values are tabulated in APPENDIX E.2..
Shaded symbols represent alkylbenzenes.

toluene reaction.[58,59,239] If the positional selectivities of the OH-aromatic reactions are similar to those of the O-aromatic reactions reported by Grovenstein and Mosher,[231] the relative preference for the ortho and para positions may vary depending on the aromatic partner. The slopes obtained by Zetzsch[220] and Atkinson[38] might be somewhat overestimated in their magnitudes if the ortho position is stericly favoured in OH-alkyl benzene reactions. Although the partial rate factors should be plotted instead of the total rate constants against such $\Sigma \sigma^+$, no such data are available at present. The correlation of ln k and $\Sigma \sigma^+$ suggested by Zetzsch [220] and Atkinson[38] is useful in roughly predicting the unknown rate constants of the OH radical reactions with aromatic compounds, but it is a crude one. From these limited correlations with $\Sigma \sigma^+$, one can only conclude that the relative reactivities of the OH-aromatic reactions are likely affected by the type of polar effects of substituents observed in solvolysis of t-cumyl chloride, but only to a small degree.

The values of σ^+ for the halogen atoms are in the order of F > H > Cl > I > Br, which does not correlate with the relative reactivities of monohalogenated benzenes (H > I > Br > Cl > F). The values of σ^+ for a chlorine atom at the meta and para positions are both positive. This predicts that the OH radical would not react faster than with benzene at any position of the chlorinated benzenes, and the addition of a chlorine as a ring substituent would always cause a retarding effect for the reaction with the OH radical. This is not the case for the OH-chlorinated benzene reactions since both m-dichlorobenzene and 1,3,5-trichlorobenzene react faster than chlorobenzene with the OH radical.

σ^+ may not be a good parameter to describe the radical reactions. Dust and Arnold[240] have suggested a different substituent parameter for radical reactions ($\sigma^\cdot$) based on ESR hyperfine coupling constants of α-hydrogen of substituted benzyl radicals. It is thought to reflect the relative spin delocalization of the radical, which indicates its stability. The values of $\sigma^\cdot$ do not necessarily correspond with those of σ^+ for the same substituent group, which implies that the stability of a radical is not necessarily determined by the same factors which govern the stability of a cation from the same substituted benzene. What is noteworthy is that chlorine was found to increase the delocalization of an unpaired electron of a benzyl radical when it was placed in the para position while fluorine had an opposite effect.[240] This implies that chlorine at the para position increases the stability of the radical while fluorine decreases it. Whether $\sigma^\cdot$ is a better parameter than σ^+ for interpreting the kinetics of the OH-aromatic reactions cannot be evaluated until the positional selectivities are studied.

A study of the stable products of the OH-aromatic reactions would provide some useful information on positional selectivities. It will be interesting to find out whether the para position to the halogen substituent is more reactive than benzene. Since one does not need to consider the solvent effect in gas-phase reactions, the study of the positional selectivities of the OH-aromatic reactions might reveal some intrinsic features of the electrophilic reactions.

V.B.2.c.3. Correlation of Rate Constants of OH-Aromatic Reactions with Ionization Potentials

There is a correlation between the rate constants of the OH-aromatic reactions and the lowest ionization potentials (IP's) of the aromatic molecules as pointed out by Rinke and Zetzsch[195]; so the kinetics show similarities to those of the OH-alkene reactions. This is shown in Figure V.22. Rate constants are taken from reference 38 and the present study. Filled symbols indicate the reactions of the present study. Values of IP's and rate constants (corrected for addition) used are tabulated in APPENDIX E.2.. The correlation is, however, not as good as that of the OH-alkene reaction (Figure IV.15). A better correlation is seen if only alkyl benzenes (shaded symbols) and benzene are taken into consideration. Rinke and Zetzsch[195] suggested a harpoon mechanism for the OH-aromatic reactions to explain the correlation. As discussed in the previous chapter (IV.B.3.d.1.a) on the OH-cycloalkene reactions, the reactive cross sections predicted from the harpoon mechanism are generally larger than those observed experimentally. This is also true for the OH-aromatic reactions. The OH-aromatic reactions are even slower by a factor of ~5 than the reactions with alkenes whose ionization potentials are similar.

The frontier orbital theory,[202] which was also discussed in section IV.B.3.d.2., might again be used to explain the correlation. The highest occupied molecular orbital (HOMO) of benzene is doubly degenerate e_{1g}. As a substituent is introduced, the degeneracy is lifted and it splits to two levels b_1 and a_2. The b_1 type MO has its maximum electron density at the substituent and the para positions while an a_2 type MO has a node at those

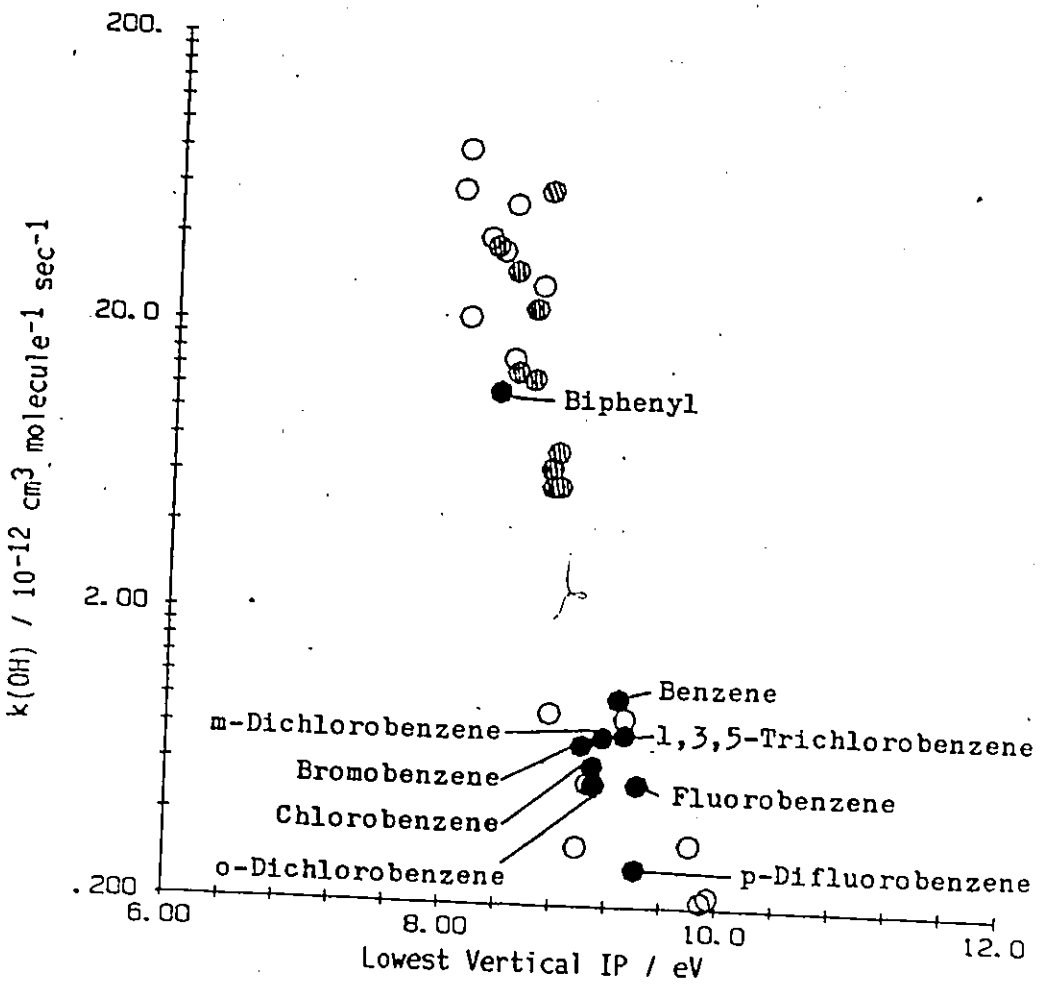

Figure V.22

The Correlation between the Reactivity of the OH Radical towards Aromatic Molecules and Lowest Vertical Ionization Potentials (IP) of Aromatic Molecules

Rate constants are taken from reference 38 and the present study (filled symbols).
The lowest vertial ionizations were taken from references 192, 194, and 241.
The values are tabulated in APPENDIX E.2..
Shaded symbols represent alkylbenzenes.

positions.[242]

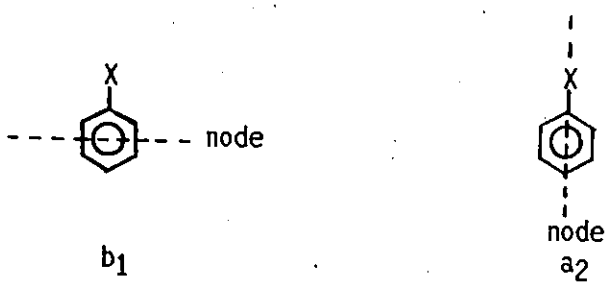

where X is a substituent. Electron-donating substituents raise the energy of b_1 resulting in smaller lowest ionization potentials than that of benzene, while electron-withdrawing substituents lower the energy of b_1 and to a lesser extent a_2 resulting in slightly larger lowest ionization potentials. This is illustrated below:

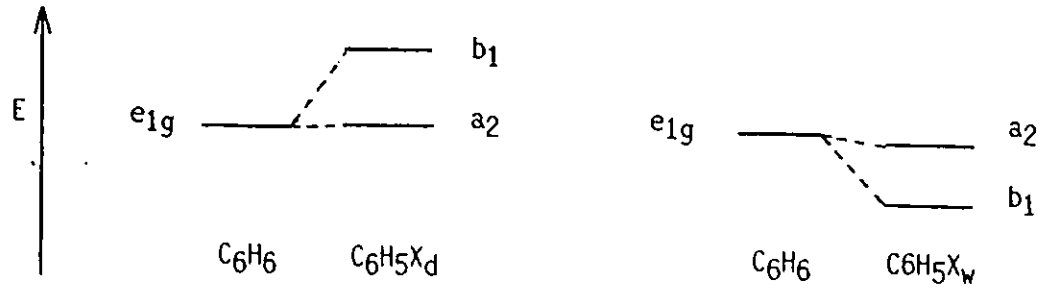

where X_d is an electron-donating group and X_w is an electron-withdrawing group. The extent of the change in the lowest ionization potential depends on the magnitude of the substituent effects. According to frontier orbital theory, the singly occupied molecular orbital (SOMO) of the OH radical should interact most strongly with HOMO of the aromatic molecule. The lower is the IP, the higher is the stabilization energy obtained by this interaction. (See section IV.B.3.d.2.) If this is the dominating factor of the reaction, the correlation between the rate constants and IP's would be expected. Although Figure V.22 shows a fair overall correlation, the

following discrepancies should be noted:

a. According to the theory, the positional selectivities of aromatic molecules with an electron donating substituent should be para > ortho > meta, but it has been observed that the ortho is dominant in the OH-toluene reaction.

b. The relative reactivities among isomers (di- and tri-substituted benzenes) are not consistent with those predicted from ionization potentials.

c. Although chloro-, bromo-, and iodobenzenes have lower IP's than that of benzene, their rate constants are smaller than that of benzene.

d. Since there does not seem to be any correlation between IP's and the activation energies of the OH-aromatic reactions, the mechanism behind the correlation is not certain. This is again similar to OH-alkene reactions.

There might be several other factors competing with the frontier orbital effect to determine the reactivity. Taking only the HOMO-SOMO interactions into account might not be adequate since the second highest occupied MO originating from the same e_{1g} is usually close to HOMO; there might be a substantial interaction with the second highest occupied MO. Since the transition state seems to be fairly tight in the OH-benzene reaction, one might expect some influence from the σ orbitals and the steric effect. This might be true especially for halogenated benzenes since halogen substituents have a strong polarity. The correlation might be indicating approximately the relative availability of the π electrons of substituted benzenes.

In summary, all three correlations (Figure V.20 - 22) examined here

support an electrophilic character of the OH radical. They also support the concept that the addition path is dominant. It is not yet certain why such correlations are exhibited since the activation energies of the OH-aromatic reactions do not correlate, and the positional selectivities, of the reactions are not known at present. Although there are general correlations among various OH-aromatic reactions, detailed reactivities of the OH-halogenated benzene reactions are not simply explained by the general trend. The extension of the study to lower temperatures would be helpful to first establish the energetics of addition process, and specifically whether there are any variations in activation energies as the substituents are altered. A study of positional selectivities of the reactions would be also helpful in extending the correlations, and evaluating the reasons for the correlations.

V.B.2.c. Implications of Kinetics of OH-Aromatic Reactions on Polychlorinated Biphenyls in the Atmosphere

Polychlorinated biphenyls (PCB's) as trace pollutants in the environment have been a serious concern for the past two decades because of their toxicological significance.[243] PCB's have been detected in the atmosphere, water, fish, seabirds, animals, and plants.[243-250] Data available on airborne pollutants suggest that PCB's are distributed through the environment primarily by the atmospheric transport process from the site of use and diposal,[243,248,251,252] and they are spread globally. Most of the airborne PCB's are in the vapour phase.[248,253] There are two classes of PCB's. The lower chlorinated biphenyls (LCB's) consist mostly of biphenyls with four or less chlorine substituents. Their mixtures were sold under

the names of Aroclor 1016 and 1242. The higher chlorinated biphenyls (HCB's) consists mostly of biphenyls with five or more chlorines substituted. Their commercial names were Aroclor 1248 and 1254. Although a larger amount of LCB's was used than HCB's until their production was banned and their use regulated in the 1970's,[243] PCB's found in animals, plants, fish, and waters are largely HCB's.[243,250] The study in the Great Lakes regions reported a significant amount of LCB's, (1242) and not HCB's (1254) in the atmosphere.[254] This pattern of PCB distribution has been attributed to the more effective loss of HCB's from the atmosphere by the wet and dry deposition.[244,245]

It is of a great interest to find out how PCB's behave chemically in the atmosphere. Photolysis and chemical reactions with some atmospheric species are potential homogeneous fates of the atmospheric PCB's. Arnts et al[255] studied the photolysis of o-chlorobiphenyl under simulated tropospheric conditions, and detected hydrogen chloride, aldehydes, phosgene, and phenolic compounds. Extremely high concentrations of aerosol were also observed. The mechanism of the system is not known yet, and the extent of the direct photolysis of 2-chlorobiphenyl is not certain.

The $OH^{\cdot}$ radical seems to be the best candidate for reaction with PCB's in the atmosphere since ozone reacts very slowly with aromatic compounds.[256] The experimental technique of the present study does not allow one to study directly the OH radical reaction with reactants whose vapour pressures are as low as those of PCB's. However, the rate constants of the OH radical reactions with biphenyl and chlorinated benzenes obtained in the present study may be used as models for the OH-PCB reactions.

The reaction of OH radical with biphenyl is moderately fast at room temperature. (Table V.4) If one assumes the concentration of the OH radical in the troposphere to be 5×10^5 molecule cm^{-3}, the halflife of biphenyl in the troposphere due to the OH radical reaction would be 33 hours. This implies that most of the biphenyl molecules would travel several hundred to several thousand kilometers from their source before they are removed from the troposphere if one assumes that the reaction with the OH radical is their only sink in the atmosphere.[118] Since all the chlorinated benzenes have been found to react with the OH radical more slowly than benzene (Table V.4), one might expect that all chlorinated biphenyls would react with the OH radical more slowly than biphenyl. The rate constant of the OH-biphenyl reaction can be considered as the upper limit of the rate constants of the OH-PCB reactions.

Experimental results for the rate constants have been obtained for the OH-monochlorobiphenyl reactions with relative rate methods by two groups. (Table V.5)[223,257] There are some significant discrepancies between their results, not only in the absolute values of rate constants but also in the relative reactivities among the three isomers of the monochlorobiphenyls. Atkinson and Aschmann[223] found the relative reactivities of the three OH-monochlorobiphenyl reactions in the order of 3- > 4- > 2-, while Dilling et al[257] found 4- > 3- > 2-. As was discussed in section V.B.2.b., the conjugation effect seems to be very important in determining the reactivities of chlorinated benzenes. A chlorine substituent should prefer electrophilic attack at positions which are ortho and para to the chlorine. Since the phenyl group also can provide π electrons to the benzene ring, it should enhance the reactivity of an electrophile at positions which are

Table V.5

Reported Rate Constants of the OH Radical Reactions with Biphnyl and Chlorobiphenyls at Room Temperature

Reactant	Atkinson and Aschmann (Ref. 223)a	Dilling et al (Ref. 257)b	This work
Biphenyl	8.2		11.7
2-Chlorobiphenyl	2.8	5.9	
3-Chlorobiphenyl	5.2	11.3	
4-Chlorobiphenyl	3.8	12.8	

All rate constants are in 10^{-12} cm^3 $molecule^{-1}$ sec^{-1}.
Rate constants in the literature were obtained with relative rate techniques.

a : relative to k(cyclohexene) = 7.28×10^{-12} cm^3 $molecule^{-1}$ sec^{-1}

b : relative to k(benzene) = 1.28×10^{-12} cm^3 $molecule^{-1}$ sec^{-1}

ortho and para to the phenyl group. If the substituent effects of the chlorine atom and the phenyl group are additive, 3-chlorobiphenyl would be expected to react faster than the 2- and the 4- isomers. Therefore, the relative reactivities obtained by Atkinson and Aschmann[223] (3- > 4- > 2-) are more reasonable than those by Dilling et al[257] (4- > 3- > 2-). The reason that 2-chlorobiphenyl is less reactive than 4-chlorobiphenyl might be that the addition to 2' position is sterically hindered. If the phenyl substituent gives ortho addition more than para addition (as a methyl substituent does), the steric hindrance of the ortho addition could reduce the observed rate constant significantly. This might be the case in the OH-2-chlorobiphenyl reaction. Since the absolute rate constant of the OH-biphenyl reaction obtained in the present study was ~43% higher than that reported by Atkinson and Aschmann[223], their relative values for the OH-monochlorobiphenyl reactions might also need to be increased.

There are 15 isomers of dichlorobiphenyls. Most of them would react with the OH radical even more slowly than monochlorobiphenyls. The 3,5-, 3,3'-, and 3,5'-dichlorobiphenyls, however, might have similar rate constants to those of 3-chlorobiphenyls if one uses the analogy of relative reactivities of monochlorobenzene and m-dichlorobenzene. Similarly, if the analogy of the relative reactivities of monochlorobenzene, m-dichlorobenzene, and 1.3.5-trichlorobenzene is used, PCB's with chlorines only on 3, 3', 5, or 5' position might react with the OH radical as fast as 3-chlorobiphenyl. Addition of a chlorine substituent to other positions could cause only a retarding effect to the reactivity. The higher chlorinated biphenyls (> Cl_4) would be chemically more persistent in the atmosphere.

In the analysis of the environmental samples, the PCB's are usually identified either by the commercial names or by the number of chlorine atoms in the PCB molecule. The specific isomers are not usually identified. How persistent the PCB's with chlorine atoms on positions 3, 3', 5, and 5' are in the atmosphere is not known. One might expect that LCB's are relatively more reactive than HCB's in the atmosphere because of their relatively fast reactions with the OH radical reactions. Since precipitation and dry deposition removes HCB's from the atmosphere more effectively than LCB's, HCB's would not have much chance to be involved in gas-phase reactions in the troposphere. LCB's, on the other hand, would be expected to stay longer in the atmosphere, and to be slowly degraded with the reactions with the OH radical or slowly removed from the atmosphere by the wet and dry depositions.

The OH radical would react with PCB's by addition. The adduct might lead to chlorinated phenylphenols which would be removed from the atmosphere more readily by wet and dry deposition because of their lower volatility. The adduct also might lead to the cleavage of the ring on which the OH radical is added, resulting in aldehydic products and substituted benzenes which might undergo further reactions in the atmosphere.

V.B.3. Summary of this chapter

The OH-benzene reaction exhibits a unique temperature dependence which has been observed previously by several groups, although there are some discrepancies among the various reports. The previously proposed mechanism involves formation and dissociation of an adduct of the OH radical and benzene, and the lifetime of the adduct plays a key role in

determining the observed kinetics. The proposed mechanism was evaluated by comparing the different kinetics observed in four temperature ranges (i) - (iv) with those simulated from the mechanism. The simulated kinetics agree fairly well with those experimentally obtained in the present study and by Tully et al.[122] Some possible sources of the discrepancies among the experimental results reported by the various groups were pointed out from the simulation study, namely an additional reaction of the thermalized adduct. Although a π complex has been proposed as an intermediate, all the experimental results reported so far can be explained with a mechanism which does not include a π complex.

The OH-chlorobenzene reaction showed a temperature dependence of the kinetics very similar to those of the OH-benzene reactions, except that temperature ranges (ii) and (iii) are shifted to slightly higher temperatures. This suggests that the adduct formed from the OH radical and chlorobenzene is more stable than that formed from the OH radical and benzene. Overall rates in the temperature range (iii) indicate that the non-addition process is significant only to about the same extent as the non-addition processes in the OH-benzene reaction.

The OH radical reactions with a series of selected halogenated benzenes were studied at room temperature. Their relative reactivities revealed an interesting feature of the halogen substituents. Their reactivity can be explained as being due to a combination of the effect of their electronegativities and that of conjugation on the π electron density of the benzene rings. The relative reactivities among the isomers of dichloro- and trichlorobenzenes indicate that the conjugation effect is important in determining the positional selectivities of the reactions.

The existence of correlations of the rate constants of OH-aromatic reactions with those of O-aromatic reactions, $\Sigma \sigma^+$, and the ionization potentials of aromatic molecules has been previously pointed out, and the correlations support the argument that the reactions occur largely by electrophilic addition to the aromatic rings. While the correlations are very useful in establishing general trends in the experimental results, there are limitations to their applications. For example, some halogenated benzenes and hetero-atom substituted benzenes deviate from the general trend of the alkyl benzenes in the $\Sigma \sigma^+$ and the IP correlations. The source of the correlation is also not clear, i.e. whether the energetics of the reactions or other factors correlate. Further studies were proposed: the extension of the temperature ranges of the kinetic study to lower than room temperature and higher than the maximum temperature of the present study, and the study of the positional selectivities by product analysis.

The relative reactivities of the OH radical with benzene and various chlorinated benzenes were used as a model to examine the reactivities of the OH-PCB reactions. The upper limit of the rate constants of any OH-PCB reactions is expected to be similar to that of biphenyl which was also determined in the present study. If some or all of 3, 3', 5, and 5' positions of a biphenyl have chlorine substituents and none of the other positions are substituted, the rate constant of the reaction with the OH radical would be expected to be larger than those of the other isomers. Addition of a chlorine atom to the other positions would cause only retarding effects. In the atmosphere, PCB's with chlorine substituents only on 3, 3', 5, or 5' positions might be lost from the atmosphere relatively quickly by the OH radical reactions. Other more highly

chlorinated PCB's (> Cl_4) would react more slowly and have higher chemical persistence in the atmosphere. They might be more effectively lost by wet and/or dry deposition.

APPENDIX A

PURITY LEVELS OF THE CHEMICALS

Table A lists the purity levels of the chemicals used in the present study. All chemicals were used as they were received from the manufacturers without further chromatographic purification. All cycloalkenes and aromatics were degassed before use. GC analyses were performed for all cycloalkenes and aromatics using a capillary column (0.25 mm i.d. and 21 m long) filled with OV101. A mixture of potential impurities and the reactant was first injected to determine the appropriate temperature programing to separate each component. Then, the reactant was injected under the same conditions. Identified impurities are listed in Table A.

Table A

Purity Levels of Chemicals Used in the Present Study

Chemical	Stated Purity Levels (%)	Manufacturer	Impurities Identified by GC Analysis
Argon	99.999 99.998	CANADIAN LIQUID AIR	
Hydrogen	99.99		
Ethene	99.5		
Propene	99.0		
Cyclopentene	99	ALDRICH	< 0.3% cyclopentane
Cyclohexene	99+		0.12% benzene, 0.11% 1,3- and 1,4-cyclohexadienes
Cycloheptene	99+		0.75% diene or triene and/or cycloheptane, 0.7% involatile substance
1,3-Cyclohexadiene	99.9	CHEM SAMP	0.2% benzene, 1% substance(s) with b.p. > 210 C
1,4-Cyclohexadiene	99.9	ALDRICH	0.27% benzene, 0.05% cyclohexene, 0.3% substance(s) with b.p. > 260 C
Benzene	99+	MATHESON	< 0.01% toluene
Fluorobenzene	99	ALDRICH	No detectable impurity
p-Difluorobenzene	98		0.05% benzene, 0.12% ortho isomer
Chlorobenzene	Analyzed Reagent	BAKER	No detectable impurity

(Continued)

(Continued)			
o-Dichloro-benzene	99+	ALDRICH	0.2% para isomer
m-Dichloro-benzene	98		0.7% ortho, 5.4% para isomers
1,3,5-Tri-chloro-benzene	98		No detectable impurity
Bromo-benzene	99+		0.28% benzene, 0.52% dibromo-benzene
Biphenyl	98	BDH	0.15% substance with b.p > 260 C

APPENDIX B

COMPUTER SIMULATION OF THE REACTION SYSTEMS

A set of computer programs was kindly provided by Dr. D. P. Santry to simulate the kinetics of the reacting systems of the present study. The set is called KINETICS, and consists of three parts: ZAUBER, VOGEL, and PLOT. The function of each part will be described using a simple reaction system:

$$\begin{aligned} A + B &\longrightarrow C \quad k_B \\ A + C &\longrightarrow D \quad k_C \end{aligned} \tag{B1}$$

This system involves two reactions with four species. Rate equations of the four species are:

$$\begin{aligned} \frac{d[A]}{dt} &= -k_B[A][B] - k_C[A][C] \\ \frac{d[B]}{dt} &= -k_B[A][B] \\ \frac{d[C]}{dt} &= k_B[A][B] - k_C[A][C] \\ \frac{d[D]}{dt} &= k_C[A][C] \end{aligned} \tag{B2}$$

ZAUBER takes chemical equations (B1) as input data, and sets up rate equations (B2) in a manner readable by VOGEL. VOGEL simultaneously and numerically solves all the rate equations (B2) for given initial concentrations

of species. Gear's method[155] was chosen to solve the series of stiff differential equations. The solutions are given in the form of the concentration of each species as a function of time. PLOT plots the solution (concentration versus time) in one of linear-linear, log-linear, or log-log scales.

B.1. Loss of the OH Radical in the Absence of a Reactant

A total of 19 reactions were taken into account to simulate the decay of the OH radical concentration in the absence of a reactant, including reactions 1 - 15 of CHAPTER III.B and diffusion loss of other species, such as H, H_2O_2, HO_2, and O. Rate constants of reactions were taken from reference 144. Rate constants at 295 K with argon as a diluent gas were used when they were available. Otherwise, those at either 298 K or 300 K with nitrogen as a diluent gas were used. Diffusion rate constants were estimated to be 6, 100, 5, 2.6, amd 3.5 sec^{-1} for OH, H, O, H_2O_2, and HO_2 respectively. As described in CHAPTER III.B, various initial concentrations of the OH radical were employed in solving the rate equations. It was found that when the initial concentration of the OH radical (and therefore that of H atom also) is $< 5 \times 10^{11}$ molecule cm^{-3}, the reactions 3 - 15 had practically no influence on the decay curves of the OH radical concentration compared with diffusion (reaction 2).

B.2. Effect of Secondary Reactions

Several simulations were performed for a reaction system of two reactions:

$$OH + R \longrightarrow P \qquad 16$$

$$OH + A \longrightarrow P1 \qquad 18$$

Diffusion loss of the OH radical was omitted for simplicity. Since [R] >> [OH] in all experiments, reaction 16 was treated as pseudo-first-order in calculation with the rate constant $k_{16(obs)} = k_{16}[R]$. For typical experimental conditions, apparent rate constants, k(app), lie between 50 and 500 sec^{-1}. Computations were performed for various $k_{16(obs)}$ between 100 and 500 sec^{-1}. Extreme conditions were assumed for the reaction 18 to estimate the maximum influence of the secondary reaction with the photolysis product of the reactant. The initial concentration of the photolysis product A was assumed to be proportional to the reactant concentration, and it was as high as that of the OH radical (10^{11} molecule cm^{-3}) when $k_{16(obs)}$ was 500 sec^{-1}. The rate constant of reaction 18 was assumed to be approximately the collision frequency ($\sim 10^{-10}$ cm^3 $molecule^{-1}$ sec^{-1}). Within the above range of $k_{16(obs)}$, it was found that decay curves of the OH radical stayed exponential for three to four halflives. If the contribution from reaction 18 is negligible, k(app) should be equal to $k_{16(obs)}$. Rate constants k(app) became, however, increasingly higher than $k_{16(obs)}$ as the values of $k_{16(obs)}$ were increased, but the maximum deviation was only ~ 10 sec^{-1} at $k_{16(obs)} = 500$ sec^{-1}. Within the typical accuracy of the present technique, this would be undetected.

The secondary reaction with the reaction product P was also considered in a simulation study by solving the rate equations of a system involving two reactions:

$$OH + R \longrightarrow P \qquad 16$$

$$OH + P \longrightarrow P2 \qquad 19$$

The collision frequency rate was again assumed for reaction 19. It was found that decay curves deviated slightly from exponentiality with time. The rate constant k(app) became faster from the first halflife to the second and the third halflives. The extent of deviation was almost independent of $k_{16(obs)}$. For example, during the first halflife, the rate constant k(app) was faster than $k_{16(obs)}$ by ~3 sec^{-1}, in the second halflife by 6 sec^{-1} and in the third by ~8 sec^{-1}. Since the deviation became noticeable only when the concentration of the OH radical became lower, it might have been difficult to observe experimentally. In addition, since the magnitudes of the deviations are independent of $k_{16(obs)}$, determination of k_{16} would hardly be affected by this secondary reaction even under this extreme condition.

APPENDIX C

ERROR ANALYSIS AND CONCENTRATION CALCULATIONS OF THE REACTANTS

C.1. Weights Used in Decay Curve Analysis

Since the uncertainty of photon counting follows the Poisson distribution, the uncertainty of a count recorded at the i-th channel P(i) is

$$\sigma(i) = P(i)^{1/2} \tag{c1}$$

The fluorescence count at the i-th channel is

$$F(i) = P(i) - ABG \tag{c2}$$

where ABG is the average background count per channel. The weighted least square analysis used was performed on a $Y(i) = \ln F(i)$ versus t_i plot to compute the observed first-order rate constant k_{obs}, where t_i was the time at i-th channel. The weight used in the analysis was calculated according to the rule of the propagation of errors:[156]

$$w(i) = F(i)^2 / P(i) \tag{c3}$$

C.2. Detection of Non-Random Errors in Decay Curve Analysis

Various halflives of decay curves were used in the calculation of k_{obs} to check if there were any systematic deviations of the fitted curves from the experimental ones. The weighted residuals and an autocorrelation function were plotted for each fit to detect the deviations. When an

observed curve with n points (Y(i) versus t_i) is fitted to a function YFIT(t), the weighted residual of the i-th point RES(i) is defined as

$$RES(i) = (Y(i) - YFIT(t_i))\ w(i)^{1/2} \qquad (c4)$$

where w(i) is the weight of a point Y(i). If RES(i) is evenly scattered around zero (Figure III.1(c)), the fit is said to be less susceptible to systematic errors. An autocorrelation function[157] is a more sensitive tool to detect non-randomness of a residual plot. It is defined as

$$C(j) = (1/m)\left(\sum_{i=1}^{m} RES(i)\ RES(i+j)\right) \Big/ (1/n)\left(\sum_{i=1}^{n} RES(i)^2\right) \qquad (c5)$$

where C(j) is an autocorrelation function, m = n/2, and j = 0,1,2,...(n-m); C(0) = 1 by definition. If the residual scatters randomly and m approaches infinity, C(j) will become zero for $j \neq 0$. In practice, however, due to the finite value for m, C(j) shows high-frequency and low-amplitude fluctuation about zero when plotted against j or t_j. (Figure II.1(d)) If a C(j) plot shows a systematic trend rather than random fluctuation, it indicates possible systematic errors in the fitted curve.

C.3. Calculation of the Concentration of a Reactant and Its Uncertainty

As described in CHAPTER II.D., three streams of gases with volumetric flow rates F_1, F_2, and F_3 were mixed before entering the reaction cell. They contained argon only, argon with water vapour, and argon with $\vec{a}$ reactant, respectively. The upstream pressures of the first two streams were maintained at atmospheric pressure P_{atm} by using a bubbler. The upstream pressure of the third stream P_R was either measured with an

electronic manometer (Figure II.9(a)) or maintained at atmospheric pressure (Figure II.9(b)) depending on the method of mixing a reactant, as described in CHAPTER II.D. The ratio of a reactant to argon in the third stream R_m was determined either by preliminary pressure measurement of a reactant (Figure II.9(a)) or from the vapour pressure of the reactant at the temperature of the condensers (Figure II.(b)). The concentration of a reactant in the mixed flow through the reaction cell was calculated from the equation

$$[R] = D\, P_{tot}\, R_m\, C\, /\, T \qquad \text{(c6a)}$$

where

$$D = F_3\, P_R\, /\{(F_1 + F_2)\, P_{atm} + F_3\, P_R\} \qquad \text{(c6b)}$$

[R] is calculated in molecule cm^{-3}. F_1, F_2, and F_3 are measured in cm^3 sec^{-1}, P_R and P_{atm} in torr. P_{tot} is the total pressure in the cell measured in torr, T is the temperature in the cell in K, and C is a conversion factor (9.658×10^{18} molecule K cm^{-1} $torr^{-1}$).

Random errors associated with [R] values are primarily from two sources: (a) random errors associated with the calibration curves of flowmeters, and (b) random errors associated with the calibration curves of u.v. absorption of a reactant if absorption was used to correct R_m values. One can estimate random errors of σF_1, σF_2, σF_3, and σR_m from the standard deviations of the calibration curves. By the propagation of errors, the random error $\sigma[R]$ associated with [R] is estimated:

$$\left(\frac{\sigma[R]}{[R]}\right)^2 = \frac{P_{atm}^2\,(\sigma F_1^2 + \sigma F_2^2)}{\{\,P_{atm}\,(F_1 + F_2) + P_R\,F_3\,\}^2} + \left(\frac{\sigma F_3}{F_3}\right)^2 + \left(\frac{\sigma R_m}{R_m}\right)^2 \qquad (c7)$$

$\sigma[R]/[R]$ is usually in the range of 1 ~ 1.5%.

Systematic errors associated with [R] are primarily due to the accuracies of various instruments:

(a) the accuracies of measurements of P_{tot}, P_{atm}, and P_R with manometers (ΔP_{tot}, ΔP_{atm}, ΔP_R),

(b) the accuracy of the temperature measurement (ΔT),

(c) the accuracies of the flowmeter measurements (ΔF_1, ΔF_2, ΔF_3),

(d) the accuracy of the absorption measurement if used, and

(e) the accuracy of the vapour pressure equation of a reactant if used.

The sources (d) and (e) determine the accuracy of R_m (i.e. ΔR_m). Using the rule of the propagation of errors, the systematic error $\Delta[R]$ associated with [R] is estimated to be

$$\left(\frac{\Delta[R]}{[R]}\right)^2 = \left(\frac{P_{atm}\,(\Delta F_1 + \Delta F_2)}{P_{atm}\,(F_1 + F_2) + P_R\,F_3}\right)^2 + \left(\frac{\Delta F_3}{F_3}\right)^2 + \left(\frac{\Delta R_m}{R_m}\right)^2$$

$$+ \left(\frac{(F_1 + F_2)\,\Delta P_{atm}}{P_{atm}\,(F_1 + F_2) + P_R\,F_3}\right)^2 + \left(\frac{\Delta P_R}{P_R}\right)^2 + \left(\frac{\Delta P_{tot}}{P_{tot}}\right)^2 + \left(\frac{\Delta T}{T}\right)^2$$

From the calculations of $\Delta[R]$ for various experimental conditions, it was found that the value of $\Delta[R]$ was primarily determined by ΔR_m, ΔP_{tot}, ΔP_R. The equation to calculate $\Delta[R]$, therefore, can be approximated to

$$\left(\frac{\Delta[R]}{[R]}\right)^2 = \left(\frac{\Delta R_m}{R_m}\right)^2 + \left(\frac{\Delta P_{tot}}{P_{tot}}\right)^2 + \left(\frac{\Delta P_R}{P_R}\right)^2 \qquad (c8)$$

It was also found that $\Delta[R] / [R]$ values were fairly constant within a series of experiments to obtain one second-order rate constant.

C.4. The Least Square Cubic Method and Calculation of the Overall Accuracy

Since both k_{obs} and the reactant concentration [R] have substantial random errors, one should use a least square analysis which takes into account the weights in both the coordinates when the slope of k_{obs} versus [R] is determined. The most unbiased method is the least square cubic method introduced by York.[158] In his method, a slope (b) and an intercept (a) are searched which minimize S:

$$S = \sum_{i=1}^{n} \{w(X_i)\ (x_i - X_i)^2 + w(Y_i)\ (y_i - Y_i)^2\} \qquad (c9)$$

where $y_i = a + bx_i$ (a fitted curve), (X_i, Y_i)'s are observed points, $w(X_i)$ and $w(Y_i)$ are weights of X_i and Y_i respectively, and n is the total number of observed points. To minimize S, one must solve

$$b^3 - 3\alpha b^2 + 3\beta b - \gamma = 0 \qquad (c10)$$

where $$\alpha = 2 \sum \frac{W_i^2 U_i V_i}{w(X_i)} \Big/ 3 \sum \frac{W_i^2 U_i^2}{w(X_i)}$$

$$\beta = -\left(\sum W_i U_i^2 - \sum \frac{W_i^2 V_i^2}{w(X_i)}\right) \Big/ 3 \sum \frac{W_i^2 U_i^2}{w(X_i)}$$

$$\gamma = -\left(\Sigma W_i U_i V_i\right) / \Sigma \frac{W_i^2 U_i^2}{w(X_i)}$$

$$W_i = \frac{w(X_i)\, w(Y_i)}{b^2 w(Y_i) + w(X_i)}$$

$$U_i = X_i - \bar{X}, \qquad V_i = Y_i - \bar{Y}$$

$$\bar{X} = \frac{\Sigma W_i X_i}{\Sigma W_i}, \qquad \bar{Y} = \frac{\Sigma W_i Y_i}{\Sigma W_i}$$

The solution of the equation (c10) is

$$b(j+1) = \alpha + 2(\alpha^2 - \beta)^{1/2} \cos\{(\theta + 2\pi j) / 3\} \qquad \text{(c11)}$$

where $j = 0, 1, 2$, and

$$\cos\theta = \frac{\alpha^2 - (3/2)\,\alpha\,\beta + (1/2)\gamma}{(\alpha^2 - \beta)^{3/2}}$$

As far as York had investigated,[157] $b(3)$ was always the satisfactory solution. W_i, however, contains b in its denominator. One must first estimate b and calculate $b(3)$ which is in turn used as b to obtain new $b(3)$. This process must be repeated until b and $b(3)$ converge. The value of b obtained from non-weighted least square analysis was used as a starting value, and iteration was repeated by computer until b and $b(3)$ converge within 0.1% of their values with one another. The uncertainties of a and b were calculated from

$$(\sigma_b)^2 = \frac{1}{n-2} \frac{\Sigma W_i (bU_i - V_i)^2}{\Sigma W_i U_i^2} \qquad (c12)$$

$$(\sigma_a)^2 = (\sigma_b)^2 \frac{\Sigma W_i X_i}{\Sigma W_i} \qquad (c13)$$

In the present study, $Y_i = k_{obs}$, $X_i = [R]$, $w(Y_i) = 1 / (\sigma k_{obs})^2$, and $w(X_i) = 1 / (\sigma[R])^2$, where σk_{obs} is the standard deviation of k_{obs} obtained in the weighted linear least square analysis and $\sigma[R]$ is the random error associated with [R] estimated in the way described in the previous section. The calculated value of b is the second-order rate constant k_{16} (shortly, k), and σ_b is the standard deviation of k (i.e. σk).

The overall accuracy of the second order rate constant k can be estimated from the equation

$$\frac{\Delta k}{k} = \frac{m\, \sigma k}{k} + \frac{\Delta[R]}{[R]} + \frac{\sigma[R]}{[R]} \qquad (c14)$$

The first term of the equation (c14) deals with the random error associated with the determination of the slope of the k_{obs} versus concentration plot, and $m = t / \sqrt{N}$, where t is the Student's t factor and N is the number of points in the plot. The confidence level of 95% was used in the present study. The second and third terms deal with the errors associated with the determination of concentrations described in the previous section C.3. The worst possible case was taken into account to calculate these terms.

C.5. Calculation of Arrhenius Parameters

Since the random error associated with the temperature was considerably smaller than that with the second order rate constant k at that temperature, only the latter was taken into account in calculating conventional Arrhenius parameters in CHAPTER IV. The weighted linear least square analysis was performed to calculate an apparent activation energy and a pre-exponential factor. The rule of the propagation of errors was used to calculate appropriate weights similar to those in section 1 of this Appendix.

APPENDIX D

MODEL STUDIES OF THE DECAY CURVES OF THE CONCENTRATION OF THE OH RADICAL BY DIFFUSION, AND DIFFUSION PLUS A FIRST-ORDER REACTION

A model was constructed to study the pattern of diffusion in the reaction zone. It assumed that initially a uniform concentration of OH radicals was present in a cylindrical form with a diameter of 1.6 cm in a coaxial cylindrical cell with a diameter of 4 cm. (Figure D(a)) This can be reduced to a two-dimensional problem. The concentration of the OH radical C is a function of radius r around the center of the cell and time t. The diffusion equation is[159]

$$\frac{\partial C(r,t)}{\partial t} = D \left(\frac{\partial^2 C(r,t)}{\partial r^2} + \frac{1}{r} \frac{\partial C(r,t)}{\partial r} \right) \qquad (d.1)$$

where D is a diffusion coefficient of the OH radical, which was estimated to be ~4.8 $cm^2\ sec^{-1}$ in 100 torr of argon. Initial and boundary conditions are

$$\text{at } t = 0,\ C(r,t) = C_0 \text{ at all } r < 0.8 \text{ cm}$$

$$\text{and } C(r,t) = 0 \text{ elsewhere}$$

$$C(r,t) = 0 \text{ at } r = 2 \text{ cm at all time.}$$

The equation (D.1) was numerically solved with a computer simulation package called FORSIM VI written by ATOMIC ENERGY OF CANADA LIMTED. The package was made available by Mr. F. Kus from the Academic Computing Center at McMaster University. The solution was given in a form of C as a function of r and t. (Figure D(b)) From the numerical solution, the average concen-

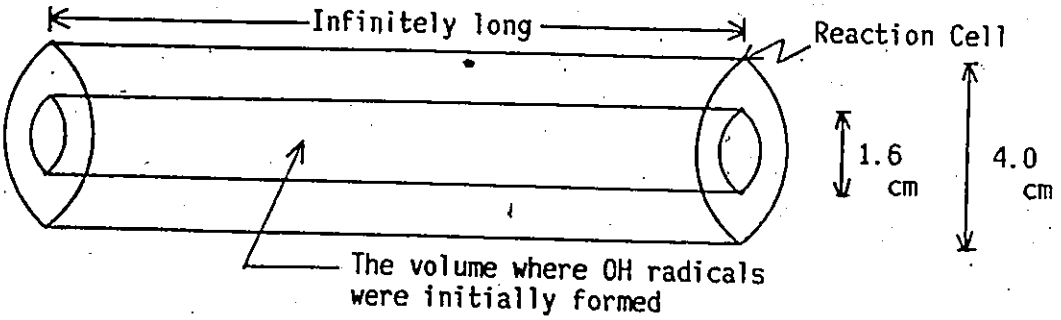

Figure D (a)

A Model Used to Study the Diffusion Pattern of OH Radicals in the Reaction Cell

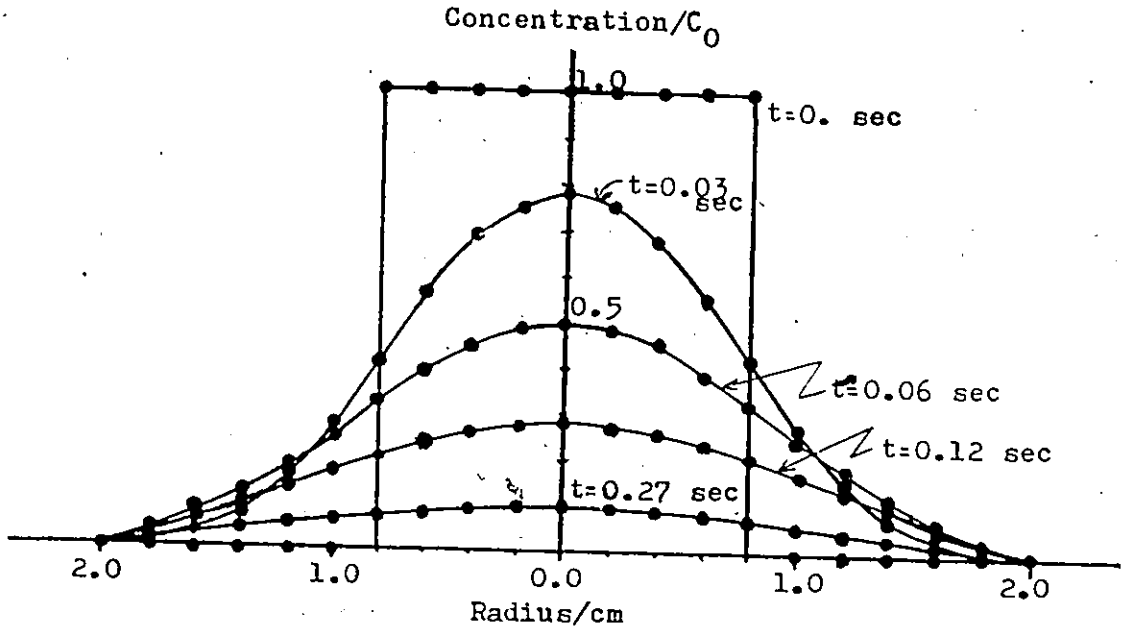

Figure D (b)

The Concentration of the OH Radical as a Function of Time and Radius in the Diffusion Model of (a)

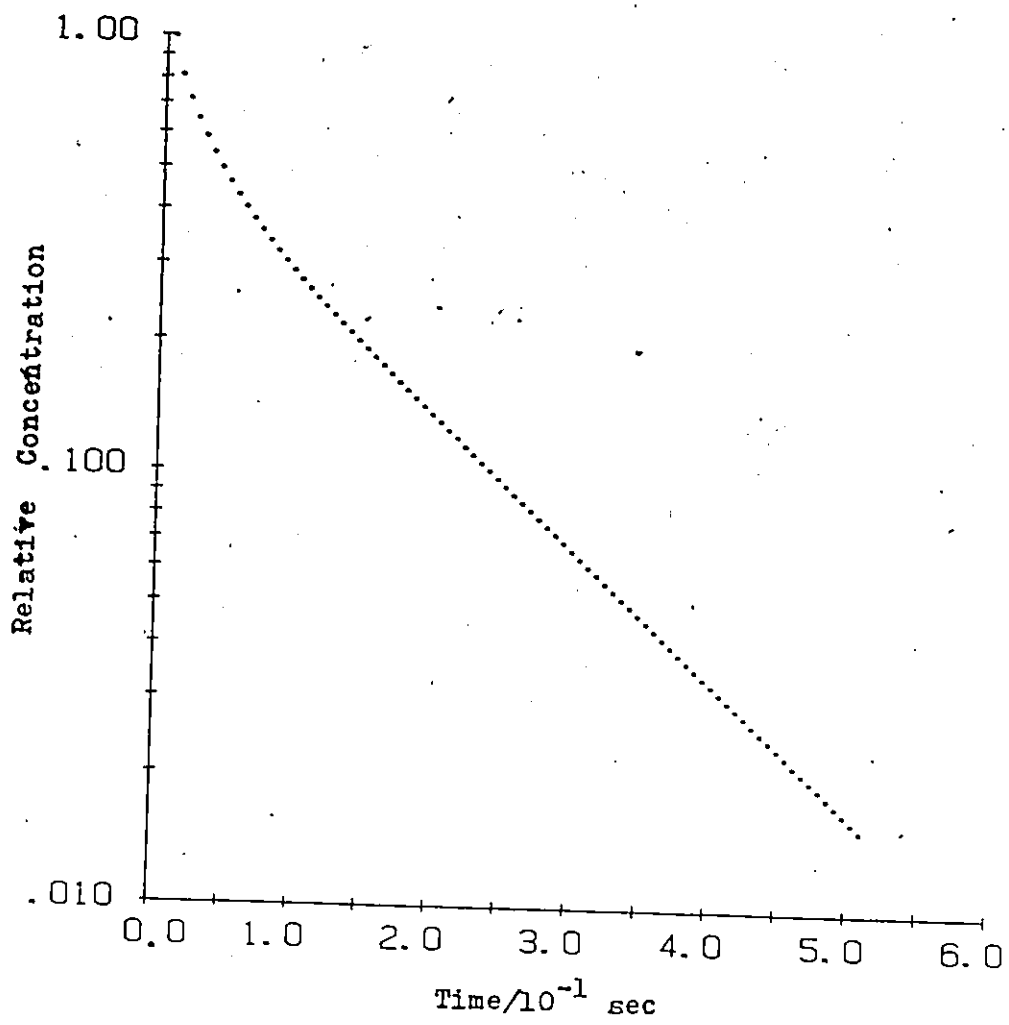

Figure D (c)

The Average Concentration of the OH Radical in the Central Area ($r \leq 0.8$ cm) as a Function of Time in the Absence of a Reaction

tration within $r \leq 0.8$ cm was calculated as a function of time. Figure D(c) shows the average concentration as a result of such a calculation. (Compare with Figure III.2)

For the system with a first-order reaction, the following equation was solved for various first-order rate constants, k, with the same initial and boundary conditions used in the previous diffusion-only calculations:

$$\frac{\partial C(r,t)}{\partial t} = D \frac{\partial^2 C(r,t)}{\partial r^2} + \frac{1}{r} \frac{\partial C(r,t)}{\partial r} - k\, C(r,t) \qquad \text{(d.2)}$$

where k is the first-order rate constant. Figure D(d) shows some examples of the results of such computations.

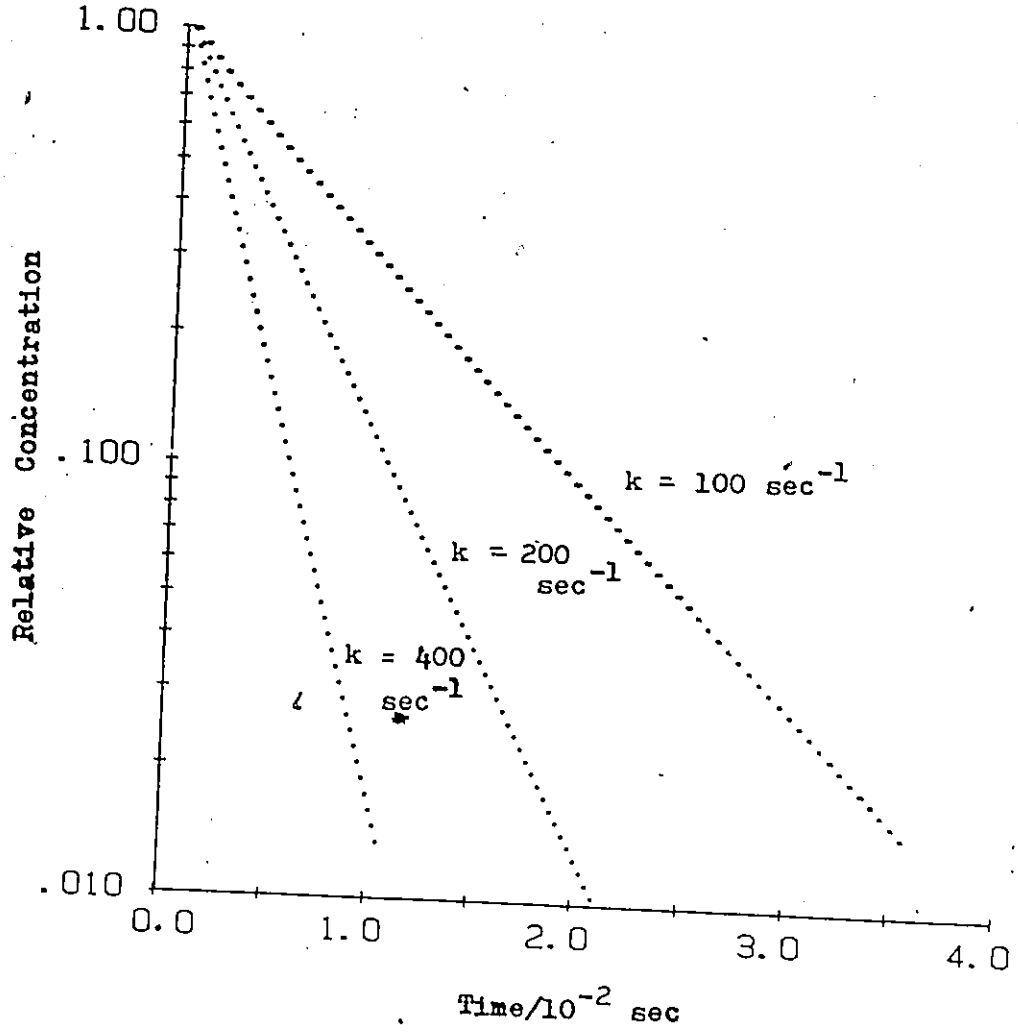

Figure D (d)

The Average Concentration of the OH Radical in the Central Area ($r \leq 0.8$ cm) as a Function of Time in the Presence of a First-Order Reaction

APPENDIX E

TABULATION OF VARIOUS PARAMETERS USED IN FIGURES IV.13, IV.15, IV.16, V.20, V.21, AND V.22

E.1. Ionization Potentials, Rate Constants of the OH Radical and the O Atom Reactions, and Reaction Cross Sections ($\bar{\sigma}_{EXP}$) of Various Alkenes

Alkene	IP/eV[a]	k(OH)[e,f]	k(O)[e,a]	$\bar{\sigma}_{EXP}/A^{2k}$
Ethene	10.52	8.54	0.76	1.1
Propene	9.74	26.3	4.46(h)	3.6
1-Butene	9.63	31.4	4.2	4.5
Isobutene	9.24	51.4	16	7.8
cis-2-Butene	9.12	56.1	18	8.1
trans-2-Butene	9.12	63.7	23	9.2
1-Pentene	9.52	31.9	4.6	4.7
2-Methyl-1-butene	9.12(b)	60.7		9.0
3-Methyl-1-butene	9.53	31.8	4.3	4.7
2-Methyl-2-butene	8.68	86.9	54	12.9
cis-2-Pentene	9.04	65.1	18	9.6
Cyclopentene	9.02	54.3(g)	23	8.0
1-Hexene	9.48	37.5	5.2	5.6
Cyclohexene	8.95	65.1(g)	22	9.6
2,3-Dimethyl-2-butene	8.27	110	80	10.6
1-Methylcyclohexene	8.67(c)	94.5	58	14.4
Cycloheptene	9.04(d)	71.9(g)		10.3
3,3-Dimethyl-1-butene	9.7(d)	28.4		4.3
1-Heptene	9.44(c)	40.5		6.2
cis-2-Pentene	9.04(c)	65.1		9.6
trans-2-Pentene	9.04(c)	67.2		9.9
Propadiene	10.16	9.79	1.2(i)	1.4
1,3-Butadiene	9.07	66.8	20.4(i)	9.6
1,3-Cyclohexadiene	8.25	137.4(g)	100	20.2
1,4-Cyclohexadiene	8.82(b)	96.1(g)		14.4
2-Methyl-1,3-Butadiene	9.04(d)	101		14.9
1,3-Cycloheptadiene	8.30(d)	139		20.1
Bicyclo[2,2,1]-2-heptene	8.81(b)	49.1		7.5
Bicyclo[2,2,1]-2,5-heptadiene	8.42(b)	120		18.2
2,4-Hexadiene	8.18(c)	135		20.3

(continued)

(continued)

4-Methyl-1,3-pentadiene	8.28(c)	132		19.8
3-Methyl-1,3-pentadiene	8.39(c)	137		20.6
1,3-Hexadiene	8.53(c)	113		17.0
2,3-Dimethyl-1,3-butadiene	8.62(c)	122		18.3
1,3-Pentadiene	8.67(c)	101		14.9
3-Methyl-1,2-butadiene	8.95(c)	57.1		8.4
1,2-Pentadiene	9.25(c)	35.6		5.3
1,4-Pentadiene	9.62(c)	53.3		7.8
Fluoroethene		5.56	0.344(j)	
Chloroethene		6.6	0.60	
Bromoethene		6.81	0.57	
α-Pinene		53.2	32	
β-Pinene		78.2	29	
d-Limonene		169	125	

a : From reference 167 if otherwise noted
b : From reference 192
c : From reference 191
d : From reference 193
e : In 10^{-12} cm^3 $molecule^{-1}$ sec^{-1}
f : From reference if 38 otherwise noted
g : From this work
h : From reference 171
i : From reference 169
j : From reference 170
k : Calculated according to the equation in IV.B.3.d.1.(a)

E.2. Rate Constants of the OH Radical and the O Atom Reactions, Ionization Potentials, and $\Sigma \sigma^+$ of Various Aromatic Compounds

Aromatic compound	k(OH)[a,b]	k(O)[a]	IP/eV[j]	$\Sigma \sigma^+$ m
Benzene	1.06[0.99][c]	0.0199[e]	9.25	0.0
Toluene	6.19[5.7]	0.0809[e]	8.78	-0.311
o-Xylene	14.7[13.4]	0.198[f]	8.57	-0.377
m-Xylene	24.5[23.5]	0.372[f]	8.57	-0.622
p-Xylene	15.2[14.1]	0.200[f]	8,45	-0.377
1,2,3-Trimethylbenzene	33.3[31.6]	1.159	8.42	-0.688
1,2,4-Trimethylbenzene	40.0[38.4]	1.004[g]	8.27	-0.688
1,3,5-Trimethylbenzene	62.4[60.5]	2.809	8.65[k]	-0.933
Phenol	28.3		8.61	-0.92
o-Cresol	40[37]		8.32	-0.986
m-Cresol	57[54]		8.40	-1.231
p-Cresol	44[41]		8.22	-0.986
Methoxybenzene	15.7[12.6]	0.265[h]	8.42[k]	-0.778
Aniline	116[~60]		8.02	-1.3
N,N-Dimethylaniline	148			-1.7
p-Chloroaniline	83		8.05	-0.901
n-Propylbenzene	5.7		8.73	-0.295
Isopropylbenzene	6.6		8.72	-0.28
o-Ethyltoluene	12.0			-0.375
m-Ethyltoluene	17.1			-0.606
p-Ethyltoluene	11.4			-0.375
Ethylbenzene	7.5		8.76	-0.295
Fluorobenzene	0.53[c]	0.0132[h]	9.40	-0.073
p-Difluorobenzene	0.27[c]		9.40[k]	0.279
n-Propylpentafluorobenzene	3.06			0.419
Hexafluorobenzene	0.219		9.93	0.837
Benzotrifluoride	0.48[0.41]	0.0058[h]		0.520
Chlorobenzene	0.61[c]	0.185[i]	9.07	0.114
o-Dichlorobenzene	0.51[c]		9.08	0.513
m-Dichlorobenzene	0.77[c]		9.14	0.228
p-Dichlorobenzene	0.32		8.97	0.513
1,2,4-Trichlorobenzene	0.50		9.04	0.627
1,3,5-Trichlorobenzene	0.79[c]		9.30[l]	0.342
Bromobenzene	0.72[c]		8.99	0.15
Iodobenzene	0.93		8.75	0.135
Benzonitrile	0.33		9.79	0.562

(continued)

(continued)

Nitrobenzene	0.21		9.88	0.674
o-Nitrophenol	0.90		9.30	-0.13
4-Chlorobenzotrifluoride	0.25			0.634
Naphthalene	21.7		8.09	
Biphenyl	11.7{5.85}[c,d]		8.34	-0.179

a : Rate constants are in 10^{-12} cm^3 $molecule^{-1}$ cm^{-1}.
b : Rate constants are from reference 38 unless otherwise stated. Values in square brackets are rate constants of addition process recommended in reference 38.
c : From this work
d : The value in a bracket is a rate constant per benzene ring which was used in Figure V.21.
e : From references 227, 229, and 230
f : From references 228 and 230
g : From reference 230
h : From reference 231
i : From references 232 and 233
j : From reference 191 unless otherwise indicated
k : From reference 193
l : From reference 239
m : From reference 38

REFERENCE

1. W. W. Watson, Astrophys. J., 60, 145 (1924)
2. K. F. Bonhoeffer and H. Reichardt, Z. Phys. Chem., 139, 75 (1928)
3. O. Oldenberg, J. Chem. Phys., 3, 266 (1935)
4. B. Lewis and G. von Elbe, Combustion, Flames, and Explosion of Gases, Academic Press, New York (1951)
5. G. J. Minkoff and C. F. H. Tipper, Chemistry of Combustion Reactions, Butterworths, London (1962)
6. D. D. Drysdale and A. C. Lloyd, Oxid. Comb. Rev., 4, 157 (1970)
7. A. G. Gaydon, Flames, Their structure, radiation, and temperature, 4th ed., Chapman and Hall, London (1979)
8. N. R. Greiner, J. Chem. Phys., 46, 3389 (1967)
9. P. A. Leighton, Photochemistry of Air Pollution, Academic Press, New York (1961) Chapter VIII
10. H. Okabe, Photochemistry of Small Molecules, Wiley-Interscience, New York (1978) pp. 334 - 336
11. J. S. Levine, The Photochemistry of Atmospheres, Academic Press, Orlando (1985)
12. H. B. Singh, Geophys. Res. Lett., 4, 101 and 453 (1977)
13. J. E. Lovelock, Nature, 267, 32, (1977)
14. W. B. Neely and J. H. Plonka, Environ. Sci. Technol. 12, 317 (1978)
15. M. A. K. Khalil and R. A. Rasmussen, Tellus, 368, 317 (1984), Chemosphere, 13, 789 (1984)
16. B. Weinstock and T. Y. Chang, Tellus, 26, 108 (1974)
17. A. Volz and K. H. Ehhalt, J. Geophys. Res., 86, 5163 (1981)
18. J. G. Calvert, Environ. Sci. Technol., 10, 256 (1976)
19. J. M. Roberts, F. C. Fehsenfeld, S. C. Liu, M. J. Bollinger, C. Hahn, D. L. Albritton, and R. E. Sievers, Atmos. Environ., 18, 2421 (1984)

20. M. J. Campbell, J. C. Sheppard, and B. F. Au, Geophys. Res. Lett., 6, 175 (1979)

21. S. C. Wofsy, J. C. McConnell, and M. B. McElroy, J. Geophys. Res., 77, 4477 (1972)

22. H. Levy II, Adv. Photochem., 9, 369 (1974)

23. P. J. Crutzen and J. Fishman, Geophys. Res. Lett., 4, 321 (1977)

24. P. J. Crutzen, I. S. A. Isaksen, and J. R. McAfee, J. Geophys. Res., 83, 345 (1978)

25. W. L. Chameides, J. Geophys. Res., 86, 5209 (1981)

26. R. J. Allan, K. S. Groves, and A. F. Tuck, J. Geophys. Res., 86, 5303 (1981)

27. C. R. Burnett, Geophys. Res. Lett., 3, 319 (1976)

28. C. R. Burnett and E. B. Burnett, J. Geophys. Res., 89, 9603 (1984)

29. D. Perner, D. H. Ehhalt, H. W. Patz, U. Platt, E. P. Roth, and A. Volz, Geophys. Res. Lett., 3, 466 (1976)

30. G. Hubler, D. Perner, U. Platt, A. Tonnissen, and D. H. Ehhalt, J. Geophys. Res., 89, 1309 (1984)

31. T. Watanabe, M. Yoshida, S. Fujiwara, K. Abe, O. Onoe, M. Hirota, and S. Igarashi, Anal. Chem., 54, 2470 (1982)

32. D. D. Davis, W. Heaps, and T. McGee, Geophys. Res. Lett., 3, 331, (1976)

33. D. D. Davis, W. S. Heaps, D. Philen, M. Rodgers, T. McGee, A. Nelson, and A. J. Moriarty, Rev. Sci. Instrum., 50, 1505 (1979)

34. C. C. Wang, L. I. Davis, Jr., P. M. Selzer, and R. Munoz, J. Geophys. Res., 86, 1181 (1981)

35. T. M. Hard, R. J. O'Brien, C. Y. Chan, and A. A. Mehrabzadeh, Environ. Sci. Technol., 18, 768 (1984)

36. R. Atkinson, K. R. Darnall, A. C. Lloyd, A. M. Winer, and J. N. Pitts, Jr., Adv. Photochem., 11, 375 (1979)

37. D. L. Baulch and I. M. Campbell, A Specialist Periodical Report: Gas Kinetics and Energy Transfer, 4, 137 (1981)

38. R. Atkinson, Chem. Rev., 85, 69 (1986)

39. J. R. Kanofsky, D. Lucas, F. Pruss, and D. Gutman, J. Phys. Chem., 78, 311 (1974)

40. I. R. Slagle, J. R. Gilbert, R. E. Graham, and D. Gutman, Int. J. Chem. Kinet. Symp., 1, 317 (1975)

41. T. M. Sloane, Chem. Phys. Lett., 54, 269 (1978)

42. T. M. Sloane and R. J. Brudzynske, J. Chem. Phys., 72, 4394 (1980)

43. K. Hoyermann and R. Sievert, Ber Bunsenges. Phys. Chem., 83, 933 (1979)

44. H. W. Biermann, G. W. Harris, and J. N. Pitts, Jr., J. Phys. Chem., 86, 2958 (1982)

45. K. Hoyermann and R. Sievert, Ber Bunsenges. Phys. Chem., 87, 1027 (1983)

46. J. P. L. Henri and R. W. Carr Jr., J. Photochem., 5, 69 (1975)

47. J. F. Meagher and J. Heicklen, J. Phys. Chem., 80, 1645 (1976)

48. H. Niki, P. D. Maker, C. M. Savage, and L. P. Breitenbach, J. Phys. Chem., 82, 135 (1978)

49. H. Takagi, N. Washida, H. Akimoto, K. Nagasawa, Y. Ushi, and M. Okuda, J. Phys. Chem., 84, 478 (1980)

50. H. Niki, P. D. Maker, C. M. Savage, and L. P. Breitenbach, Chem. Phys. Lett., 80, 499 (1981)

51. H. Niki, P. D. Maker, C. M. Savage, and L. P. Breitenbach, Int. J. Chem. Kinet., 15, 647 (1983)

52. H. Niki, P. D. Maker, C. M. Savage, L. P. Breitenbach, J. Phys. Chem., 87, 4978 (1983)

53. E. C. Tuazon, R. Atkinson, H. MacLeod, H. W. Biermann, A. M. Winer, W. P. L. Carter, and J. N. Pitts, Jr., Environ. Sci. Technol., 18, 981 (1984)

54. P. B. Shepson, E. O. Edney, and E. W. Corse, J. Phys. Chem., 88, 4122 (1984)

55. S. Hatakeyama and H. Akimoto, J. Phys. Chem., 87, 2387 (1983)

56. K. R. Darnall, R. Atkinson, J. N. Pitts, Jr., J. Phys. Chem, 83, 1943 (1979)

57. A. C. Besemer, Atmos. Environ., 16, 1599 (1982)

58. R. A. Kenley, J. E. Davenport, and D. G. Hendry, J. Phys. Chem., 82, 1095 (1978)

59. R. A. Kenley, J. E. Davenport, and D. G. Hendry, J. Phys. Chem., 85, 2740 (1981)

60. Ref. 11, H. Okabe, pp.338, Table VIII-1A

61. F. Sakamaki, H. Akimoto, and M. Okuda, Environ. Sci. Technol., 14, 985 (1980)

62. H. Akimoto, M. Hoshino, G. Inoue, F. Sakamaki, N. Washida, and M. Okuda, Environ. Sci. Technol., 13, 471 (1981)

63. J. N. Pitts, Jr., D. Grosjean, K. Van Cauwenberghe, J. P. Schmid, and D. R. Fitz, Environ. Sci. Technol. 12, 946 (1978)

64. W. P. L. Carter, A. M. Winer, K. R, Darnall, and J. N. Pitts Jr., Env. Sci. Tech., 13, 1094 (1979)

65. A. M. Winer, R. A. Graham. G. J. Doyle, P. J. Bekowies, J. M. McAfee and J. N. Pitts, Jr., Adv. Environ. Sci. Technol., 10, 461 (1980)

66. W. P. L. Carter, A. C. Lloyd, J. L. Sprung, and J. N. Pitts, Jr., Int. J. Chem. Kinet., 11, 45 (1979)

67. R. Atkinson, W. P. L. Carter, K. R. Darnall, A. M. Winer, and J. N. Pitts, Jr., Int. J. Chem. Kinet., 12, 779 (1980)

68. N. A. Kelly, Environ. Sci. Technol., 16, 763 (1982)

69. J. A. Leone, R. C. Flagan, D. Grosjean, and J. H. Seinfeld, Int. J. Chem. Kinet., 17, 177 (1985)

70. G. Z. Whitten, H. Hogo, and J. P. Killus, Environ. Sci. Technol., 14, 690 (1980)

71. J. P. Killus and G. Z. Whitten, Atmos. Environ., 16, 1973 (1982)

72. R. Atkinson, A. C. Lloyd, and L. Winges, Atmos. Environ., 16, 1341 (1982)

73. A. C. Lloyd, R. Atkinson, F. W. Lurmann and B. Nitta, Atmos. Environ. 17, 1931 (1983)

74. J. P. Killus and G. Z. Whitten, Environ. Sci. Technol., 18, 142 (1984)

75. J. A. Leone and J. H. Seinfeld, Int. J. Chem. Kinet., 16, 159 (1984)

76. K. R. Darnall, A. C. Lloyd, A. M. Winer, and J. N. Pitts, Jr.,

Environ. Sci Technol., 10, 692 (1976).

77. R. Perry, R. Atkinson, J. N. Pitts, Jr., J. Chem. Phys., 67, 5577 (1977)

78. J. S. Robertshaw and I. W. M. Smith, J. Phys. Chem., 86, 785 (1982)

79. W. Braun and M. Lenzi, Discuss. Faraday Soc., 44, 252 (1967)

80. B. A. Ridley, J. A. Davenport, L. J. Stief, and K. H. Welge, J. Chem. Phys., 57, 520 (1972)

81. D. D. Davis and R. B. Klemm, Int. J. Chem. Kinet., 5, 841 (1973)

82. R. B. Klemm and L. J. Stief, J. Chem. Phys., 61, 4900 (1974)

83. M. J. Kurylo and W. Braun, Chem. Phys. Lett., 37, 232 (1976)

84. R. J. Donovan, H. M. Gillespie, and R. H. Strain, J. Chem. Soc. Faraday Trans. 2, 73, 1553 (1977)

85. D. Husain, L. Krause, and N. K. H. Slater, J. Chem. Soc. Faraday Trans. 2, 73, 1678 (1978)

86. F. Stuhl and H. Niki, J. Chem. Phys., 57, 3671 (1971)

87. H. H. Nelson, W. J. Marinelli, and H. S. Johnston, Chem. Phys. Lett., 78, 495 (1981)

88. G. W. Harris and J. N. Pitts, Jr., J. Chem. Phys., 70, 2581 (1979)

89. J. J. Lamb, L. T. Molina, C. A. Smith, and M. J. Molina, J. Phys. Chem., 87, 4467 (1983)

90. W. J. Marinelle and H. S. Johnston, J. Chem. Phys., 77, 1225 (1982)

91. I. W. M. Smith and R. Zellner, J. Chem. Soc. Faraday Trans. 2, 69, 1617 (1973)

92. C. Morley and I. W. M. Smith, J. Chem. Soc. Faraday Trans. 2, 68, 1016 (1972)

93. A. R. Ravishankara, P. H. Wine, and A. O. Langford, J. Chem. Phys., 70, 984 (1979)

94. F. P. DelGreco and F. Kaufman, Discuss. Faraday Soc., 33, 128 (1962)

95. J. H. Brophy, J. A. Silver, and J. L. Kinsey, J. Chem. Phys., 62, 3820 (1975)

96. C. J. Howard, J. Chem. Phys., 65, 4771 (1976)

97. E. D. Morris, Jr., D. H. Stedman, and H. Niki, J. Am. Chem. Soc., 93, 3570 (1971)

98. C. J. Howard, J. Phys. Chem., 83, 3 (1979)

99. F. Kaufman, J. Phys. Chem., 88, 4909 (1984)

100. T. Ohta, J. Phys. Chem., 87, 1209 (1983)

101. T. Ohta, Int. J. Chem. Kin., 16, 879 (1984)

102. G. J. Doyle, A. C. Lloyd, K. R. Darnall, A. M. Winer, and J. N. Pitts, Jr., Environ. Sci. Technol., 9, 237 (1975)

103. A. C. Lloyd, K. R. Darnall, A. W. Winer, and J. N. Pitts, Jr., J. Phys. Chem., 80, 789 (1976)

104. C. H. Wu, S. M. Japar, and H. Niki, J. Environ. Sci. Health, A11, 191 (1976)

105. H. Niki, P. D. Maker, C. M. Savage, and L. P. Breitenbach, J. Phys. Chem., 82, 132 (1978)

106. R. A. Cox, K. F. Patrick, and S. A. Chant, Environ. Sci. Technol., 15, 587 (1981)

107. R. Atkinson, W. P. L. Carter, A. M. Winer, and J. N. Pitts, Jr., J. Air Pollut. Con. Ass., 31, 1090 (1981)

108. R. Atkinson, S. M. Aschmann, W. P. L. Carter, Int. J. Chem. Kinet., 15, 1161 (1983)

109. D. R. Darnall, R. Atkinson, and J. N. Pitts, Jr., J. Phys. Chem., 82, 1581 (1978)

110. R. Atkinson, S. M. Aschmann, and J. N. Pitts, Jr., Environ. Sci. Technol., 18, 110 (1984)

111. C. N. Plum, E. Sanhueza, R. Atkinson, W. P. L. Carter, and J. N. Pitts, Jr., Environ. Sci. Technol., 17, 479 (1983)

112. H. W. Biermann, H. MacLeod, R. Atkinson, A. M. Winer, and J. N. Pitts, Jr., Environ. Sci. Technol., 19, 244 (1985)

113. E. C. Tuazon, W. P. L. Carter, R. Atkinson, A. M. Winer, and J. N. Pitts, Jr., Environ. Sci. Technol., 18, 49 (1984)

114. I. M. Campbell, B. J. Handy, R. M. Kirby, J. Chem. Soc. Faraday Trans. 1, 71, 867 (1975)

115. E. C. Tuazon, W. P. L. Carter, R. Atkinson, J. N. Pitts, Jr., Int. J. Chem. Kinet., 15, 619 (1983)

116. Th. Klein, I. Barnes, K. H. Becker, E. H. Fink, and F. Zabel, J. Phys. Chem., 88, 5020 (1984)

117. D. Grosjean and S. K. Friedlander, Adv. Environ. Sci. Technol., 9, 435 (1980)

118. T. E. Graedel, Chemical Compounds in the Atmosphere, Academic Press, New York (1978)

119. K. R. Darnall, A. M. Winer, A. C. Lloyd, and J. N. Pitts, Jr., Chem. Phys. Lett., 44, 415 (1976)

120. R. A. Perry, R. Atkinson, and J. N. Pitts, Jr., J. Phys. Chem., 81, 296 (1977)

121. R. A. Perry, R. Atkinson, and J. N. Pitts, Jr., J. Phys. Chem., 81, 1607 (1977)

122. F. P. Tully, A. R. Ravishankara, R. L. Thompson, J. M. Nicovich, R. C. Shah, N. M. Kreutter, and P. H. Wine, J. Phys. Chem., 85, 2262 (1981)

123. K. Lorenz and R. Zellner, Ber. Bunsenges. Phys. Chem., 87, 629 (1983)

124. M. J. Kurylo, Chem. Phys. Lett., 23, 467 (1973)

125. D. D. Davis, S. Fischer, and R. Schiff, J. Chem. Phys., 61, 2213 (1974)

126. R. Atkinson, D. A. Hansen, and J. N. Pitts, Jr., J. Chem. Phys., 62, 3284 (1975)

127. L. J. Stief, D. F. Nava, W. A. Payne, and J. V. Michael, J. Chem. Phys., 73, 2254 (1980)

128. F. P. Tully and A. R. Ravishankara, J. Phys. Chem., 84, 3126 (1980)

129. J. J. Margitan and R. T. Watson, J. Phys. Chem., 86, 3819 (1982)

130. C. L. Lin, Int. J. Chem. Kinet., 14, 593 (1982)

131. A. Wahner and C. Zetzsch, J. Phys. Chem., 87, 4945 (1983)

132. C. A. Smith, L. T. Molina, J. J. Lamb, and M. J. Molina, Int. J. Chem. Kinet., 16, 41 (1984)

133. R. Zellner and K. Lorenz, J. Phys. Chem., 88, 984 (1984)

134. J. R. McNesby and H. Okabé, Adv. Photochem., 3, 157 (1964)

135. P. Borrell, P. Cashmore, and A. E. Platt, J. Chem. Soc., A, 1969, 3063 (1968)

136. L. C. Glasgow and P. Potzinger, J. Phys. Chem., 76, 138 (1972)

137. F. C. Fehsenfeld, K. M. Evenson, and H. P. Broida, Rev. Sci. Instrum., 36, 294 (1965)

138. Advances in Chemistry Series: 15 Physical Properties of Chemical Compounds, American Chemical Soc., Washington D. C. (1955)

139. G. W. Sears and E. R. Hopke, J. Am. Chem. Soc., 71, 2575 (1949)

140. L. P. Burkhard, D. E. Armstrong, and A. W. Andren, J. Chem. Eng. Data, 29, 248 (1984)

141. J. V. Michael and J. H. Lee, J. Phys. Chem., 83, 10 (1979)

142. D. M. Golden, F. P. DelGreco, and F. Kaufman, J. Chem. Phys., 39, 3034 (1963)

143. T. Carrington and H. P. Broida, J. Molecular Spec., 2, 273 (1958)

144. R. F. Hampson, "Chemical Kinetics and Photochemical Data Sheets for Atmospheric Reactions", Technical Report No. FAA-EE-80-17, U. S. Department of Transportation (1980)

145. G. L. Pratt, Gas Kinetics, John Wiley, London, (1969)

146. F. P. Tully and J. E. M. Goldsmith, Chem. Phys. Lett., 116, 345 (1985)

147. R. Atkinson, D. A. Hansen, and J. N. Pitts, Jr., J. Chem. Phys., 63, 1703 (1975)

148. A. R. Ravishankara, J. M. Nicovich, R. L. Thompson, and F. P. Tully, J. Phys. Chem., 85, 2498 (1981)

149. V. Schmidt, G. Y. Zhu, K. H. Becker, and E. H. Fink, Ber. Bunsenges. Phys. Chem., 89, 321 (1985)

150. D. D. Davis, S. Fischer, R. Schiff, R. T. Watson, and W. Bollinger, J. Chem. Phys., 63, 1707 (1975)

151. R. Atkinson, R. A. Perry, and J. N. Pitts, Jr., J. Chem. Phys., 66, 1197 (1977)

152. F. P. Tully, Chem. Phys. Lett., 96, 148 (1983)

153. R. Atkinson and J. N. Pitts, Jr., J. Chem. Phys., 63, 3591 (1975)

154. A. R. Ravishankara, S. Wagner, S. Fischer, G. Smith, R. Schiff, R. T. Watson, G. Tesi, and D. D. Davis, Int. J. Chem. Kinet., 10, 783 (1978)

155. C. W. Gear, Commun. ACM, 14, 176 (1971)

156. R. J. Cvetanovic, D. L. Singleton, and G. Paraskevopoulos, J. Phys. Chem., 83, 50 (1979)

157. A. Grinvald and I. Z. Steinberg, Anal.Biochem., 59, 583 (1974)

158. D. York, Can. J. Phys., 44, 1079 (1976)

159. J. Crank, The Mathematics of Diffusion, Clarendon Press, Oxford (1956)

160. R. A. Cox, R. G. Derwent, and M. R. Williams, Environ. Sci. Technol., 14, 57 (1980)

161. I. Barnes, V. Bastian, K. H. Becker, E. H. Fink, and F. Zabel, Atmos. Environ., 16, 545 (1982)

162. R. J. Cvetanovic, The 12th International Symposium on Free Radicals, Languna Beach, CA., (1976) referred in ref. 44, 154, and 163.

163. R. Atkinson, R. A. Perry, and J. N. Pitts, Jr., J. Chem. Phys., 67, 3170 (1977)

164. M. Bartels, K. Hoyermann, and R. Sievert, Proceedings of the 19th International Symposium on Combustion, The Combustion Institute, 1982, pp. 61-72

165. T. Ohta, Int. J. Chem. Kinet., 16, 1495 (1982)

166. R. Atkinson, E. C. Tuazon, and W. P. L. Carter, Int. J. Chem. Kinet., 17, 725 (1985)

167. R. D. Grant, E. Rizzardo, and D. H. Solomon, J. Chem. Soc. Perkin Trans. 2 , 379 (1985)

168. J. S. Gaffney and S. Z. Levine, Int. J. Chem. Kinet., 11, 1197 (1979)

169. R. Atkinson, Int. J. Chem. Kinet., 12, 761 (1980)

170. W. S. Nip, D. L. Singleton, and R. J. Cvetanovic, Can. J. Chem., 57, 949 (1979)

171. J. -Y. Park, P. F. Sawyer, M. C. Heaven, and D. Gutman, J. Phys. Chem., 88, 2821 (1984)

172. R. A. Perry, J. Chem. Phys., 80, 153 (1984)

173. R. J. Cvetanovic and D. L. Singleton, Rev. Chem. Intermed., 5, 183 (1984)

174. J. Heicklen, Int. J. Chem. Kinet., 13, 651 (1981)

175. J. -P. Martin and G. Paraskevopoulos, Can. J. Chem., 61, 861 (1983)

176. G. S. Jolly, G. Paraskevopoulos, and D. L. Singleton, Int. J. Chem. Kinet., 17, 1 (1985)

177. D. F. McMillen and D. M. Golden, Annu. Rev. Phys. Chem., 33, 493 (1982)

178. G. P. Smith, P. W. Fairchild, J. B. Jeffries, and D. R. Crosley, J. Phys, Chem., 89, 1269 (1985)

179. W. A. Pryor, Free Radicals, McGraw-Hill, New York (1966) p.156

180. R. L. Huanh, S. H. Goh, and S. H. Ong, The Chemistry of Free Radicals, Edward Arnold, London (1974), pp.25,26

181. M. Szwarc, "The Transition State in Radical Reactions" in The Transition State, Chemical Society Special Publication No. 16, London (1962), pp.109

182. D. C. McKean, Chem. Soc. Rev., 7, 399 (1978)

183. N. B. Colthup, L. H. Daly, and S. E. Wiberley, Introduction to Infrared and Raman Spectroscopy, 2nd ed., Academic Press, New York (1975)

184. F. P. Tully, A. R. Ravishnkara, K. Carr, Int. J. Chem. Kinet., 15, 1111 (1983)

185. F. P. Tully, A. T. Droege, M. L. Koszykowski, and C. F. Melius, J. Phys. Chem., 90, 691 (1986)

186. R. Atkinson, and S. M. Aschmann, Int. J. Chem. Kinet., 16, 1175 (1984)

187. A. Fontijn and R. Zellner, "Influence of Temperature on Rate Coefficients of Bimolecular Reaction" in Reactions of Small Transient Species Kinetics and Energetics, Ed. by A. Fontijn and M. A. A. Clyne, Academic Press, New York (1983), pp.1-61

188. M. Eliason and J. O. Hirschfelder, J. Chem. Phys., 30, 1426 (1959)

189. R. Zellner, "Bimolecular Reaction Rate Coefficients" in Combustion Chemistry, Ed. by W. C. Gardiner; Springer-Verlag, Heidelberg (1984)

pp.127

190. S. Glasstone, K. Laidler, and H. Eyring, The Theory of Rate Processes, McGraw-Hill, New York (1941)

191. D. L. Singleton and R. J. Cvetanovic, J. Am. Chem. Soc., 98, 6812 (1976)

192. H. Gusten, L. Klasinc, and D. Maric, J. Atmos. Chem., 2, 83 (1984)

193. D. A. Demeo and M. A. El-Sayed, J. Chem. Phys., 52, 2622 (1970)

194. CRC Handbook of Spectroscopy, Vol. I, Ed. by J. W. Robinson, CRC Press, Cleveland, (1974)

195. M. Rinke and C. Zetzsch, Ber. Bunsenges. Phys. Chem., 88, 55 (1984)

196. J. L. Magee, J. Chem. Phys., 8, 687 (1940)

197. K. J. Laidler, Theories of Chemical Reaction Rates, McGraw-Hill, New York (1969) pp.172

198. CRC Handbook of Chemistry and Physics, 66th Edition, 1985-1986, CRC Press, Boca Raton, Florida, pp.E62,E63

199. R. P. Ruiz and K. D. Bayes, J. Phys. Chem., 88, 2592 (1984)

200. R. Paltenghi, E. A. Ogryzlo, and K. D. Bayes, J. Phys. Chem., 88, 2595 (1984)

201. K. Fukui, Theory of Orientation and Stereoselection, Springer-Verlag, Berlin (1975)

202. I. Fleming, Frontier Orbitals and Organic Chemical Reactions, Wiley, New York (1977)

203. S. W. Benson, Thermochemical Kinetics, 2nd ed., Wiley Interscience New York (1976)

204. K. N. Houk, N. G. Rondan, and J. Mareda, Tetrahedron, 41, 1555 (1985)

205. P. S. Skell and M. S. Cholod, J. Am. Chem. Soc., 91, 7131 (1969)

206. B. Giese and J. Meister, Angew Chem. Int. Edit., 17, 595 (1978)

207. B. Giese and W-B Lee, Angew Chem. Int. Edit., 19, 835 (1980)

208. D. Schuetzle, D. Cronn, A. L. Crittenden, and R. J. Charlson, Environ. Sci. Technol., 9, 838 (1975)

209. D. Grosjean, K. Van Cauwenberghe, J. P. Schmid, P. E. Kelley, and J.

N. Pitts, Jr., Environ. Sci. Technol.,12, 313 (1978)

210. A. P. Altshuller, Adv. Environ. Sci. Technol., 10, 181 (1980)

211. R. Atkinson, S. M. Aschmann, W. P. L. Carter, and J. N. Pitts, Jr., Int. J. Chem. Kinet., 15, 721 (1983)

212. D. D. Davis, W. Bollinger, and S. Fischer, J. Phys. Chem., 79, 293 (1975)

213. D. A. Hansen, R. Atkinson, and J. N. Pitts, Jr., J. Phys. Chem., 79, 1763 (1975)

214. S. Madronich and W. Felder, J. Phys. Chem., 89, 3556 (1985)

215. C.-Y. Lin and M. C. Lin, Presented at the Fall Technical Meeting, Eastern Sction, The Combustion Instutute (1984) referred in ref. 214

216. P. R. Bevington, Data Reduction and Error Analysis for the Physical Sciences, MacGraw-Hill, New York (1969)

217. D. V. Banthorpe, Chem. Rev., 70, 295 (1970)

218. B. Fritz, V. Handwerk, M. Preidel, and R. Zellner, Ber. Bunsenges. Phys. Chem., 89, 343 (1985)

219. R. Atkinson, S. A. Aschmann, A. M. Winer, and J. N. Pitts, Jr., Arch. Environ. Con. and Tox., 14, 417 (1985)

220. C. Zetzsch, 15th Informal Conference on Photochemistry, Stanford, CA., June 27- July 1 (1982) referred in ref. 38 and 219

221. R. Koster and K.-D. Asmus, J. Phys. Chem., 77, 749 (1973)

222. S. W. Provencher, J. Chem. Phys., 64, 2772 (1976) (Mr. F. Kus of the Academic Computing Service of McMaster University kindly provided the computer program of curve fittings using an eigenfunction expansion method, and assisted its adaptation to the present study.)

223. R. Atkinson and S. M. Aschmann, Environ. Sci. Technol., 19, 462 (1985)

224. B. Giese, Angew. Chem. Int. Ed. Engl., 16, 125 (1977)

225. J. A. Kerr and M. J. Parsonage, Evaluated Kinetic Data on Gas Phase Addition Reactions, Butterworths, London, (1972)

226. G. W. Klumpp, Reactivity in Organic Chemistry, Wiley Interscience, New York (1982)

227. J. M. Nicovich, C. A. Gump, and A. R. Ravishankara, J. Phys. Chem.,

86, 1684 (1982)

228. J. M. Nicovich, C. A. Gump, and A. R. Ravishankara, J. Phys. Chem., 86, 1690 (1982)

229. R. Atkinson and J. N. Pitts, Jr., Chem. Phys. Lett., 63, 485 (1979)

230. R. Atkinson and J. N. Pitts, Jr., J. Phys. Chem., 78, 1780 (1974)

231. E. Grovenstien, Jr. and A. J. Mosher, J. Am. Chem. Soc., 92, 3810 (1970)

232. I. Mani and M. C. Sauer, Jr., Adv. Chem. Ser., 82, 142 (1968)

233. S. Furuyama and N. Ebara, Int. J. Chem. Kinet., 7, 689 (1975)

234. R. E. Huie and J. T. Herron, Prog. React. Kinet., 8, 1 (1975)

235. W. Exner, "The Hammet Equation, the Present Position" in Advances in Linear Free Energy Relationships, Ed. by N. B. Chapman and J. Shorter, Plenum Press, New York (1972) Chapter 1

236. H. C. Brown and Y. Okamoto, J. Am. Chem. Soc., 80, 4979 (1958)

237. Ref. 180., pp. 32, 110-116

238. Ref. 226, Chapter 3

239. R. Atkinson, W. P. L. Carter, and A. M. Winer, J. Phys. Chem., 87, 1605 (1983)

240. J. M. Dust and D. R. Arnold, J. Am. Chem. Soc., 105, 1221 (1983)

241. K. Kimura, S. Katsumata, Y. Achiba, T. Yamazaki, and S. Iwata, Handbook of HeI Photoelectron Spectra of Fundamental Organic Molecules, Japan Science Soc., Tokyo, (1981)

242. A. D. Baker, D. P. May, and D. W. Turner, J. Chem. Soc., B, 22 (1968)

243. BACKGROUND to the REGULATION of POLYCHLORINATED BIPHENYLS (PCB) in Canada: A report of the TASK FORCE on PCB, April 1, 1976 to the ENVIRONMENTAL CONTAMINATION COMMITTEE of ENVIRONMENT CANADA and HEALTH & WELFARE CANADA, TECHNICAL REPORT 76-1, Environment Canada & Health and Welfare Canada

244. E. Atlas and C. S. Giam, Science, 211, 163 (1981)

245. T. F. Bidleman and C. E. Olney, Science, 183, 516 (1974)

246. W. R. Swain, J. Great Lakes Res., 4, 398 (1978)

247. W. M. J. Strachan and H. Huneault, J. Great Lakes Res., 5, 61 (1979)

248. S. J. Eisenreich, B. B. Looney, and J. D. Thornton, Environ. Sci. Technol., 15, 30 (1981)

249. E. H. Buckley, Science, 216, 520 (1982)

250. M. P. Brown, M. B. Werner, R. J. Sloan, and K. W. Simpson, Environ. Sci. Technol., 19, 656 (1985)

251. T. J. Murphy, L. J. Formanski, B. Brownawell, and J. A. Meyer, Environ. Sci. Technol., 19, 942 (1985)

252. G. R. Harvey and W. G. Steinhauer, Atmos. Environ., 8, 777 (1974)

253. Polychlorinated Biphenyls: A Report Prepared by the Committee on the Assessment of Polychlorinated Biphenyls in the Environmnet, National Academy of Sciences, Washington, D.C. (1979) pp.11-25

254. T. J. Murphy and C. P. Rzeszutko, J. Great Lakes Res., 3, 305 (1977)

255. R. R. Arnts, A. Appleby, D. Lillian, and H. B. Singh, 172nd Meeting, American Chemical Society, San Francisco, Cal., (1976), Paper ENVT-68

256. R. Atkinson and W. P. L. Carter, Chem. Rev., 84, 437 (1984)

257. W. L. Dilling, G. E. Miracle, and G. U. Boggs, 186th National Meeting of the American Chemical Society, Washington, D.C., (1983), Paper ENVR-126